

**A STUDY ON COP IMPROVEMENT OF A
HOUSEHOLD REFRIGERATOR BY USING AN
ADSORPTION HEAT PUMP**

**A Thesis Submitted to
the Graduate School of Engineering and Sciences of
İzmir Institute of Technology
in Partial Fulfillment of the Requirements for the Degree of**

MASTER OF SCIENCE

in Mechanical Engineering

**by
Gizem ARSLAN**

**June, 2015
İZMİR**

ACKNOWLEDGEMENTS

I would like to express my deepest gratitude to Prof. Dr. Moghtada MOBEDI, for his excellent guidance, caring, patience, and providing me an excellent research atmosphere. Many thanks to him not just for encouraging and believing me also for teaching me the meaning of the word educationist. I have always been proud of being Prof. Dr. Moghtada MOBEDI's student. The things I learned from him are immeasurable. From now on, I will do the best I can to hear from him that he is proud of me.

Special thanks to Dr. Gamze GEDIZ ILIS. It was a pleasure study with her. I never forget her support during my conferences. Her advices have enlightened my life and academic path, doubtlessly.

I also would like to thank to my advisor, Dr. BARISIK for supporting my research. Countless thanks to my friends in the Mechanical Engineering. I would like to show my gratitude to Ersin YAZGAN and his co-workers for the construction of the experimental setup. Also, thanks to Indesit company for funding my thesis.

I would like to thank Ahmet Sadik YORULMAZ who, as a good friend, was always willing to help and give his best suggestions.

Finally, my research would not have been possible without help of my mom Ayşe ARSLAN, my dad Kemal ARSLAN and my brother Can ARSLAN. It was their support what lift me up and kept me motivated. The last thank to my beloved one Cem OZGEN. He was always with me to cheer me up and stood by me through the good times and bad.

I would never have been able to finish my dissertation without the guidance of my committee members, help from friends, and support from my family.

ABSTRACT

A STUDY ON COP IMPROVEMENT OF A HOUSEHOLD REFRIGERATOR BY USING AN ADSORPTION HEAT PUMP

The thesis aims to increase the coefficient of performance of a domestic type household refrigerator.

A household refrigerator is a kind of mechanical heat pump which works based on the vapor compression cycle. On the other hand, adsorption heat pump is a thermal heat pump and it can directly operate with any kind of third energy source such as solar, waste heat.

The heat released from the condenser of a mechanical heat pump provides the desorption of the adsorbate in the adsorbent bed and helps the transfer of the adsorbate to the condenser of the adsorption heat pump. Then, the adsorbent bed which has low level adsorbate concentration provides the evaporation of the adsorbate in the evaporator and generates a cooling effect. By this way, an additional cooling effect can be generated without the increase of energy consumption of refrigerator.

In this thesis, a detailed literature survey on the combination of hybrid cooling systems is done. The suggested hybrid cooling systems are classified, and their advantages and disadvantages are discussed. In order to analyze heat and mass transfer of an adsorption heat pump, different conditions for adsorbent bed design are studied, theoretically. To design an adsorption heat pump the effects on the heat and mass transfer should be well known. Theoretical studies on heat and mass transfer in a rectangular adsorbent bed is performed to understand what can be effected on the heat and mass transfer in an adsorbent bed. Heat and mass transfer equations for a rectangular adsorbent bed are derived for non-uniform pressure approaches and numerically solved to determine temperature and concentration profiles in the bed with using Comsol Software. Furthermore, our CFD program coded in FORTRAN language. The code is used to validate the obtained results from Comsol. An experimental setup was designed and constructed in the light of these numerical studies. The enhancement of performance of a household refrigerator is calculated by using an adsorption heat pump.

ÖZET

ADSORPSİYONLU ISI POMPASI KULLANIMI İLE BİR EV TİPİ BUZDOLABININ ETKİNLİK KATSAYISININ ARTTIRILMASI ÜZERİNE BİR ÇALIŞMA

Bu tezde, bir ev tipi buzdolabında bulunan yoğuşturucudan ortama atılan atık ısının bir adsorpsiyonlu ısı pompası vasıtası ile değerlendirilerek buzdolabının etkinlik katsayısının artırılması amaçlanmıştır.

Ev tipi buzdolabı bir mekanik ısı pompası olup buhar sıkıştırırmalı soğutma çevrimi ve mekanik bir iş girişi ile çalışmaktadır. Adsorpsiyonlu ısı pompası ise termal bir ısı pompası olup üçüncül ısı kaynağı (güneş enerjisi, jeotermal enerji, atık ısı vs.) ile soğutma etkisi yaratabilmektedir. Mekanik çevrim yoğuşturucusundan atılan ısı, adsorbent yatağında bulunan adsorbatın desorplanmasını ve adsorpsiyonlu sistemin yoğuşturucusuna transfer edilmesini sağlamaktadır. Düşük adsorbat konsantrasyonunda bulunan yatak ise adsorpsiyonlu sistemin buharlaştırıcısında bulunan sıvı adsorbatın buharlaşmasına ve soğutma etkisi yaratmasına neden olmaktadır. Böylece elektrik tüketmeden sağlanan ilave bir soğutma etkisi yaratılabilmektedir.

Bu tezde, buhar sıkıştırırmalı ısı pompalarının adsorpsiyonlu ısı pompası veya komponentleri ile nasıl kombine edilebileceği literatürdeki verileri çerçevesinde kıyaslanmıştır. Önerilen sistemler tek çevrimli ve çift çevrimli hibrit sistemler olarak sınıflandırılmıştır. Önerilen hibrit sistemlerin elde edilen veriler ışığında etkinlik katsayısı ve verim artış oranı incelenmiş, aralarında mukayese edilmiş, avantaj ve dezavantajları tartışılmıştır. Adsorpsiyonlu ısı pompasının ısı ve kütle transferi üzerine teorik ve deneysel çalışmalar yapılmıştır. Hibrit soğutma sistemlerinin oluşturulabilmesi için önerilen adsorpsiyonlu ısı pompası tasarımı önemlidir. Adsorpsiyonlu ısı pompası tasarımı yapmak için ısı ve kütle transferini etkileyen etkenler iyi bilinmelidir. Sabit olmayan basınç yaklaşımı kullanılarak dikdörtgensel bir adsorbent yataktaki ısı ve kütle transferi denklemleri çıkarılmış, yataktaki sıcaklık ve konsantrasyon profilleri Comsol Yazılımı kullanılarak hesaplanmıştır. Elde edilen sayısal sonuçları doğrulamak için tarafımızca oluşturulan kod yardımıyla FORTAN Programı kullanılmıştır. Sayısal sonuçlar ışığında, bir deney düzeneği geliştirilmiştir. Deneysel çalışmalar sonucunda bir ev tipi buzdolabının adsorpsiyonlu ısı pompası kullanılarak performans artışı hesaplanmıştır.

TABLE OF CONTENTS

LIST OF FIGURES.....	x
LIST OF TABLES.....	xv
LIST OF SYMBOLS.....	xvii
CHAPTER 1. INTRODUCTION.....	1
CHAPTER 2. HEAT PUMP.....	5
2.1. Classifications of Heat Pumps	5
2.1.1. Mechanical Heat Pumps	6
2.1.2. Thermal Driven Heat Pumps	8
2.1.3. Hybrid Heat Pumps	15
CHAPTER 3. LITERATURE SURVEY.....	19
3.1. Classification of the Hybrid Cooling Systems	19
3.1.1. Survey on Single-Loop Hybrid Cooling Systems	20
3.1.2. Survey on Double-Loop Hybrid Cooling Systems.....	25
CHAPTER 4. PRELIMINARY STUDY ON SUGGESTED HYBRID COOLING SYSTEM.....	29
4.1. The Aim of the Proposed System.....	29
4.2. Working Principle of the Proposed Hybrid Cooling System.....	31
4.3. Performance Calculations of the Proposed Hybrid Cooling System	33
CHAPTER 5. EXPERIMENTAL SETUP AND PROCEDURE.....	40
5.1. Components of the Experimental Setup.....	40
5.1.1. Adsorbent Bed	42
5.1.2. Condenser	44
5.1.3. Evaporator	45
5.1.4. Silica Gel	46

5.1.5. The Water Bath.....	47
5.1.6. The Vacuum Pump	48
5.1.7. The Pressure Gauge	48
5.1.8. The Thermocouples in the Adsorbent Bed	48
5.1.9. The Software	48
5.1.10. The Data Loggers	49
5.2. The Revised Adsorption Heat Pump Setup.....	49
CHAPTER 6. GOVERNING EQUATIONS.....	54
6.1. Adsorption Phenomenon	54
6.1.1. Isotherms	55
6.2. Uniform and Non-Uniform Pressure Approach.....	57
6.2.1. Uniform Pressure Approach	58
6.2.2. Non-Uniform Pressure Approach.....	59
6.3. The Governing Equations	60
6.4. The Governing Equations with Metal Additives	64
CHAPTER 7. NUMERICAL SOLUTION METHODOLOGIES	66
7.1. The Solution Method with Comsol Software.....	66
7.2. Introduction of COMSOL Multiphysics Software.....	68
7.3. Validation of Comsol Results	68
7.4. The Comparison between Uniform and Non-Uniform Pressure Approaches	71
CHAPTER 8. SIMULATION RESULTS	74
8.1. Simulation of Heat and Mass Transfer in Adsorbent Bed of Adsorption Heat Pump Operating with Released Heat of a Household Refrigerator	75
8.2. The Use of Metal Additives for Improving Heat Transfer in a Granular Adsorbent Bed.....	83

8.3. Optimum Design of an Adsorbent Bed of Adsorption Refrigeration System for Highest SCP	92
CHAPTER 9. EXPERIMENTAL RESULTS	101
9.1. Experimental Results	102
9.2. Experimental Procedure of the Adsorption Heat Pump	102
9.3. The Performance Calculation of the Experiments for the Adsorption Heat Pump Setup	105
9.4. The Tests of the First Adsorption Heat Pump Setup	106
9.4.1. The Leakage Test of the Adsorption Heat Pump	106
9.4.2. The Calibration Test Results of the Measurement Devices on the Adsorption Heat Pump Setup	108
9.4.3. The Results of the Experiments of the First Adsorption Heat Pump Setup	109
9.5. The Results for Revised Setup	116
9.5.1. The Tests of the Revised Adsorption Heat Pump Setup	117
CHAPTER 10. CONCLUSION	128
REFERENCES	131
APPENDICES	
APPENDIX A. TABLE OF PROPERTIES	135
APPENDIX B. DERIVATION OF THE HEAT AND MASS TRANSFER EQUATIONS	1358
APPENDIX C. COMSOL MODEL REPORT	143
APPENDIX D. FURTHER EXPERIMENTAL RESULTS	153
APPENDIX E. UNCERTAINTY ANALYSIS	180

LIST OF FIGURES

<u>Figure</u>	<u>Page</u>
Figure 2.1. Heat pump working principle.....	6
Figure 2.2. Vapor compression cycle of the refrigerator.....	7
Figure 2.3. Absorption heat pump cycle and its components.....	9
Figure 2.4 Adsorption heat pump a) a schematic view, b) a cycle of an AHP on Clapeyron diagram.....	12
Figure 2.5 The sample of a single-cycle hybrid systems.....	16
Figure 2.6. The sample of a double-cycle hybrid systems.....	17
Figure 4.1. The schematic demonstration of the vapor compression cycle with the adsorption heat pump cycle combination in a household refrigerator.....	29
Figure 4.3. Proposed hybrid system (EP2775236A1, TR2013/02766).....	30
Figure 4.4. COP change of the vapor compression and hybrid refrigerator for different ambient temperatures.....	37
Figure 5.1. A schematic view of the first designed setup.....	40
Figure 5.2. A view of the first experimental setup.....	40
Figure 5.3. The technical drawing of the adsorbent bed design.....	41
Figure 5.4. Side view of the adsorbent bed.....	42
Figure 5.5. Top view of the adsorbent bed.....	42
Figure 5.6 (a) The details of the serpentine for heating and the pipes for cooling.	
Figure 5.7. The build phase of the pipes that made from the gauze with using special glue for enduring the high temperatures and the view of the cover that made from the gauze for adsorbent bed.....	43
Figure 5.8. The details of the condenser.....	44
Figure 5.9. Condenser, reservoir, fan and measurement devices on the condenser.....	44
Figure 5.10. The Evaporator.....	45
Figure 5.11. The mixture of aluminum and silica gel particles.....	46
Figure 5.12. The process of to minimize the 2 mm diameter of the silica gel particles to 0.25 mm.....	46

Figure 5.13. a) Data logger E680 to measure temperature, b) PCLD 8710 datalogger to measure pressure.....	48
Figure 5.14. The view of the mesh pipes that are located inside of the adsorbent bed.....	49
Figure 5.15. The relief valve between the adsorbent bed and evaporator tank after the revision of experimental setup.....	50
Figure 5.16. The view of the evaporator is located near the adsorbent bed after the revision of experimental setup.....	50
Figure 5.17. The Clapeyron Diagram of the adsorbent bed.....	52
Figure 6.1. Illustration of adsorption phenomena.....	54
Figure 6.2. The adsorption behaviors of Freundlich, Henry, and Toth's isotherms.	55
Figure 6.3. Schematic representation of inter-particle and intra-particle flow.....	57
Figure 6.4. A section of adsorbent bed for uniform pressure approach.....	57
Figure 6.5. A section of adsorbent bed for non-uniform pressure approach.	59
Figure 6.6. A schematic view of the adsorption-desorption process on Clapeyron Diagram.	60
Figure 7.1. The operation conditions of the adsorption cycle on the Clapeyron Diagram.	67
Figure 7.2. The comparison of the results belong to the variation of temperature in the bed.....	68
Figure 7.3. The comparison of the change of adsorptive pressure in the bed obtained from the COMSOL and FORTRAN.....	68
Figure 7.4. The comparison of the water concentration in the bed obtained from COMSOL and FORTRAN.	69
Figure 7.5. The 2D adsorbent bed with filled with silica gel particles.	69
Figure 7.6. The temperature and concentration distributions for Uniform Pressure Approach of an adsorption process.....	70
Figure 7.7. The temperature, concentration and pressure distributions for Non- Uniform Pressure Approach of an adsorption process.	70
Figure 8.1. The schematic view of analyzed adsorbent bed filled with the adsorbent granules.	74
Figure 8.2. A schematic view of the adsorption-desorption process on Clapeyron Diagram.	75

Figure 8.3. The change of compressor outlet refrigerant temperature while the compressor is on and off.	76
Figure 8.4. The adsorbate concentrations and pressures of the adsorption desorption process on Clapeyron Diagram for the considered adsorbent bed.....	79
Figure 8.5. The distribution of the temperature and adsorbate concentration of the adsorbent bed for adsorption (d-a) process after 2 min, 5 min, 10 min, and of the process a) temperature, b) concentration.	80
Figure 8.6. The distribution of the temperature and adsorbate concentration of the adsorbent bed for desorption (b-c) process after 1 min, 2min, 3min, and of the process a) temperature, b) concentration.	81
Figure 8.7. The distribution of the pressure and velocity vectors of the adsorbent bed after 2min, and end of the process a)adsorption (d-a) process, b) desorption (b-c) process.....	82
Figure 8.8. The distribution of the average temperature and average adsorbate concentration of the considered adsorbent bed during the cycle.	83
Figure 8.9. Schematic view of the adsorbent bed a) the adsorbent bed, b) the two dimensional representative domain.	83
Figure 8.10. Aluminum pieces and aluminum pieces added silica gel granules.	84
Figure 8.11. Adsorption, heating, desorption, cooling processes for all volume fractions	88
Figure 8.12. The variation of temperature and concentration inside the adsorbent bed with no additive, 20, and 50% fractions at different time steps for adsorption, a) temperature, b) concentration.	89
Figure 8.13. The variation of temperature and concentration inside the adsorbent bed with no additive, 20 and 50% fractions at different time steps for desorption, a) temperature, b) concentration.	90
Figure 8.14. Adsorption-desorption time vs aluminum fraction.	90
Figure 8.15. Schematic view of the adsorbent bed a) the adsorbent bed, b) the two dimensional representative domain.....	91
Figure 8.16. SCP and amount of silica gel for all volume fractions from 10 to 90%.....	92
Figure 8.17. SCP and amount of mass of bed for all volume fractions from 10 to 90%.....	94

Figure 8.18. The effects of design parameters of A, B, C, and D on SCP of the adsorbent bed.	99
Figure 8.19. The contribution ratio of each parameter on SCP of the adsorbent bed.....	101
Figure 9.1. The ideal adsorption heat pump cycle.....	103
Figure 9.2. The adsorption process of the adsorption heat pump cycle on the Clapeyron Diagram.....	104
Figure 9.3. The heating process of the adsorption heat pump cycle on the Clapeyron Diagram.....	105
Figure 9.4. The desorption period of the adsorption heat pump cycle on the Clapeyron Diagram.....	106
Figure 9.5. The cooling process of the adsorption heat pump cycle on the Clapeyron Diagram.....	106
Figure 9.6. Leakage test results.....	109
Figure 9.7. Calibration test results of the Pt-100 thermocouples.....	110
Figure 9.8. a) Temperature variation of the adsorbent bed, evaporator and condenser during the adsorption and desorption processes. b) Pressure variation of the adsorbent bed, evaporator and condenser during the adsorption and desorption processes. c) Clapeyron Diagram of the adsorbent bed with the operation temperature and pressure values of the adsorbent bed.....	112
Figure 9.9. a) Temperature variation of the adsorbent bed, evaporator and condenser during the adsorption and desorption processes. b) Pressure variation of the adsorbent bed, evaporator and condenser during the adsorption and desorption processes. c) Clapeyron Diagram of the adsorbent bed with the operation temperature and pressure values of the adsorbent bed.....	114

Figure 9.10. a) Temperature variation of the adsorbent bed, evaporator and condenser during the adsorption and desorption processes. b) Pressure variation of the adsorbent bed, evaporator and condenser during the adsorption and desorption processes. c) Clapeyron Diagram of the adsorbent bed with the operation temperature and pressure values of the adsorbent bed.....	116
Figure 9.11. The leakage test results of the revised adsorption heat pump setup.....	118
Figure 9.12. a) Temperature variation of the adsorbent bed, evaporator and condenser during the adsorption and desorption processes. b) Pressure variation of the adsorbent bed, evaporator and condenser during the adsorption and desorption processes. c) Clapeyron Diagram of the adsorbent bed with the operation temperature and pressure values of the adsorbent bed.....	120
Figure 9.13. a) Temperature variation of the adsorbent bed, evaporator and condenser during the adsorption and desorption processes. b) Pressure variation of the adsorbent bed, evaporator and condenser during the adsorption and desorption processes. c) Clapeyron Diagram of the adsorbent bed with the operation temperature and pressure values of the adsorbent bed.....	122
Figure 9.14. a) Temperature variation of the adsorbent bed, evaporator and condenser during the adsorption and desorption processes. b) Pressure variation of the adsorbent bed, evaporator and condenser during the adsorption and desorption processes. c) Clapeyron Diagram of the adsorbent bed with the operation temperature and pressure values of the adsorbent bed.....	124
Figure 9.15. a) Temperature variation of the adsorbent bed, evaporator and condenser during the adsorption and desorption processes. b) Pressure variation of the adsorbent bed, evaporator and condenser during the adsorption and desorption processes. c) Clapeyron Diagram of the adsorbent bed with the operation temperature and pressure values of the adsorbent bed.....	127

LIST OF TABLES

<u>Figure</u>	<u>Page</u>
Table 3.1. The single-cycle hybrid systems developed by the researchers and the systems' efficiency.....	23
Table 3.2. The double-cycle hybrid systems developed by the researchers and the systems 'efficiency.....	26
Table 4.1. Operation temperatures of a vapor compression cycle of a domestic type refrigerator for different ambient temperatures.	34
Table 4.2. Consumed work, cooling and heating capacities and COP values of the domestic type refrigerator for different ambient temperatures.	34
Table 4.3. Adsorption heat pump cycle design values.	35
Table 4.4. The minimum and maximum adsorbate concentrations, mass of silicagel and evaporator capacity for the designed adsorption heat pump.....	36
Table 4.5. The calculated data for a vapor compression heat pump cycle of a refrigerator for different ambient temperatures.....	36
Table 4.6. The calculated data of an adsorption heat pump cycle.	37
Table 4.7. The COP values of the MHP, AHP and the suggested hybrid system.....	78
Table 8.1. The initial and boundary conditions of the considered problem.	85
Table 8.2. Thermophysical properties of the additive aluminum considered in the present study.....	86
Table 8.3. The initial and boundary conditions of the considered problem.....	91
Table 8.4. The COP, energy transfer from heating, desorption and evaporation processes for different volume fractions of the considered adsorbent bed.....	94
Table 8.5. The considered parameters of the bed and their levels.....	96
Table 8.6. The initial and boundary conditions of the considered problem.	97
Table 8.7. The initial temperature and concentration values for runs.	98
Table 8.8. Experimental plan of L9 orthogonal array for SCP values.....	101
Table 8.9. Response table of S/N ratios.....	101
Table 9.1. The comparison of obtained results from the first experimental setup and second experimental setup.....	125

Table 9.2. The contribution of the proposed hybrid system on the performance of a household refrigerator is calculated when ambient temperature is 20°C.....	128
--	-----

LIST OF SYMBOLS

C_p	specific heat of adsorbent, $\text{J kg}^{-1} \text{K}^{-1}$
D_{eff}	effective mass transfer diffusivity, $\text{m}^2 \text{s}^{-1}$
D_k	Knudsen diffusivity, $\text{m}^2 \text{s}^{-1}$
D_m	molecular diffusivity, $\text{m}^2 \text{s}^{-1}$
D_{bed}	effective diffusivity of adsorptive in adsorbent bed, $\text{m}^2 \text{s}^{-1}$
D_o	reference diffusivity, $\text{m}^2 \text{s}^{-1}$
E	diffusional activation energy, J mol^{-1}
K_{inh}	inherent permeability of adsorbent bed, m^2
K_{app}	apparent permeability of adsorbent bed, m^2
M	molecular weight of adsorptive, kg mol^{-1}
P	pressure, Pa
r_p	radius of adsorbent granule, m
R	radius of bed, m; ideal gas constant, $\text{J mol}^{-1} \text{K}^{-1}$
T	temperature, K
t	time, sec
v	adsorptive velocity, m s^{-1}
\bar{W}	average adsorbate concentration, kg_v/kg_s
W_∞	local adsorbate concent., kg_v/kg_s
Q_{evap}	energy transfer from evaporation, kJ

Greek symbols

ρ	density, kg m^{-3}
ΔH_{ads}	heat of adsorption, J kg^{-1}
φ	porosity
β	volume fraction
λ	thermal conductivity, $\text{W m}^{-1} \text{K}^{-1}$
μ	adsorptive viscosity, Ns m^{-2}
σ	collision diameter for Lennard–Jones potential, A^0
Ω	collision integral
τ	tortuosity

Subscriptions

a, d	final and initial conditions of adsorption
add	additive
eff	effective
i	inner
l	adsorptive
m_{add}	mass of additive aluminum
m_b	mass of bed
m_s	mass of silica gel
o	outer
s	adsorbent
sat	saturation
v	adsorbate
∞	equilibrium

CHAPTER 1

INTRODUCTION

As a result of the demand for higher comfort conditions and industrial development, energy consumption has considerably increased in recent years. Many studies have been performed to develop systems or methods to improve the energy efficiencies of house appliances and utilize the waste heat of the systems. The developments of innovative systems that are efficient and environmentally friendly are the new goal of researchers and designers. In the light of these developments, the present project aims to increase the coefficient of performance of a domestic type household refrigerator. The increase of performance yields the reduction of energy consumption and increase in the energy labeling level of a refrigerator. There is no doubt that the reduction of energy consumption of a refrigerator will considerably reduce energy consumption not only in our country but also around the world due to the huge number of operated refrigerators in houses, shops and restaurants. As it is known, heat pumps can be separated into two groups as mechanical and thermal heat pumps. A household refrigerator is a kind of mechanical heat pump which works based on the vapor compression cycle.

Vapor compression refrigeration cycles are the most common cooling cycles and have advantages of having high performance (i.e. COP, coefficient of performance) and the feasibility for industrial applications. However, they operate using the electricity produced by fossil fuel resources such as oil, coal, natural gas and hence extensive use of vapor compression cycles causes a rapid decrease in these energy resources due to low energy conversion efficiencies. Therefore in last decades, the interest in thermally driven systems which can use alternative energy sources and waste heat has increased. These systems can eliminate the disadvantages of electrically driven systems. They use heat sources such as solar, geothermal or waste heat without using any fuel. The ability to use thermal energy directly also enables making the recovery of waste heat.

Thermal heat pumps can operate with sustainable thermal sources such as geothermal energy, solar energy, and waste heat. There are three kinds of thermal driven heat pumps as absorption, adsorption, and chemical heat pumps. The absorption heat pump is produced by many manufacturers whereas the adsorption and chemical

heat pumps are still under investigation. Adsorption heat pump can directly operate with any kind of thermal energy source such as solar and geothermal energy. Absorption and adsorption cooling cycles are briefly compared in Chapter 2. Although adsorption cooling cycles show similarities to absorption cycles in the type of heat sources and in the physical events performed during the cycle, there are distinct differences between two. In absorption process, gas or liquid penetrates (diffuses) into a liquid or solid material producing a solution and resulting in a chemical reaction or phase change while in adsorption process, gas or liquid is accumulated at the surface of solid or liquid substance by the utilization of unbalanced surface forces. Absorption is a bulk phenomenon and the concentration is uniform throughout the bulk of absorbent. However, the adsorption is a surface phenomenon and the concentration of adsorbate on the surface of adsorbent is higher than that in the bulk of adsorbent.

An adsorption heat pump has significant advantages compared to the absorption or the mechanical heat pump. The utilization of low level temperature thermal energy source for heating and cooling purposes, lack of moving components, noiseless, and long life time are some of adsorption heat pumps' advantages.

As can be known, the function of a condenser in a mechanical heat pump is to condense or sub-cool the refrigerant from saturated vapor to the liquid phase. Therefore, the heat which is released from the condenser is a kind of waste heat that can be utilized for the desorption process of an adsorption heat pump. On the other hand, adsorption heat pump is a thermal heat pump and it can directly operate with any kind of third energy source such as solar, geothermal energy and waste heat. Many researchers and manufacturers have focused on the development and production of adsorption heat pumps due to their environmental friendly structure and advantage of their working with low level temperature thermal energy sources.

Combination of thermal and mechanical heat pump is one of the attempts of researchers for improving COP in recent years. Sward and LeVan examined thermodynamically a compression-driven adsorption cooling cycle. Three different adsorbate/adsorbent pairs used in this cycle: CO₂/zeolite, CO₂/activated carbon, and ammonia/silica gel based on two-bed system. The heat of desorption was transferred from the thermal reservoir which is in contact with the low pressure bed. As a result of this research, the COP of the system was changed according to the heat capacity of the adsorbent strongly. Another combined system is adsorption–ejector refrigeration. A hybrid system powered by solar energy was proposed and simulated by Zhang and

Wang. Zeolite/water pair was chosen in this hybrid system. The ejector and adsorber were used instead of mechanical compressors to compress the refrigerant vapor from the evaporator to the condenser. Banker et al. studied the performance of mechanical and adsorption hybrid compression refrigeration cycles with HFC 134a. The mechanical compression was tied up with thermal compression using an adsorption compressor as.

A basic adsorption heat pump consists of four main components: an adsorber, a condenser, an evaporator, and an expansion valve. The heat released from the condenser of a mechanical heat pump provides the desorption of the adsorbate in the adsorbent bed and helps the transfer of the adsorbate to the condenser of the adsorption heat pump. Then, the adsorbent bed which has low level adsorbate concentration provides the evaporation of the adsorbate in the evaporator and generates a cooling effect. By this way, an additional cooling effect can be generated without the increase of energy consumption of refrigerator.

The thesis consists of ten chapters. The classification of heat pumps as mechanical and thermal heat pump with their performance analysis is given in Chapter 2 besides the brief information about hybrid heat pumps. The working principle of an adsorption heat pump, performance analysis, definition of parameters such as COP and SCP/SHP, advantages and disadvantages of adsorption heat pump, comparison of heat pumps are given, also. The performed studies on hybrid heat pumps were reviewed in literature and presented in Chapter 3. The methods used for combination hybrid heat pumps categorized and presented also in Chapter 3 at the first time in the literature. In Chapter 4, the preliminary study on suggested hybrid system is given. The details of suggested hybrid system such as aims and components are presented in Chapter 4. The study consists on the selection of the pair used in the adsorption heat pump, steady and dynamical analysis of adsorption heat pump cycle is also given in Chapter 4. The description and construction of the designed adsorption heat pump is given in Chapter 5. The information about design and equipments of setup is given, also. The revised setup, its components and experimental procedure is explained in details in Chapter 5. The heat and mass transfer equations with no metal additive and when adding metal additive that solved for the proposed adsorption heat pump are given with the details such as effective mass diffusivity, and thermal diffusivity, in Chapter 6. In chapter7, numerical solution methodology of this study is presented. A detailed information about Comsol Software is given. A CFD code is written by using FORTRAN language. The results performed by using CFD solver. The results are compared with the results are

obtained from COMSOL. Furthermore, in Chapter 8 numerical studies on the suggested adsorbent bed is given in detailed. The change of performance of the adsorbent bed is investigated, based on the effect of different working condition. The experimental part of this study is performed with two constructed experimental setups. Chapter 9 includes results and discussion for the experiments performed in both first and second setups. The coefficient of performance, specific cooling power and cooling capacity of the adsorption experiments were calculated and its contribution to the existent vapor compression cycle of a household refrigerator is discussed based on the experimental results. Chapter 10 gives the conclusions of studies performed. The evaluations and the comments made about the study are presented in this chapter.

CHAPTER 2

HEAT PUMP

Due to the demand of higher comfort conditions and industrial development, energy consumption has increased in the world; therefore, the energy saving and renewable energy applications have gained importance. The development of energy systems that are environmentally friendly and designed based on innovative technologies using less energy or renewable sources is the focus of numerous studies.

A heat pump is a device which transfers heat from low temperature to high temperature source. Heat transfer from low to high temperature source is only possible by a third energy source, according to the second law of thermodynamics. The third energy source determines whether the heat pump is mechanical or thermal driven. If this third energy is mechanical, the heat pump can be named as mechanical and if it is thermal then it will be called as thermal heat pump. Thermal heat pumps can operate with sustainable thermal sources such as geothermal energy, solar energy, and waste heat.

In this section, more information is given about the mechanical heat pumps and thermally driven heat pumps. Their working principles, their components, and the performance calculations are also expressed in details.

2.1. Classifications of Heat Pumps

Heat pump is a device which transfers heat from low to high temperature heat source by using a third energy source. As given in Figure 2.1, heat pump applies external work to extract an amount of energy Q_L from a cold reservoir and delivers heat Q_H to a hot reservoir by using a third energy source. Q_L denotes the heat taken from the low temperature heat reservoir, while Q_H refers to the heat transferred to the high temperature one. If the third energy source is mechanical or thermal, the transferred energy is expressed by W_{in} or Q_{in} , respectively.

Heat pumps can be classified into two groups as mechanical and thermal heat pumps. There are three kinds of thermal driven heat pumps as absorption, adsorption, and chemical heat pumps. Detailed discussions and more information about mechanical and thermal heat pumps are presented in the next sections.

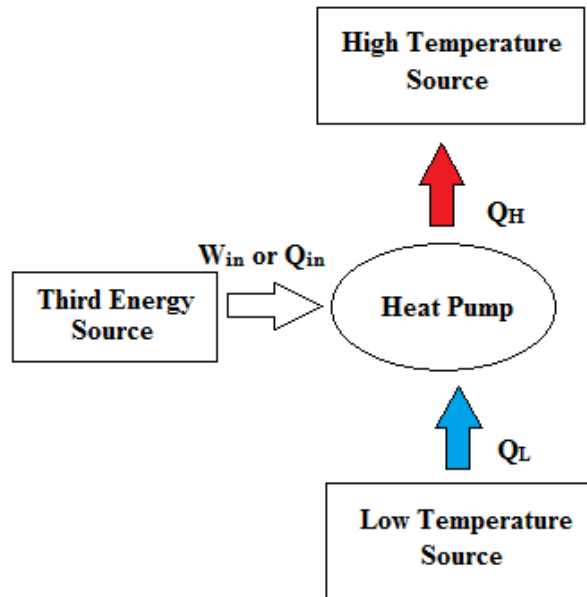


Figure 2.1. Heat pump working principle.

2.1.1. Mechanical Heat Pumps

The vapor compression cycle is widely used refrigeration system for the household refrigerators and HVAC systems. Vapor compression refrigeration cycle is used in various industrial, commercial and residential applications due to their continuous cooling and heating process. Also, they have practical design for the construction and application. On the other hand, the vapor compression heat pump uses hazardous refrigerants and requires periodic maintenance. Besides, the vapor compression heat pump has noisy operating conditions. Basically, the mechanical heat pump consists of four components such as an evaporator, a compressor, a condenser and an expansion valve (Figure 2.2). The refrigerant enters the compressor as saturated vapor and it is compressed to the condenser pressure. Then the refrigerant enters the condenser as superheated vapor and leaves the condenser as saturated (or sub-cooled) liquid. The pressure of refrigerant is dropped to the evaporator pressure by a capillary tube and after that it, enters the evaporator with a low quality saturated mixture. In the evaporator, the refrigerant evaporates by absorbing heat from the refrigerator interior space.

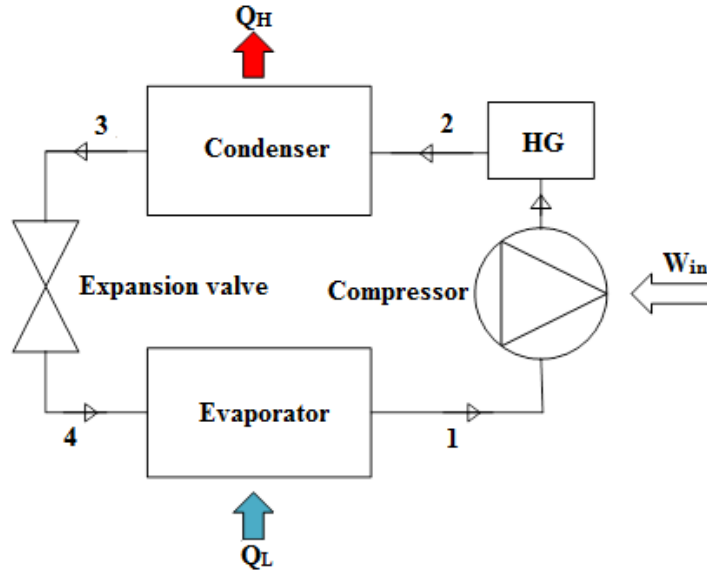


Figure 2.2. Vapor compression cycle of the refrigerator.

The COP value can be calculated by using the correlations given below for a basic vapor compression cycle of the refrigerator. The basic vapor compression cycle of the refrigerator is displayed in Figure 2.2.

$$COP_{vap} = \frac{Q_{evap}}{W_{in}} \quad (2.1.)$$

where

$$W_{in} = \dot{m}(h_{comp,out} - h_{comp,in}) \quad (2.2)$$

$$Q_{evap} = \dot{m}(h_{evap,out} - h_{evap,in}) \quad (2.3)$$

where \dot{m} represents the mass flow rate of the refrigerant in the cycle. Furthermore, the released heat from the hot gas and phase change can be calculated as:

$$Q_{hg} = \dot{m}C_p(T_{evap,out} - T_{vaporsat}) \quad (2.4)$$

$$Q_{phc} = \dot{m}(h_{vaporsat} - h_{cond,out}) \quad (2.5)$$

The total heat released from the vapor compression cycle can be calculated as:

$$Q_{cond} = Q_{hg} - Q_{phc} \quad (2.6)$$

2.1.2. Thermal Driven Heat Pumps

Thermal heat pumps can operate with sustainable thermal sources such as geothermal energy, solar energy, and waste heat. There are three kinds of thermal driven heat pumps as absorption, adsorption, and chemical heat pumps. The absorption heat pump is produced by many manufacturers whereas the adsorption and chemical heat pumps are still under investigation. Adsorption heat pump can directly operate with any kind of thermal energy source such as solar and geothermal energy.

2.1.2.1. Absorption Heat Pump

According to Adewusi and Zubair (2003), the absorption refrigeration system (ARS) has an important role because it has a higher cooling capacity than vapor compression system. Also, absorption heat pumps operate by a heat source such as natural gas, propane, solar-heated water, or geothermal-heated water, not electricity. Ammonia-water absorption refrigeration technology has been in existence since 1860. Ammonia-water is the most commonly used in absorption heat pumps as working pair. Because Ammonia-water has lower cost, better cycle efficiency, higher heat transfer coefficient. (Cengel and Boles, 2006). Basically the absorption heat pump cycle is the variation on a simple vapor compression refrigerator cycle. In the absorption cycle (Figure 2.3), the role of the mechanical compressor in compression cycle is replaced by thermal compressor which consists of a generator, an absorber, a heat exchanger, a pump and a throttling valve. The pump requires less energy input than the compressor. This is the reason of the less energy requirement. The high temperature source requires for the generator and the high temperature source would be solar energy, waste heat etc. The pure ammonia circulates the left part of the cycle as vapor compression cycle without a compressor. The pure ammonia goes to the absorber and the water cools it and the water comes from the generator to the absorber. The ammonia and water mixture goes to the pump. In the generator the mixture is separated by adding heat such as solar energy, waste heat, etc. The vapor ammonia goes to the condenser again and the water turns to the absorber.

The coefficient of performance values of heating and refrigeration processes for an absorption heat pump are given with the following equations (Cengel and Boles 2002):

$$COP_H = \frac{Q_{cond}}{Q_{gen} + W_{pump}} \quad (2.7)$$

$$COP_C = \frac{Q_{evap}}{Q_{gen} + W_{pump}} \quad (2.8)$$

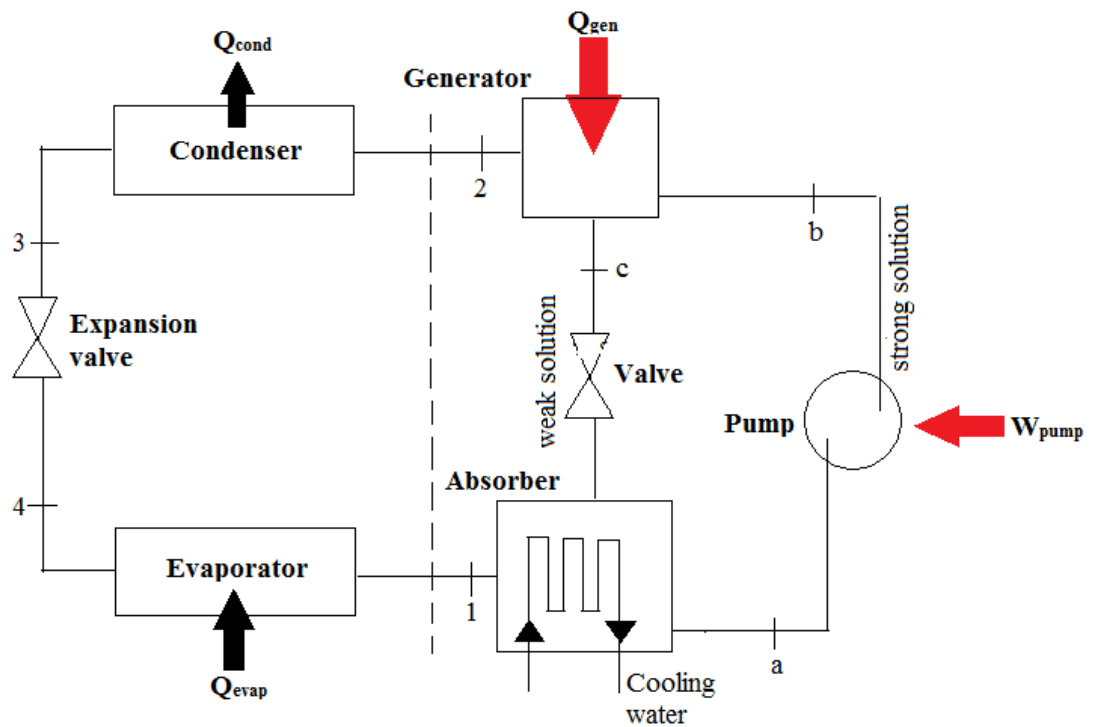


Figure 2.3. Absorption heat pump cycle and its components.

The comparison between compression and absorption refrigeration systems is also listed below.

Compression Systems

- Work operated
- High COP
- Lot of heat loss
- Regular maintenance required
- Higher noise
- Many moving parts
- Higher cost due to electricity as energy input

Absorption Systems

- Heat operated
- Low COP
- Less heat loss
- Very low maintenance required
- Less noise
- Less moving parts
- Cheap fuel such as waste heat

2.1.2.2. Chemical Heat Pumps

Chemical heat pumps (CHPs) utilize the reversible chemical reaction to change the temperature level of the thermal energy stored by chemical substances (Kawasaki, 1999). CHPs take the advantage of chemical reactions between a gas and a solid inside a reactor (Wongsuwan 2001; Mbaye 1998). A chemical heat pump involves desorption and adsorption/absorption processes. For absorbing and releasing heat, the properties of chemical substances are really important (Kato, 1996). Chemical heat pump is an option for energy upgrading of low temperature heat. The low temperature can be waste heat or solar energy. The thermochemical energy has advantages such as having a high storage capacity, lower heat loss (Ranade, 1990). Chemical heat pumps are more environmentally friendly than the conventional vapor compression heat pumps, as the compressor component consumes more electrical energy.

2.1.2.3. Adsorption Heat Pump

Adsorption heat pump can be directly operated with any kind of thermal energy source such as solar and geothermal energy. An adsorption heat pump has significant advantages compared to the absorption or the mechanical heat pump. The adsorption heat pump has significant advantages when compared to the absorption or the mechanical heat pumps. Adsorption heat pumps can work with a low level temperature heat reservoir. Adsorption heat pumps do not have moving components and adsorption heat pumps are noiseless systems. Adsorption heat pumps have a long-term performance besides having simple principle of working. The advantages and disadvantages of adsorption heat pump (AHP) are given in this section.

The advantages of adsorption heat pump system can be listed as:

1. It can operate with thermal driving energy sources such as waste heat, solar, and geothermal energies etc.
2. It can work with low temperature driving energy sources.
3. It does not require moving parts for circulation of working fluid.
4. It has long life time.
5. It operates without noise and vibration.
6. It has simple principle of working.
7. It does not require frequent maintenance.

8. It is environmental friendly.
9. It can be employed as thermal energy storage device.

It has disadvantages such as:

1. It has low COP values.
2. It has intermittently working principles.
3. It requires high technology and special designs to maintain high vacuum.
4. It has large volume and weight relative to traditional mechanical heat pump systems.

2.1.2.3.1. Working principle of Adsorption Heat Pump

A basic adsorption heat pump consists of four main components: an adsorber, a condenser, an evaporator, and an expansion valve as shown in Figure 2.4 (a). The adsorber contains adsorbent material which practically can be zeolite, silica gel or active carbon. Adsorbent can be coated on the surface of the adsorber or it may exist as granular in the bed. Adsorbents have large surface areas which can adsorb considerable amount of gas or liquids. The fluid circulating in the cycle of adsorption heat pump, which can be water, methanol etc., is called adsorbate.

The cycle of adsorption heat pump can be schematically represented on the Clapeyron diagram ($\ln(P)$ vs. $-(1/T)$) as shown in Figure 2.4 (b). Clapeyron diagram represents equilibrium condition between adsorbent and adsorbate. Considering Figure 2.4(a), both valves (V_1 and V_2) are closed at the beginning of adsorption process (point d). The adsorbent bed and evaporator are both at the evaporator pressure, P_{evap} . The concentration of adsorbate in the adsorbent bed is W_1 . By opening the valve V_1 , the evaporator starts to get heat from the space required to be cooled. The evaporated adsorbate in the evaporator is adsorbed by the adsorbent in the adsorbent bed. The process continues until the concentration of adsorbate in adsorbent attains to W_2 level. After the isobaric adsorption process, the valve V_1 is closed and then isosteric heating process starts (a-b). During this process, the adsorbent bed is heated and the temperature of the adsorbent bed rises from T_a to T_b while the adsorbate concentration in the bed remains constant at W_2 . The pressure of the adsorbent bed increases from P_{evap} to P_{cond} during the isosteric heating process. The next process is desorption process (b-c) which starts by opening of valve V_2 placed between the adsorber and the condenser. During the desorption process, the temperature of adsorbent bed increases from T_b to T_c while

its pressure remains at P_{cond} . The desorbed adsorbate leaves the adsorber, and it condenses in the condenser and as a result the adsorbate concentration falls from W_2 to W_1 . Finally, both valves (V_1 and V_2) are closed and the adsorbent bed is cooled to reduce its pressure from P_{cond} to P_{evap} . During this process, which is known as isosteric cooling process, the temperature of adsorbent bed falls from T_c to T_d .

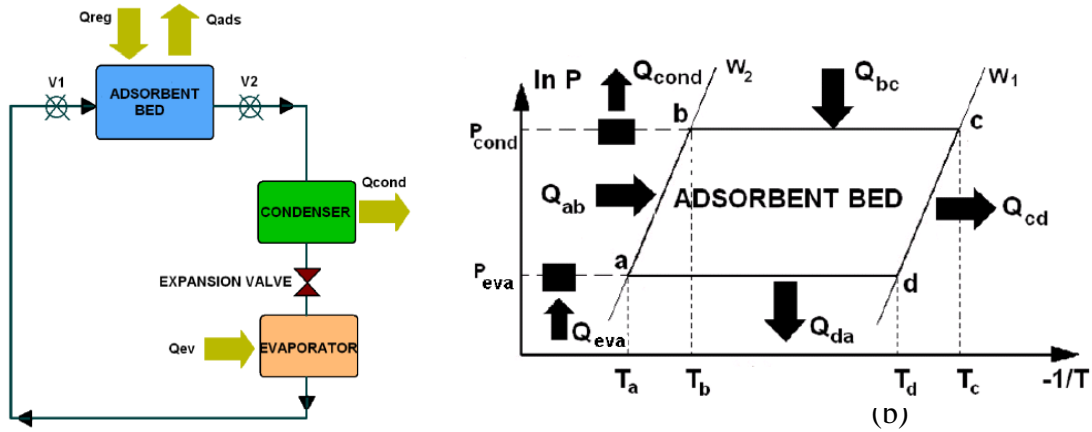


Figure 2.4. Adsorption heat pump a) a schematic view, b) a cycle of an AHP on Clapeyron Diagram.

2.1.2.3.2. Performance Analysis

The equations listed below are used to calculate the performance of an adsorption heat pump. The amount of heat from isosteric heating process (Q_{ab}), isobaric desorption process (Q_{bc}), isosteric cooling process (Q_{cd}), and isobaric adsorption process (Q_{da}) is stated below.

- The amount heat (Q_{ab}) should be transferred to increase the temperature of adsorbent. The formula for the amount of heat to increase the temperature of adsorbent bed from T_a to T_b is presented below.

$$Q_{ab} = \int_{T_a}^{T_b} \left[m_s \left(C_{p_s} + WC_{p_v} \right) + m_{bed} C_{p_{bed}} \right] dT \quad (2.9)$$

- (Q_{bc}) is the amount of heat which is transferred to the adsorbent bed for increasing the temperature of adsorbate-adsorbent pair and adsorbent bed for desorption process. Q_{bc} is calculated by using Eq. (2.10).

$$Q_{bc} = \int_{T_b}^{T_c} \left[m_s \left(C_{p_s} + WC_{p_v} \right) + m_{bed} C_{p_{bed}} \right] dT + \int_b^c m_s \Delta H_{ads} dW \quad (2.10)$$

- (Q_{cd}) is the heat loss when the valve between the condenser and adsorbent bed is closed, the temperature of adsorbent bed (T_c) is decreased to T_d .

$$Q_{cd} = \int_{T_d}^{T_c} \left[m_s \left(C_{p_s} + WC_{p_v} \right) + m_{bed} C_{p_{bed}} \right] dT \quad (2.11)$$

- (Q_{da}) is the heat loss due to heat of adsorption when the valve between the adsorbent bed and evaporator is opened and in the evaporator vaporization of the adsorbate is started.

$$Q_{da} = \int_{T_d}^{T_a} \left[m_s \left(C_{p_s} + WC_{p_v} \right) + m_{bed} C_{p_{bed}} \right] dT + \int_d^a m_s \Delta H_{ads} dW \quad (2.12)$$

- Q_{evap} is the heat of evaporation that causes cooling effect. Q_{evap} can be determined by the following relation:

$$Q_{ev} = \int_{T_{cond}}^{T_{evap}} \left[m_s \Delta W \Delta H_{va} \right] dT + \int_{T_{cond}}^{T_{evap}} m_s \Delta WC_{p_v} dT \quad (2.13)$$

- Q_{cond} is the heat of condensation which can be employed for heating purpose.

Q_{cond} can be determined by the following relation:

$$Q_{cond} = m_s \Delta W \Delta H \quad (2.14)$$

The cooling and heating COP of an adsorption heat pump can be calculated by using these formulas below.

$$COP_{cooling} = \frac{Q_{eva}}{Q_{ab} + Q_{bc}} \quad (2.15)$$

$$COP_{heating} = \frac{Q_{cond} + Q_{cd} + Q_{da}}{Q_{ab} + Q_{bc}} \quad (2.16)$$

Specific cooling power (SCP) or specific heating power (SHP) is the ratio of cooling/heating power per mass of adsorbent per cycle time. The definition of SCP/SHP involves the period of cycle and the period of cycle has important role to compare the various adsorption heat pump designs due to the cycle time changes according to the design of the adsorption heat pump. To have an enhancement on SCP/SHP value of an adsorbent bed, some improvements such as using multi-bed designs can be done on an adsorption heat pump.

$$SCP = \frac{Q_{evap}}{m_s \tau_{cycle}} \quad (2.17)$$

$$SHP = \frac{Q_{cond}}{m_s \tau_{cycle}} \quad (2.18)$$

where m_s is the mass of the adsorbent (silica gel, active carbon etc.) in the adsorbent bed.

2.1.3. Hybrid Heat Pumps

The aim of combining the mechanical heat pumps with the adsorption heat pumps is to improve the COP of a household refrigerator by developing a hybrid system. Developing a hybrid system can be possible with the combination of an adsorption heat pump or its components with a vapor compression heat pump. Adsorbent beds can be adapted into the mechanical heat pumps as a single cycle works. Another way is that the mechanical heat pump and adsorption heat pump can be tied up by a component and two separate refrigeration cycles operate in the hybrid system.

As a result, the COP value of the hybrid system can be calculated by the following equation:

$$COP_{hybrid} = \frac{Q_{evap} + Q_{evap}^*}{W_{in}} \quad (2.19)$$

where Q_{evap} is refers to the heat extracted from low temperature heat source in evaporator of mechanical heat pump, Q_{evap}^* is the amount of heat in evaporator of adsorption heat pump. Compressor requires the work input as presented W_{in} .

$$Q_{evap}^* = m_s \Delta H (W_2 - W_1) \quad (2.20)$$

where is the W_2 and W_1 maximum and minimum concentration values of the adsorption heat pump. Also, m_s represents the mass of silica gel and ΔH is the heat of desorption.

The combination of thermal and mechanical heat pump has been one of the attempts of researchers for improving COP in recent years. The detailed information about these studies with their proposed hybrid system and the COP values or the efficiency of the system given in Chapter 3. The classification of the proposed hybrid systems is performed according to combination of the components of adsorption heat pump and mechanical heat pump. The studies reported in the literature are reviewed and the proposed systems are classified as single-cycle and double-cycle hybrid systems. In a single-loop cycle hybrid system, the same refrigerant is circulated in both cycles of vapor compression and adsorption heat pumps. The double-cycle hybrid system has two separate cycles and heat exchange is taken place between these cycles.

2.1.3.1. The Single-Loop Hybrid Cooling Systems

In a single-loop hybrid cooling system, the adsorbent bed is adapted into the vapor compression heat pump cycle. The same refrigerant is circulated in a single-loop hybrid cooling cycle. The refrigerant is adsorbed/desorbed in the adsorbent bed and the refrigerant circulates in the vapor compression cycle, also.

The schematic figure of single-loop hybrid cooling system is illustrated in Figure 2.5. The adsorbent bed is used to help the compressor for increasing the pressure of the refrigerant in the single-loop hybrid cooling system. To adapt an adsorbent bed into the vapor compression cycle, there are two methods can be used. The adsorbent bed can be located before compressor to provide the low stage compression. The other possibility is to use mechanical compression for the lower stage. The two methods to compose a single-loop hybrid cooling system are given in detailed in literature survey of this thesis.

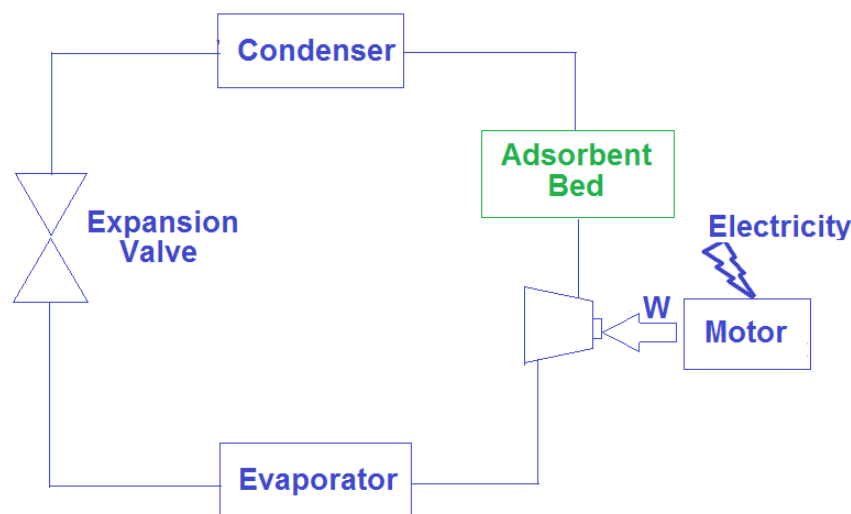


Figure 2.5. The sample of a single-cycle hybrid systems.

Banker et al. studied the performance of mechanical and adsorption hybrid compression refrigeration cycles with HFC 134a. Michel van der Pala et al. used the single-cycle hybrid system for their investigation. They used the silica gel-water as a working pair. Mitsui et al. used the same method in their investigation. Also, they used two adsorbent bed to compensate the some work of mechanical compressor. Inoue et Honda adapted an adsorbent bed to their vapor compression cycle. Sward and LeVan examined thermodynamically a compression-driven adsorption cooling cycle. Three

different adsorbate/adsorbent pairs used in this cycle: CO₂/zeolite, CO₂/activated carbon, and ammonia/silica gel based on two-bed system.

2.1.3.2. Double-Cycle Hybrid Cooling Systems

The double-cycle hybrid system has two separate cycles. In double-cycle hybrid cooling system, there is a heat exchange between the vapor compression cycle and the adsorption heat pump cycle. The refrigerant of the vapor compression cycle and the working fluid of the adsorption cycle does not mixed in the double-cycle hybrid cooling system. The refrigerant circulates in vapor compression cycle and the working fluid that adsorbed by the adsorbent bed.

The enhancement of performance of suggested hybrid systems has been examined in the light of performed literature research. The classification of the hybrid cooling systems are given in the Chapter 3. The advantages and disadvantages of the proposed hybrid systems were compared and discussed in the Chapter 3, also.

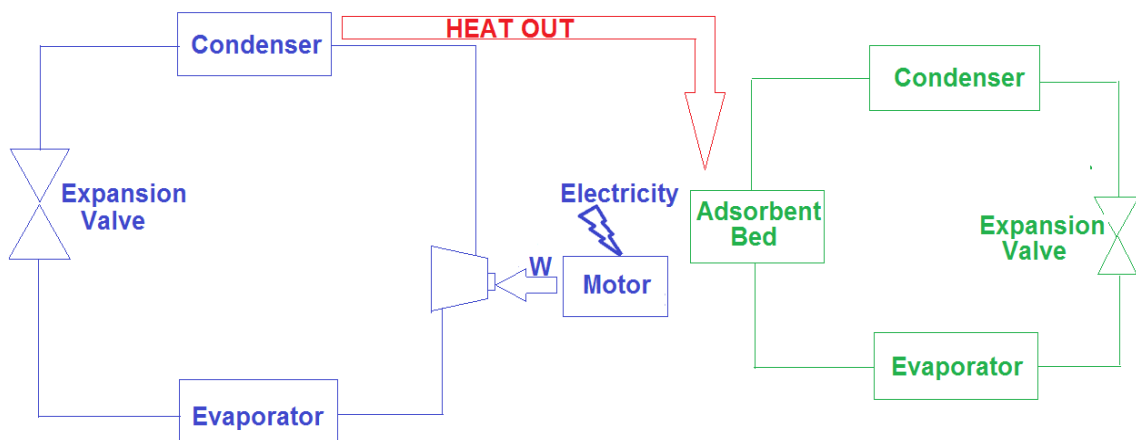


Figure 2.6. The sample of a double-cycle hybrid systems.

An experimental study was performed on investigation of double-cycle hybrid cooler system by Athanasiou. There are two cooler system to cool evaporator that are mechanical and adsorption system. Another system is developed by Sklenak. The hybrid system is implemented on a cooler that cooling the computer rooms. A. Asselman and Van Vensvoort studied on a system to perform on the household refrigerators. Silica gel or zeolite type adsorbent can be suggested for this system. An experimental study on investigation of a hybrid cooler system that can be performed by using silica

gel-water as a working pair for adsorption heat pump part of the system is investigated by Ilis, Mobedi and Ülkü use the waste that have high temperature and is discarded from the compressor is transferred to the adsorbent bed with using a heat exchanger to actualize the regeneration process.

The detailed information about the hybrid cooling system studies that developed by the researchers in the literature is given in Chapter 3, as illuminating as possible.

CHAPTER 3

LITERATURE SURVEY

This chapter is a review of previous studies performed on hybrid systems that are combination of mechanical heat pump and adsorption heat pump. In this chapter, the hybrid systems from literature are presented. Furthermore, the methods for combination of mechanical heat pump and adsorption heat pump are also investigated and categorized. The hybrid cooling systems are classified as single-loop hybrid cooling systems and double-loop hybrid cooling systems according to their combination method. Two main tables are presented to summarize the performed studies. The tables cover the name of the researchers, the original figure of the proposed hybrid systems and the COP values or the efficiency of the hybrid cooling systems. Table 3.1 represents the proposed single-loop hybrid cooling systems with the COP values or the efficiency of the proposed single-loop hybrid cooling systems and Table 3.2 represents the proposed double-loop hybrid cooling systems, respectively.

3.1. Classification of the Hybrid Cooling Systems

Hybrid systems use the technology of vapor compression refrigeration systems. The adsorption cooling cycle can be adapted to existing vapor compression cycle in the hybrid cooling systems. Thus, without requiring high investments in existing cooling systems, the increase of efficiency can be achieved. Recently considerable researches on the development of hybrid systems are carried out for the improvement of heat pumps' COP values. A detailed review on the hybrid cooling systems is presented in this chapter. The methods for combination of adsorption heat pumps and mechanical heat pumps are summarized and classified. Two main tables are presented to summarize the proposed hybrid systems, briefly. The tables (Table 3.1 and Table 3.2) represent the schematic diagrams, the coefficient of performance or efficiency values of the proposed hybrid cooling systems.

There is no classification for the hybrid cooling systems in the literature. A classification is done according to the combination method of the hybrid cooling systems by Mobedi et al. for the first time (Mobedi et al. 2015). The classification of the proposed hybrid systems are performed according to combination of the components of

adsorption heat pump and mechanical heat pump. The studies in the literature are reviewed and reported in this chapter. The proposed hybrid cooling systems are classified as single-loop and double-loop hybrid systems. In a single-loop hybrid system, the same refrigerant is circulated in both cycles of vapor compression and adsorption heat pump. Adsorbent bed of the adsorption cooling cycle is adapted to the existing vapor compression cycle to compose a single-loop hybrid system. The double-loop hybrid system has two separate cycles. The refrigerant that is operating in the vapor compression cycle and the working fluid that is adsorbed by the silica gel particles are different in the double-loop hybrid cooling cycles. The refrigerant of the vapor compression cycle and the working fluid of the adsorption cycle are not mixed in the double-loop hybrid cooling systems. Heat exchange is taken place between these cycles, only. The enhancement of performance of suggested hybrid systems has been examined in the light of the performed literature survey. The advantages and disadvantages of the proposed hybrid cooling systems are discussed.

3.1.1. Survey on Single-Loop Hybrid Cooling Systems

As mentioned in Chapter 2, basically, the single-loop hybrid cooling systems have adsorbent bed which is located in the existing vapor compression heat pump cycle. The adsorbent bed is called as adsorption compressor or thermal compressor in the literature, also (Banker, 2008). The thermal compressor can be used before or after mechanical compressor in the single-loop cycle. The thermal compressor provides the low-stage compression when the thermal compressor is located before mechanical compressor. The other possibility is to use mechanical compressor for the lower stage. If the thermal compressor use after the mechanical compressor, the thermal compressor provides high-stage compression. The refrigerant circulates in the vapor compression cycle and the refrigerant is adsorbed in the thermal compressor. The working fluid of the vapor compression cycle and the adsorption cycle is same. The developed single-loop cooling systems are searched in the literature and listed in Table 3.1. Table 3.1 presents a brief review on the performed studies. The name of the researchers, figure of the proposed hybrid system and their efficiency or COP values presented in Table 3.1.

As seen from Table 3.1, Banker et al. (2008) studied the utility of a hybrid compression refrigeration cycle using HFC 134a as a refrigerant. The conventional mechanical compression is supplemented by adsorption compressor. Activated carbon

is the adsorbent for the thermal compression component. This paper presents the results of an analysis of a hybrid compression system where the mechanical compression process is the dominant means of raising the pressure. Also, the thermal compression supplements the pressure rise enhancement of the vapor compression heat pump. Thus, the thermal compressor roles on the reduction of energy consumption of a mechanical refrigeration system. In the first proposed system, the thermal compressor is located after the mechanical compressor in the hybrid cycle. As given in the schematic diagram of the suggested hybrid refrigeration system, the adsorption compressor provides the low stage compression. The refrigerant from evaporator is transferred to the thermal compressor, where it gets adsorbed by activated carbon. After the adsorbent bed gets near the condensation pressure, the refrigerant is desorbed by supplying heat. The desorbed refrigerant is passed through an intercooler and its temperature is decreased. Then it enters into a mechanical compressor for high stage compression. Finally, refrigerant at high temperature and pressure enters to the condenser. In the second proposed of the Banker et al. (2008), the thermal compressor is located before the mechanical compressor. In this hybrid refrigeration system, the mechanical compressor provided the low stage compression and thermal compressor operates at high stage. The cycle has same components with the first cycle as an evaporator, a mechanical and an adsorption compressor, a condenser and an expansion valve. There is no intercooler in this suggested reverse cycle. The study showed that almost 40% energy saving is realizable with the hybrid system when compared with the case of a single-stage mechanical compressor. The main disadvantage of the proposed hybrid system is the intermittent refrigeration cycle due to the adsorption and the desorption periods.

Michel van der Pala et al. (2011) used the single-loop hybrid system for their investigation. They used the silica gel-water as a working pair. The aim of this study is increasing the efficiency of the adsorption heat pump with using mechanical compressor. The thermal efficiency of the adsorption chiller increase from 40% to 60% with using mechanical compressor. In this paper, the heat pump use both the waste heat and the heat gained from a compressor. The system comprises of a condenser, an evaporator and a reactor vessel. During the regeneration phase of the cycle, the reactor is heated to high temperature (60°C to 90°C) while the condenser is kept at ambient temperature. During the discharge phase of the cycle, the reactor is cooled down to ambient and the evaporator kept at desired cooling temperature. By measuring the temperature and the flow rate of the water entering and leaving the components

(evaporator, condenser and reactor), the amount of heat consumed or released was calculated. Furthermore the temperature and pressures in the components were measured. In the first proposed hybrid configuration, they placed the mechanical compressor between the evaporator and the reactor. The effect of the compressor on the discharge phase of the cycle is analyzed. In the second proposed hybrid configuration, they placed mechanical compressor between the reactor and the condenser. The effect of the compressor on the regeneration phase of the cycle is analyzed.

Mitsui et al. (1999) used two adsorbent bed to compensate the some work of mechanical compressor. The aim of using two adsorbent bed to provide continuity of the cooling system. So, adsorption process continues in one bed where the desorption process starts in the second bed. The thermal compressor is placed after the mechanical compressor in their system. The concept of their work is based on single-loop hybrid system. The efficiency of the proposed system is not mentioned in their study.

Inoue and Honda (1999) adapted an adsorbent bed to their vapor compression cycle. The refrigerant that comes from the compressor has high pressure and temperature provides the regeneration of the adsorbent from the adsorbent bed. When the system stops, it adsorbed by the adsorbent in the adsorbent bed, this situation brings along additional cooling effect for the system. The efficiency of the system is not mentioned in their study.

Sward and LeVan (1999) examined thermodynamically a compression-driven adsorption cooling cycle. Three different adsorbate/adsorbent pairs used in this cycle: CO₂/zeolite, CO₂/activated carbon, and ammonia/silica gel. The proposed two-bed system. The heat of desorption was transferred from the thermal reservoir which is in contact with the low pressure bed. The single-loop hybrid cooling cycle consists of two adsorbent bed in this study. The condenser of a vapor compression heat pump and replaces it with an adsorbing bed, as shown in Figure 1(a). The evaporator would then be replaced by a second, desorbing bed. The heat of desorption was transferred from the thermal reservoir which is in contact with the low pressure bed. During the cooling stages of the cycle, the working fluid comes from the compressor at low temperature to the desorbing bed, and passes it into the high temperature, adsorbing bed. Following compression and adsorption in the high temperature bed, the heat of adsorption is released to a second thermal reservoir. In this study, the influence of the shape and slope of the isotherm, the heat of adsorption and the sensible heat of the adsorbent are investigated on the performance of the cycle. When compared with three different

working pairs based on coefficients of performance, the ammonia system provides the best performance, followed by the CO₂/activated carbon, with the worst results generated by CO₂/NaX zeolite. As a result of this research, the COP of the system was changed according to the heat capacity of the adsorbent strongly.

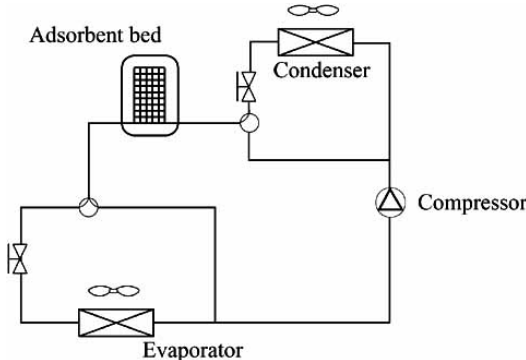
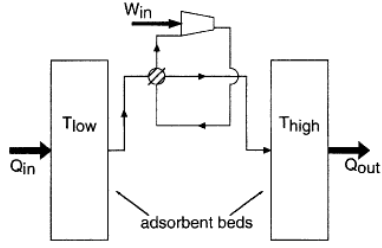
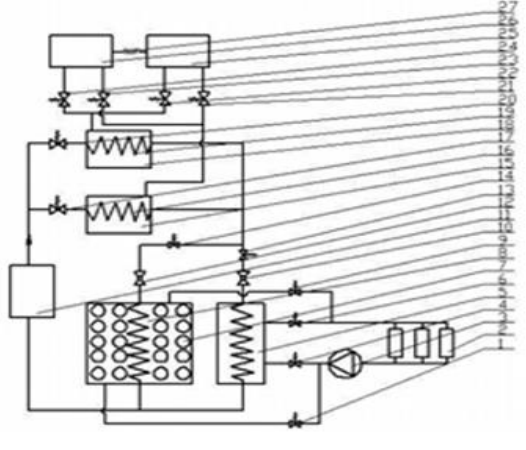
In patent CN102444950 (2011), Lin Yong developed a single-loop hybrid system which is the combination of the adsorption and vapor compression cycle. The ice obtained from the adsorption cycle is stored in two ice tank and the ice use to cool the condenser of the vapor compression cycle. Although there are two separate refrigeration cycle systems, these two systems are connected by valves and in the same refrigerant circulates in both the refrigeration cycle. The invention refers an ice cold accumulation adsorption heat recycling air-conditioner which is compose of a fan coil, a water pump, twelve magnetic valve and two throttling valve between components, a shell-tube evaporator, a cold accumulation ice ball, a cold accumulation box, a compressor, two adsorbent bed, two condenser pipe, an evaporator with a condenser of the adsorption cycle and a capillary tube. The capillary tube connects the condenser and evaporator of the adsorption cycle. The compressor, the seventh magnetic valve, the first adsorption bed, the fifth magnetic valve, the first throttling valve and the evaporator are connected in a closed loop. The ice cold accumulation adsorption heat recycling air-conditioner has the advantages of recycling heat of condensation after being used. The situation means the energy saving is achieved.

Table 3.1. The single-cycle hybrid systems developed by the researchers and the systems' efficiency.

Researchers	The Proposed Hybrid System	Efficiency/COP
<p>Banker et al. (2008)</p>		<p>%40</p>
<p>Michel van der Pala et al. (2011)</p>		<p>%60</p>
<p>Kakiuchi (1999)</p>		<p>n/a</p>

(cont.on next page)

Table 3.1. (cont.)

Researchers	The Proposed Hybrid System	Efficiency/COP
<p>Inoue and Honda (1999)</p>		<p>n/a</p>
<p>Sward and Levan (1999)</p>		<p>%40</p>
<p>Lin Yong (2011)</p>		<p>n/a</p>

3.1.2. Survey on Double-Loop Hybrid Cooling Systems

As mentioned in Chapter 2, in the double-loop hybrid cooling systems have adsorption cycle and vapor compression cycle works separately. The refrigerant circulates in the vapor compression cycle and the working fluid is adsorbed in the adsorption cycle are the different. The double-loop hybrid cooling system has two separate cycles. Heat exchange is taken place between these cycles. In double-cycle

hybrid system, the working fluid that is adsorbed by the adsorbent bed and the refrigerant circulates in the vapor compression cycle does not mixed. The enhancement of performance of suggested double-loop hybrid systems has been examined in the light of performed literature research and the advantages and disadvantages of the proposed double-loop hybrid systems were discussed. Double-cycle hybrid cooling systems are given on the Table 3.2 with their original proposed designs taken from the literature.

An experimental study was performed on investigation of double-loop hybrid cooler system by Athanasiou (2010). There are two cooler systems to cool evaporator that are mechanical and adsorption system. Athanasiou applied this proposed system on the household refrigerator. There is no information about the desorption process how to occurs by the compressor and condenser.

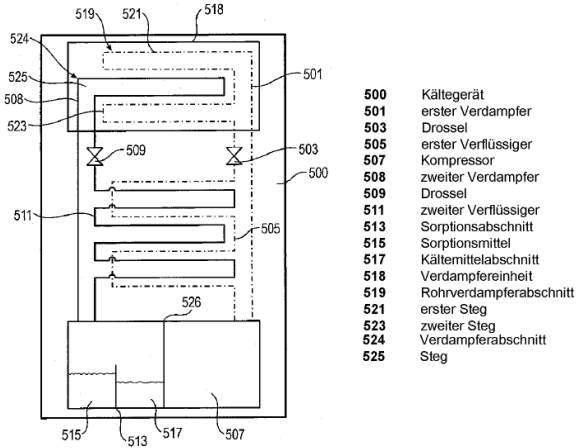
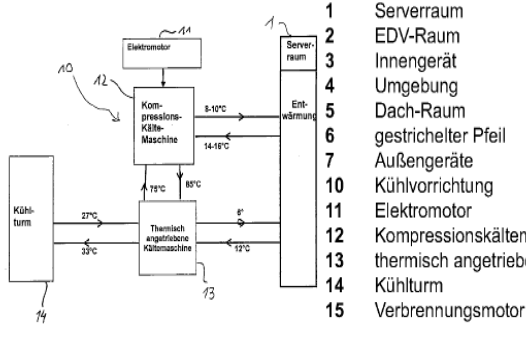
Another system is developed by Sklenak (2008). The hybrid system is implemented on a cooler that cooling the computer rooms. The heat discarded from the compressor is transferred to the adsorption cooler and run the adsorption process. So, the additional cooler effect can be provided and the performance of the system can be increased. The system that is developed by Sklenak showed how to use the waste heat in the adsorption heat pump extracted from the vapor compression cycle.

A. Asselman and Van Vensvoort (1983) studied on a system to perform on the household refrigerators. The system separated two sections that are chiller and freezer. The vapor compression cycle works for the freezer part. The refrigerant that comes from the evaporator in the freezer part, condenses the vapor phase adsorbate by using a heat exchanger. By means of the condensation is the adsorbate can be liquid phase from the vapor phase at low temperatures cools the refrigeration section. The amount of the vapor adsorbent is calibrated by the adsorbent in the adsorbent bed and an electrical heater. Silica gel and zeolite type adsorbent can be suggested for this system.

An experimental study on investigation of a hybrid cooler system was performed by Ilis, Mobedi and Ulku (2014). The system includes two separate refrigeration cycles. For the vapor compression system, the refrigerant is R600a and the silica gel-water pair is used for the adsorption heat pump cycle. The adsorption refrigeration system can be added to a vapor compression system as a secondary cycle. The adsorption heat pump cycle and vapor compression systems can be tied up by the condenser. By this way, both the hot gas and phase change released heats can be utilized in the desorption process of an adsorption refrigeration cycle. The waste that have high temperature and is discarded from the compressor is transferred to the adsorbent bed by using a heat

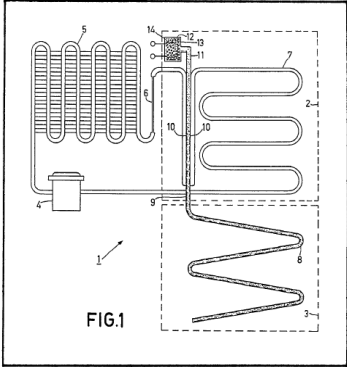
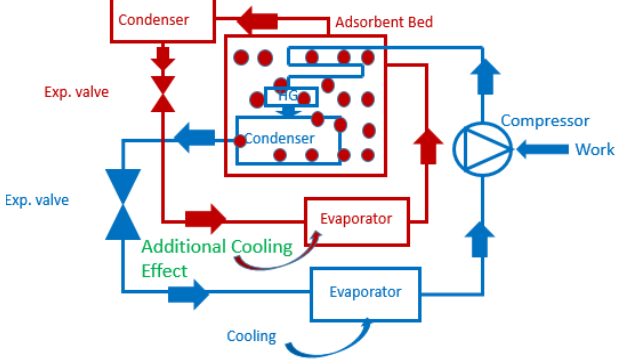
exchanger to actualize the regeneration process. Hence, the cooling effect and consequently the COP value of the vapor compression system are improved. For the low ambient temperatures up to 35°C. The suggested hybrid cycle can increase the COP value of the vapor compression refrigerator from 33 to 21%. However, further studies with different type of adsorbent/adsorbate pairs should be performed in order to investigate the improvement of COP by combination of vapor compression and adsorption heat pump cycle such as zeolite. Table 3.2 presents a brief information about the proposed the double-loop hybrid cycle. The name of researchers, the original figures of the suggested systems and the efficiency or COP value are given in Table 3.2. Table 3.2 is given below.

Table 3.2. The double-cycle hybrid systems developed by the researchers and the systems' efficiency.

Researchers	The Proposed Hybrid System	Efficiency/COP
Athanansiou (2010)	 <p>500 Kältegerät 501 erster Verdampfer 503 Drossel 505 erster Verflüssiger 507 Kompressor 508 zweiter Verdampfer 509 Drossel 511 zweiter Verflüssiger 513 Sorptionsabschnitt 515 Sorptionsmittel 517 Kältemittelabschnitt 518 Verdampfereinheit 519 Rohrverdampferabschnitt 521 erster Steg 523 zweiter Steg 524 Verdampferabschnitt 525 Steg</p>	n/a
B. Sklenak (2008)	 <p>1 Serverraum 2 EDV-Raum 3 Innengerät 4 Umgebung 5 Dach-Raum 6 gestrichelter Pfeil 7 Außengeräte 10 Kühlvorrichtung 11 Elektromotor 12 Kompressionskältemaschine 13 thermisch angetriebene Kältemaschine 14 Kühlturm 15 Verbrennungsmotor</p>	COP=6.7

(cont.on next page)

Table 3.2. (cont.)

Researchers	The Proposed Hybrid System	Efficiency/COP
<p>A.Asselman, Van Vensvoort (1983)</p>	 <p>FIG.1</p>	<p>n/a</p>
<p>Ilis, Mobedi, Ulku (2014)</p>		<p>%30</p>

CHAPTER 4

PRELIMINARY STUDY ON SUGGESTED HYBRID

COOLING SYSTEM

In the light of the literature survey, a double loop cooling hybrid system is proposed to increase the COP of a household refrigerator. As mentioned in the literature survey chapter, the adsorption heat pump system is adopted to a vapor compression cycle of a household refrigerator. This hybrid system is separated from each other, and the refrigerants of vapor compression and the adsorption heat pump systems are R600a and water, respectively. The details of this proposed hybrid cooling system are given in this chapter.

4.1. The Aim of the Proposed System

Adsorption technology has wide applications in pollution control, gas separation, drying process, catalytic reaction, and water and air purification. A new application of adsorption technology in recent years is adsorption based heat storage and refrigeration systems. Several theoretical and numerical studies have been performed on adsorption heat pump due to its advantages such as operation with low temperature heat reservoir, utilization of waste heat and alternative energy sources. A review on the reported studies, and advantages and disadvantages of adsorption heat pump is summarized by Demir et al. (2008). Due to the global warming and ozone layer depletion, the standards of the refrigeration industry force the manufacturers not only to find out new working fluids but also to develop new innovative thermodynamic cycles. Several studies have been performed on different parameters of cycles in order to improve the performance of a vapor compression refrigeration system. As a new idea in recent years, the combination of thermal and vapor compression refrigeration cycles for improving the performance. The details of these systems are also given in literature survey chapter of this thesis.

As it is well known, the duty of condenser in the most of mechanical refrigeration systems is to release heat to environment. The released heat can be utilized in the desorption process of an adsorption refrigeration cycle. As it is well known, the

duty of condenser in mechanical refrigeration systems is to release heat to environment and change the working fluid phase from superheated to saturated or sub-cooled phase. The heat released in vapor compression system refrigerators can be divided to two parts as:

- Hot gas released heat which involves the heat released from working fluid between compressor outlet and saturated vapor,
- Phase change released heat which contains the heat released from working fluid between condenser saturated vapor and saturated liquid (or sub-cooled).

Hence, an adsorption refrigeration system can be added to a vapor compression system as a secondary cycle as mentioned in literature survey chapter.

The proposed system focuses on the vapor compression cycle of a household refrigerator. The adsorption heat pump cooling system is adopted to the existing vapor compression cycle of a refrigerator. As known, the released heat of the refrigerator from hot gas and condenser can be accepted as a low source heat reservoir for the desorption process of an adsorption heat pump. Figure 4.1 summarizes this idea. The heat from hot gas and the condenser of a refrigerator can be used for the desorption. Also this system has another benefit such as using environmentally friendly refrigerants for improvement of the existing performance. Instead of designing completely a new heat pump of a household refrigerator based on new technology, improving the COP of the existent vapor compression heat pump by adding an adsorption heat pump cycle may be more logical and practical. There is no need any construction modification on the refrigerator.

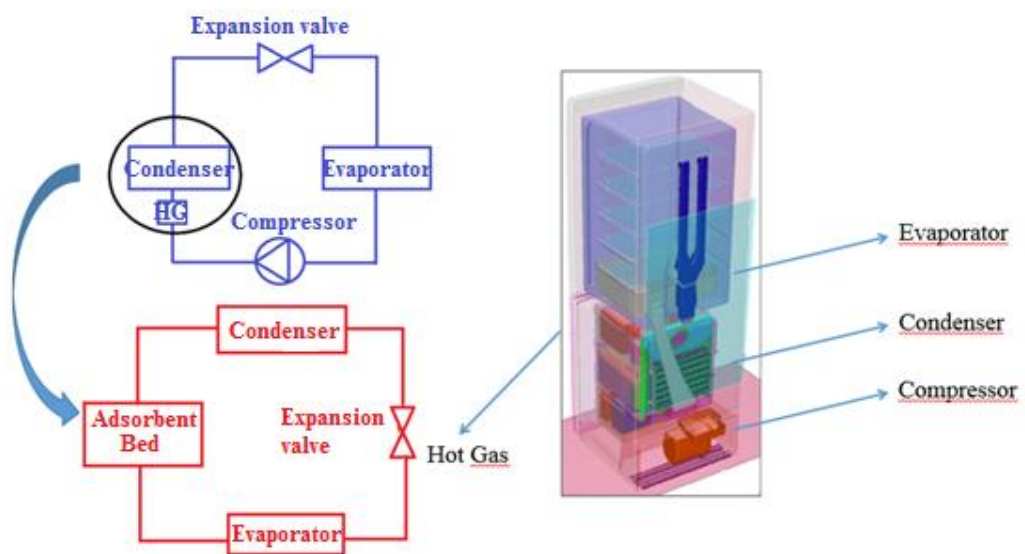


Figure 4.1. The schematic demonstration of the vapor compression cycle with the adsorption heat pump cycle combination in a household refrigerator.

To improve of COP of a household refrigerator by developing a hybrid system, the heat released in hot gas pipe and condenser can be utilized by adsorption heat pump cycle and additional cooling effect can be generated as illustrated in Figure 5.2. Two separate refrigeration cycles will operate in the hybrid system, however they are tied up by the condenser in the system. For the vapor compression cycle, the refrigerant is R600a and the silica gel-water pair is used for the adsorption cycle.

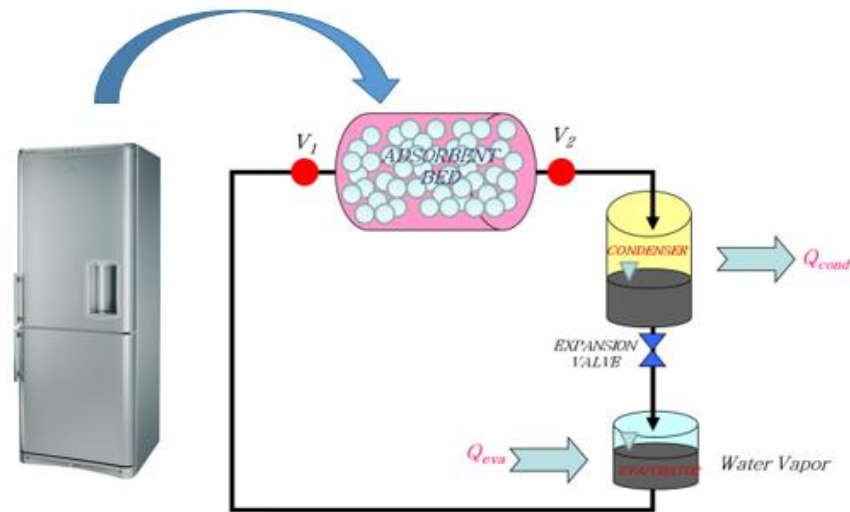


Figure 4.2. The demonstration of the utilizing the waste heat in the hybrid refrigeration system, basically.

4.2. Working Principle of the Proposed Hybrid Cooling System

As mentioned in Chapter 2, the standard vapor compression cycle used in refrigerators comprises a compressor which compresses the refrigerant fluid to the condenser pressure; a condenser which releases the heat out during of the cooling cycle, an evaporator which provides the cooling effect and a capillary tube which decreases the pressure of refrigerant fluid to the pressure of evaporator. In a household type refrigerator, the compressor which operates with electric power compresses the refrigerant fluid (R600 a, R134a etc.) to the condenser pressure. The pressure of the compressed gas is decreased to the evaporator pressure by passing from the capillary tube and thus, the cooling effect is obtained.

Adsorption heat pumps as explained in details in Chapter 2, they have four main components: an adsorber, a condenser, an evaporator, and an expansion valve. As condenser, evaporator, expansion valve, and adsorbent bed. The adsorber contains

adsorbent material which practically can be zeolite, silica gel, active carbon etc. Adsorbent can be coated on the surface of adsorber or it may exit as granular in the adsorber. Adsorbents have large surface areas which can adsorb considerable amount of gas or liquids. The fluid circulated in cycle of adsorption heat pump, which can be water, methanol etc., is called as adsorbate. The isobaric adsorption, isosteric heating, isobaric desorption, and isosteric cooling processes are its cooling cycle. The adsorption heat pump uses waste heat for the desorption process.

In Figure 4.2, the schematic view showing the adsorption cycle which is integrated to the system in addition to the standard cooling cycle is given. The adsorption cycle comprises at least one adsorbent bed which is filled with adsorbents such as silica gel, zeolite etc., a condenser which releases out the heat of the new adsorption cycle, an evaporator which creates the cooling effect and an expansion valve which decreases the pressure of the refrigerant fluid (water etc.) to the evaporator pressure and operates in vacuum. The adsorption cycle with adsorption is a closed cycle and has its unique evaporator and condenser. Adsorptive (water etc.) is circulated in the evaporator and condenser in vacuum. It is completely different from the vapor compression cycle. The adsorbent bed filled with adsorbent (silica gel, zeolite etc.) adsorbs the heat of the condenser and uses it in desorption. The cooling effect can be obtained in the evaporator of the adsorption cycle. By using this effect in the refrigerator, the cooling performance of the refrigerator can be improved (EP2775236A1, TR2013/02766).

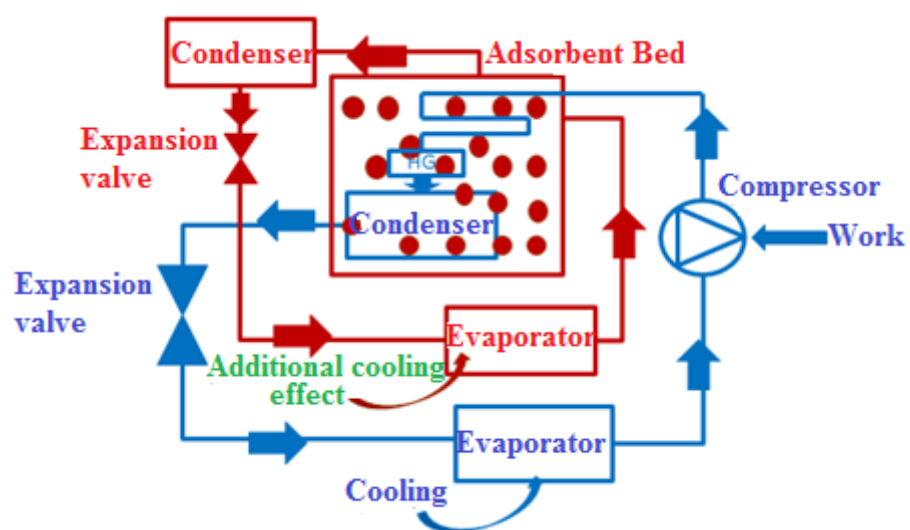


Figure 4.3. Proposed hybrid system (EP2775236A1, TR2013/02766).

4.3. Performance Calculations of the Proposed Hybrid Cooling System

The thermodynamic cycle of the refrigerator varies with time. The cooling load is not constant and it changes by time. The reason is that the refrigerator works and stops based on the required cooling capacity. For household domestic refrigerator, the compressor works for a period of 25 minutes in an hour which means an operation value between 44 to 46% of an hour. The COP value for vapor compression cycle can be calculated by using the correlations given below for a basic vapor compression cycle of the refrigerator:

$$COP_{vap} = \frac{Q_{evap}}{W_{in}} \quad (4.1)$$

where

$$W_{in,comp} = \dot{m}(h_{comp,out} - h_{comp,in}) \quad (4.2)$$

$$Q_{evap} = \dot{m}(h_{evap,out} - h_{evap,in}) \quad (4.3)$$

where \dot{m} represents the mass flow rate of the refrigerant in the cycle. Furthermore, the released heat from the hot gas and phase change can be calculated as:

$$Q_{hg} = \dot{m}C_p(T_{comp,out} - T_{vaporsat}) \quad (4.4)$$

$$Q_{phc} = \dot{m}(h_{vaporsat} - h_{cond,out}) \quad (4.5)$$

The total heat released from the vapor compression cycle can be calculated as:

$$Q_{cond} = Q_{hg} + Q_{phc} \quad (4.6)$$

As it was mentioned before, the main focus of this study is to improve the COP value of the household refrigerator cooling cycle. In order to achieve the aim of this study, the heat of the condenser used in the vapor compression cycle (Q_{cond}) is utilized in the desorption process of the adsorption cycle. The cooling effect generated by the

adsorption cycle is used for the refrigerator's cooling effect. The compressor works approximately 20 min. in an hour in a standard household refrigerator system. The desorption period can be considered as 15 min.

Then, the required mass of the silica gel for the adsorbent bed can be calculated from the following equation:

$$Q_{cond} t_{desorp} = m_s C_{p,s} (T_c - T_a) + m_s \Delta H_{desorp} (W_2 - W_1) \quad (4.7)$$

where the specific heat of the silica gel was taken as 0.921 kJ/kg K. ΔH_{desorp} is the heat of desorption. The adsorption/desorption period is considered to be taken an hour. $Q_{evap,ads}$ can be found from the following equation:

$$Q_{evap}^* = m_s \Delta H_{desorp} (W_2 - W_1) / 3600 \quad (4.8)$$

As a result, the COP value of the hybrid system can be calculated from the following equation:

$$COP_{hyb} = \frac{Q_{evap} + Q_{evap}^*}{W_{in}} \quad (4.9)$$

In the above equations, W represents adsorbate equilibrium concentration and it can be found from Eq. (4.2).

As a result of this study, for the low ambient temperatures up to 35°C, the suggested hybrid cycle can increase the COP value of the vapor compression refrigerator from 33 to 21%. However, further studies with different type of adsorbent–adsorbate pairs should be performed in order to investigate the improvement of COP by combination of vapor compression and adsorption heat pump cycle. The suggested hybrid cycle for domestic refrigerator is given Figure 4.3.

Table 4.1 represents the change of compressor and condenser outlet with ambient temperature for a real household refrigerator operating with R600a. The consumed work, cooling capacity, condenser capacity and COP are calculated by using equations for basic vapor compression cycle of the refrigerator and presented in Table 5.2. As expected by increase of ambient temperature, the consumed work increases while cooling capacity decreases. This causes a shape decrease of COP of vapor compression refrigerators with increase of ambient temperature.

Table 4.1. Operation temperatures of a vapor compression cycle of a domestic type refrigerator for different ambient temperatures.

Vapor Compression Cycle						
T_{amb} (°C)	20	25	30	35	40	45
$T_{comp,out}$ (°C)	105	112	120	127	134	141
$T_{sat,cond}$ (°C)	38	42	46.5	51	56	60

Table 4.2. Consumed work, cooling and heating capacities and COP values of the domestic type refrigerator for different ambient temperatures.

Vapor Compression Cycle						
T_{amb} (°C)	20	25	30	35	40	
$W_{in,comp}$ (W)	111.32	110.16	119.28	121.98	128.97	
Q_{evap} (W)	187.69	180.69	174.23	168.22	161.88	
Q_{cond} (W)	304.10	301.59	300.87	300.25	300.25	
$COP_{cooling}$	1.68	1.64	1.46	1.38	1.26	

In order to keep the cabinet of the refrigerator at 5°C, the adsorption cycle evaporator should be kept at a value lower than the cabinet temperature. The water is chosen as adsorbate for the adsorption cycle and the evaporator temperature is chosen 2°C. As it was mentioned before, the adsorbent is considered as silica gel RD. The condenser temperature is chosen 5°C higher than the ambient temperature. The temperature at the end of desorption period is chosen as the average of the condenser and the compressor outlet temperatures of the vapor compression cycle. According to the considered evaporator and condenser temperatures, the evaporator and the condenser pressures of the adsorption heat pump are calculated and the design values of the adsorption heat pump are illustrated in Table 4.3.

Table 4.3. Adsorption heat pump cycle design values.

AHP Cycle $T_{eva}^*=2^{\circ}\text{C}$						
T_{amb} ($^{\circ}\text{C}$)	20	25	30	35	40	45
T_a^* ($^{\circ}\text{C}$)	25	30	35	40	45	50
T_c^* ($^{\circ}\text{C}$)	71.5	77	83.5	89	95	100.5
T_{cond}^* ($^{\circ}\text{C}$)	25	30	35	40	45	50
P_{eva}^* (Pa)	775	775	775	775	775	775
P_{cond}^* (Pa)	3250	4310	5665	7380	9535	12220

According to the design temperatures and pressures presented in Table 4.3, the minimum and maximum water concentration and circulated water in the cycle are calculated and shown in Table 4.4. As seen from Table 4.4, the amount of water circulated in the cycle decreases by increase of ambient temperature. The hybrid cycle does not work when the ambient temperature is greater than 30°C .

Table 4.4. The minimum and maximum adsorbate concentrations, mass of silica gel and evaporator capacity for the designed adsorption heat pump.

AHP Cycle $T_{eva}^*=2^{\circ}\text{C}$						
T_{amb} ($^{\circ}\text{C}$)	20	25	30	35	40	45
W_2 (kg_v/kg_s)	0.128	0.096	0.073	-	-	-
W_1 (kg_v/kg_s)	0.0525	0.055	0.0555	-	-	-
ΔW (kg_v/kg_s)	0.0755	0.041	0.0175	-	-	-
m_s (kg)	1.2	1.9	3.1	-	-	-
Q_{evap}^* (W)	62.1	53.1	37.3	-	-	-

The COP of the hybrid system is calculated by using Eqn. 2.19. In the light of the given data and equations of the vapor compression cycle of a refrigerator the work done by the compressor, the heat extracted of the evaporator, the released heat from the condenser and the coefficient of the performance is calculated and presented in Table 4.5.

Table 4.5. The calculated data for a vapor compression heat pump cycle of a refrigerator for different ambient temperatures.

T_{amb} (°C)	20	25	30	35	40	45
$W_{in,comp}$ (W)	111.32	110.16	119.28	121.98	128.97	134.92
Q_{evap} (W)	187.69	180.69	174.23	168.22	161.88	155.83
Q_{cond} (W)	304.10	301.59	300.87	300.25	300.25	299.52
$COP_{cooling}$	1.68	1.64	1.46	1.38	1.26	1.16

The maximum and minimum concentration values, the mass of silica gel and the heat extracted from environment to the evaporator are calculated for different ambient temperature of an adsorption heat pump cycle. The results are presented in Table 4.6.

Table 4.6. The calculated data of an adsorption heat pump cycle.

T_{amb} (°C)	20	25	30	35	40	45
W_2 (kg _v /kg _s)	0.128	0.096	0.073	-	-	-
W_1 (kg _v /kg _s)	0.0525	0.055	0.0555	-	-	-
ΔW (kg _v /kg _s)	0.0755	0.041	0.0175	-	-	-
m_s (kg)	1.2	1.9	3.1	-	-	-
Q_{evap} (W)	62.1	53.1	37.3	-	-	-

The coefficient of the performance (COP) is calculated for the mechanical heat pump (MHP), adsorption heat pump (AHP) and for the suggested hybrid system. Table 4.7 is propounded the comparison of this results.

Table 4.7. The COP values of the MHP, AHP and the suggested hybrid system.

T_{amb} (°C)	20	25	30	35	40	45
COP of AHP	0.22	0.20	0.16	-	-	-
COP of AHP	0.22	0.20	0.16	-	-	-
COP of Proposed Hybrid System	2.24	2.12	1.77	-	-	-
% increase vs MHP	33%	29%	21%	-	-	-

The change of total COP with ambient temperature is presented in Figure 4.4. As it can be seen, the COP of hybrid refrigerator increases by decreasing of ambient temperature. For a vapor compression refrigerator operates at the ambient temperature of 20°C, the combination of adsorption and vapor compression systems can increase COP of the system by 33%.

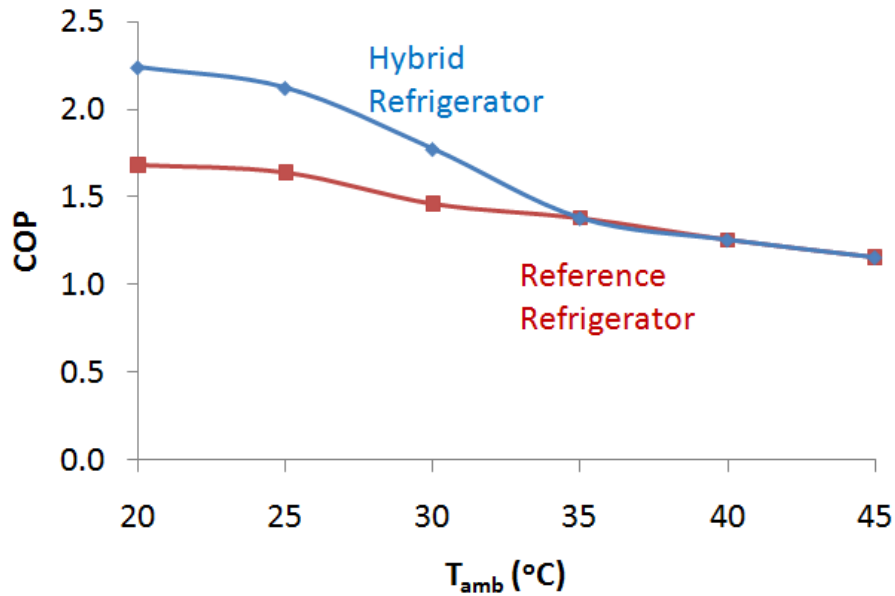


Figure 4.4. COP change of the vapor compression and hybrid refrigerator for different ambient temperatures.

In this chapter, a hybrid refrigeration system consists of vapor compression and adsorption heat pump cycles is designed and analyzed, theoretically. In this proposed hybrid system, the adsorption heat pump cycle is combined by vapor compression cycle to utilize the heat which is released by the condenser. Hence, the cooling effect and consequently the COP value of the vapor compression system are improved. The system

includes two separate refrigeration cycles. For the vapor compression system, the refrigerant is R600a and the silica gel-water pair is used for the adsorption heat pump cycle. For the low ambient temperatures up to 35°C, the suggested hybrid cycle can increase the COP value of the vapor compression refrigerator from 33 to 21%.

CHAPTER 5

EXPERIMENTAL SETUP AND PROCEDURE

As mentioned in Chapter 4, the aim of this thesis is to use the released heat from the pipe between the compressor and condenser outlets of a household refrigerator for the isosteric heating (a-b) and desorption (b-c) processes. For this purpose, an adsorption heat pump was designed and constructed.

In this chapter, the details of the experimental setup are explained. The setup was designed to investigate heat and mass transfer in an adsorbent bed of an adsorption heat pump. The silica gel RD/water pair was used. The adsorbent bed is a rectangular bed. The main objective of this setup is to find out temperature, concentration and pressure distributions in the bed of an adsorption heat pump for specified adsorption and desorption durations of a household refrigerator. In order to simulate the waste heat of the vapor compression refrigeration cycle, the water was used instead of refrigerant. The first setup was constructed as given in details below and many experiments were performed to simulate the adsorption heat pump cycle. This setup was revised in order to accelerate the mass transfer of the water vapor inside of the bed. Small arrangements were done on this first experimental setup to have enhancement of the adsorption heat pump performance. The adsorption experiments were performed on the revised experimental setup, again. The second setup was constructed by the help of the first setup experimental results. The second setup has better cycle period when compared with the first constructed setup.

5.1. Components of the Experimental Setup

The constructed adsorption heat pump setup is illustrated in Figure 5.1. The experimental set up involves four main components: Adsorbent bed, evaporator, condenser and the expansion valves. Two electrical fans were placed on the setup; one for the adsorbent bed and one for the condenser ventilation. Four thermocouples were placed on the setup in order to measure the temperature of each component. Three pressure gauges were placed to the adsorbent bed, the condenser and the evaporator. The details of the components are given in Figure 5.1 and the view of the experimental setup from the laboratory is represented as Figure 5.2.

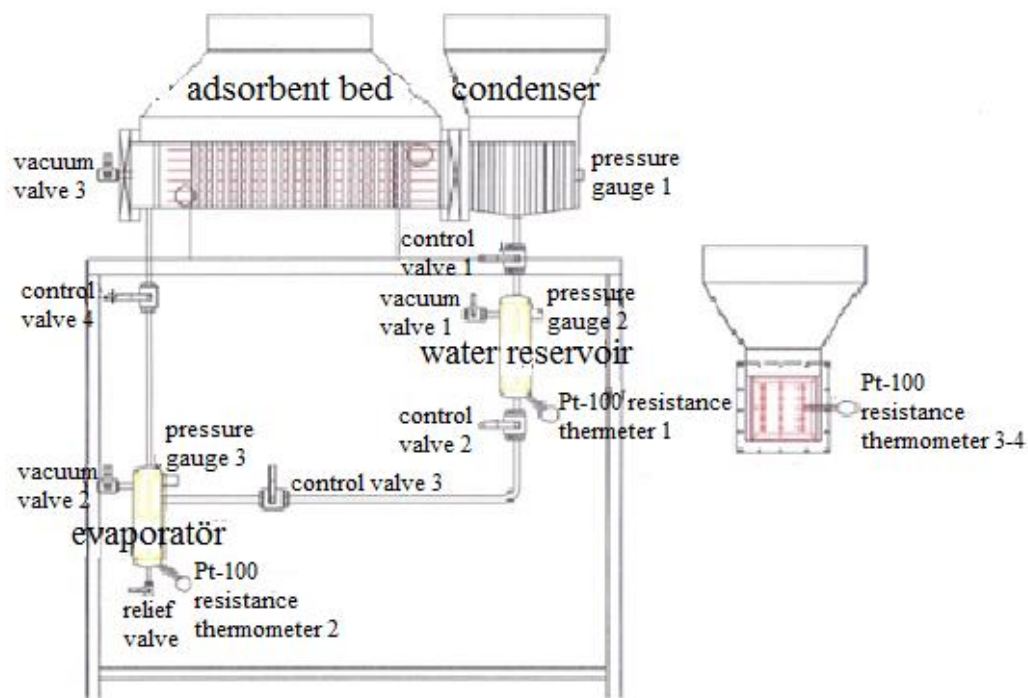


Figure 5.1. A schematic view of the first designed setup.

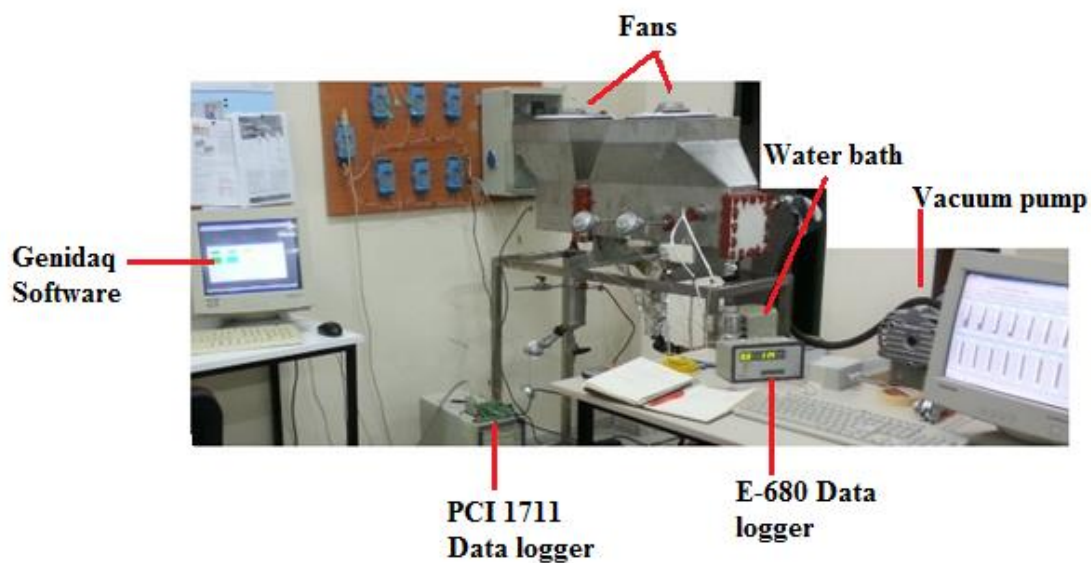


Figure 5.2. A view of the first experimental setup.

5.1.1. Adsorbent Bed

The adsorbent bed has a rectangular shape filled with the silica gel RD granules. The material of the casing is made from stainless steel. The length, width, and thickness of the bed are 60 x 12 x 12 cm, respectively. Inside the casing, 5 parallel plates assisted with pipe were located in order to circulate the refrigerant from the compressor outlet of the household refrigerator (Figure 5.3). And in Figure 5.4, the side view of the adsorbent bed is given with the details of fans that are located on the adsorbent bed and condenser. The cooling channels are represented in the top view of the adsorbent bed (Figure 5.5). Instead of using refrigerant, water was circulated from these aluminum pipes. The details of the serpentine are shown in Figure 5.6 (a). The serpentine has two inlets and outlets. The pipes were located on the aluminum plates as illustrated in Figure 5.6 (b). The distance between each plate is 20 mm and the silica gel granules were placed between these distances. Forty two pipes with 10 mm diameter were placed from the top to bottom surfaces of the adsorbent bed casing. These pipes were placed in order to cool the adsorbent bed with the fan placed on the bed for adsorption and cooling processes.

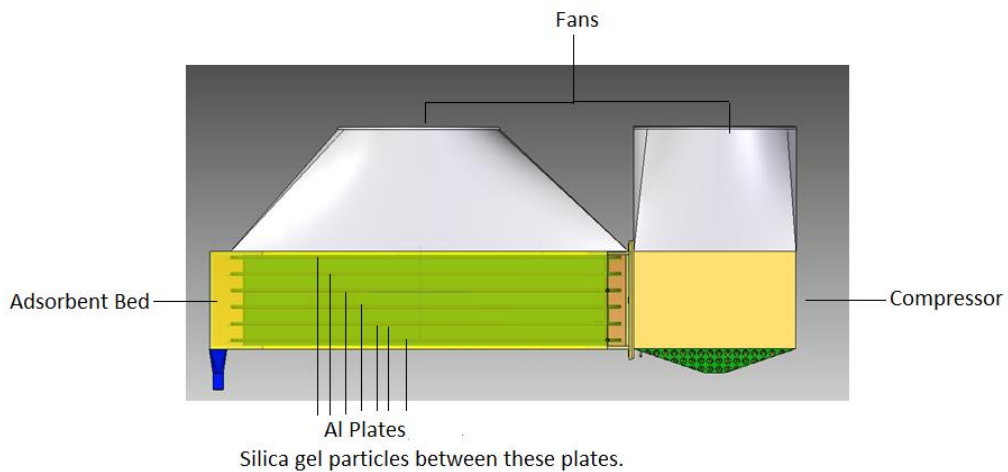


Figure 5.3. The technical drawing of the adsorbent bed design.

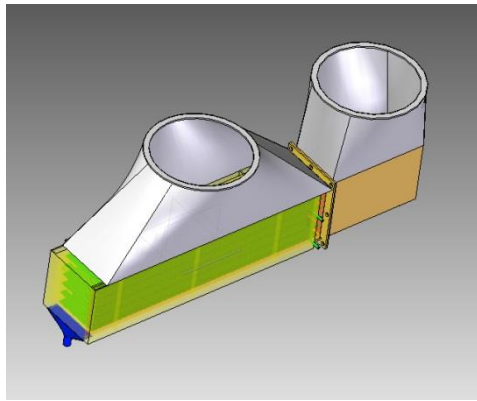


Figure 5.4. Side view of the adsorbent bed.

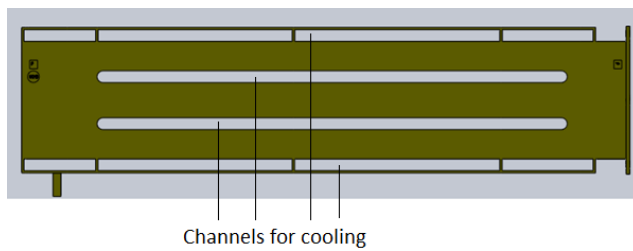


Figure 5.5. Top view of the adsorbent bed.

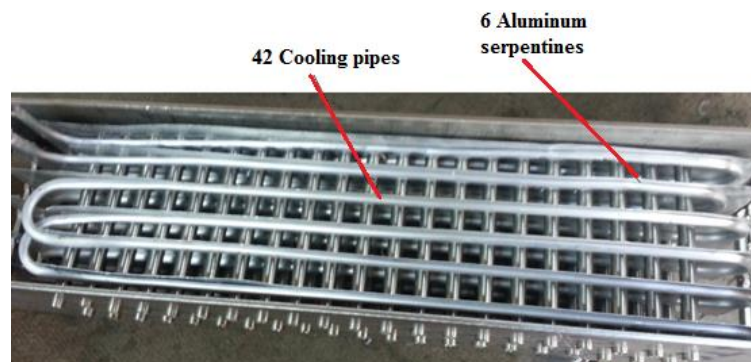


Figure 5.6 (a). The details of the serpentine for heating and the pipes for cooling.

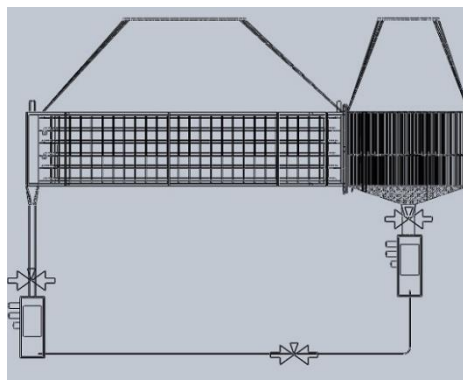


Figure 5.6 (b). The details of the serpentine for heating and the pipes for cooling.

The right and left side of the adsorbent bed closed with 325 mesh sieve to prevent pouring of the silica gel particles from the adsorbent bed. (Figure 5.7). The vapor comes from the evaporator passes inside of the adsorbent bed through the condenser for condensing. Eleven pipes were made as cylindrical shape from the 325 mesh sieve and places into the adsorbent bed for increasing the progress of the moving vapor through the condenser (Figure 5.7). The adsorbent bed was closed by a delrin sheet from one side to the other side where the condenser was placed.

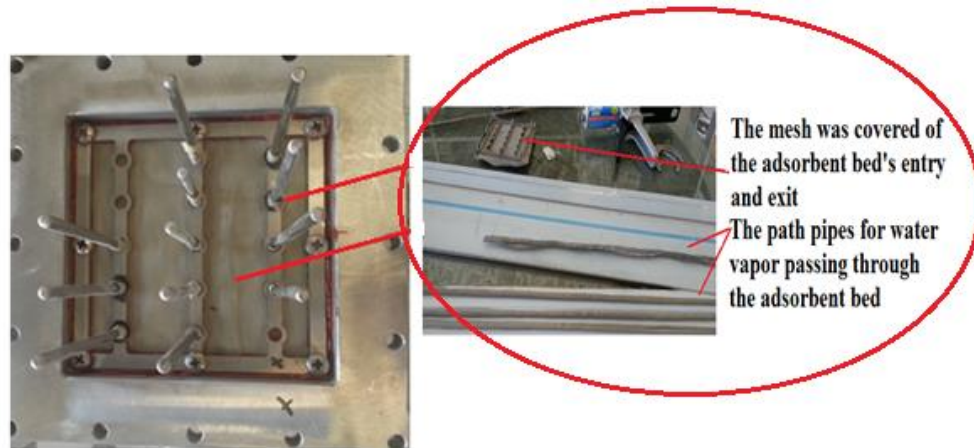


Figure 5.7. The construction phase of the pipes that made from the gauze with using special glue for enduring the high temperatures and the view of the cover that made from the gauze for adsorbent bed.

5.1.2. Condenser

The length, width, and thickness of the condenser tank are 12 x12 x 20 cm, respectively. An electric fan was located on the top side of the condenser to cool the condenser by air for the desorption process. Cooling pipes are constructed in the condenser which are 10 mm diameter, to condense vapor more efficiently (Figure 5.8). The condenser basically consists of a stainless steel container, a pressure transducer, a thermocouple, and a vacuum valves (a valve for water supply inlet, a valve for vacuum connector, a valve to drain water and a valve between the condenser and the evaporator, a valve between the condenser and the container) as shown in Figure 5.9. A container which is 0.4 lt. capacity is located below the condenser to save the water that is condensed from the vapor in the condenser (Figure 5.9). The water level in the container can be observed from the sight glass located in front of the condenser. The

length of the sight glass is 12 cm and the width is 1 cm. The amount of the desorbed water can be determined by measuring and scaling from this sight glass.

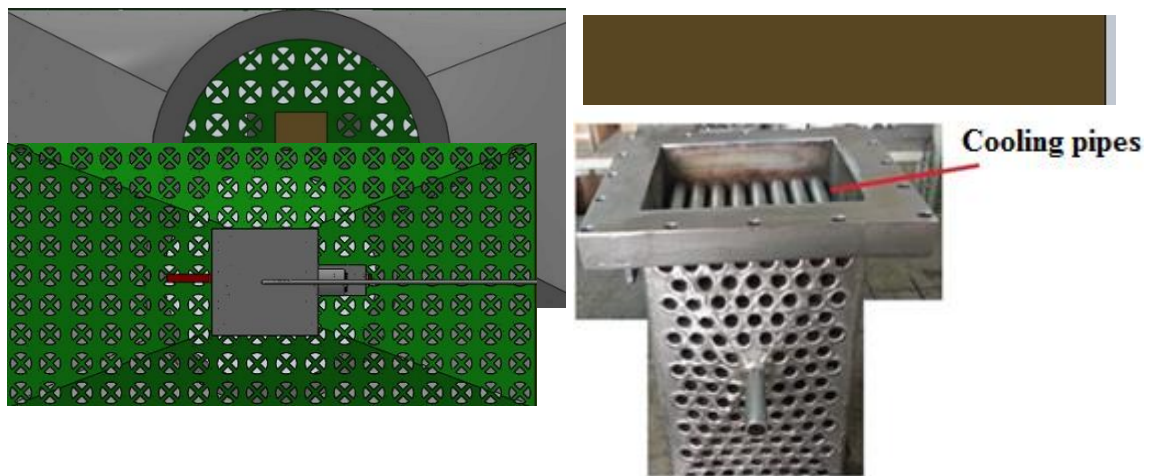


Figure 5.8. The details of the condenser.

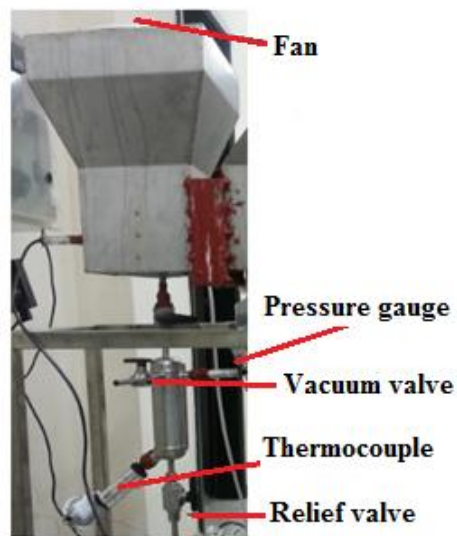


Figure 5.9. Condenser, reservoir, fan and measurement devices on the condenser.

5.1.3. Evaporator

The setup has one evaporator tank which has a volume of 0.4 L. made of stainless steel. The evaporator basically consists of a pressure transducer, a thermocouple, and a vacuum valves (a valve for water supply inlet, a valve for vacuum connector, a valve to drain water and a valve between the evaporator and the adsorbent

bed) as shown in Figure 5.10. The water level in the container can be observed from the sight glass located in front of the evaporator. The length and the width of the sight glass is 12 and 1 cm, respectively. The amount of the adsorbed water can be determined by measuring the water level inside of the evaporator from this sight glass.

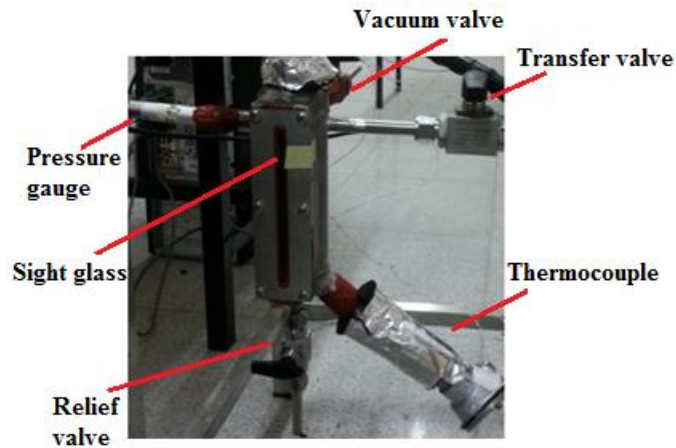


Figure 5.10. Evaporator.

5.1.4. Silica Gel

The silica gel used in the adsorbent bed was supplied from Fuji Silysia Chemical Ltd. The shape of silica gel is assumed spherical and the equivalent diameter of adsorbent granules is 2 mm. It has 25% water adsorption capacity by weight. BET (Braunauer Emmet and Teller - the physical adsorption of gas molecules on a solid surface) surface area and average pore diameter of silica gel were given as $626 \text{ m}^2\text{g}^{-1}$ and 2.0-2.5 nm respectively. The specific heat and the density of the silica gel were given as $0.921 \text{ kJ/kg}^\circ\text{C}$ and 700 kg/m^3 , respectively. The heat of adsorption per kg adsorbed water is taken as 2693kJ from the Ref (Demir et al. 2013-microwave). Random sized aluminum chips are used to enhance the heat transfer in the adsorbent bed for 4kg RD type silica gel. The aluminum piece were added to the silica gel according to the 22.5% of adsorbent bed's volume (Figure 5.11).

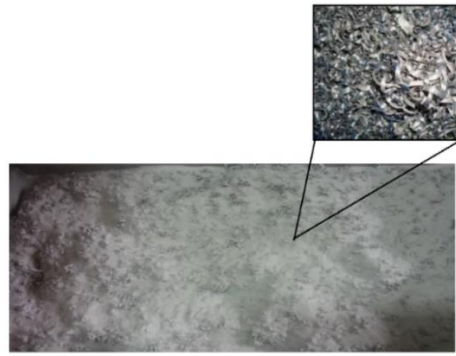


Figure 5.11. The mixture of aluminum and silica gel particles.

The silica gel diameter is important for the heat transfer. At the first step, the silica gel particles have 2 mm diameter. This situation can increase the adsorption time, considerably. So the silica gel particles diameter was reduced to 0.25 mm by using muller. The reduction of diameter of a silica gel procedure are summarized and illustrated in Figure 5.12.

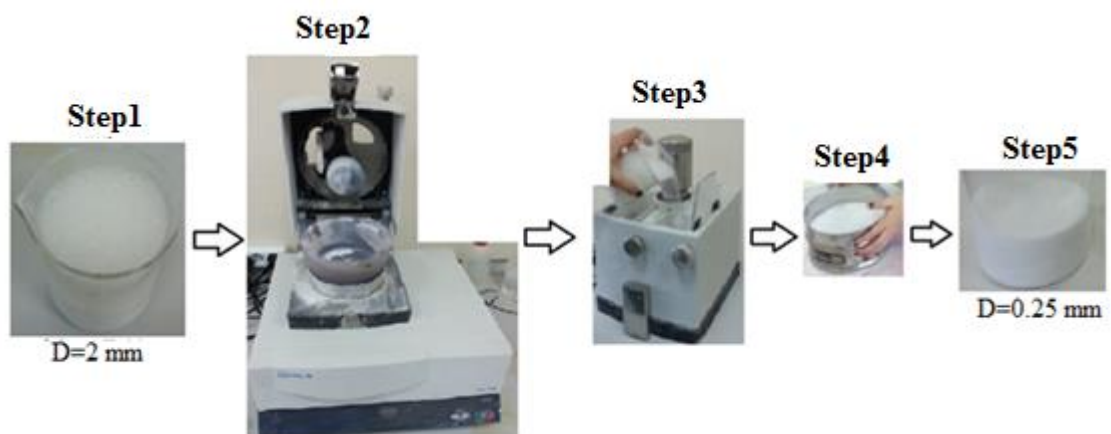


Figure 5.12. The process of to minimize the 2 mm diameter of the silica gel particles to 0.25 mm. 1. Step: The silica gel particles that have 2mm diameter. 2. Step: To prepare the special machine for this process. 3. Step: To minimize the silica gel particles with using this machine. 4. Step: To mesh the silica gel particles for having the ones have 0.25 mm, 5. Step: The silica gel particles that have 0.25 mm diameter.

5.1.5. The Water Bath

The temperature stability of the inlet water for the heat exchanger (serpentine) was maintained by a constant temperature water bath which has 7 lt water capacity and its operating temperature range changes from -40 to 200°C with $\pm 0.01^\circ\text{C}$ stability. The temperature setting is digital. The bath has been made out of stainless steel.

5.1.6. The Vacuum Pump

A small dry nXDS10i rotary vane vacuum pump from Edwards Co. was used for vacuuming. The vacuum pump is non-oiled type. At high vacuum mode, the ultimate min. pressure of the pump is 7×10^{-3} mbar. The motor powers at 50/60 Hz is 280 W.

5.1.7. The Pressure Gauge

Three identical pressure gauges were used on the setup to measure the pressures of the evaporator and the adsorbent bed. These pressure gauges have $\pm 0.4\%$ accuracy and have a range 1 to 5 V output. The stainless steel pressure gauges have a measurement range 101.6 kPa to 0 kPa. They can endure temperatures range -29 to 71°C. The pressure data measured by pressure gauges were obtained using Genidaq Software.

5.1.8. The Thermocouples in the Adsorbent Bed

Pt-100 are the resistance thermometers used for the experimental setup because of high susceptibility according to the thermocouples. The resistance thermometers were located inside of the adsorbent bed, evaporator and condenser which all of them are thermally insulated with a flexible wire. They measure the local temperature at certain positions. The response time of the K type thermocouples is 0.5 sec. Their operation temperature is from -200 to 850°C. Pt-100 has 100 ohm resistance value at 0°C. The temperature data measured with Pt-100 can be obtained using E-680 datalogger.

5.1.9. The Software

The software used for monitoring and data logging includes task, script, and display configuration is provided by the Advantech Co. named as Advantech Genidaq. The software provides an object based graphical interface that simplifies control and display setup. The software provides to configure the parameters and connect the toolbox. The data are saved automatically and can be transferred to Excel data file.

5.1.10. The Data Loggers

The resistance thermometers located in the adsorbent bed, in the evaporator, and in the condenser of the setup are Pt-100. E-680 datalogger is used to collect the data from the resistance thermometers (Figure 5.13 (a)). E-680 each have 16-bit 31-channel analog input module that provides programmable input ranges on all channels. The module sends the data to the host computer through a standard RS-485 interface. Their operation temperature is from -10 to 55°C. The datalogger have $\pm 0.5^\circ\text{C}$ % accuracy.

The another data logger is PCI 1711 card connected to the PCLD 8710 card which is used to collect the data from the pressure gauges. PCI 1711 card input provides from 4 ~ 20 mA to 1 ~ 5 VDC to convert sensor voltage or current into digital data. The data logger use a 16-bit microprocessor-controlled sigma-delta A/D converter to convert sensor voltage or current into digital data. The module sends the data to the host computer through a standard RS-485 interface. Genitaq Software is used to save and see the data measured (Figure 5.13 (b)).



a)

b)

Figure 5.13. a) Data logger E680 to measure temperature, b) PCLD 8710 datalogger to measure pressure.

5.2. The Revised Adsorption Heat Pump Setup

After performing experiments with this first experimental setup, sealing was provided and cooling effect was created. However, the cycle time was quite long as it seems. The long cycle time has been attributed to the following reasons:

- Water vapor does not move instantly across the whole bed. To go from one part to another takes time. This may be due to the narrow pipes made from mesh placed through in the bed.

- The tube is too long between the adsorbent bed and evaporator results pressure drop. A larger valve between adsorbent bed and evaporator with a shorter pipe should be used to prevent the pressure drop.

Therefore, the following revisions were planned.

- Expanding the diameter of the mesh pipes placed into the adsorbent bed to get up steam, the water vapor moves through to the adsorbent bed of will be more comfortable. Thus, water vapor can reach every point on the bed and in a shorter time. Expansion of ways reduces the amount of silica gel increase. But the duration of adsorption and desorption are decreased, also. As can be seen from Figure 5.14, the pipes are larger than the ones from the first experimental set up.

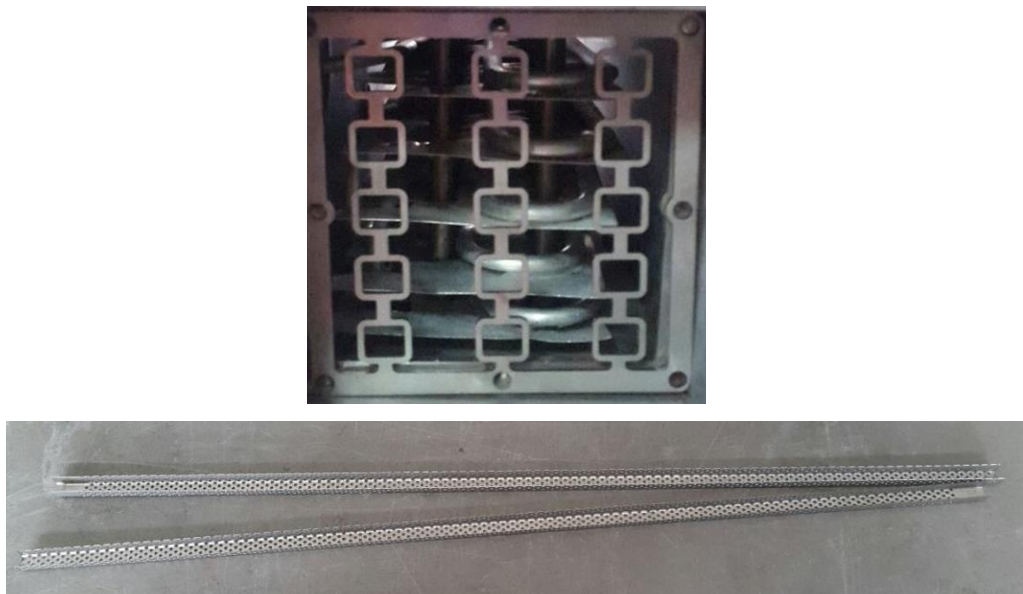


Figure 5.14. The view of the mesh pipes that are located inside of the adsorbent bed.

- Evaporator should be located near to the adsorbent bed in order to reduce the pressure drop between adsorbent bed and evaporator, as much as possible. To enlarge the diameter of the valve between the evaporator and the adsorbent bed, the steam from the evaporator should reach the adsorbent bed, easily. Figure 5.15 shows the 1 inch relief valve between the adsorbent bed and evaporator tank. In Figure 5.16, the evaporator were located closed to the adsorbent bed as much as possible.



Figure 5.15. The relief valve between the adsorbent bed and evaporator tank after the revision of experimental setup.



Figure 5.16. The view of the evaporator is located near the adsorbent bed after the revision of experimental setup.

As the conclusion of this revision, when the duration of adsorption/desorption is same, the amount of adsorbed water by the silica gel particles and desorbed vapor from the silica gel particles are increased. The details of the revision are given in the Chapter 9. As a result of these arrangements on the experimental setup, higher COP and SCP values are obtained. The experimental procedure is not changed after this revision which is same as first experimental setup.

5.3. The Experiment Procedure

- Four steps were followed to perform an experiment by the setup. These steps are given below:

- I.** Considering Figure 5.16, both valves between the evaporator-adsorbent bed and the condenser-adsorbent bed (V_1 and V_2) are closed at the beginning of adsorption process (point d). The adsorbent bed and evaporator are both at the evaporator pressure, P_{eva} . The concentration of adsorbate in the adsorbent bed is W_1 which is the minimum concentration value. By opening the valve V_1 between the evaporator and the adsorbent bed, the evaporator starts to get heat from the space needed to be cooled. The evaporated water in the evaporator is adsorbed by the silica gel in the adsorbent bed. The process continues until the concentration of adsorbate in adsorbent attains to W_2 level which is the maximum concentration value. At the isobaric adsorption process, the temperature of the adsorbent bed cooled from T_d to T_a .
- II.** After isobaric adsorption process, the valve V_1 is closed and then isosteric heating process is started (a-b). During this process, the adsorbent bed is heated by using the water bath. The temperature of the adsorbent bed rises from T_a to T_b while the adsorbate concentration in the bed remains constant at W_2 . The pressure of the adsorbent bed is increased from P_{eva} to P_{cond} during the isosteric heating process. During this process, the adsorbent bed is insulated to prevent the heat loss.
- III.** The next process is desorption process (b-c) which starts by opening the valve V_2 placed between the adsorbent bed and the condenser. During the desorption process, the temperature of adsorbent bed is increased from T_b to T_c while its pressure remains at P_{cond} . The desorbed vapor leaves the silica gel particles, and it is condensed in the condenser and, as a result, the water concentration falls from W_2 to W_1 . Finally, both valves V_1 and V_2 are closed and the adsorbent bed is cooled to reduce its pressure from P_{cond} to P_{eva} . During this process, which is known as isosteric cooling process, the temperature of adsorbent bed falls from T_c to T_d which is the initial condition before experiment. These experiments are done by using different timing for adsorption and desorption process to see the effect of the amount desorbed/adsorbed water during the processes.

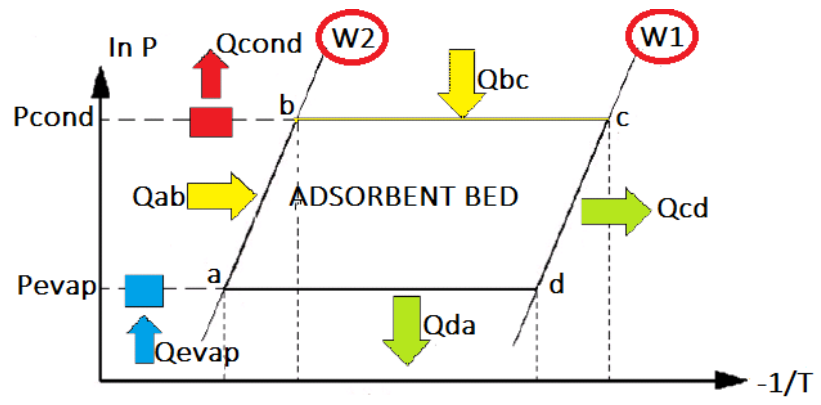


Figure 5.17. The Clapeyron Diagram of the adsorbent bed.

CHAPTER 6

GOVERNING EQUATIONS

The adsorption phenomenon including isotherms and meaning of the uniform/non-uniform pressure approaches are discussed in this chapter. This discussion also provides governing equations for the adsorption heat pump system suggested in the previous chapter. Equations are required to determine the adsorption rate in an adsorbent particle. For this reason, isotherm equations are introduced and the most suitable one for silica gel RD adsorbent was chosen. The heat and mass transfer equations of an adsorbent bed were written for two dimensional rectangular form based on non-uniform pressure approach. Detailed equations such as permeability, diffusivity, effective thermal capacitance and conductivity of the proposed adsorbent bed are given in this chapter.

6.1. Adsorption Phenomenon

The term sorption include both processes, while desorption is the reverse process of adsorption. Adsorption phenomenon occurs at the interface of two phases, a solid and a fluid. It is different from absorption, in which a fluid or gas diffuses into a solid to form a solution. Adsorbate, adsorptive and adsorbent are the concepts of the adsorption phenomenon. In an adsorption process, the fluid adsorbed (adsorbate; e.g. water) on the solid surface is referred to as adsorbent (e.g. silica gel), while the adsorbable substance which is in the gas phase is known as adsorptive (e.g. water vapor). Adsorptive tends to be diffused into the pores of the adsorbent as adsorbate according to the thermophysical properties of the adsorbent.

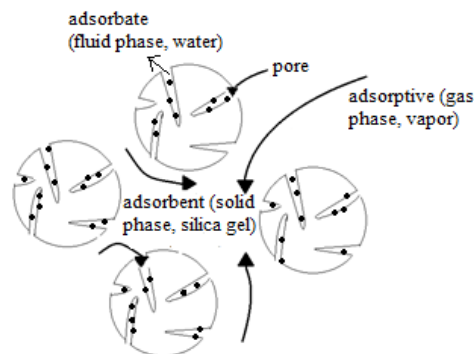


Figure 6.1. Illustration of adsorption phenomena.

The adsorption can be classified into as physical or chemical adsorption depending upon the forces existing between adsorbate molecules and adsorbent. If the force of attraction existing between adsorbate and adsorbent are Van der Waal's forces, the adsorption is called physical adsorption. In physical adsorption the force of attraction between the adsorbate and adsorbent are very weak. If the force of attraction existing between adsorbate and adsorbent are almost the same strength as chemical bonds, which is very strong, is called as the chemical adsorption.

6.1.1. Isotherms

Adsorption is usually described through isotherms connecting the amount of adsorbate in the adsorbent as a function of its pressure or concentration at constant temperature. Adsorption isotherm is the correlation between the amounts of adsorbate adsorbed in the adsorbent and the pressure of the adsorptive at constant temperature. In the literature, several models can be found for mathematically describing process of adsorption, namely Freundlich isotherm (Saha et al.2009, Liu and Leong et al.2006), Henry isotherm (Ng et al. 2001), Toth's isotherm (Terzyk et al. 2003), etc. The isotherm equations refer the adsorption behavior of the working pair. In order to understand the adsorption for the proposed working pair, isotherms should be investigated. For Fuji Type silica gel-RD, the experiments concluded that Toth's isotherm should be used to define the adsorption of this adsorbent with water vapor (Gundogan, 2014). In this section, the equations are compared with each other according to their adsorption behavior of isotherms as seen in Figure 6.2.

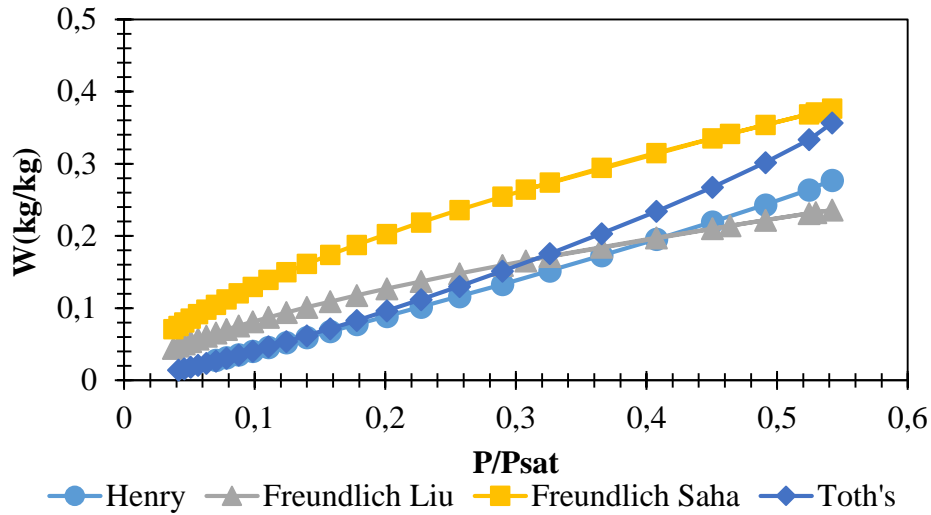


Figure 6.2. The adsorption behaviors of Freundlich, Henry, and Toth's isotherms.

6.1.1.1. Freundlich's Equation

Freundlich's equation is commonly used in adsorption heat pumps studies (Xia et al. 2008). There are different coefficients for Freundlich equation which are experimentally estimated in the literature. The relation is given in equation 6.1.

$$\bar{W}_{\infty} = k \left(\frac{P}{P_{sat}} \right)^{\frac{1}{n}} \quad (6.1)$$

W refers to the equilibrium adsorbed amount, p is the pressure and P_{sat} is the saturation pressure at a determined temperature in kPa. k and n are dimensionless equation constants which are 0.346 (Liu and Leong 2006) or 0.552 (Saha et al.2009) are used for k and 1.6 (Liu and Leong 2006, Saha et al.2009) for n constants.

6.1.1.2. Henry's Equation

Henry's equation is used to define the isotherm of silica gel-water pair, commonly. The equation can be given as:

$$\bar{W}_{\infty} = K_o \exp \left(\frac{\Delta H_{ads}}{RT} \right) P \quad (6.2)$$

where W refers the equilibrium adsorbed amount, P is the pressure in Pa and T is the temperature in K; R is gas constant in kJ/kgK; ΔH_{ads} is isosteric heat of adsorption in kJ/kg; K_0 is a constant in Pa⁻¹. K_0 and ΔH are dimensionless equation constants which are 2510 and 5.5×10^{-12} (Ng et al.2001).

6.1.1.3. Toth's Equation

Toth's equation is derived from Henry's equation which is related with the isosteric heat of adsorption of the pair. It is used to define the isotherm of silica gel-water pair. The equation is given below:

$$\bar{W}_\infty = \frac{K_0 \exp[\Delta H_{ads}/(RT)]P}{\left\{ \left[1 + K_0/q_m \exp[\Delta H_{ads}/(RT)]P \right]^t \right\}^{1/t}} \quad (6.3)$$

where W refers the equilibrium adsorbed amount, P is the pressure in Pa and T is the temperature in K; R is gas constant in kJ/kgK; ΔH_{ads} is isosteric heat of adsorption in kJ/kg; q_m denotes the monolayer coverage (kg_v/kg_s); K_0 is a constant in Pa⁻¹. q_m , K_0 and t are dimensionless equation constants and 0.45, 7.3×10^{-10} and 12, respectively (Chua et al. 2002).

6.2. Uniform and Non-Uniform Pressure Approach

Two main approaches are used to analyze heat and mass transfer in an adsorbent bed. These are uniform and non-uniform pressure approaches related to the named of the mass transfer in a closed type adsorbent bed. Two types of mass transfer occur in a closed type granular adsorbent bed as mass transfer within the adsorbent particle (intraparticle mass transfer) and mass transfer in the voids between adsorbent particles (interparticle mass transfer). The intraparticle mass transfer is formed generally by diffusion mode of transport in the adsorbent particle. As a consequence, LDF model is used to determine the gradient of adsorbate concentration in the adsorbent particle. The interparticle mass transfer mostly occurs due to the pressure difference (i.e., adsorptive

concentration) of adsorptive in the adsorbent bed. The intraparticle mass transfer is generally formed due to mass diffusion in the particle. The reason of the interparticle mass transfer is the change of adsorptive concentration in the adsorbent bed.

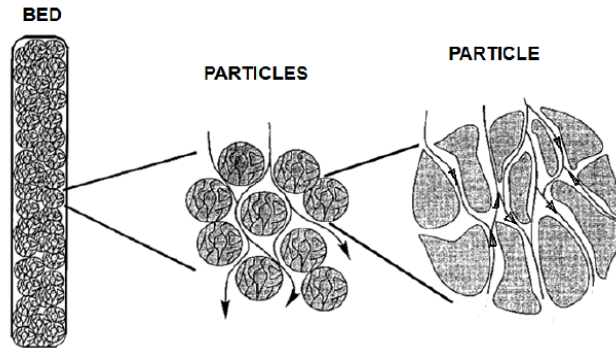


Figure 6.3. Schematic representation of inter-particle and intra-particle flow
(Source: Ilis 2012)

6.2.1. Uniform Pressure Approach

The interparticle mass transfer resistance may be assumed as negligible where the adsorptive pressure in the entire adsorbent bed is uniform. The temperature gradient and intraparticle mass transfer resistance are two parameters that influence adsorbate concentration change inside the bed. The temperature in the bed changes both in time and space. A heat transfer equation without convective term is solved to determine local temperature throughout the adsorption process (Figure 6.4). The governing equations that use for the uniform approach are given below.

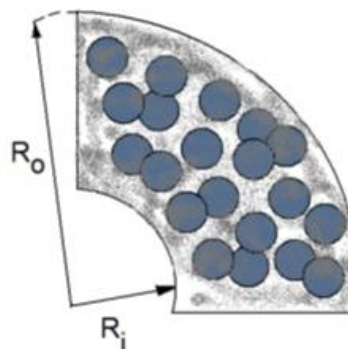


Figure 6.4. A section of adsorbent bed for uniform pressure approach
(Source: Ilis 2012)

Since the pressure inside of the bed is uniform, there is no need to write a mass transfer equation for water vapor flow through the bed.

The heat transfer equation for the adsorbent bed, water vapor and adsorbed water can be written as:

$$\left(\rho C_p \right)_{eff} \frac{\partial T}{\partial t} = \lambda_{eff} \frac{1}{R} \frac{\partial}{\partial R} \left(R \frac{\partial T}{\partial R} \right) + (1 - \phi) \rho_s \Delta H_{ads} \frac{\partial \bar{W}}{\partial t} \quad (6.4)$$

However, an equation is required for determination of adsorption rate in the adsorbent particle. Three different models can be written as;

a) The instantaneous equilibrium model:
$$\frac{\partial \bar{W}}{\partial t} = \frac{\partial \bar{W}_\infty}{\partial t} \quad (6.5)$$

b) The solid diffusion model:
$$\frac{\partial W}{\partial t} = \frac{1}{r^2} \frac{\partial}{\partial r} \left(r^2 D_{eff} \frac{\partial W}{\partial t} \right) \quad (6.6)$$

c) LDF model:
$$\frac{\partial \bar{W}}{\partial t} = \frac{15 D_{eff}}{r_p^2} (\bar{W}_\infty - \bar{W}) \text{ where } D_{eff} = D_o e^{-E/RT} \quad (6.7)$$

6.2.2. Non-Uniform Pressure Approach

The interparticle mass transfer resistance is taken into account and the space gradient of adsorptive pressure is determined in this approach (Figure 6.5). The space gradient of adsorptive pressure have to be determined. The convective transport term appears in the heat transfer equation. Two simultaneous additional equations (i.e. continuity and Darcy equations) should be solved to obtain the adsorptive concentration profile and adsorptive velocity in the bed. The non-uniform pressure approaches (Marletta et al., 2002, Demir et al., 2009, Restruccia et al, 2002, Maggio et al., 2009, Li Yong and Sumathy, 2004, Saha et al., 2009, Ilis et al., 2011, Bird et al., 2002, Karger and Ruthven, 1992) were preferred by many researchers in order to simulate heat and mass transfer in an adsorbent bed. Radial adsorbent bed was considered in the most of the studies except the study of Sun et al. (1995) in which a rectangular bed was

analyzed. Most of the researchers performed one dimensional study, and the changes of temperature and adsorbate concentration with time were obtained only in radial direction. The two dimensional studies were performed by Saha et al. (2009), Ben Amar et al. (Ben Amar et al., 1996), Marletta et al. (2002), Maggio et al. (2009), and Ilis et al. (2011). In addition, the comparison of uniform and non-uniform pressure approaches was performed by Ilis et al. (2013a), based on this study used the governing equations arranged according to the non-uniform approach, which is sensible for small size adsorbent bed particle. Consequently, the governing equations studied in this thesis are listed in the next section.

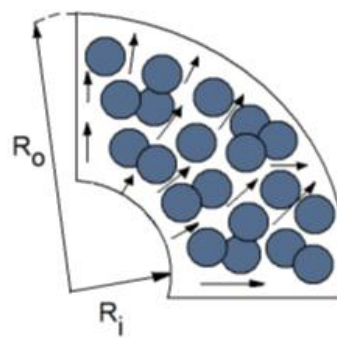


Figure 6.5. A section of adsorbent bed for non-uniform pressure approach.

6.3. The Governing Equations

In this part, the adsorbent bed is assumed in rectangular shape filled with the adsorbent particles. The adsorptive from evaporator and condenser during adsorption and desorption process can easily flow in the bed. The thermal resistance of the metal casing is neglected. The silica gel RD-water pair is chosen. The mechanisms of heat and mass transfer in a granular adsorbent bed are coupled and complicated; hence some assumptions have to be made to pose the governing equations.

The assumptions are; 1) the adsorbent bed consists of uniform size spherical adsorbent particles, 2) the particles arrangement is assumed cubical and thus the bed porosity is constant, 3) the adsorptive and adsorbent particle are in thermal equilibrium, 4) the thermal resistance within the adsorbent particle is neglected, 5) thermal properties of the adsorbent, adsorptive and adsorbate are constant, 6) wall thermal resistance between the bed surface and particle is not considered, 7) the heat of adsorption is assumed constant.

Figure 6.6 shows whole the cycle on Clapeyron diagram. The adsorption process is started when the adsorbate concentration in the adsorbent bed is W_d and bed temperature is at T_d . Desorption process is started when the adsorbate concentration is attained to W_2 while the bed temperature is increased to T_b . Desorption process finishes when the bed temperature reaches to T_c .

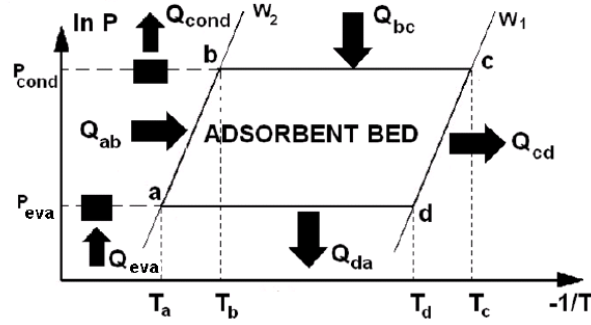


Figure 6.6. A schematic view of the adsorption-desorption process on Clapeyron Diagram.

The governing equations for the heat and mass transfer in the adsorbent bed are separately presented in this section. The derivation of the equations are also given in Appendix B.

The continuity equation based on conservation of mass for water vapor flow through the adsorbent bed can be written as:

$$(\varphi - 1)\rho_s \frac{\partial \bar{W}}{\partial t} = \frac{\partial}{\partial x}(\rho_v V_x) + \frac{\partial}{\partial y}(\rho_v V_y) + \varphi \frac{\partial \rho_v}{\partial t} \quad (6.8)$$

The heat transfer equation for the adsorbent bed, water vapor and adsorbed water can be written as:

$$(1 - \varphi)\rho_s \Delta H_{ads} \frac{\partial \bar{W}}{\partial t} + \frac{\partial}{\partial x}(\lambda_{eff} \frac{\partial T}{\partial x}) + \frac{\partial}{\partial y}(\lambda_{eff} \frac{\partial T}{\partial y}) = \frac{\partial}{\partial x}(\rho_v C_{v,x} V_x T) + \frac{\partial}{\partial y}(\rho_v C_{v,y} V_y T) + (\rho C_p)_{eff} \frac{\partial T}{\partial t} \quad (6.9)$$

where $(\rho C_p)_{eff}$ and λ_{eff} are the effective thermal capacitance and conductivity of the adsorbent bed and can be calculated by using the following relations:

$$(\rho C_p)_{eff} = (1-\phi) \left\{ (\rho C_p)_s + \rho_s C_{p_l} \bar{W} \right\} + \phi (\rho C_p)_v \quad (6.10)$$

$$\lambda_{eff} = (1-\phi)\lambda_s + \phi\lambda_v \quad (6.11)$$

Linear Drive Force (LDF) model is used to determine the change of mean adsorbate concentration in the adsorbent particle with time;

$$\frac{\partial \bar{W}}{\partial t} = \frac{15D_{eff}}{r_p^2} (\bar{W}_\infty - \bar{W}) \quad (6.12)$$

where D_{eff} and r_p represent effective diffusivity and radius of the adsorbent particle.

D_{eff} can be found from Arrhenius equation (Ben Amar et al., 1996):

$$D_{eff} = D_o e^{-E/RT} \quad (6.13)$$

where D_o is the reference diffusivity and E is the diffusion activation energy. In order to solve mass transfer equation for the particle (Eq. (5)), a relation for equilibrium state (i.e. \bar{W}_∞) must be known.

The following isotherm equation can be used to determine adsorbate equilibrium concentration in the silica gel particle for a given pressure and temperature (Chua et al., 2002):

$$\bar{W}_\infty = \frac{K_o \exp\left(\frac{\Delta H}{RT}\right) P}{\left\{ 1 + \left[\frac{K_o}{W_m} \exp\left(\frac{\Delta H}{RT}\right) P \right]^b \right\}^{1/b}} \quad (6.14)$$

where K_o , b and W_m are the constants for the specific adsorbent-adsorbate pair. The values of K_o , b and W_m are 7.3×10^{-10} , 12, and 0.45, respectively. The symbol P represents water vapor pressure at the considered temperature.

In Eqs. (6.8) and (6.9), V_x and V_y are facial water vapor velocities and can be calculated by Darcy law. Darcy's law is a simple proportional relationship among the fluid flow rate through a porous medium, the fluid viscosity and the pressure drop for a given distance.

For the present problem, it can be written as:

$$v_x = \frac{K_{app}}{\mu} \left(-\frac{\partial P}{\partial x}\right) \quad v_y = \frac{K_{app}}{\mu} \left(-\frac{\partial P}{\partial y}\right) \quad (6.15)$$

where K_{app} and μ are apparent permeability of the silica gel bed and the water vapor viscosity. The ideal gas relation is used to calculate the pressure change of the water vapor in the silica gel bed.

The apparent permeability of the silica gel bed, K_{app} can be calculated by the following relation (Leong and Liu, 2004):

$$K_{app} = K_{inh} + \frac{\phi\mu}{\tau P} D_{bed} \quad (6.16)$$

where K_{inh} is the inherent permeability and D_{bed} is the mass diffusivity of the bed. The inherent permeability can be obtained by using Blake–Kozeny relation which is valid for void fractions less than $\phi=0.5$ (Bird and Steward, 2002):

$$K_{inh} = \frac{r^2 \phi^3}{37.5(1-\phi)^2} \quad (6.17)$$

The water vapor can also be diffused in the voids between silica gel particles. Two diffusion mechanisms which are Knudsen and molecular diffusions should be taken into account. As known, when the collisions between a molecule and the pore walls occur more frequently than collisions between diffusing molecules, the diffusion is called as Knudsen diffusion, and it can be calculated from the following equation:

$$D_k = 97r_{pore}\sqrt{T/M} \quad (6.18)$$

When the pore diameter is larger than the average distance between molecular collisions and the collisions between diffusing molecules occur more frequently than collisions between molecules and the pores wall, the diffusion mechanism is called as molecular diffusion. The molecular diffusivity can be obtained from Eq. (6.19).

$$D_m = 0.02628 \frac{\sqrt{T^3/M}}{P\sigma^2\Omega} \quad (6.19)$$

The effect of overall diffusion in the voids between the particles in the adsorbent bed can be obtained by considering both effects of Knudsen and molecular diffusion (Karger and Ruthven, 1992):

$$\frac{1}{D_{bed}} = \frac{1}{D_m} + \frac{1}{D_k} \quad (6.20)$$

6.4. The Governing Equations with Metal Additives

In this section, the governing equations are given if metal is added to the adsorbent bed between the silica gel particles. The continuity equation based on conservation of mass for water vapor flow through the adsorbent bed can be written as:

$$(\varphi - 1)(1 - \beta)\rho_s \frac{\partial \bar{W}}{\partial t} = \frac{\partial}{\partial x}(\rho_v V_x) + \frac{\partial}{\partial y}(\rho_v V_y) + \varphi \frac{\partial \rho_v}{\partial t} \quad (6.21)$$

where φ is the porosity and β is the volume fraction of the metal additives.

The heat transfer equation for the adsorbent bed, water vapor and adsorbed water can be written as:

$$(1 - \varphi)(1 - \beta)\rho_s \Delta H_{ads} \frac{\partial \bar{W}}{\partial t} + \frac{\partial}{\partial x}(\lambda_{eff} \frac{\partial T}{\partial x}) + \frac{\partial}{\partial y}(\lambda_{eff} \frac{\partial T}{\partial y}) = \frac{\partial}{\partial x}(\rho_v C_v V_x T) + \frac{\partial}{\partial y}(\rho_v C_v V_y T) + (\rho C_p)_{eff} \frac{\partial T}{\partial t} \quad (6.22)$$

where $(\rho C_p)_{eff}$ is the effective thermal capacitance can be calculated by using the following relation:

$$(\rho C_p)_{eff} = (1-\phi) \left\{ \beta(\rho C_p)_{add} + (1-\beta)(\rho C_p)_s \right\} \quad (6.23)$$

ρ_{add} is the density and $C_{p,add}$ is the thermal capacitance of the additive which is aluminum, ρ_s is the density and C_p is the thermal capacitance of the silica gel.

The λ_{eff} is the effective thermal conductivity of the adsorbent bed which can be calculated from Maxwell's model (Maxwell, 1873):

$$\frac{\lambda_{eff}}{\lambda_s} = \frac{\frac{\lambda_{add}}{\lambda_s} + 2 - 2\beta(1 - \frac{\lambda_{add}}{\lambda_s})}{\frac{\lambda_{add}}{\lambda_s} + 2 + \beta(1 - \frac{\lambda_{add}}{\lambda_s})} \quad (6.24)$$

where λ_{add} is the thermal conductivity of the additive which is aluminum and λ_s is the thermal conductivity of adsorbent which is the silica gel in this study.

The LDF model, permeability, diffusivity and Darcy law equations are the same from Eq. (6.10) to Eq. (6.20) for metal additive cases.

CHAPTER 7

NUMERICAL SOLUTION METHODOLOGIES

In this chapter, the brief description on numerical solution methodologies of this thesis is given. The considered problem is explained in Chapter 5 and the governing equations of this problem is given in Chapter 4, extendedly. The Comsol Software is used to analyze heat and mass transfer of the suggested adsorption heat pump. The details of the solution method is given with a brief information about the Comsol Software. To ensure the validation of the Comsol Software, our CFD software is used to solve the adsorption cycle that has same operation conditions for a simple geometry. The results of the Comsol Software and our CFD Programme are compared with each other to validate the achieved results of Comsol. The comparison of numerical results for the adsorbent bed are plotted and given in this Chapter.

7.1. The Solution Method with Comsol Software

Finite difference method is used to solve the governing equations for uniform and non-uniform approaches. The model geometry is meshed by using extremely fine mesh. Solver parameter has a relative tolerance of 0.01 and an absolute tolerance 0.001 enabling high accuracy and convergence. The conservation of mass and energy equations, Linear Drive Force (LDF) model and Darcy Law equations are solved to find temperature, water concentration, water vapor velocity, and pressure in the adsorbent bed for entire cycle. The ideal gas equation is used to relate the water vapor pressure with its density and temperature. The governing equations are solved for the rectangular bed shape by using Comsol Software. The local temperature, concentration, and pressure distributions are calculated in the bed for four processes of the cycle. The mean values of local temperature, concentration, and pressure of the adsorbent bed are found and the mean values of those parameters are plotted against the time. Furthermore, the adsorption heat pump cycle is shown on Clapeyron diagram by using the mean values of temperature and concentration. The Coefficient of Performance (COP) and Specific Cooling Power (SCP) of the considered adsorption refrigeration system are found. The coupled heat and mass transfer models make an analytical solution impossible because of their complicacy and nonlinearity. Numerical methods include the finite difference

method, the finite volume method and the finite element method. Finite difference methods are generally used for solving this set of equations due to its simplicity and ease of varying initial and boundary conditions. In this study, coupled heat and mass transfer model is used to investigate both heat and mass transfer inside the bed. In this model, temperature distributions for the HTF, the adsorbent bed, and variations of pressure, amount adsorbed, equilibrium adsorption capacity and mass transfer coefficient in the adsorbent bed are investigated for isobaric adsorption, isosteric heating, isobaric desorption, isosteric cooling processes. Solutions are presented by domain distributions that show the results in multi-colored 2D domain besides of the graphs for the gradient of the properties. Before presenting the results, a detailed information about Comsol Multiphysics is given in this chapter.

The results are given for the comparison of uniform and non-uniform pressure approximation. As mentioned before, the results are obtained for silica gel-water pair. The adsorption process is started at 353 K and ended 303 K. For the uniform pressure approach, the water vapor pressure is assumed uniform as 775 Pa in the entire bed during the adsorption process. For the non-uniform approach, the water vapor pressure inside the adsorbent bed is not uniform and it varies. However, the water vapor pressure at the entrance of the bed is at 775 Pa. Figure (7.2) and (7.3) shows the obtained numerical results of both uniform and non-uniform pressure approaches for an adsorbent bed with length of 15 mm and height of 10 mm for the silica gel particle radius of 1 mm. Figure (7.2) and (7.3) represents the change in average water concentration, pressure and temperature by time for uniform and non- uniform pressure approaches. The average bed temperature decreases while the average of water concentration increases with time. The changes T and W versus time for both approaches are very close to each other.

The first result is for the adsorbent particle radius of 0.01 mm so the solution is considering uniform pressure approximation. The adsorbent bed temperature decreases over time and consequently the adsorbate concentration in the adsorbent particle increases due to the adsorbate vapor entering to the bed from the left and right sides. According to these results, the Non-Uniform Pressure Approach Approximation gives more accurate results. The heat and mass transfer equations to find temperature, concentration and pressure distributions by using uniform and non-uniform pressure approaches for a two-dimensional rectangular adsorbent bed are given in Chapter 5. In

consequence of solving this governing equations to determine the size of the adsorbent bed and silica gel, the results are obtained as listed below.

7.2. Introduction of COMSOL Multiphysics Software

Computer simulation has become an essential part of science and engineering. COMSOL is a Multiphysics modeling tool that solves various coupled physical problems based on Finite Element Analysis (FEM) and all kinds of engineering problems based on partial differential equations (PDEs). COMSOL provides a user-friendly interface for mesh generation, equations configuration, and results visualization. COMSOL Multiphysics (known as FEMLAB before 2005) is a commercial finite element software package designed to address a wide range of physical phenomena [1]. It is for solving systems of time-dependent or stationary second order partial differential equations in one, two, and three dimensions.

Comsol Multiphysics solves is an all-in-one geometry creator and mesher, solver and postprocessor. Comsol Multiphysics is much simpler to use than traditional finite element method software packages. Comsol Multiphysics enables to perform stationary and time-dependent analysis. Comsol Multiphysics can be used in many application areas, from chemical reactions to fluid dynamics and from heat transfer o porous media flow since it can solve a system of PDEs [147]. Comsol Multiphysics automatically meshes geometry when the geometry is completed and various parameters defined. In the solution stage, Comsol Multiphysics uses suitable solvers for stationary, eigenvalue, and time-dependent problems. A sample Comsol model report created by the program is given in Appendix D.

7.3. Validation of Comsol Results

The governing equations should be solved to simulate heat and mass transfer in the adsorbent bed as given in the Figure 7.1. The height and length of the adsorbent bed is 15 mm and 10 mm. The porosity value was 0.45 (Collins 1961, Heinemann 2005). The density and the specific heat of the silica gel were taken from the silica gel product manual as 700 kg/m³ and 1 kJ/kg°C, respectively. The heat of adsorption for the silica gel-water pair was taken as 2693 kJ/kg (Appendix A). The effective thermal conductivity was 0.198 W/mK (Appendix A).

The radius of the silica gel particles is 0.5 mm. The evaporator pressure is 775 Pa and the condenser pressure is 3250 Pa. The properties are used as given in Appendix A.

The adsorption cycle conditions are given in the Figure 7.1 on the Clapeyron Diagram.

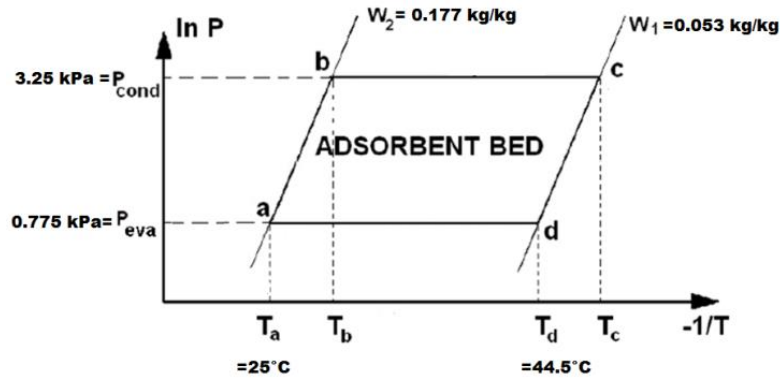


Figure 7.1. The operation conditions of the adsorption cycle on the Clapeyron Diagram.

The adsorption problem is solved by using our own CFD program coded in FORTRAN language and Comsol Software. The obtained numerical results are compared to validate the results for the Comsol Software. The comparison of the results are given from Figure (7.2) to (7.4). In the Fig. 7.2 is given the variation of the temperature with the time at the end of adsorption process. As can be seen there is a neglected differences between the results are taken from our CFD solver and Comsol. The reason of the small difference is the difference in mesh types. The change of pressure and concentration in the adsorbent bed with the time is given in the Figure (7.3) and (7.4).

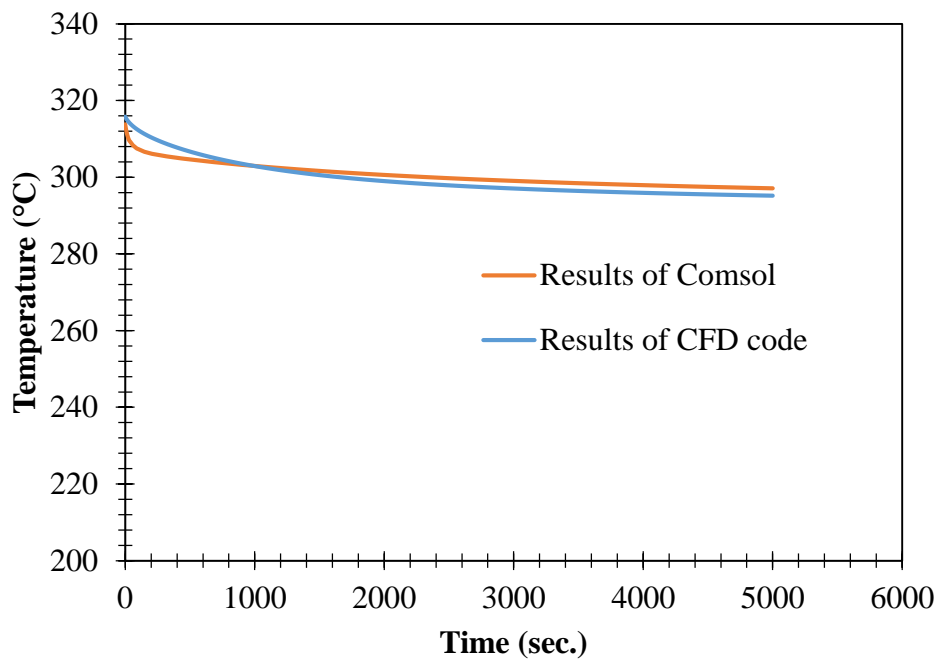


Figure 7.2. The comparison of the results belong to the variation of temperature in the bed.

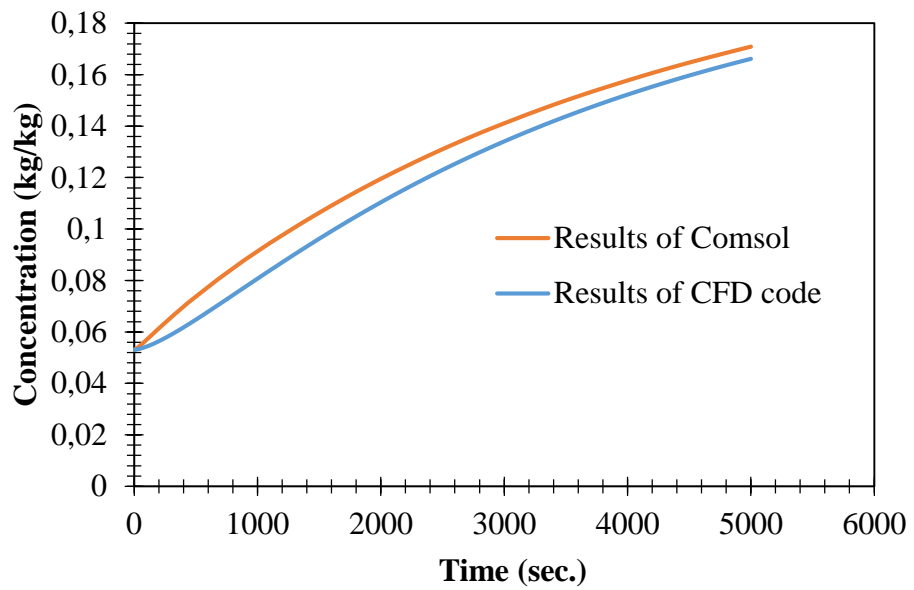


Figure 7.3. The comparison of the change of adsorptive pressure in the bed obtained from the Comsol and our CFD code.

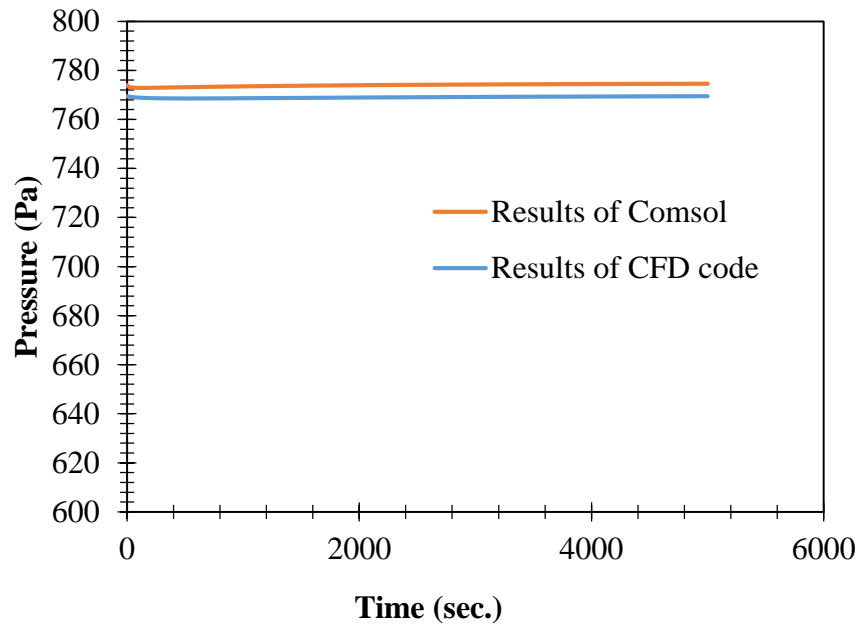


Figure 7.4. The comparison of the water concentration in the bed obtained from the Comsol and our CFD code.

7.4. The Comparison between Uniform and Non-Uniform Pressure Approaches

Heat and mass transfer equations are solved for a two dimensional rectangular adsorbent bed filled with silica gel particles (bed length and thickness of 80 and 20 mm, Figure 7.5) with using uniform and non-uniform pressure approaches under specified temperature and pressure conditions in the adsorption process. Initial temperature and pressure values are given as 317K and 775 Pa besides of surface temperature values is taken 298 K as ambient temperature.

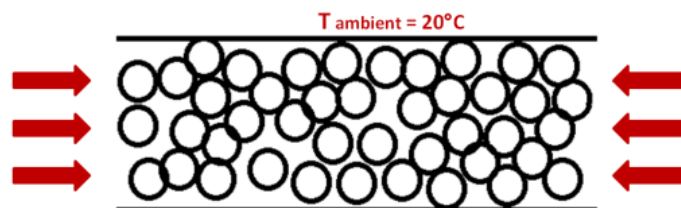
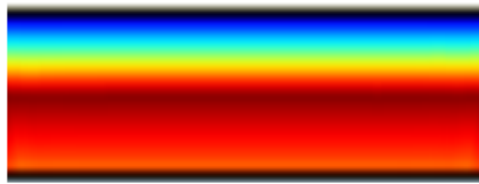
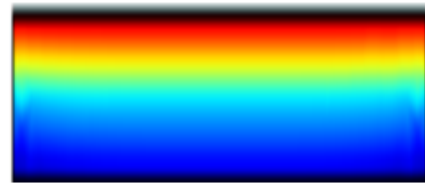


Figure 7.5. The 2D adsorbent bed filled with silica gel particles.

For 0.01 mm silica gel radius with using uniform pressure approach the temperature and concentration distributions are found at the end of 20 minutes of an adsorption process for specified adsorbent bed section is shown in Figure 7.6



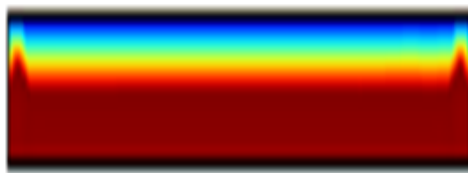
The temperature distribution for **adsorption** process (d-a) at the end of 20 minutes.



The concentration distribution for **adsorption** process (d-a) at the end of 20 minutes.

Figure 7.6. The temperature and concentration distributions for Uniform Pressure Approach of an adsorption process.

For 0.01 mm silica gel radius with using non-uniform pressure approach the temperature and concentration distributions are found at the end of 20 minutes of an adsorption process for specified adsorbent bed section is shown in Figure 7.3.



The temperature distribution for **adsorption** process (d-a) at the end of 20 minutes.



The concentration distribution for **adsorption** process (d-a) at the end of 20 minutes.



The pressure distribution for **adsorption** process (d-a) at the end of 20 minutes.

Figure 7.7. The temperature and concentration distributions for Non-Uniform Pressure Approach of an adsorption process.

The non-uniform pressure approach was considered since the used adsorbent particles are small and there are insufficient space between the particles. Water vapor cannot move between silica gel particles and interparticle mass transfer resistance is considered. But the advantage of using small size particles the thermal resistance in the adsorbent particle can be neglected. Non-Uniform Approach Pressure provides more

precise results than the Uniform Pressure Approach, so Non-Uniform Pressure Approach is used for next studies. The results of these simulation studies reached the following conclusions:

- 20 minutes of adsorption and desorption periods are sufficient.
- Silica gel particle diameter will be 0.25 mm.
- The thickness, the length and depth of the adsorbent bed will be 100, 500 and 100 mm.

CHAPTER 8

SIMULATION RESULTS

In this chapter, the theoretical studies performed during this thesis are given. The governing equations of these problems are given in Chapter 4 in extend. The theoretical studies were performed in order to understand the heat and mass transfer mechanism of an adsorption heat pump in a granular rectangular adsorbent bed. By the help of the theoretical results, the experimental setup part of this thesis was tried to be optimized. The studies were performed for silica gel RD-water pair. The two dimensional rectangular coordinate based governing equations on the heat and mass transfer mechanism of an adsorption bed were written by using Non-Uniform Pressure Approach. The heat and mass transfer equations for the adsorbent bed, equation of the mass transfer for adsorbent granule, and the Darcy law were solved under the corresponding initial and boundary conditions for each theoretical study. The solution of these coupled and non-linear equations were performed by using Comsol Software. Details on solution procedures such as number of grids, convergence criterion, and determination of averages of the unknowns are explained in this chapter.

Three theoretical studies were performed. In the first theoretical study, simulation of heat and mass transfer in adsorbent bed of adsorption heat pump operating with released heat of a household refrigerator was performed. As mentioned in previous chapter, the released heat of the condenser and hot gas of a household refrigerator was used to desorp the adsorbent bed (Ilis et al., 2013). That's why the adsorption and desorption periods should be considered with the on and off time of the refrigerator's compressor. When the compressor is on, the heat of hot gas and condenser is transferred to the adsorbent bed and desorption process occurs. For this reason, a bed was considered in order to understand the relationship with the period of a compressor of a refrigerator. In the second theoretical study, the effects of aluminum metal piece additives on adsorption-desorption process of an unconsolidated adsorbent bed filled with silica gel Fuji RD were investigated. The temperature and concentration distribution in the rectangular adsorbent bed during the adsorption and desorption processes were plotted during the cycle period for different volume fractions of the aluminum piece additives added to the bed silica gel volume. In the last study, the effect of geometrical parameters of a rectangular bed length and height, diameter of adsorbent

particle, and minimum and maximum temperatures of adsorption cycle on the performance of an adsorbent bed were numerically investigated in order to find a proper adsorbent bed design for the Highest Specific Cooling Power (SCP).

The numerical studies led the way for design of the proposed hybrid system. Inferences were obtained from these results to have optimum adsorption heat pump design in order to get the maximum efficiency from the household refrigerator where the adsorption heat pump was adapted.

8.1. Simulation of Heat and Mass Transfer in Adsorbent Bed of Adsorption Heat Pump Operating with Released Heat of a Household Refrigerator

In this study, simulation of heat and mass transfer in adsorbent bed of adsorption heat pump operating with the released heat of a household refrigerator is performed (Ilis et al. 2014). The adsorbent bed has a rectangular design. To transfer the heat between the outlets of compressor and condenser into the adsorbent bed, a heat exchanger consists of two parallel plates on which the adsorbent bed is located is designed. The R600a refrigerant leaving the compressor flows into the parallel plate. The temperature of refrigerant between compressor outlet and expansion valve inlet is obtained from experimental data of a household refrigerator. The top of the adsorbent bed is cooled by a fan which operates only during adsorption process. Adsorptive enters and leaves the bed from two ends. Heat and mass transfer equations are solved numerically to determine temperature and concentration distributions in the bed for both adsorption and desorption process. The distribution of these parameters are plotted for the bed and discussed. The study is performed for Fuji RD silica gel-water pair with Freundlich isotherm relationship.

In this study, the interparticle mass transfer resistance is taken into account and the space gradient of adsorptive pressure is determined. The convective transport term appears in the heat transfer equation. Two simultaneous additional equations (i.e. continuity and Darcy equations) should be solved to obtain the adsorptive concentration profile and adsorptive velocity in the bed.

In this study, the released heat from the condenser and hot gas of a household refrigerator is used to desorb the adsorbent bed (Ilis et al., 2013b). That's why the adsorption and desorption periods should be considered with the on and off time of the

refrigerator's compressor. When the compressor is on, the heat of hot gas and condenser is transferred to the adsorbent bed and desorption process occurs.

Figure 8.1 shows the schematic view of the analyzed rectangular adsorbent bed filled with the adsorbent particles. The upper surface of the adsorbent bed is in contact with the ambient. The bottom surface contacts with a pipe where the heating fluid flows. The adsorptive from evaporator and condenser during adsorption and desorption process can easily flow into/from the left and right surfaces toward the mid part of the bed. The thermal resistance of the metal casing is neglected. The study is performed for silica gel RD-water pair. The porosity of the adsorbent bed is assumed as 0.45. The thermophysical properties of the analyzed silica gel RD-water pair are given in Appendix A. The adsorbent particle diameter is 0.7 mm, the length and the thickness of the bed are considered as 80 mm and 5 mm, respectively. The depth of the bed depends on mass flow rate of the refrigerant. The length of adsorbent bed is short and convective heat transfer coefficient between refrigerant and bottom surface is high. The upper surface is cooled by air via an external fan. The reason for the assumption that the upper and bottom surface temperatures of the adsorbent bed are constant during adsorption and desorption processes.

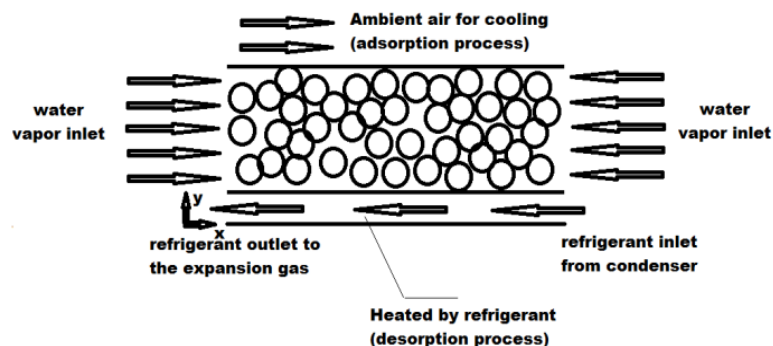


Figure 8.1. The schematic view of analyzed adsorbent bed filled with the adsorbent granules.

The mechanisms of heat and mass transfer in a granular adsorbent bed are coupled and complicated; hence some assumptions have to be made to pose the governing equations. The assumptions are; 1) the adsorbent bed consists of uniform size spherical adsorbent particles, 2) the particles arrangement is assumed cubical and thus the bed porosity is constant, 3) the adsorptive and adsorbent particle are in thermal equilibrium, 4) the thermal resistance within the adsorbent particle is neglected, 5) thermal properties of the adsorbent, adsorptive and adsorbate are constant, 6) wall

thermal resistance between the bed surface and particle is not considered, 7) the heat of adsorption is assumed constant.

Figure 8.2 shows whole the cycle on Clapeyron diagram. The adsorption process is started when the adsorbate concentration in the adsorbent bed is W_d and bed temperature is at T_d . Desorption process is started when the adsorbate concentration is attained to W_2 while the bed temperature is increased to T_b . Desorption process finishes when the bed temperature reaches to T_c . (Chapter 2)

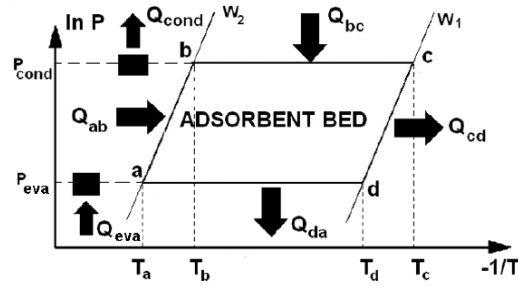


Figure 8.2. A schematic view of the adsorption-desorption process on Clapeyron Diagram.

The governing equations of the problem used in the analysis of the heat and mass transfer in the adsorbent bed are separately presented in previous chapters. The continuity equation based on conservation of mass for water vapor flow through the adsorbent bed can be written as given in Eq. (4.8).

The heat transfer equation for the adsorbent bed, water vapor and adsorbed water can be written as Eq. (4.9). The effective thermal capacitance and conductivity of the adsorbent bed can be calculated by using Eq. (4.10) and Eq. (4.11).

Linear Drive Force (LDF) model is used to determine the change of mean adsorbate concentration in the adsorbent particle with time presented in Eq. (4.12). The D_{eff} can be found from Eq. (4.13) and D_o is the reference diffusivity and E is the diffusion activation energy as given in the Appendix A. In order to solve mass transfer equation for particles (Eq. (6.15)), a relation for equilibrium state (i.e. \bar{W}_∞) must be known. The following isotherm equation can be used to determine adsorbate equilibrium concentration in the silica gel particle for a given pressure and temperature as given Eq. (4.14).

Darcy's law is a simple proportional relationship among the fluid flow rate through a porous medium, the fluid viscosity and the pressure drop for a given distance. For the present problem, it can be written as Eq. (4.15) to find V_x and V_y .

The ideal gas relation is used to calculate the pressure change of the water vapor in the silica gel bed. The apparent permeability of the silica gel bed (K_{app} , K_{inh}) is the inherent permeability and D_{bed} is the mass diffusivity of the bed besides of the Knudsen diffusion and the molecular diffusivity are calculated as Eq. (4.16) to Eq. (4.20). The initial and the boundary conditions are given in Table 8.1.

Figure 8.3 illustrates the compressor outlet temperature of the refrigerant when the compressor is on or off. As shown in the Figure 8.3, the compressor of a household refrigerator starts to work while the temperature of the cabinet of the refrigerator (i.e., inside temperature of refrigerator) drops to a higher specified temperature. Similarly, when the temperatures of the inner cabinets of the refrigerator reach to the lower specified temperature, compressor stops. The period of on and off of the compressor changes by the inner set temperature of the cabinets, type of the refrigerator, type of compressor etc. Based on the performed experimental data, the period of on and off of the compressor were taken 30 min and 35 min in this study, respectively.

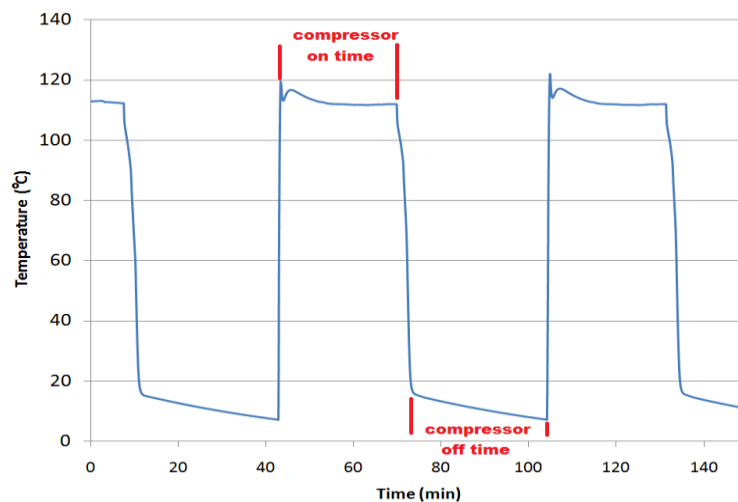


Figure 8.3. The change of compressor outlet refrigerant temperature while the compressor turns on and off.

In this study, the released heat from pipe between the compressor and condenser outlets is considered to be used for the isosteric heating (a-b) and desorption (b-c) processes. That's why, the total process period of both desorption (b-c) and the isosteric heating (a-b) processes of the adsorption heat pump should not be greater than 30 min. During the off time of the compressor, the adsorption (d-a) and the isosteric cooling (c-d) processes are performed and the adsorption and isosteric cooling processes should be performed in 35 min. Due to the constraint of the compressor on and off period, the

adsorbent bed should be designed carefully. The adsorbent particle size, the thickness and the width of the bed should be optimized. The related Clapeyron diagram can be seen from Figure 7.4 for the considered bed. As seen, during the cycle, the adsorbate concentration changes between 0.053 and 0.177 kg_v/kg_s. The evaporator pressure is taken at 0.775 kPa where the temperature of the evaporator is 2°C. The condenser pressure is at 3.25 kPa where the ambient temperature is 20°C. As it was mentioned before, the water vapor pressure inside the adsorbent bed is not uniform and it varies with the local adsorption rate and temperature. However, the water vapor pressure at the adsorbent bed entrance during the adsorption process is 0.775 kPa.

Table 8.1. The initial and boundary conditions of the considered problem.

Processes	Dependent Variable	Boundary Conditions at Bottom Side	Boundary Conditions at Upper Side	Boundary Conditions at Left Side	Boundary Conditions at Right Side	Initial Conditions
Isobaric adsorption process (start-up)	Temperature (K)	$\partial T/\partial x = 0$	$T = T_{amb}$	$\partial T/\partial x = 0$	$\partial T/\partial x = 0$	$T = T_d$
	Adsorbate pressure (kPa)	$\partial P/\partial x = 0$	$\partial P/\partial x = 0$	P=constant	P=constant	$P = f(P, T)$
	Adsorbate density (kg/m ³)	$\rho_v = f(P, T)$	$\rho_v = f(P, T)$	$\rho_v = f(P, T)$	$\rho_v = f(P, T)$	$\rho_v = \text{initial value at } T_d$
	Amount of adsorbate (kgw/kg _s)	$W = f(P, T)$	$W = f(P, T)$	$W = f(P, T)$	$W = f(P, T)$	$W = \text{initial value at } T_d$
	Adsorbate velocity (m/s)	$\partial u/\partial x = 0$	$\partial u/\partial x = 0$	$v_x = f(\rho_v)$ $v_y = f(\rho_v)$	$v_x = f(\rho_v)$ $v_y = f(\rho_v)$	$v_x = 0$ $v_y = 0$
Isosteric heating process	Temperature (K)	$T = T_{pipe}$	$\partial T/\partial x = 0$	$\partial T/\partial x = 0$	$\partial T/\partial x = 0$	Last values of isobaric adsorption process
	Adsorbate pressure (kPa)	$\partial P/\partial x = 0$	$\partial P/\partial x = 0$	$\partial P/\partial x = 0$	$\partial P/\partial x = 0$	
	Adsorbate density (kg/m ³)	$\rho_v = f(P, T)$	$\rho_v = f(P, T)$	$\rho_v = f(P, T)$	$\rho_v = f(P, T)$	
	Amount of adsorbate (kgw/kg _s)	$W = f(P, T)$	$W = f(P, T)$	$W = f(P, T)$	$W = f(P, T)$	
	Adsorbate velocity (m/s)	$\partial u/\partial x = 0$	$\partial u/\partial x = 0$	$\partial u/\partial x = 0$	$\partial u/\partial x = 0$	
Isobaric desorption process	Temperature (K)	$T = T_{pipe}$	$T = T_{amb}$	$\partial T/\partial x = 0$	$\partial T/\partial x = 0$	Last values of isosteric heating process
	Adsorbate pressure (kPa)	$\partial P/\partial x = 0$	$\partial P/\partial x = 0$	P=constant	P=constant	
	Adsorbate density (kg/m ³)	$\rho_v = f(P, T)$	$\rho_v = f(P, T)$	$\rho_v = f(P, T)$	$\rho_v = f(P, T)$	
	Amount of adsorbate (kgw/kg _s)	$W = f(P, T)$	$W = f(P, T)$	$W = f(P, T)$	$W = f(P, T)$	
	Adsorbate velocity (m/s)	$\partial u/\partial x = 0$	$\partial u/\partial x = 0$	$v_x = f(\rho_v)$ $v_y = f(\rho_v)$	$v_x = f(\rho_v)$ $v_y = f(\rho_v)$	
Isosteric cooling process	Temperature (K)	$\partial T/\partial x = 0$	$T = T_{amb}$	$\partial T/\partial x = 0$	$\partial T/\partial x = 0$	Last values of isobaric desorption process
	Adsorbate pressure (kPa)	$\partial P/\partial x = 0$	$\partial P/\partial x = 0$	$\partial P/\partial x = 0$	$\partial P/\partial x = 0$	
	Adsorbate density (kg/m ³)	$\rho_v = f(P, T)$	$\rho_v = f(P, T)$	$\rho_v = f(P, T)$	$\rho_v = f(P, T)$	
	Amount of adsorbate (kgw/kg _s)	$W = f(P, T)$	$W = f(P, T)$	$W = f(P, T)$	$W = f(P, T)$	
	Adsorbate velocity (m/s)	$\partial u/\partial x = 0$	$\partial u/\partial x = 0$	$\partial u/\partial x = 0$	$\partial u/\partial x = 0$	

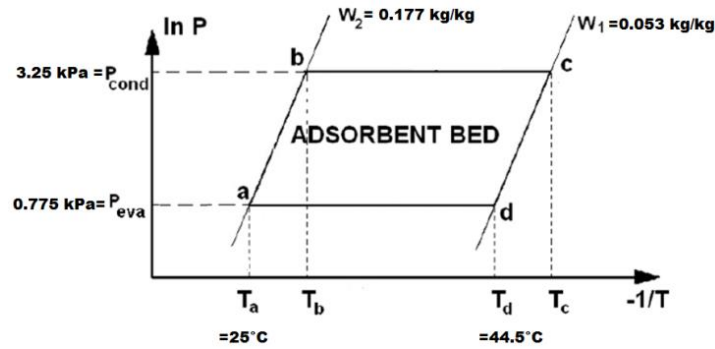


Figure 8.4. The adsorbate concentrations and pressures of the adsorption-desorption process on Clapeyron diagram for the considered adsorbent bed.

The distributions of temperature and adsorbate concentration in the bed for adsorption process are shown in Fig. 8.5. Left side of the Fig. 8.5 shows the distribution of temperature in the bed at four time steps of adsorption period. The bed initial temperature is 44.5°C and suddenly the bed outer surface temperature drops to 20°C, as a result, the temperature of region close to the top surface is also reduced to 20°C in 2 min. The distributions of temperature in the adsorbent bed after 5 and 10 minutes are also shown in Figure 8.5 (a). The temperature of the region close to the bed outer surface is smaller than the temperature of center region. As seen from Figure 8.5 (a), the temperature decreases by time in vertical direction (i.e., from the top to bottom surface) and it seems like a one dimensional heat transfer occurs in the bed. The distributions of adsorbate concentration at the four time steps of adsorption process of 8.5 (a) are shown in Figure 8.5 (b). The adsorbate concentration in the adsorbent particles is 0.053 kg_v/kg_s at the beginning of the adsorption process. The adsorbent bed temperature decreases over time and consequently the adsorbate concentration in the adsorbent particle increases (Figure 8.5 (b)) due to the adsorbate vapor entering to the bed from the left and right sides. There might be an intraparticle resistance in direction of the adsorbate vapor from ends to the center due to the small size of the adsorbent particle (i.e. 0.7 mm). This mass transfer resistance causes the concentration of adsorbate in the center region of the bed becomes slower than end region. The average adsorbate concentration in the bed is 0.177 kg_v/kg_s at the end of adsorption period.

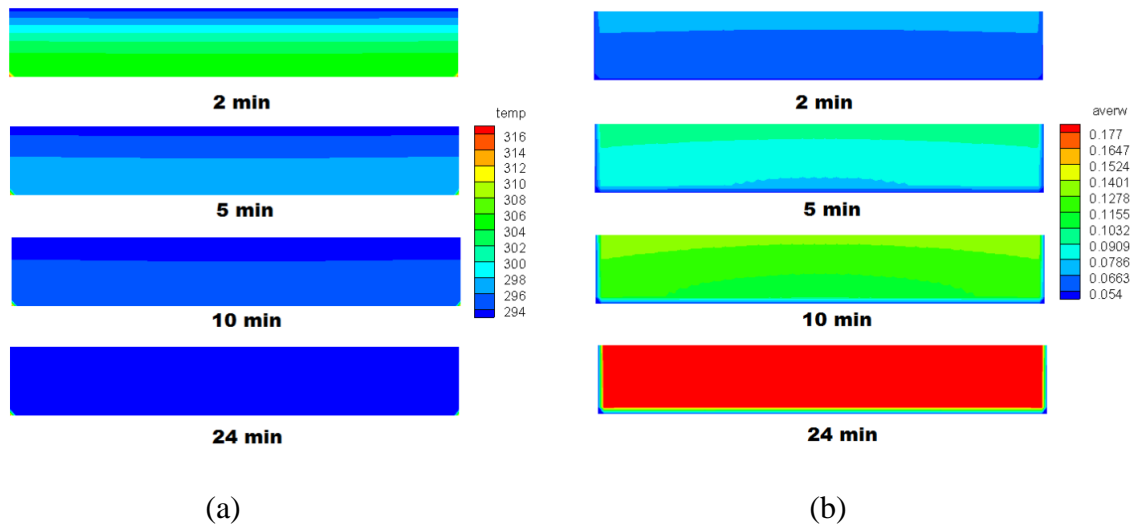


Figure 8.5. The distribution of a) temperature and b) adsorbate concentration of the adsorbent bed for adsorption (d-a) process after 2 min, 5 min, 10 min, end of the process.

The adsorbate concentration and temperature distributions for desorption process of Figure 8.4 are shown in Figure 8.6. The bed is heated by refrigerant (leaves the compressor) at 90°C from the bottom side of the bed. The wall temperature of the bottom surface of the adsorbent bed is taken 90°C due to high convective heat transfer coefficient. At the beginning of the desorption process, the temperature of the region closed to the bed bottom surface increases to 90°C. After 2 and 3 min, the temperature of the bed increases and the vapor starts to leave the bed (Figure 8.6 (b)). The distributions of adsorbate concentration at the four time steps of adsorption process are shown in Figure 8.6 (b). The average adsorbate concentration in the adsorbent bed starts to drop from 0.177 to 0.053 kg_v/kg_s at the end of the desorption process. Desorption process ends after 5 min. The comparison between periods of adsorption and desorption processes shows that adsorption process is longer than desorption process. This might be due to the refrigerant temperature of the desorption process. The adsorbent bed is cooled by ambient air which is at 20°C. The difference between ambient temperature and T_a is 5°C. However, the temperature of refrigerant for desorption process is 90°C which is 19°C above the T_c . This high temperature difference between the refrigerant and adsorbent bed accelerates heat transfer through the adsorbent bed during desorption process and reduce desorption periods.

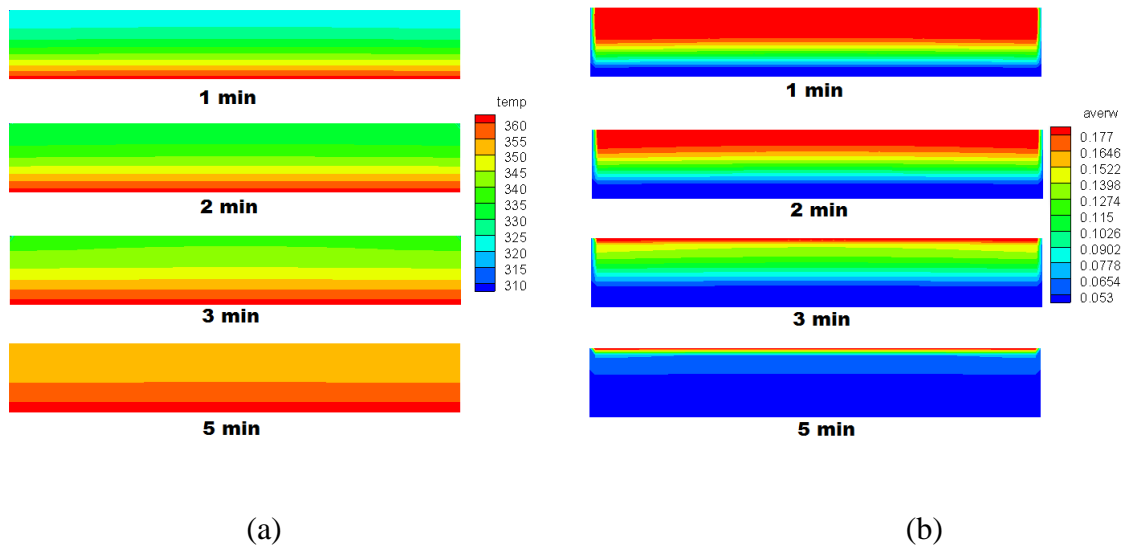


Figure 8.6. The distribution of a) temperature and b) adsorbate concentration of the adsorbent bed for desorption (b-c) process after 1 min, 2 min, 3 min, at the end of the process.

Figure 8.7 shows the distribution of the pressure and the velocity vectors of the bed after 2 min and at the end of the adsorption (8.7 (a)) and desorption processes (8.7 (b)). For both adsorption and desorption processes, the adsorptive flows from high pressure to low pressure. For adsorption and desorption processes, the average pressure inside of the bed is approximately 0.775 kPa and 3.25 kPa, respectively. As seen from Figure 8.7, the adsorptive inlet and outlet is from the right and left side of the adsorbent bed. The adsorptive starts to flow inside of the bed in adsorption process where it flows in the opposite direction during the desorption process to the outer of the bed.

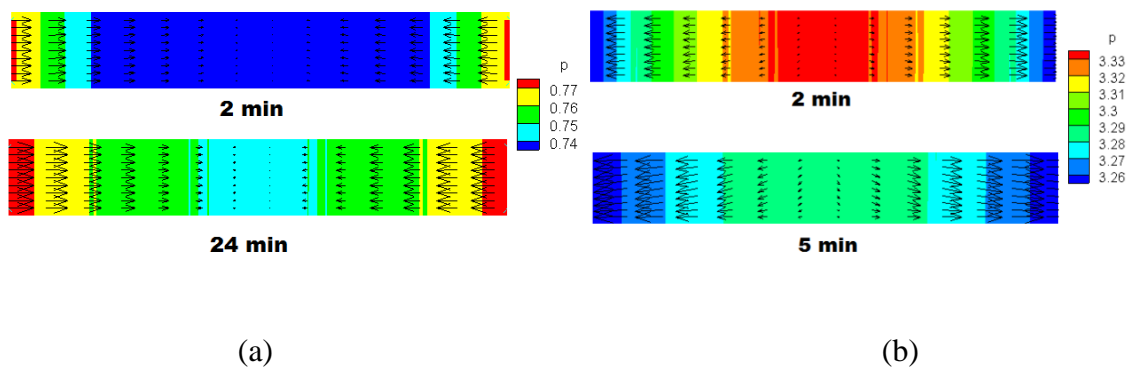


Figure 8.7. The distribution of the pressure and velocity vectors of the adsorbent bed after 2 min, and end of the process a) adsorption (d-a) process, b) desorption (b-c) process.

The change of the average temperature and average adsorbate concentration of the adsorbent bed during the four process of the cycle obtained by the numerical method are illustrated in Figure 8.8. At the beginning of the adsorption process, the average

temperature of the bed is approximately $T_d = 44^\circ\text{C}$, and it gradually drops to $T_a = 25^\circ\text{C}$. During the isosteric heating process the temperature of the bed increases approximately to $T_b = 58^\circ\text{C}$ and then it continues to be increased to $T_c = 74^\circ\text{C}$ during isobaric desorption process. As shown, the longest period of the cycle is the isobaric adsorption process. During the isobaric adsorption process the average adsorbate concentration increases from 0.053 to 0.177 kg_v/kg_s. The adsorbent bed is cooled during the isosteric cooling process to reduce the bed pressure to the evaporator pressure. The period of the cycle is approximately 33 min and it is appropriate with the compressor on and off period.

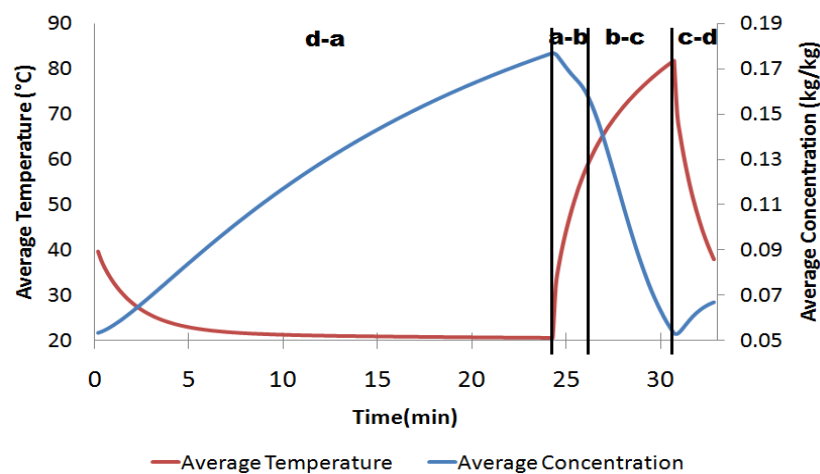


Figure 8.8. The distribution of the average temperature and average adsorbate concentration of the considered adsorbent bed during the cycle.

8.2. The Use of Metal Additives for Improving Heat Transfer in a Granular Adsorbent Bed

The effects of aluminum metal piece additives on adsorption-desorption process of an unconsolidated adsorbent bed filled with silica gel Fuji RD were investigated in this study (Ilis et al. 2015-1).

Figure 8.9 shows the schematic view of the analyzed rectangular adsorbent bed filled with Fuji RD silica gel granules. A section is analyzed in order to understand the heat and mass transfer in the whole bed. So a section is considered and the length and the height of the adsorbent bed section are 15 mm and 10 mm, respectively.

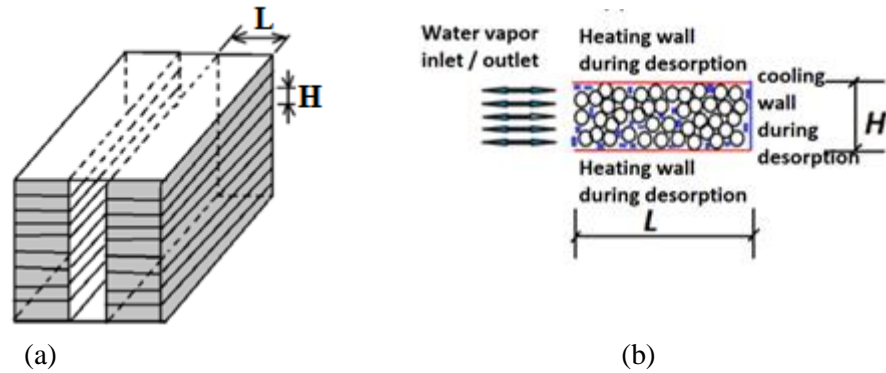


Figure 8.9. Schematic view of the adsorbent bed a) the adsorbent bed, b) the two dimensional representative domain.

In this study, the aluminum metal additive is added by the volume fraction from 10% to 90% to the granular adsorbent bed. The additive of aluminum and the silica gel particles in real cases can be seen from Figure 8.10.

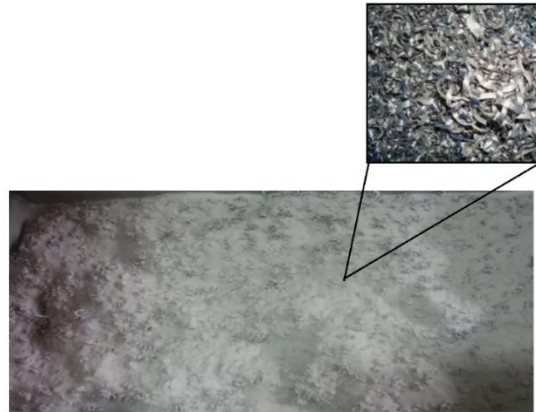


Figure 8.10. Aluminum pieces and aluminum pieces added silica gel granules.

The Eq. (4.20) can be used to the continuity equation based on conservation of mass for water vapor flow through the adsorbent bed. The heat transfer equation for the adsorbent bed, water vapor and adsorbed water is also given in Eq. (4.21). For the effective thermal capacitance Eq. (4.22) can be used for this problem. Eq. (4.23) is the effective thermal conductivity of the adsorbent bed with metal additive cases.

Linear Drive Force (LDF) model is given as Eq. (4.12) to determine the change of mean adsorbate concentration in the adsorbent particle with time. The LDF model, permeability, diffusivity and Darcy law equations are the same from Eq. (4.10) to Eq. (4.20) for metal additive cases. The thermophysical properties of the considered silica

gel–water pair and the metal additive aluminum are given in Appendix A with the thermophysical properties of the additive aluminum, additionally as given in Table 8.2.

Table 8.2. Thermophysical properties of the additive aluminum considered in the present study.

Parameter	Symbol	Value
Density of aluminum, kg/m ³	ρ_{add}	2702
Specific heats of additive aluminum, kJ/kgK	$C_{p_{add}}$	0.903
Thermal conductivity of additive aluminum, kW/mK	λ_{add}	237×10^{-3}

The initial and the boundary conditions with dimensional and dimensionless forms are given in Table 8.3.

The cooling COP and the specific cooling power of the intermittent adsorption heat pump can be calculated by the following equations.

$$COP = \frac{Q_{evap}}{Q_{ab} + Q_{bc}} \quad (8.1)$$

$$SCP_{ms} = \frac{Q_{evap}}{m_s \tau} \quad (8.2)$$

$$SCP_{mb} = \frac{Q_{evap}}{m_{bed} \tau} \quad (8.3)$$

where SCP_{ms} and SCP_{mb} represents the specific cooling power of the device based on the mass of silica gel and mass of the bed, respectively. m_s and m_{bed} are calculated by using these formulas:

$$m_s = V_{bed}(1 - \beta)\rho_s \quad (8.4)$$

$$m_{bed} = m_s + m_{add} \quad (8.5)$$

Table 8.3. The initial and boundary conditions of the considered problem.

Processes	Depend. Variable	Bound. Cond. at Bottom Side	Bound. Cond. at Upper Side	Bound. Cond. at Left Side	Bound. Cond. at Right Side	Initial Cond.
Isobaric adsorp. process (start-up)	Temperature (K)	$\frac{\partial T}{\partial x} = 0$	$\frac{\partial T}{\partial x} = 0$	$\frac{\partial T}{\partial x} = 0$	$T = T_{amb} = 293.15$	$T = T_d = 317.15$
	Adsorbate pressure (kPa)	$\frac{\partial P}{\partial x} = 0$	$\frac{\partial P}{\partial x} = 0$	$P=775$ Pa	$P=775$ Pa	$P = f(P, T)$
	Adsorbate density (kg/m ³)	$\rho_v = f(P, T)$	$\rho_v = f(P, T)$	$\rho_v = f(P, T)$	$\rho_v = f(P, T)$	$\rho_v = initial$
	Amount of adsorbate (kg/kg)	$W = f(P, T)$	$W = f(P, T)$	$W = f(P, T)$	$W = f(P, T)$	$W = initial = 0.03$
	Adsorbate velocity (m/s)	$\frac{\partial u}{\partial x} = 0$	$\frac{\partial u}{\partial x} = 0$	$v_x = f(\rho_v)$ $v_y = f(\rho_v)$	$v_x = f(\rho_v)$ $v_y = f(\rho_v)$	$v_x = 0$ $v_y = 0$
Isosteric heating process	Temperature (K)	$T = T_{pipe} = 353.15$	$T = T_{pipe} = 353.15$ K	$\frac{\partial T}{\partial x} = 0$	$\frac{\partial T}{\partial x} = 0$	Last values of isobaric adsorption process
	Adsorbate pressure (kPa)	$\frac{\partial P}{\partial x} = 0$	$\frac{\partial P}{\partial x} = 0$	$\frac{\partial P}{\partial x} = 0$	$\frac{\partial P}{\partial x} = 0$	
	Adsorbate density (kg/m ³)	$\rho_v = f(P, T)$	$\rho_v = f(P, T)$	$\rho_v = f(P, T)$	$\rho_v = f(P, T)$	
	Amount of adsorbate (kg/kg)	$W = f(P, T)$	$W = f(P, T)$	$W = f(P, T)$	$W = f(P, T)$	
	Adsorbate velocity (m/s)	$\frac{\partial u}{\partial x} = 0$	$\frac{\partial u}{\partial x} = 0$	$\frac{\partial u}{\partial x} = 0$	$\frac{\partial u}{\partial x} = 0$	
Isobaric desorp. process	Temperature (K)	$T = T_{pipe} = 353.15$	$T = T_{pipe} = 353.15$ K	$\frac{\partial T}{\partial x} = 0$	$\frac{\partial T}{\partial x} = 0$	Last values of isosteric heating process
	Adsorbate pressure (kPa)	$\frac{\partial P}{\partial x} = 0$	$\frac{\partial P}{\partial x} = 0$	$P=3250$ Pa	$P=3250$ Pa	
	Adsorbate density (kg/m ³)	$\rho_v = f(P, T)$	$\rho_v = f(P, T)$	$\rho_v = f(P, T)$	$\rho_v = f(P, T)$	
	Amount of adsorbate (kg/kg)	$W = f(P, T)$	$W = f(P, T)$	$W = f(P, T)$	$W = f(P, T)$	
	Adsorbate velocity (m/s)	$\frac{\partial u}{\partial x} = 0$	$\frac{\partial u}{\partial x} = 0$	$v_x = f(\rho_v)$ $v_y = f(\rho_v)$	$v_x = f(\rho_v)$ $v_y = f(\rho_v)$	
Isosteric cooling process	Temperature (K)	$\frac{\partial T}{\partial x} = 0$	$\frac{\partial T}{\partial x} = 0$	$\frac{\partial T}{\partial x} = 0$	$T = T_{amb} = 293.15$	Last values of isobaric desorption process
	Adsorbate pressure(kPa)	$\frac{\partial P}{\partial x} = 0$	$\frac{\partial P}{\partial x} = 0$	$\frac{\partial P}{\partial x} = 0$	$\frac{\partial P}{\partial x} = 0$	
	Adsorbate density (kg/m ³)	$\rho_v = f(P, T)$	$\rho_v = f(P, T)$	$\rho_v = f(P, T)$	$\rho_v = f(P, T)$	
	Amount of adsorbate (kg/kg)	$W = f(P, T)$	$W = f(P, T)$	$W = f(P, T)$	$W = f(P, T)$	
	Adsorbate velocity (m/s)	$\frac{\partial u}{\partial x} = 0$	$\frac{\partial u}{\partial x} = 0$	$\frac{\partial u}{\partial x} = 0$	$\frac{\partial u}{\partial x} = 0$	

The effect on cooling performance of metal additive on the adsorbent bed is concluded in this section. As mentioned, adsorbent bed section having 10 mm height and 15 mm length is analyzed in this study and the mass of the silica gel inside of the

bed without no metal additive is 0.1 kg. The temperature and the concentration change during the whole cycles of the adsorption process by adding the aluminum additive with volume fraction from 10% to 90% are presented in Figure 8.6. As can be seen from Figure 8.6 (a), the temperature of the bed is started the adsorption process at 317.5 K and decreases to 293 K. The heating process starts at 293 K and by this process, the pressure starts to increase from 775 Pa to 3250 Pa. After this pressure, the temperature increases up to 353 K in the desorption process. The pressure starts to decrease to 775 Pa and also the temperature drops to 317.5 K which is the temperature at the beginning of the process. Also the concentration change during the whole cycle of the process is plotted and illustrated in Figure 8.11 (b). At the beginning of the adsorption process, the silica gel is dry with concentration of 0.03 kg_v/kg_s. The concentration increases to 0.24 kg_v/kg_s at the end of the adsorption process. At the desorption process, it drops again to 0.03 kg_v/kg_s. As can be seen from Figure 8.11 (a), the whole process including, adsorption, heating, desorption, and cooling processes filled with pure silica gel takes approximately 29000 sec. The duration of the whole process if 10% aluminum metal additive is added to the silica gel inside of the bed decreases to 24000 sec which is 17% lower than, the case with no additive. The whole process period if 30%, 50%, 70% aluminum metal additive is added to the silica gel inside of the bed decreases 36%, 43%, 57% lower according to the no additive cycle period. When the mass of silica gel decreases by increasing of percentage of the aluminum such as 90%, the concentration inside of the bed starts to not change which means there is no adsorption inside of the bed due to amount of silica gel.

The distributions of temperature and adsorbate concentration in the bed for adsorption process are shown in Figure 8.12. Figure 8.12 (a) shows the distribution of temperature in the bed at three time steps of adsorption period for 0%, 20%, and 50% volume fractions. The bed initial temperature is 317.5 K and suddenly the right surface temperature drops to 293 K, as a result, the temperature of region close to the right is also reduced to 293 K in 10 sec. for all volume fractions. The distributions of temperature in the adsorbent bed after 1000 and 10000 seconds are also shown in Fig. 8.12 (a) for specified volume fractions. The temperature of the region close to the bed right surface is smaller than the temperature of left region. As seen from Fig. 8.12 (a), the temperature decreases by time in horizontal direction (i.e., from the right to left surface) and it seems like a one dimensional heat transfer occurs in the bed. As can be seen, the heat transfer inside of the bed can be enhanced by increasing of volume

fraction. This is the proof of the enhancement of the heat transfer by adding the metal additives inside of the silica gel particles.

The distributions of adsorbate concentration for the three time steps of adsorption process of Fig. 8.12 (a) are shown in Figure 8.12 (b). The adsorbate concentration in the adsorbent particles is $0.03 \text{ kg}_v/\text{kg}_s$ at the beginning of the adsorption process. The adsorbent bed temperature decreases over time and consequently the adsorbate concentration in the adsorbent particle increases (Figure 8.12 (b)) due to the adsorbate vapor entering to the bed from the left side. The average adsorbate concentration in the bed reaches to $0.245 \text{ kg}_v/\text{kg}_s$ at the end of adsorption period. It can be mentioned that the concentration rate can be increased by adding metal additives into the adsorbent bed.

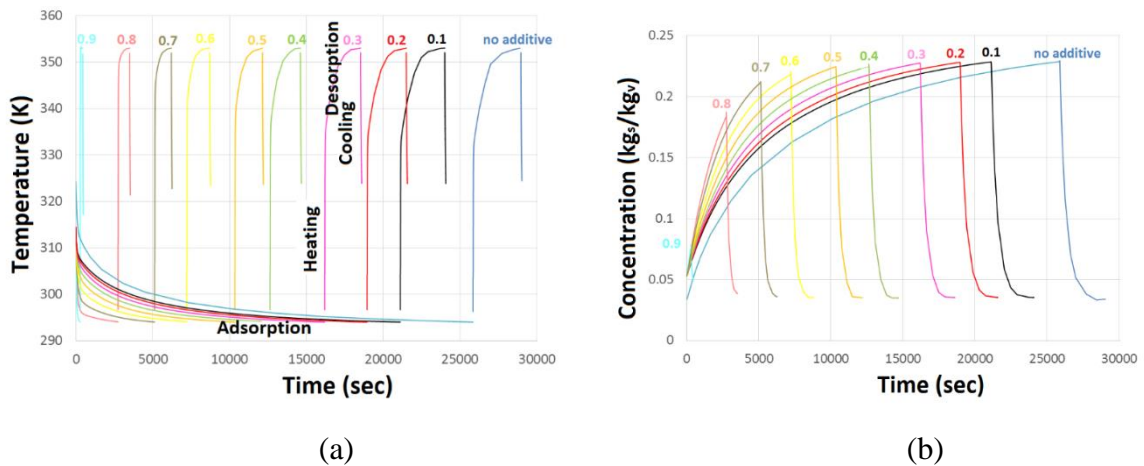


Figure 8.11. Adsorption, heating, desorption, cooling processes for all volume fractions from 10 to 90%, a) temperature variation, b) concentration variation.

The adsorbate concentration and temperature distributions for desorption process of Figure 8.12 shown in Figure 8.13. The bed is heated at 353 K from the bottom and the top sides of the bed. The wall temperature of the bottom and top surfaces of the adsorbent bed are taken 353 K due to high convective heat transfer coefficient. At the beginning of the desorption process, the temperature of the region closed to the bed bottom and top surfaces increase to 353 K. After 10 sec. the temperature of the bed increases and the vapor starts to leave the bed (Fig. 8.13 (b)). The distributions of adsorbate concentration at the three time steps of desorption process are shown in Fig. 8.13 (b). The average adsorbate concentration in the adsorbent bed starts to drop from 0.245 to $0.03 \text{ kg}_v/\text{kg}_s$ at the end of the desorption process. Desorption process ends after 3000, 2500, 1800 sec. for 0, 20, 50% volume

fractions, respectively. As same with the adsorption process, the concentration rate can be increased by adding metal additives into the adsorbent bed for desorption process

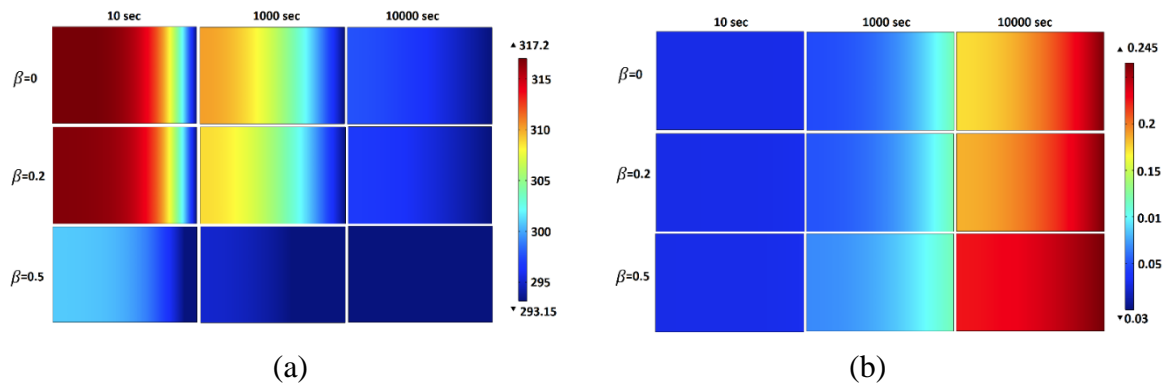
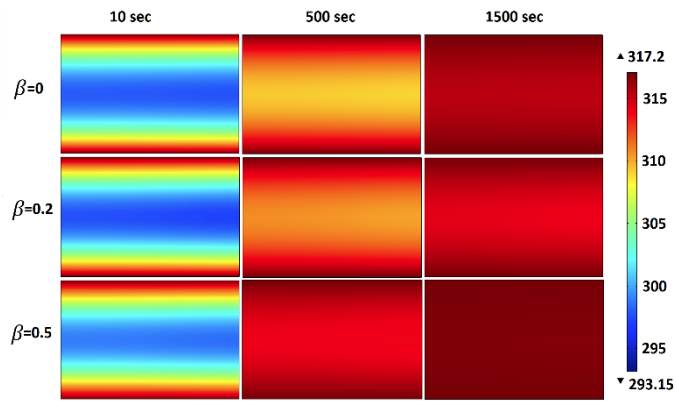


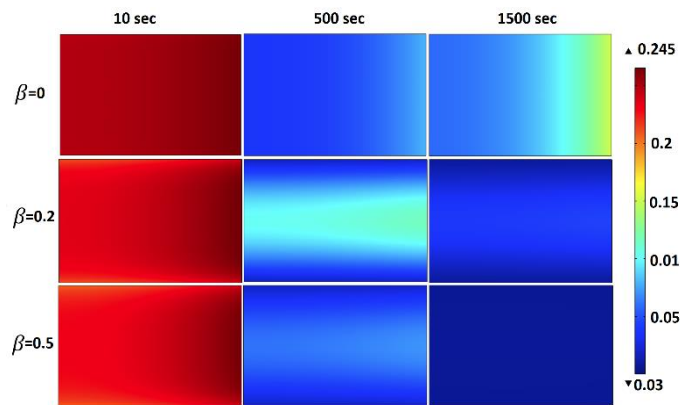
Figure 8.12. The variation of temperature and concentration inside the adsorbent bed with no additive, 20, and 50% fractions at different time steps for adsorption, a) temperature, b) concentration.

The results show that the heat transfer can be enhanced by using the metal additives inside of the bed. The increase of volume fraction of metal additive causes decreasing on the period of the adsorption and desorption. As can be seen from Fig. 8.14, the adsorption and desorption time decreases in inverse ratio with increasing of volume fraction. But a little change has occurred after the high values of aluminum volume fraction such as 80%. After this volume fraction such as 80%, the adsorption and desorption time have almost no change and the durations of these processes change insignificantly.

The energy transfer from heating, desorption, and the evaporation processes have to be calculated in order to define the COP of the system. As mentioned, the mass of the silica gel decreases with the change of the aluminum additive and also the duration of the process decreases in parallel. So, the energy transfer from the from heating, desorption and evaporation processes for different volume fractions of the considered adsorbent bed are calculated and illustrated in Table 8.4. As shown, the COP of the heat pump is same for all volume fractions.



(a)



(b)

Figure 8.13. The variation of temperature and concentration inside the adsorbent bed with no additive, 20, and 50% fractions at different time steps for desorption, a) temperature, b) concentration.

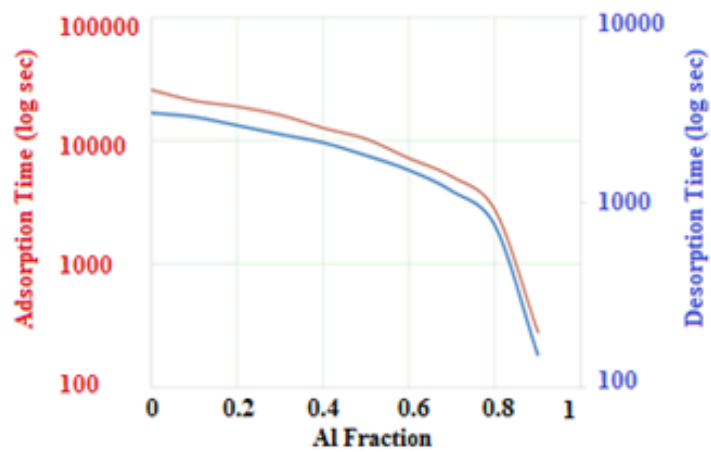


Figure 8.14. Adsorption-desorption time vs aluminum fraction.

Table 8.4. The COP, energy transfer from heating, desorption and evaporation processes for different volume fractions of the considered adsorbent bed.

VOLUME FRACTION	Q_{heating} (kJ)	$Q_{\text{desorption}}$ (kJ)	Q_{evap} (kJ)	COP
0	0.884	6.291	52.776	7.356
10%	0.796	5.662	47.498	
20%	0.708	5.032	42.221	
30%	0.619	4.403	36.943	
40%	0.531	3.774	31.666	
50%	0.442	3.145	26.388	
60%	0.354	2.516	21.110	
70%	0.265	1.887	15.833	
80%	0.177	1.258	10.555	
90%	0.088	0.629	5.278	

As given in Eq. (8.3) and (8.4), the SCP have to be defined in two different approaches. As illustrated in Figure 6.16, the amount of silica gel decreases by increasing of volume fraction of aluminum inside of the bed. As a result of this, the SCP based on mass of silica gel has inverse ratio with the mass of the silica gel and the duration of the process. As given in the results, the process time decreases by decreasing of mass of the silica gel. Also the results showed us that, the energy transfer from the evaporator also decreases. So the SCP based on the mass of the silica gel increases by increasing of volume fraction as seen from Figure 8.15.

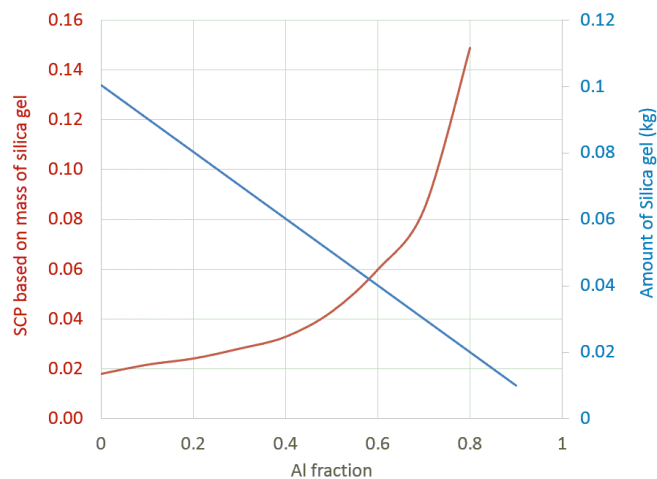


Figure 8.15. SCP and amount of silica gel for all volume fractions from 10 to 90%.

The SCP based on the mass of the total amount of the bed have to be calculated in the light of the results showed in Figure 8.15. By decreasing the mass of the silica gel, the mass of the aluminum increases. Also the mass of the bed increases, too. Even

the duration of the process reduces with the increasing of the volume fraction, the mass of the bed increases and causes decrease in SCP as seen from Figure 8.16. But the decrease of the SCP based on amount of the total mass of the bed starts to not change after 40% volume fraction.

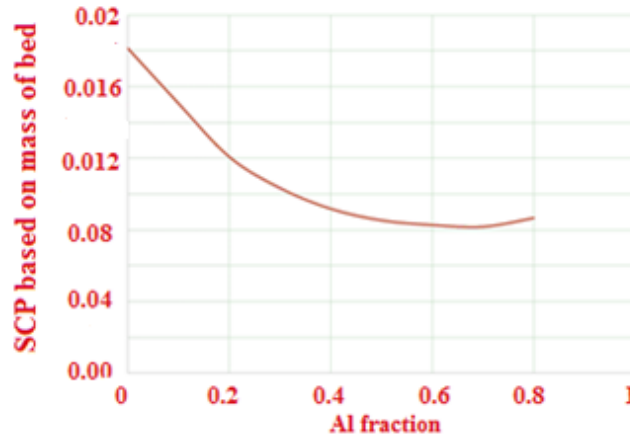


Figure 8.16. SCP and amount of mass of bed for all volume fractions from 10 to 90%.

8.3. Optimum Design of an Adsorbent Bed of Adsorption Refrigeration System for Highest SCP

A reason of the low cooling power of an adsorption heat pump is the slow heat and mass transfer in adsorbent bed. Many researchers focus on the accelerating heat and mass transfer in the adsorbent bed [1, 2]. There are many parameters that have to be considered during design of an adsorbent bed. The effects of parameters such as bed thickness, porosity, particle size, mass diffusivity and the operating temperature on the heat and mass rate have to be studied [3- 6]. Practically, it is difficult to consider all geometrical and operational parameters to find out the best design for an adsorbent bed. Some of the parameters are coupled and the increase of one parameter reduces the effect of another parameter. That's why some statistics methods may be employed to consider all affected parameters and find out a proper design. One of popular method is Taguchi method that reduces number of runs and saves time. In Taguchi method, based on the number of parameters and their levels, an orthogonal array is selected and runs or experiments are performed only for the levels of the orthogonal array. The methods were used by some researchers in order to find a proper design for heat exchangers. For instance, Jamshidi et al. [7] used Taguchi method to find a proper helical coil design in

which nano-fluid flows, theoretically. Tzu-Chen Hung et al [8] studied on optimal design of a concentric heat exchanger for high-temperature systems using CFD simulations by using Taguchi method.

The effects of four parameters of an adsorbent bed of adsorption heat pump on the performance of adsorption heat pump are numerically studied and a proper design is found. The height and length of the rectangular adsorbent bed, the granule size, and the operating temperatures are changed and the optimum bed design is concluded for the problem. The conservation of mass and energy equations and Darcy Law equations are solved to find temperature, water concentration in the adsorbent bed for entire cycle. The ideal gas equation is used to relate the water vapor pressure with its density and temperature. The equations are solved for the rectangular bed by using Comsol Software. The Taguchi method is applied to the considered problem in order to reduce the numerical run and find a proper design (Ilis et al. 2015-2).

Figure 8.17 shows the schematic view of the analyzed rectangular adsorbent bed filled with Fuji RD silica gel granules. As can be seen, there are many horizontal parallel heating plates and the adsorbent particles are located in between (Fig. 8.17 (a)). The adsorbent bed is cooled from the right side and the adsorptive (water vapor) enters from the left side of the bed (Fig. 8.17 (b)). A representative section is analyzed and there is no doubt that the analyzed section resemble the entire bed. The porosity of the adsorbent bed is assumed as 0.45.

In order to optimize the adsorbent bed design, the length and width of the bed are changed from 5 to 15 mm, the adsorbent granule particle radius is considered from 0.25 to 1 mm, and the maximum and minimum temperature difference of the bed varies between 30 to 50°C. The values of considered parameter are given in Table 8.5. As seen, there are four main parameters and each parameter has three levels. The thermo-physical properties of the considered silica gel–water pair are given in Appendix A. All these parameters are constant for entire present study. The made assumptions are given in section 7.1 to pose the governing equations.

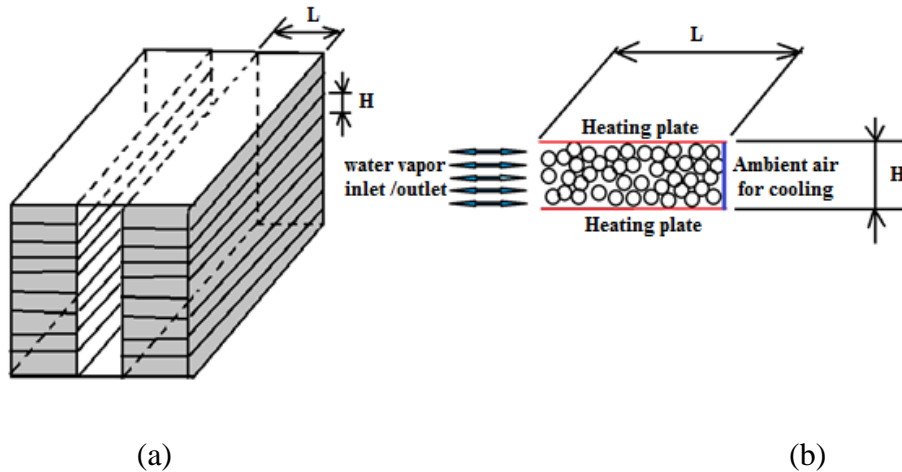


Figure 8.17. Schematic view of the adsorbent bed a) the adsorbent bed, b) the two dimensional representative domain.

Table 8.5. The considered parameters of the bed and their levels.

Parameter	Symbol	Levels		
		1	2	3
A, Length	L	5 mm	10 mm	15 mm
B, Height	H	5 mm	10 mm	15 mm
C, Radius of the granular adsorbent	r_p	0.25 mm	0.5 mm	1 mm
D, Temperature difference of the bed and the ambient	ΔT	30°C	40°C	50°C

Figure 8.2 shows the entire cycle on Clapeyron diagram. The adsorption process can be started when the adsorbate concentration in the adsorbent bed is W_d and bed temperature is at T_d . The adsorption process continues until the concentration value reaches to the W_2 while the bed temperature is T_a . Then, the bed temperature and pressure are increased to the condenser pressure and temperature. When the pressure value attains to the condenser pressure, desorption process is started. Desorption process is finished when the adsorbate concentration reaches to W_1 while the bed temperature is T_c . The cooling process continues to return to the evaporator pressure again.

The governing equations of the problem used in the analysis of the heat and mass transfer in the adsorbent bed are separately presented in Section 7.1. The continuity equation, the heat and mass transfer equation, the LDF model, permeability, diffusivity and Darcy law equations are the same from Eq. (4.8) to Eq. (4.20)

The specific cooling power of the intermittent adsorption heat pump can be calculated by the following equations.

$$SCP = \frac{Q_{evap}}{m_s \tau} \quad (8.6)$$

The initial and boundary conditions of the considered problem is illustrated in Table 8.6. Table 8.7 represents the initial temperatures and the concentrations at the beginning of the adsorption and desorption processes.

Table 8.6. The initial and boundary conditions of the considered problem.

Processes	Depend. Variable	Bound. Cond. at Bottom Side	Bound. Cond. at Upper Side	Bound. Cond. at Left Side	Bound. Cond. at Right Side	Initial Cond.
Isobaric adsorp. process (start-up)	Temperature (K)	$\partial T / \partial x = 0$	$\partial T / \partial x = 0$	$\frac{\partial T}{\partial x} = 0$	$T = T_{amb} = 293.15 \text{ K}$	$T = T_d$
	Adsorbate pressure (kPa)	$\partial P / \partial x = 0$	$\partial P / \partial x = 0$	$P=775 \text{ Pa}$	$P=775 \text{ Pa}$	$P = f(P, T)$
	Adsorbate density (kg/m ³)	$\rho_v = f(P, T)$	$\rho_v = f(P, T)$	$\rho_v = f(P, T)$	$\rho_v = f(P, T)$	$\rho_v = \text{initial value at } T_d$
	Amount of adsorbate (kg _w /kg _s)	$W = f(P, T)$	$W = f(P, T)$	$W = f(P, T)$	$W = f(P, T)$	$W = \text{initial value at } T_d$
	Adsorbate velocity (m/s)	$\partial u / \partial x = 0$	$\partial u / \partial x = 0$	$v_x = f(\rho_v)$ $v_y = f(\rho_v)$	$v_x = f(\rho_v)$ $v_y = f(\rho_v)$	$v_x = 0$ $v_y = 0$
Isosteric heating process	Temperature (K)	$T = T_{pipe} = 353.15 \text{ K}$	$T = T_{pipe} = 353.15 \text{ K}$	$\frac{\partial T}{\partial x} = 0$	$\partial T / \partial x = 0$	Last values of isobaric adsorption process
	Adsorbate pressure (kPa)	$\partial P / \partial x = 0$	$\partial P / \partial x = 0$	$\frac{\partial P}{\partial x} = 0$	$\partial P / \partial x = 0$	
	Adsorbate density (kg/m ³)	$\rho_v = f(P, T)$	$\rho_v = f(P, T)$	$\rho_v = f(P, T)$	$\rho_v = f(P, T)$	
	Amount of adsorbate (kg _w /kg _s)	$W = f(P, T)$	$W = f(P, T)$	$W = f(P, T)$	$W = f(P, T)$	
Isobaric desorp. process	Temperature (K)	$T = T_{pipe} = 353.15 \text{ K}$	$T = T_{pipe} = 353.15 \text{ K}$	$\frac{\partial T}{\partial x} = 0$	$\partial T / \partial x = 0$	Last values of isosteric heating process
	Adsorbate pressure (kPa)	$\partial P / \partial x = 0$	$\partial P / \partial x = 0$	$P=3250 \text{ Pa}$	$P=3250 \text{ Pa}$	
	Adsorbate density (kg/m ³)	$\rho_v = f(P, T)$	$\rho_v = f(P, T)$	$\rho_v = f(P, T)$	$\rho_v = f(P, T)$	
	Amount of adsorbate (kg _w /kg _s)	$W = f(P, T)$	$W = f(P, T)$	$W = f(P, T)$	$W = f(P, T)$	
	Adsorbate velocity (m/s)	$\partial u / \partial x = 0$	$\partial u / \partial x = 0$	$v_x = f(\rho_v)$ $v_y = f(\rho_v)$	$v_x = f(\rho_v)$ $v_y = f(\rho_v)$	
Isosteric cooling process	Temperature (K)	$\partial T / \partial x = 0$	$\partial T / \partial x = 0$	$\frac{\partial T}{\partial x} = 0$	$T = T_{amb} = 293.15 \text{ K}$	Last values of isobaric desorption process
	Adsorbate pressure(kPa)	$\partial P / \partial x = 0$	$\partial P / \partial x = 0$	$\frac{\partial P}{\partial x} = 0$	$\partial P / \partial x = 0$	
	Adsorbate density (kg/m ³)	$\rho_v = f(P, T)$	$\rho_v = f(P, T)$	$\rho_v = f(P, T)$	$\rho_v = f(P, T)$	
	Amount of adsorbate (kg _w /kg _s)	$W = f(P, T)$	$W = f(P, T)$	$W = f(P, T)$	$W = f(P, T)$	
	Adsorbate velocity (m/s)	$\partial u / \partial x = 0$	$\partial u / \partial x = 0$	$\frac{\partial u}{\partial x} = 0$	$\partial u / \partial x = 0$	

Table 8.7. The initial temperature and concentration values for runs.

T _a (°C)	T _d (°C)	W _d (kg _v / kg _s)	W _a (kg _v / kg _s)
25	75	0.045	0.177
30	70	0.057	0.128
35	65	0.073	0.094

Taguchi method is widely used in science and industry to reduce number of experiments for achieving sufficient data in order to understand the effects of relevant parameters. It uses a mathematical tool named as orthogonal arrays and signal to noise ratio (S/N) to consider large number process variables with small number of experiments (Taguchi, 1987). Following steps should be considered to use Taguchi method as an optimization technique:

- Target (or targets) for the considered problem should be specified. The aim of this study is to have a design to provide maximum cooling power with minimum amount of adsorbent. That's why SCP is selected as the quality character for the problem.
- The parameters influence the target should be specified. In this study, as presented in Table 8.5, four independent parameters which are the length and height of adsorbent bed, radius of the particle and the temperature difference (ΔT) are considered and their effects on SCP are investigated. For each independent parameter 3 values are considered.
- The orthogonal array should be selected. Since there are four dependent parameters and each dependent parameters have three level, L₉ array is chosen based on the Taguchi method. This means that for the considered parameters with three levels $3^4=81$ runs is required but Taguchi method reduces it to 9 runs.
- Signal to Noise analysis should be performed. The S/N ratio is a quality metric linked to the loss function. The loss related with the process can be minimized by maximizing the S/N ratio.
- The S/N ratio can be divided into three categories:

Smaller is better:
$$\frac{S}{N} = -10 \log \frac{1}{n} (\Sigma y^2) \quad (8.7)$$

$$\text{Nominal is better: } \frac{S}{N} = -10 \log \frac{1}{n} \left(\sum \frac{\bar{y}}{S_y^2} \right) \quad (8.8)$$

$$\text{Larger is better: } \frac{S}{N} = -10 \log \frac{1}{n} \left(\sum \frac{1}{y^2} \right) \quad (8.9)$$

where \bar{Y} is the average of observed data, S_y^2 is the variation of y , n is the number of observations, and y is the observed data. In this study, the Signal-to-Noise (S/N) ratios determined by using Minitab 17.0 software. Larger is better characteristic used for our problem since the maximum value for SCP is required.

The experimental plan described above is used and by considering Table 8.8, the found results of SCP by numerical runs are given in Table 6.10.

Table 8.8. Experimental plan of L_9 orthogonal array for SCP values.

Ru ns	A (bed length)	B (bed height)	C (particle radius)	D (Temp. diff.)	SCP (W/kg)
1	A1	B1	C1	D1	229.15
2	A1	B2	C2	D2	100.44
3	A1	B3	C3	D3	33.51
4	A2	B1	C2	D3	81.20
5	A2	B2	C3	D1	25.92
6	A2	B3	C1	D2	100.08
7	A3	B1	C3	D2	52.98
8	A3	B2	C1	D3	64.43
9	A3	B3	C2	D1	33.56

The effects on specific cooling performance of four parameters such as the length, and height of the bed, the adsorbent granule particle radius, and the maximum and minimum temperature difference of the adsorbent bed are concluded in this section. In order to understand the effect of these parameters on the optimum adsorbent bed design, Fig. 8.18 should be evaluated. The effects of four design parameters on SCP are plotted in Fig. 8.18.

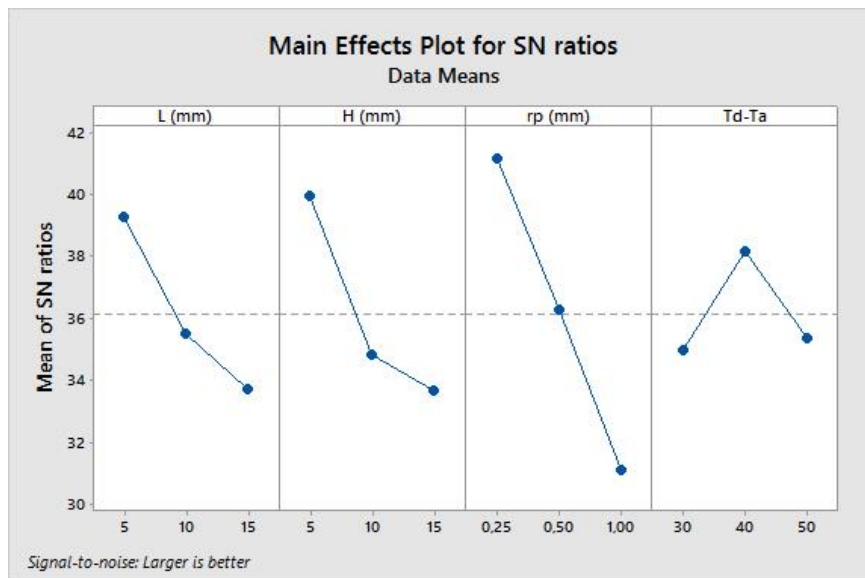


Figure 8.18. The effects of design parameters of A, B, C, and D on SCP of the adsorbent bed.

If the first curve from left side of the Figure 8.18 is considered, it is seen that the SCP value takes optimum value at the first level ($L = 5 \text{ mm}$) and then decreases and takes its minimum value at the third level for the parameter A (Length). If Figure 8.17 is considered, it is clearly seen that the distance for water vapor to move to the end of plate and the heat which should transferred to the surrounding during the adsorption increases by increase of L . This causes the period of the cycle to increase and consequently the SCP value will decrease. The second curve of Figure 8.18 relates to parameter B which is height. The SCP decreases by increase of height value from 5 to 15 mm. By increasing of the H , the heat transfer from the plate to the center of channel takes a long time and consequently desorption period increases. The third curve of Figure 8.18 refers to the effect of particle size. The SCP value tends to decrease with the increase of parameter C (adsorbent particle radius) from first level (0.25 mm) to its third level (1 mm).

By reducing the particle size, the intraparticle mass transfer resistance decreases and this causes the water content in the silica gel to be released faster and consequently SCP increases. The effect of maximum and minimum temperature of the cycle on the SCP is interesting. This study shows that there is an optimum temperature difference. By increasing the temperature difference, the SCP value increases, then takes a maximum value at 40°C and finally it decreases when the temperature difference becomes 50°C . The reason of this behavior of SCP with the temperature difference may be the adsorbate concentration difference. For low values of the maximum and

minimum temperature difference of the cycle, the cycle period is low but the amount of adsorbate evaporation is also very low which causes the SCP value to decrease. For high values of temperature difference, the amount of the evaporated adsorbate is high however the period of the cycle is also increased and consequently the SCP value drops. Then it should be an optimum maximum and minimum temperature difference for the cycle. For the present problem, the temperature difference is 40°C is the best if Figure 8.18 is considered. The analysis of the obtained results yields that the highest SCP value belongs to case where the bed and cycle have the properties of $L=5$ mm (A_1), $H=5$ mm (B_1), $r_p=0.25$ mm (C_1), $\Delta T=40^\circ\text{C}$ (D_2). In conclusion, $A_1B_1C_1D_2$ can be defined as the optimum design with SCP of 229.15 W/kg.

Response table of S/N ratios for SCP is illustrated in Table 8.9. The delta values are calculated by using maximum and minimum S/N ratios of all parameters. The contribution ratio is the ratio of delta values of each parameter to the total delta values of all parameters as presented Table 8.9. The results of Table 8.9 is shown graphically in Figure 8.19. It is seen that the radius of the adsorbent particles contributes by 35.2% of the total effect on SCP. This means that the parameter C is the most effective one on the performance of the bed. The parameter A which is the bed length has less effect on SCP with ratio of 26.5%, comparing to the parameter A. The contribution ratios of parameters B which is the height of the bed and D which is the maximum and minimum temperature difference are 24.6% and 13.7%, respectively. As seen clearly, the difference between the maximum and minimum working temperatures of the adsorbent bed has the lowest effect on the cooling performance of the considered adsorbent bed.

Table 8.9. Response table of S/N ratios.

	L	H	r_p	
Level	(mm)	(mm)	(mm)	ΔT (°C)
1	121.04	121.11	131.22	59.72
2	69.07	63.60	71.73	84.50
3	50.33	55.72	37.47	96.21
Delta	70.71	65.40	93.75	36.49
Rank	2	3	1	4
Contribution ratio (%)	26.5%	24.6%	35.2%	13.7%

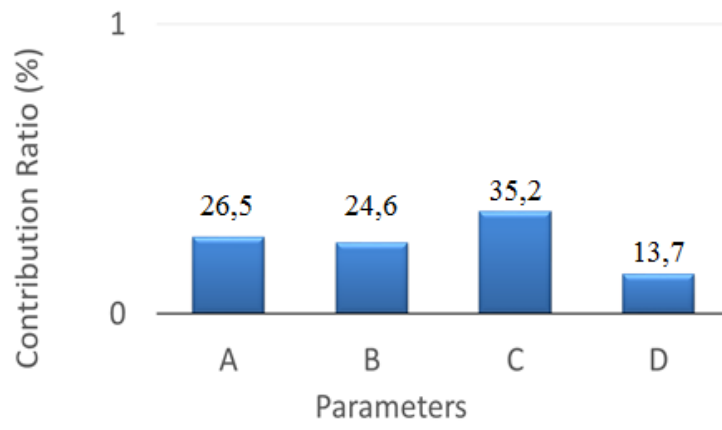


Figure 8.19. The contribution ratio of each parameter on SCP of the adsorbent bed.

CHAPTER 9

EXPERIMENTAL RESULTS

The aim of this experimental study was to investigate the enhancement of performance for a household refrigerator with using an adsorption heat pump. Hence, an adsorption heat pump experimental setup was designed and constructed. To have better results for the adsorption heat pump experiments, the first experimental setup was revised. The experiments were done with using the revised experimental setup. The results obtained from the first experimental setup and revised experimental setup, are compared each other. The comparison shows that there is an enhancement for the experimental results after revision. And then, the Fuji RD Type silica gel-water adsorption experiments were performed with the experimental procedure that described in this Chapter. The results were grouped as first setup results and revised setup results. The pressure and temperature change with time was logged and plotted for both of them. The results of performed studies such as leakage tests, adsorption experiments are presented with plots or calculations.

In this chapter, the results of the experimental studies which were carried out in this thesis are given. The adsorption experiments were performed to change cycle time of the experiment to see the effect of the time on cooling capacity, COP, SCP. Based on the obtained experimental results, the variation of temperature and pressure with time of the adsorbent bed, evaporator, condenser during the isobaric adsorption, isosteric heating, isobaric desorption, isosteric cooling process are plotted. Also the cooling capacity, coefficient of performance (COP), specific cooling power (SCP) are calculated and presented as table for each experiment. Vapor amount desorbed from the adsorbent during the adsorption process and water amount during desorption processes are also given to calculate the cooling capacity of the adsorption heat pump. The enhancement of the performance of a household refrigerator by using an adsorption heat pump is calculated, also.

9.1. Experimental Results

The silica gel-water vapor adsorption experiments were performed on the constructed setup which was explained in details in this chapter. The measured temperature and pressures were logged by data loggers and software. The leakage tests were done to provide leaktightness in the adsorbent bed, evaporator and condenser, completely. Even many experiments were done for the different cycle period conditions, the temperature and pressure variations are plotted for adsorbent bed, condenser and evaporator. The adsorbed vapor amount to adsorbent and the desorbed water amount from the adsorbent during the adsorption experiments are journalized for each experiment. The contribution to the performance of a household refrigerator when it is combined with the suggested adsorption heat pump is calculated also.

9.2. Experimental Procedure of the Adsorption Heat Pump

A basic adsorption heat pump consists of four main components as an adsorbent bed, an evaporator, a condenser, an expansion valve. Basically, adsorption heat pump operates by circulating adsorbate between these four components. Adsorption heat pump experiments were performed the duration of four process that are include: adsorption, heating, desorption and cooling processes. Four steps were followed to perform an experiment by the setup are given in detail on the Clapeyron diagram, as shown in Figure 9.1.

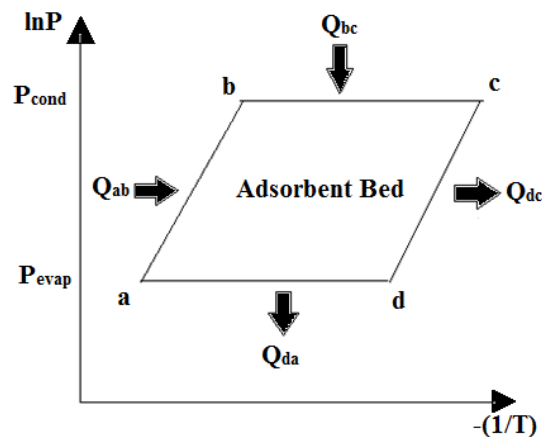


Figure 9.1. The ideal adsorption heat pump cycle (Clapeyron Diagram).

Step 1: Isobaric Adsorption Process:

The cycle begins with isobaric adsorption (d-a) process. Before starting the adsorption process, the whole system has to be under vacuumed. The temperature of the evaporator chamber is between 7-10°C and the inside is filled with deionized water. The water level inside of the evaporator was marked to determine the amount of adsorbed water by the silica gel particles. And then the valve between the adsorbent bed and evaporator is opened and water vapor starts to evaporate. During adsorption of the water vapor in the silica gel particles, heat is released that called as heat of adsorption. The heat of adsorption is removed from the adsorbent bed to decrease the temperature of the adsorbent bed from $T_d = 45-50^\circ\text{C}$ to $T_a=20-25^\circ\text{C}$. The fan on the adsorbent bed works during the adsorption process to remove this generated heat. The isobaric adsorption process was continued until the level of water inside the evaporator becomes fixed which indicates that the silica gel particles reach their equilibrium condition. Throughout the adsorption process, the adsorbent bed concentration increase that is full with dry silica gel particles at the minimum concentration, before the adsorption. The water level inside of the evaporator was marked at the end of the adsorption process to measure amount of the adsorbed water. During the adsorption process, the adsorbent bed, evaporator and condenser temperature and pressure values are collected. The temperature of the adsorbent bed decrease at the constant pressure during the adsorption process as can be seen from Figure 9.2.

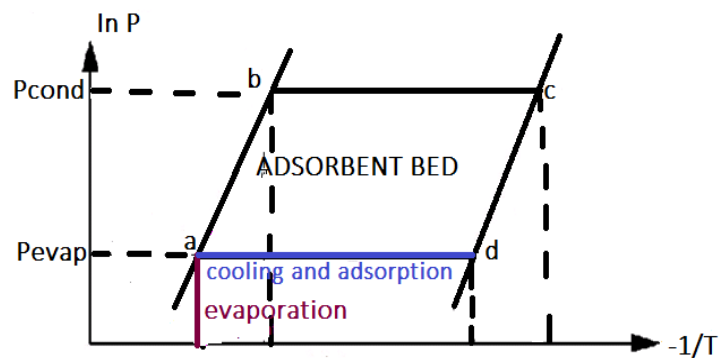


Figure 9.2. The adsorption process of the adsorption heat pump cycle on the Clapeyron Diagram.

Step 2: Isosteric Heating Process:

After the isobaric adsorption process, the isosteric heating process is started. The adsorbent bed temperature is 20-25°C and it reaches maximum concentration value. The valve between the adsorbent bed and the condenser and the evaporator are closed. The temperature of the adsorbent bed is increased from T_a to T_b by heating the adsorbent bed with the constant temperature that is provided from the water bath. The temperature of water in the water bath is fixed to 85°C to heating the adsorbent bed. Firstly, the plastic hose which are between water bath and adsorbent bed covered with insulation material to prevent heat loss. However the adsorbent bed inlet temperature of the hot water that is 60-65°C occur. The temperature and pressure of the adsorbent bed increases with time during the heating process (Figure 9.3). Temperature of the adsorbent bed reaches 50-55°C at the end of heating process.

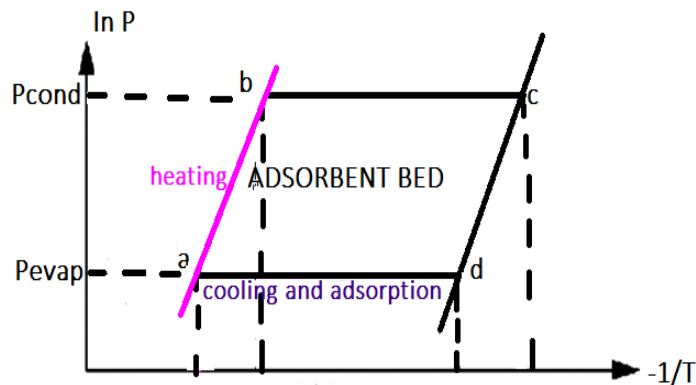


Figure 9.3. The heating process of the adsorption heat pump cycle on the Clapeyron Diagram.

Step 3: Isobaric Desorption Process:

The next process is isobaric desorption process. The valve between the adsorbent bed and condenser is opened. Desorption process is started and water vapor is condensed in the condenser, when the pressure of the cycle is constant. The fan on the condenser works during the desorption to cooling for condensing of water vapor. The condenser chamber fills with the condensed water that remove from the silica gel particles during the desorption in the condenser. The temperature of the adsorbent bed begins to increase at constant pressure and the adsorbent bed reaches 60-65°C. As can be seen from Figure 8.4, the desorption process actualizes at the constant pressure when the adsorbent temperature increases.

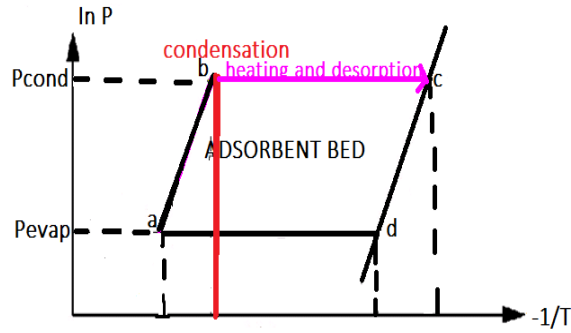


Figure 9.4. The desorption period of the adsorption heat pump cycle on the Clapeyron Diagram.

Step 4: Isostatic Cooling Process:

At the end of desorption, the adsorbent bed has high temperature and pressure conditions. The valve between the condenser and adsorbent bed is closed and the temperature of the adsorbent bed (T_c), which is the maximum temperature of the adsorbent bed are decreased to the evaporator conditions as can be seen in Figure 9.5.

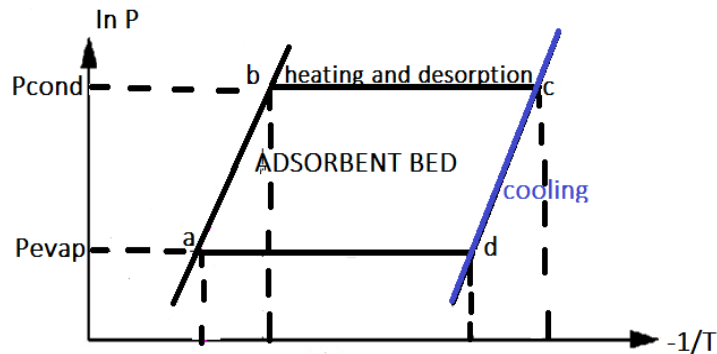


Figure 9.5. The cooling process of the adsorption heat pump cycle on the Clapeyron Diagram.

9.3. The Performance Calculation of the Experiments for the Adsorption Heat Pump Setup

Adsorption heat pumps experiments with different cycle time were performed. SCP (Specific Cooling Power) and COP (Coefficient of Performance) values were calculated. The experiments are given in details below.

SCP value is found using the following equation:

$$SCP = \frac{Q_{evap}}{m_{silica} \Delta\tau} \quad (9.1)$$

Q_{ev} , m_{silica} , $\Delta\tau$ represents the heat withdrawn from the evaporator, the mass of silica gel and the duration of the cycle. A high value is desired SCP. High SCP value shows ability to create a high cooling effect in a short time with a little mass of silica gel.

The COP value is found using the following equation:

$$COP = \frac{Q_{evap}}{Q_{heating}} \quad (9.2)$$

Q_{evap} and $Q_{heating}$ are the amount of heat supplied to the evaporator and the heat is given to the adsorbent bed. The cooling capacity is found using the following equation:

$$Cooling\ capacity = \frac{Q_{evap}}{\Delta\tau} \quad (9.3)$$

9.4. The Tests of the First Adsorption Heat Pump Setup

The connections of the pressure gauge on the heat pump with computers is provided with a data logger and PCI cards. Temperature measurements are done with using the E-680 datalogger software. And the computer connection are completed and operation of the first measurements made on and measuring devices are tested. The results section for the experiments can be started with the illustration of the leakage rate versus time (Figure 9.1). After leakage test, the calibration of temperature measuring device provided it is done. Experiments were initiated after the completion of the control of the measuring device. All these steps are described in detail below.

9.4.1. The Leakage Test of the Adsorption Heat Pump

Even though the experimental setup was designed and constructed to work under vacuum, many leakage problems were observed. So leakage tests are must be done on the adsorption heat pump setup before starting the experiments. The adsorption experiments could not be performed with this leakage rate, thus some further improvements were done to reduce leakage. After improvement, the leakage test repeated to resolve, completely. The valves that are located between the evaporator with the adsorbent bed and the condenser with the adsorbent bed are closed for vacuuming to test the leakage of the adsorption heat pump setup. The Genidaq Software is used to

take pressure data during the vacuuming of this system. The data are transferred to the computer to collect. At the first step, there was leak on the adsorption heat pump setup. To determine where the leak is, soapy water test is done on the setup. Based on experimental observations, the most important leakage problem occurs from thermocouple jacks, connections of the valves and the welding points on the adsorbent bed. So the connections and the adsorbent bed were covered with a red silicone sealant (Loctite Co.) which has thermally resists up to 300°C is used to overcome the leak of the system, several times. As a result of the leakage rate was found only 1 kPa/24 hours from all of the setup and the leakage test is completed. The results of the tests are listed and the pressure values according to time of the adsorption heat pump setup during the vacuuming are plotted.

- **Test 1:** The adsorption heat pump setup is under vacuuming during 16 hours for the first leakage test. The data that are collected through this test with help of the pressure gauges on the setup. The first test results showed that there are leaks in the system. An attempt was done to determine the location of the leak (Figure 9.6 - Date of 1.Test: 21.11.2014).
- **Test 2:** After eliminating some leaks detected in the initial test results, the adsorbent bed stays during the 4 days under vacuum. The results obtained by closing the vacuum pump still showed that the current leakage (Figure 9.6 - Date of 2.Test: 26.11.2014)
- **Test 3:** The third leakage test continue with giving hot water to the adsorbent bed. The hot water gives from the hot water bath to the adsorbent bed under the vacuum during 4 days again. After eliminating the detected leakage in the system, after 8 hours that are the under the vacuum have been found to continued leakage in the adsorbent bed as shown in Figure 9.6. (Figure 8.6 - Date of 3.Test: 29.11.2014).
- **Test 4:** Substantially leak has been corrected prior to testing, but there is still leakage, as shown in Figure 8.6. After this test, leakage is determine on the evaporator and is fixed (Figure 9.6 - Date of 4.Test: 02.12.2014).
- **Test 5:** 5. Leakage test was performed on the adsorption heat pump setup, again to eliminate completely. There are leaks in the system, still. To provide vacuum in the adsorbent bed has an important role for an adsorption heat pump, as said in Chapter 2 (Figure 9.6 - Date of 5.Test: 03.12.2014)

- **Test 6:** 6. Leakage test was performed on the adsorption heat pump setup. There are leaks on the cooling pipes where is under the adsorbent bed leak is fixed with the help of red silicon (Figure 9.6 - Date of 6.Test: 04.12.2014)
- **Test 7:** In this test, the leakage on the connection between adsorbent bed and condenser is fixed (Figure 9.6 - Date of 7.Test: 08.12.2014)
- **Test 8:** The leaks are corrected leaks in the bed, condenser and evaporator, completely after this experiment (Figure 9.6 - Date of 8.Test: 12.12.2014).

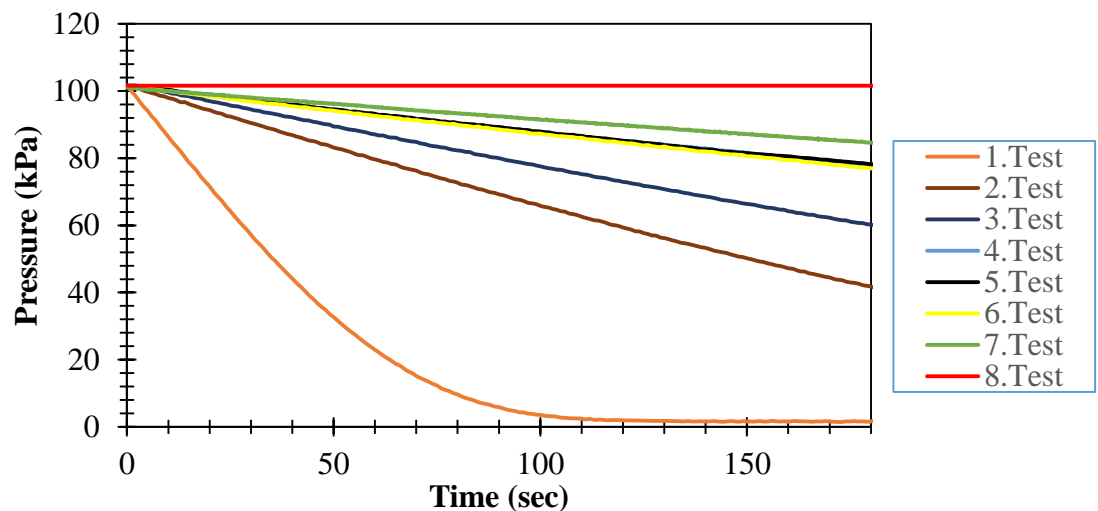


Figure 9.6. Leakage test results.

9.4.2. The Calibration Test Results of the Measurement Devices on the Adsorption Heat Pump Setup

E-680 data logger and its software was used in order to get results from the Pt-100 resistance thermometers on the adsorbent bed, condenser and evaporator for temperature measurement. The calibration of thermometers were done with following method that is explained, carefully. The method is collecting instant temperature measurements from a thermometer besides of E-680 that connected to Pt-100 to compare these results. X-axis is the temperature values that are measured by the thermometer. Y-axis is the temperature values that are measured by Pt 100 resistance thermocouples. Calibration test results are shown in Figure 9.7.

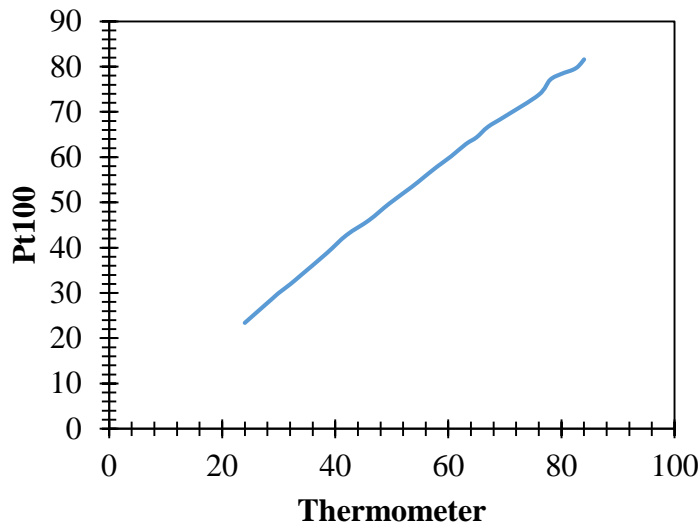


Figure 9.7. Calibration test results of the Pt-100 thermocouples.

9.4.3. The Results of the Experiments of the First Adsorption Heat Pump Setup

The adsorption heat pump experiments were performed on the constructed setup which was explained in details in this Chapter. The measured temperature and pressures were logged by data loggers and software. The related diagrams were plotted and illustrated via diagrams. The experiments which were done are quotable. Even many experiments were done to determine the optimum conditions, the temperature and pressure variations are plotted only for three of them. The experimental part of this study is performed with two constructed experimental setups. A lot of experiments are done with the first experimental setup for operating different cycle time. On the design and equipments of first setup were changed to increase the performance of the adsorption heat pump. Therefore the experimental procedure was not changed after revision. The revised setup with its components is explained in details in Chapter 8.

The three experiments that were performed for operating different cycle time with the first experimental setup are below. Some decisions are determined as a result of these experiments by using the first experimental setup. Revisions can be done on the first adsorption heat pump setup to get more productive results such as high COP and SCP. The results of the revised experimental setup are given in next Section 9.5.

9.4.3.1. The Results of the First Experiment on the Adsorption Heat Pump Setup

The results of the experimental study are presented by the graphs. X-axis is the time and Y-axis is temperature or pressure in all plots. The experiments were performed to investigate the effect of cycle time on the adsorption heat pump performance.

Experiment 1:

In this experiment, 3 hours adsorption / desorption processes were occurred. The heating and cooling processes are in a total of 1.5 hours. Therefore, adsorption heat pump cycle is completed 7.5 hours. 4.3 cm of water is vaporized in the evaporator during the adsorption process and 2 cm of water vapor is condensed in the process of desorption. Obtained in this experiment COP, SCP and cooling capacity are found as 0.82, 8.614 and 34 W using the equations as given 9.1, 9.2, and 9.3. The adsorption cycle of four thermodynamic steps (isobaric adsorption, isosteric heating, isobaric desorption and isosteric cooling) is presented by Clapeyron diagram, as shown in Figure 9.8 (c). Furthermore, temperature and pressure changes are measured during all processes for evaporator, adsorbent bed and condenser as shown in Figures 9.8 (a) and (b), respectively.

In Figure 9.8 (a) temperature decreases at the constant pressure in the adsorbent bed throughout adsorption process from 51°C to 24°C. And then the adsorbent bed is heated to increase temperature and pressure when all valves are closed between adsorbent bed, evaporator and condenser. The bed temperature reaches to the 60°C after heating process. And the pressure of the adsorbent bed increase from 2.604 to 4.527 kPa. The temperature of the adsorbent bed enhances from 60°C to 65°C with the heat that is given by the water bath at the constant pressure. In the isobaric desorption process, the water vapor starts to leave from the silica gel particles in the adsorbent bed, it is called as desorption. The water vapor is condensed in the condenser tubes by help of the fan on the condenser. And then the cooling process is started on the adsorbent bed by natural convection to turn evaporator conditions.

Figure 9.8 (a) shows that the variation of the temperature of evaporator, condenser and adsorbent bed for each process of adsorption heat pump cycle. The change of pressure of evaporator, condenser and adsorbent bed for all processes is also given in Figure 9.8 (b). The Clapeyron diagram of the adsorbent bed is presented in

Figure 9.8 (c). The X-axis is given as logarithmic pressure and the Y-axis is a function of temperature as $-(1/T)$.

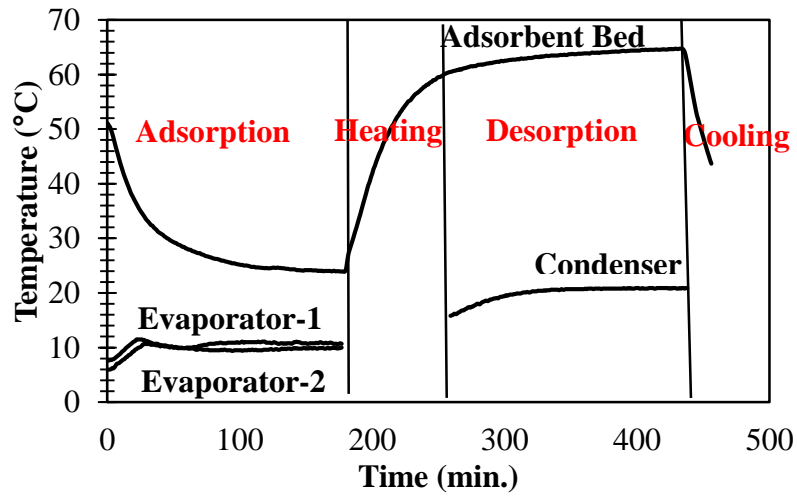


Figure 9.8. a) Temperature variation of the adsorbent bed, evaporator and condenser during the adsorption and desorption processes.

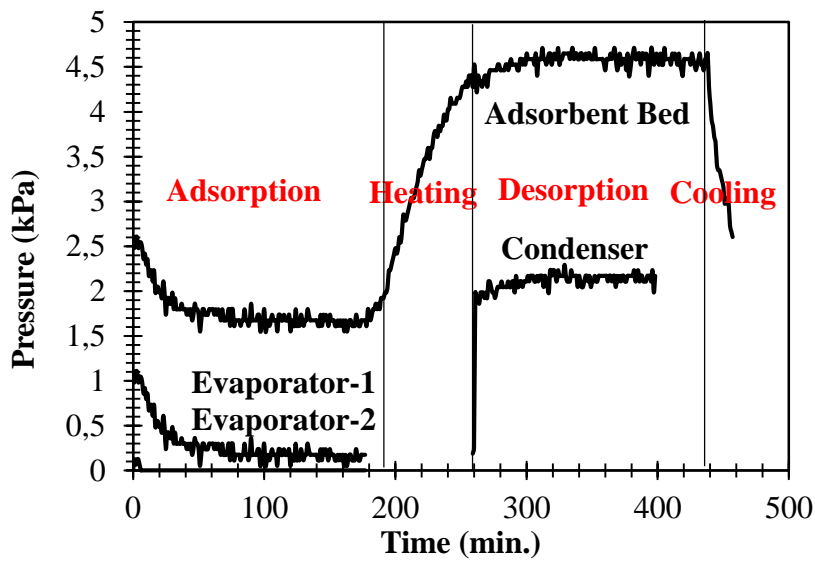
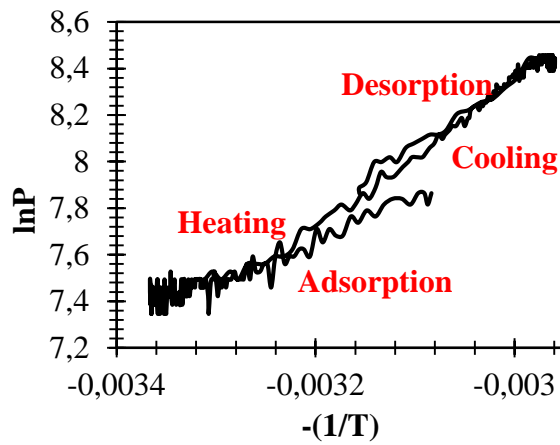


Figure 9.8. b) Pressure variation of the adsorbent bed, evaporator and condenser during the adsorption and desorption processes.



	Adsorbent Bed	
	Temperature (°C)	Pressure (kPa)
Adsorption	51.15	2.604
Heating	24.15	2.736
Desorption	60.55	4.527
Cooling	65	4.589

Figure 9.8. c) Clapeyron Diagram of the adsorbent bed with the operation temperature and pressure values of the adsorbent bed.

Experiment 2:

This duration of this experiment is 23.5 hours as 6 hours adsorption, 16 hours desorption and the heating and cooling processes are in a total of 1.5 hours. The amount of absorbed water in the silica gel particles is 3.5 cm of water and 2 cm of water vapor is condensed in the desorption process. The COP, SCP and cooling capacity are calculated as 0.778, 2.237, and 9 W. In the experiment pressure and temperature variations are presented in the adsorbent bed on the Clapeyron diagram as shown in Figure 8.9 (c). The temperature and pressure changes are saved for evaporator, adsorbent bed and condenser duration of the adsorption cycle process as shown in Figures 9.9 (a) and (b).

At the start of adsorption process, the temperature of adsorbent bed decreases from 49°C to 20°C. Then the adsorbent bed temperature reaches to the 60°C and the pressure increase from 3.659 to 5.783 kPa at the end of heating process. The temperature of the adsorbent bed is enhanced from 60°C to 65°C as a result of isobaric desorption process. Figure 9.9 (a) shows that the variation of the temperature of evaporator, condenser and adsorbent bed for all processes of adsorption heat pump cycle. The change of pressure of evaporator, condenser and adsorbent bed for all processes is also given in Figure 9.6 (b). The Clapeyron diagram of the adsorbent bed is presented in Figure 9.6 (c).

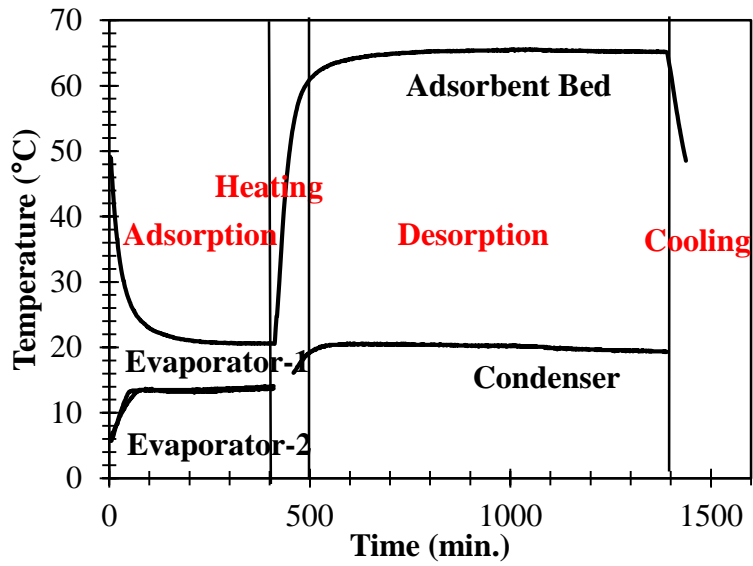


Figure 9.9. a) Temperature variation of the adsorbent bed, evaporator and condenser during the adsorption and desorption processes.

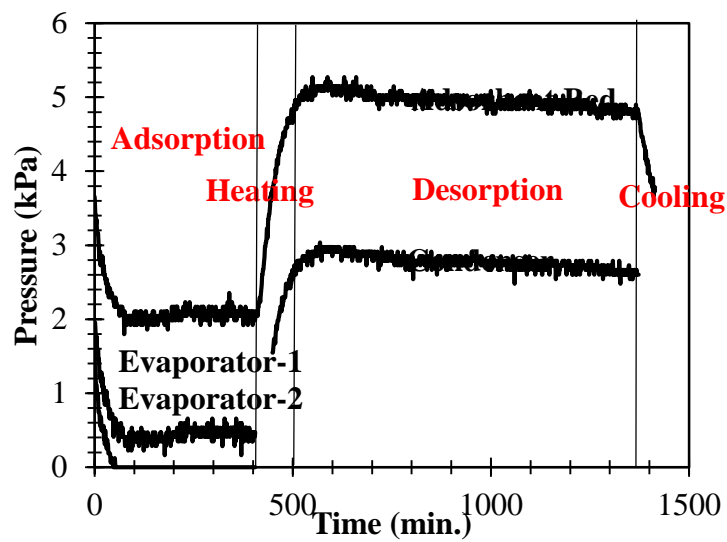


Figure 9.9. b) Pressure variation of the adsorbent bed, evaporator and condenser during the adsorption and desorption processes.

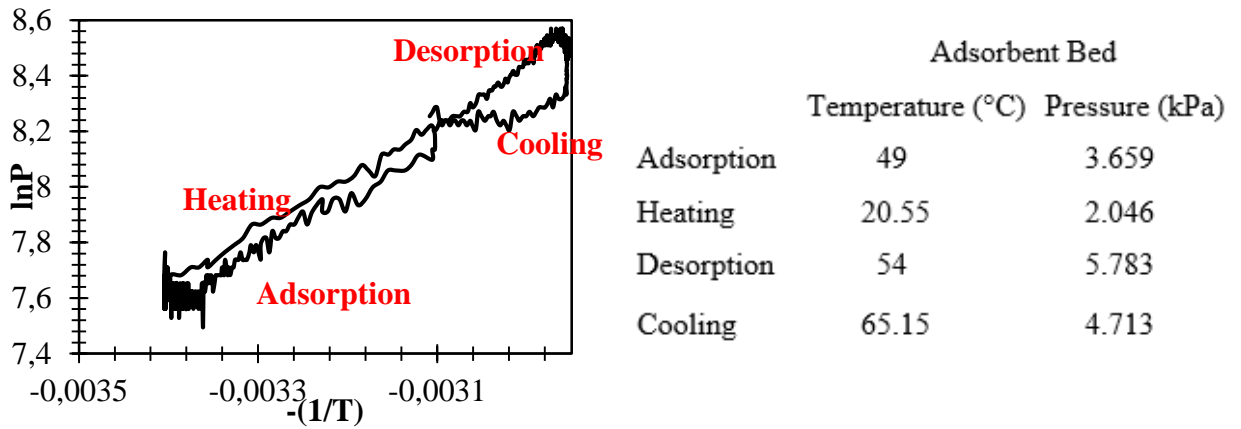


Figure 9.9. (c) Clapeyron Diagram of the adsorbent bed with the initial conditions of each process for the adsorbent bed.

Experiment 3:

In this experiment, 24 hours adsorption / desorption processes were carried out. The duration of heating and cooling processes are 1.5 hours, totally. The adsorption experiment is performed throughout 49.5 hours. COP, SCP and cooling capacity are found as 0.891, 3.642 and 14 W, also. The Clapeyron diagram of the adsorption cycle of this experiment is plotted as Figure 9.10 (c). Furthermore, the variation of pressure and temperature in the adsorbent bed for evaporator, adsorbent bed and condenser during all processes, as shown in Figures 9.10 (a) and (b).

In Figure 9.10 (a) temperature decreases in the adsorbent bed during adsorption process from 49°C to 22°C. For the next step, the adsorbent bed is heated to 60°C with the help of water bath. The temperature of the adsorbent bed increases to 65°C at the constant pressure for desorption. In the desorption process, the water vapor starts to leave from the silica gel particles in the adsorbent bed as the amount 12 cm and the water vapor is condensed in the condenser during desorption as measured 10 cm at the end of process. And then the temperature and pressure goes down to return evaporator conditions. Figure 9.10. (a) is presented the variation of the temperature of evaporator, condenser and adsorbent bed of adsorption heat pump cycle for adsorption cycle processes. In Figure 9.10 (b) the variation of pressure of evaporator, condenser and adsorbent bed is shown. Figure 9.10 (c) gives the Clapeyron diagram of the adsorbent bed as X-axis is logarithmic pressure and Y-axis is $-(1/T)$.

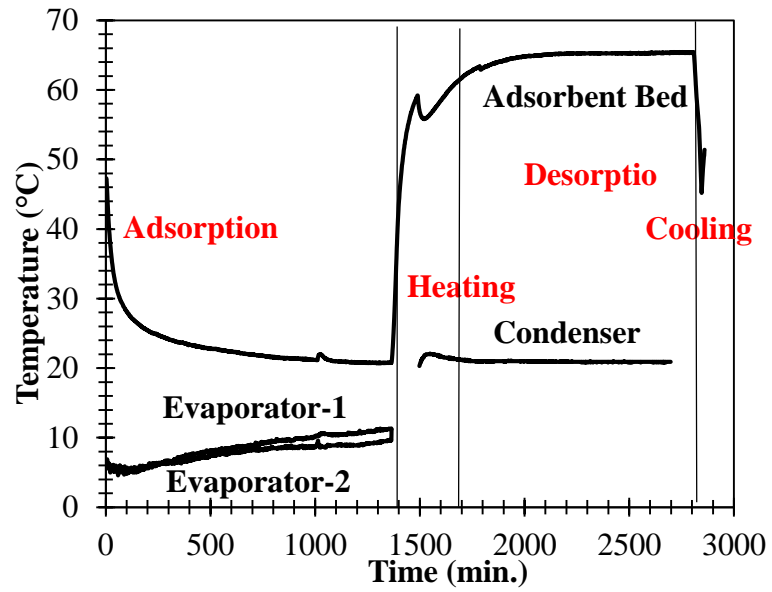


Figure 9.10. a) Temperature variation of the adsorbent bed, evaporator and condenser during the adsorption and desorption processes.

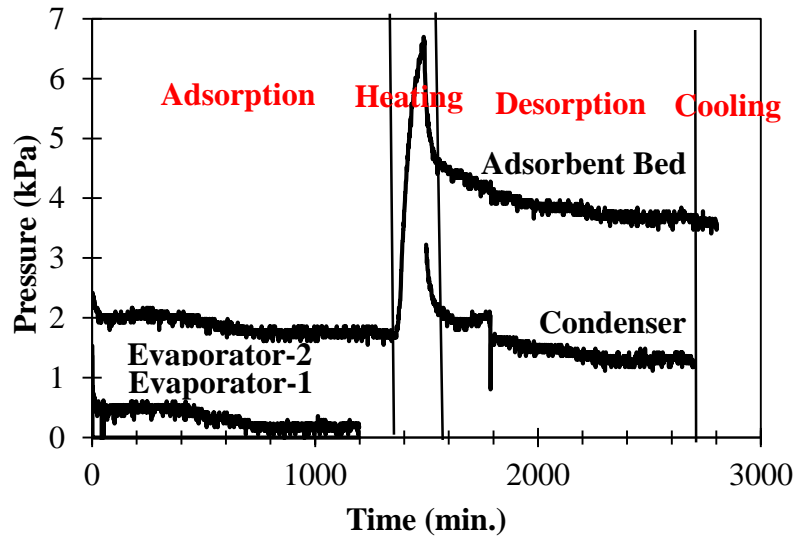


Figure 9.10. b) Pressure variation of the adsorbent bed, evaporator and condenser during the adsorption and desorption processes.

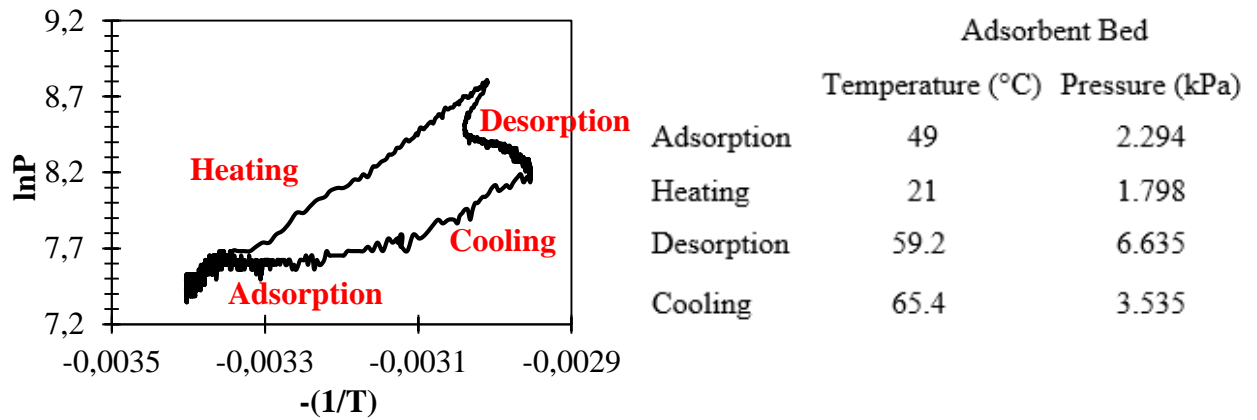


Figure 9.10. (c) Clapeyron Diagram of the adsorbent bed with the initial conditions of each process for the adsorbent bed.

9.5. The Results for Revised Setup

The modifications on the first constructed adsorption heat pump setup was occurred that given in this section. The modifications are listed as below.

- The high pressure drop that occurs on the evaporator pipe that connects to the adsorbent bed is one of the problem of first experimental setup. In the adsorption process, the water evaporates in the evaporator and moves on to the adsorbent bed. The high pressure drop in the pipe due to be long and thin, the water cannot be adsorbed by the silica gel particles in the adsorbent bed. The solution of this problem is shortening the pipe that connects adsorbent bed and evaporator.
- Another important issue is the size of mesh pipes inside of the adsorbent bed for making easier water vapor passing to the condenser. The pipes size was changed because the size of the first one is not suitable for water vapor passing. This situation was understood after experimental observations. The small changes on the design and equipments of setup were changed, therefore the experimental procedure was not changed after revision.

9.5.1. The Tests of the Revised Adsorption Heat Pump Setup

The leakage test is done to control vacuum of the revised adsorption heat pump before to start the experiments. After the leakage test was completed, the experiments with the same cycle time that were performed on the first adsorption heat pump set up. The results of the experiments that were performed on the first experimental setup and on the revised experimental setup are compared with each other. The aim of this comparison is to see improvements by revision. The leakage test and the experiments are presented in this section in depth.

9.5.1.1. The Leakage Test of the Revised Adsorption Heat Pump Setup

Figure 8.11 shows the results of the leakage tests on the revised adsorption heat pump. To overcome the air leakage in the first setup, the resistance thermometers cable ports and pressure gauge jacks which are coming out of the adsorbent bed, evaporator and condenser were covered with a red silicone sealant (Loctite Co.) which has thermally resists up to 300°C. As a result of the insulation for the first setup, the leakage rate was found only 1 kPa/8 hours of the revised setup. The final view of the experimental setup is illustrated in Figure 8.11.

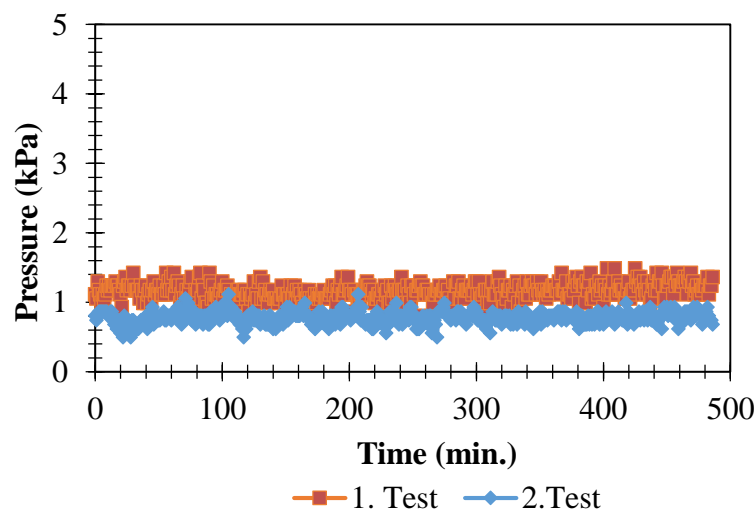


Figure 9.11. The leakage test results of the revised adsorption heat pump setup.

The experiments that have duration adsorption/desorption process is 3 hours, 24 hours and 6 hours adsorption/ 16 hours desorption is performed again on the revised setup to compare the first results of the first experimental setup.

Experiment 1:

The first experiment of the revised setup has same conditions as cycle time, working temperatures of cycle with the first experiment of the first setup. The duration of this experiment is 7.5 hours as 6 hours adsorption, 16 hours desorption and the heating and cooling processes are in a total of 1.5 hours. The amount of absorbed water in the silica gel particles is 4.7 cm of water and 4 cm of water vapor is condensed in the desorption process. The COP, SCP and cooling capacity are calculated as 0.841, 9.629 and 38.5 W. The enhancement ratio of the cooling capacity and SCP is 60% according to the first setup experiment that has same cycle time. 8% is the percentage increase of the COP when first setup COP result and revised setup COP result compare.

The variation of temperature and pressure and the Clapeyron Diagram are presented with the first results. The black lines belong to the first setup and the red lines are belong to the revised setup. In the experiment pressure and temperature variations are presented in the adsorbent bed on the Clapeyron diagram as shown in Figure 9.11 (c). The temperature and pressure changes are saved for evaporator, adsorbent bed and condenser duration of the adsorption cycle process as shown in Figures 9.11 (a) and (b). The change of pressure of evaporator, condenser and adsorbent bed for all processes is also given in Figure 9.11 (b). The Clapeyron diagram of the adsorbent bed is presented in Figure 9.11 (c).

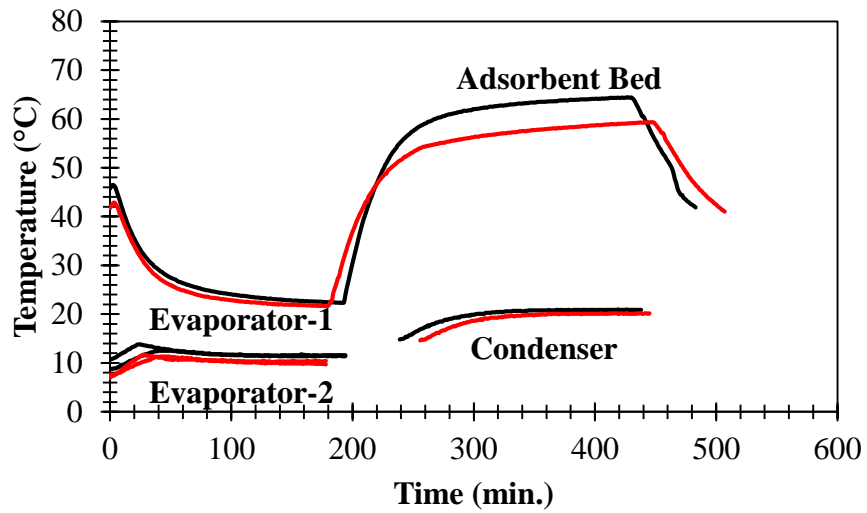


Figure 9.12. a) Temperature variation of the adsorbent bed, evaporator and condenser during the adsorption and desorption processes.

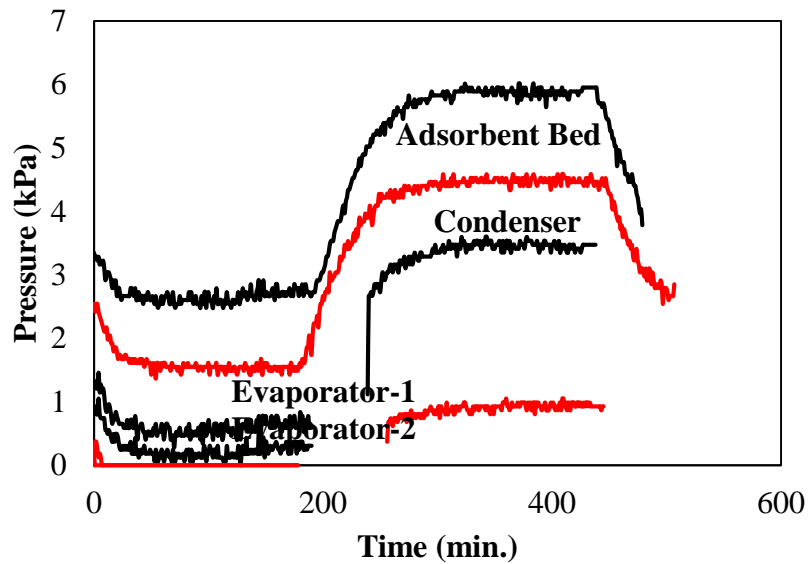
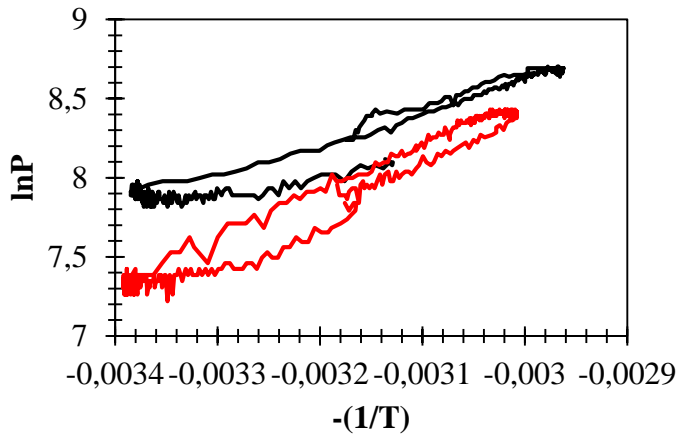


Figure 9.12. b) Pressure variation of the adsorbent bed, evaporator and condenser during the adsorption and desorption processes.



	Adsorbent Bed	
	Temperature (°C)	Pressure (kPa)
Adsorption	41.75	2.542
Heating	22	1.612
Desorption	55	4.527
Cooling	60	4.659

Table 9.12. (c) Clapeyron Diagram of the adsorbent bed with initial conditions of each process for the adsorbent bed.

Experiment 2:

In the experiment 2, the cycle time is of this experiment is 23.5 hours as 6 hours adsorption, 16 hours desorption and the heating and cooling processes are in a total of 1.5 hours. The amount of absorbed water in the silica gel particles is 5 cm of water and 6 cm of water vapor is condensed in the desorption process. The COP, SCP and cooling capacity are calculated as 0.810, 3.06 and 12 W. In the experiment pressure and temperature variations are presented in the adsorbent bed on the Clapeyron diagram as shown in Figure 9.12 (c). The temperature and pressure changes are saved for evaporator, adsorbent bed and condenser duration of the adsorption cycle process as shown in Figures 9.6 (a) and (b). Figure 9.12 (a) shows that the variation of the temperature of evaporator, condenser and adsorbent bed for all processes of adsorption heat pump cycle. The change of pressure of evaporator, condenser and adsorbent bed for all processes is also given in Figure 9.12 (b). The Clapeyron diagram of the adsorbent bed is presented in Figure 9.12 (c). 400% 39%

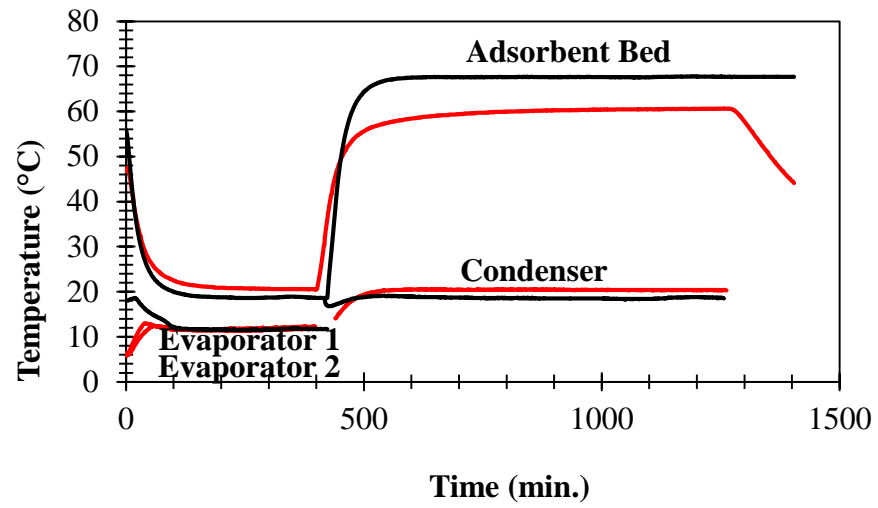


Figure 9.13. a) Temperature variation of the adsorbent bed, evaporator and condenser during the adsorption and desorption processes.

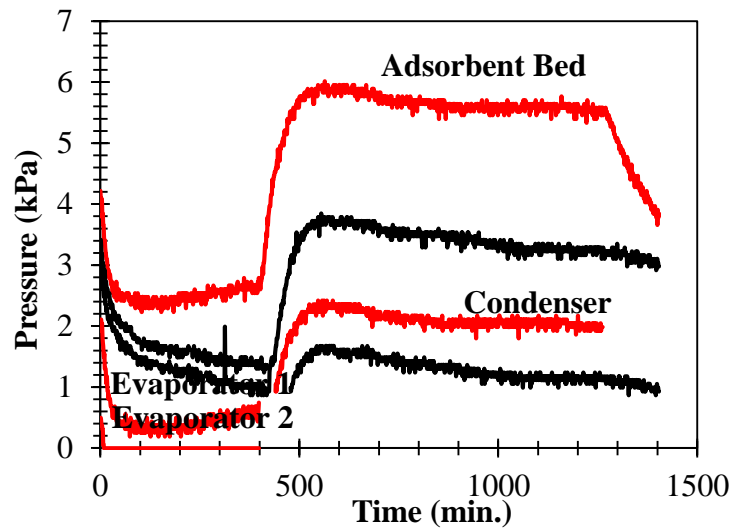
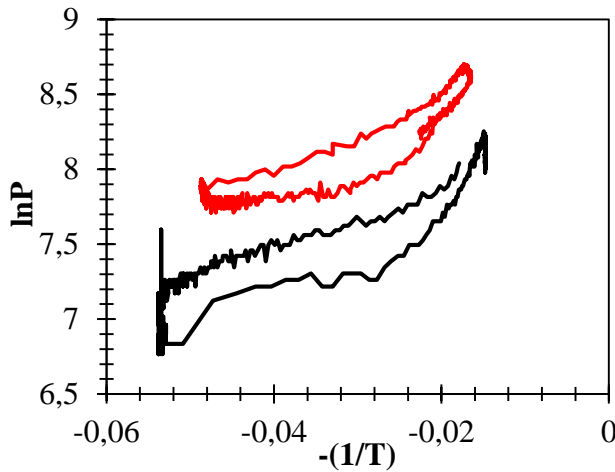


Figure 9.13. b) Pressure variation of the adsorbent bed, evaporator and condenser during the adsorption and desorption processes.



	Adsorbent Bed	
	Temperature (°C)	Pressure (kPa)
Adsorption	46.75	4.217
Heating	22	2.667
Desorption	58	5.923
Cooling	61	5.705

Figure 9.13. (c) Clapeyron Diagram of the adsorbent bed with the initial conditions of each process.

Experiment 3:

This duration of this experiment is 49.5 hours as 24 hours adsorption/desorption and the heating and cooling processes are in a total of 1.5 hours. The amount of absorbed water in the silica gel particles is 20 cm of water and 2 cm of water vapor is condensed in the desorption process. The COP, SCP and cooling capacity are calculated as 0.778, 2.237 and 9 W. In the experiment pressure and temperature variations are presented in the adsorbent bed on the Clapeyron diagram as shown in Figure 9.13 (c). The temperature and pressure changes are saved for evaporator, adsorbent bed and condenser duration of the adsorption cycle process as shown in Figures 9.13 (a) and (b). Figure 9.13 (a) shows that the variation of the temperature of evaporator, condenser and adsorbent bed for all processes of adsorption heat pump cycle. The change of pressure of evaporator, condenser and adsorbent bed for all processes is also given in Figure 9.13 (b). The Clapeyron diagram of the adsorbent bed is presented in Figure 9.13 (c). 70% 1.8%

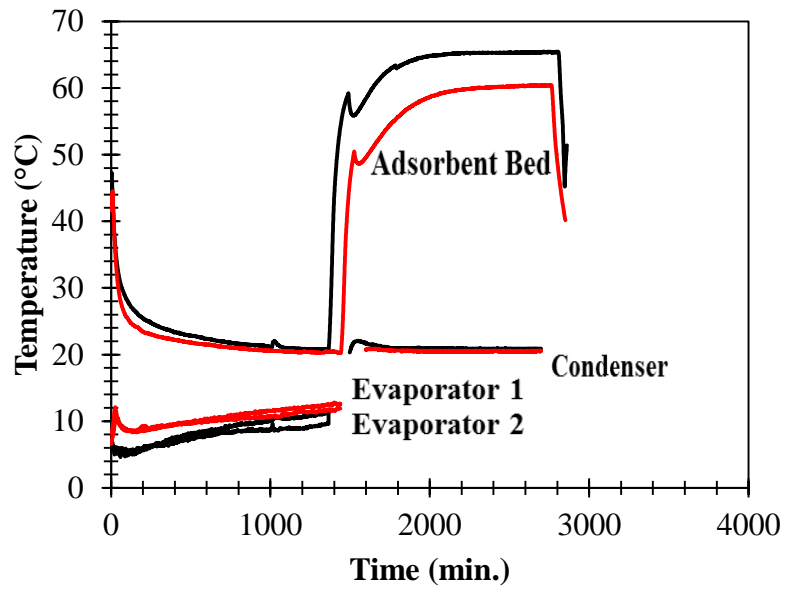


Figure 9.14 a) Temperature variation of the adsorbent bed, evaporator and condenser , during the adsorption and desorption processes.

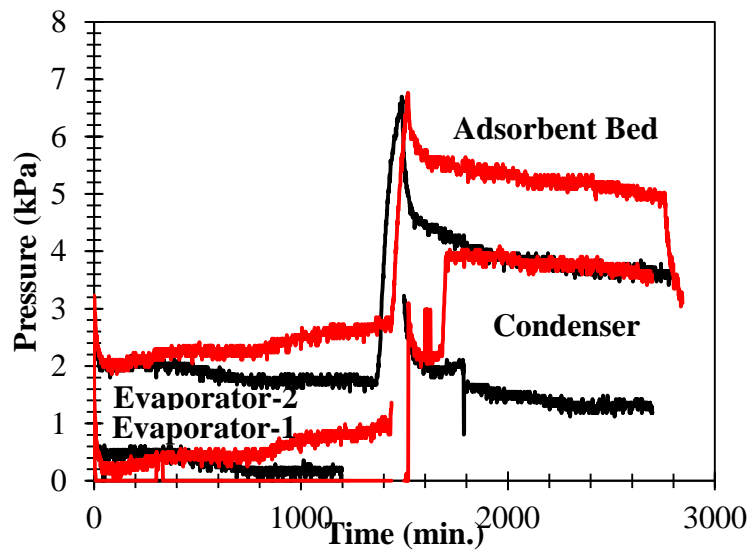


Figure 9.14. b) Pressure variation of the adsorbent bed, evaporator and condenser during the adsorption and desorption processes.

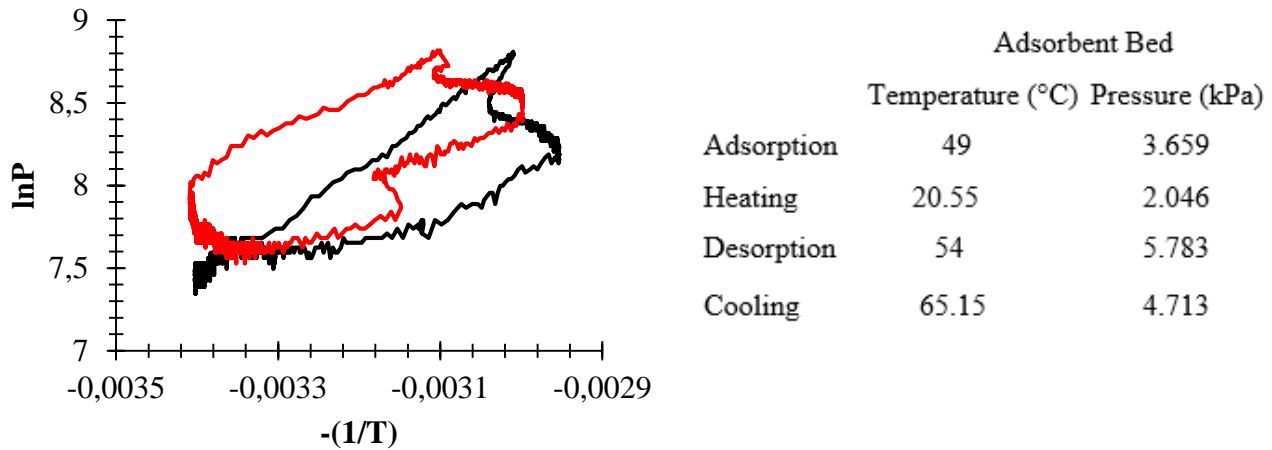


Figure 9.14. (c) Clapeyron Diagram of the adsorbent bed.

In table 9.1 the amount of adsorbed water during the adsorption, desorbed water vapor from the silica gel during the desorption process, the water mass besides of the cooling capacity that is taken from the experiment, COP and SCP are given to compare other experiments which have different cycle time. According to the achieved results as a consequence of these experiments, to revise the first experimental setup makes a progress. In Table 9.1 the obtained results from the second experimental setup is written in bold.

Table 9.1. The comparison of obtained results from the first experimental setup and second experimental setup.

	Ads. Time (hour)	h_{evap} (cm)	Des. Time (hour)	h_{cond} (cm)	Water mass (kg)	Cooling Capacity (W)	COP	SCP (W/kg)
Exp.1	3	4.3	3	2	0.372	34	0.82	8.61
Exp.1	3	4.7	3	4	0.406	38.5	0.84	9.62
Exp.2	6	3.5	16	2	0.303	9	0.77	2.23
Exp.2	6	5	16	6	0.432	12.26	0.81	3.06
Exp.3	24	12	24	10	1.038	14.57	0.89	3.64
Exp.3	24	20.5	24	21	1.774	24.8	0.91	6.22

The consumed work, cooling capacity and COP values of the domestic type refrigerator for 20 °C ambient temperatures are presented in the Table 9.1. Table 9.1 represents the results for first experimental setup and revised experimental setup. Hence, the results have an improvement after revision of first experimental setup.

The contribution of the suggested adsorption heat pump to the performance of a household refrigerator is calculated with using the results of the revised experimental setup. The cycle period is taken as 1 hour and an experiment was done with the revised experimental setup.

Experiment 4:

This duration of this experiment is 1 hours as 20 minutes adsorption/desorption and the heating and cooling processes are in a total of 10 minutes. The amount of absorbed water in the silica gel particles is 1 cm of water and 0,3 cm of water vapor is condensed in the desorption process. The COP, SCP and cooling capacity are calculated as 0.611, 15.025 and 60 W. In the experiment pressure and temperature variations are presented in the adsorbent bed on the Clapeyron diagram as shown in Figure 9.14 (c). The temperature and pressure changes are saved for evaporator, adsorbent bed and condenser duration of the adsorption cycle process as shown in Figures 9.14 (a) and (b). Figure 9.14 (a) shows that the variation of the temperature of evaporator, condenser and adsorbent bed for all processes of adsorption heat pump cycle. The change of pressure of evaporator, condenser and adsorbent bed for all processes is also given in Figure 9.14 (b). The Clapeyron diagram of the adsorbent bed is presented in Figure 9.14 (c).

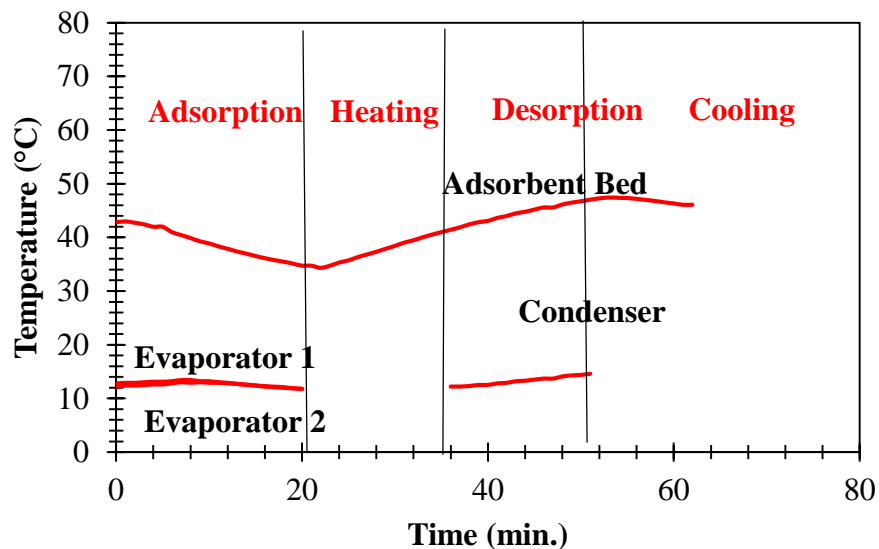


Figure 9.15. a) Temperature variation of the adsorbent bed, evaporator and condenser during the adsorption and desorption processes.

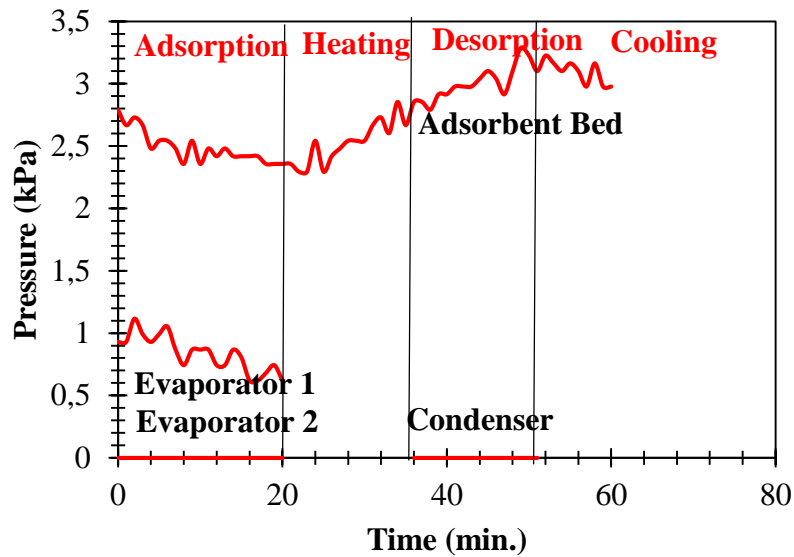


Figure 9.15. b) Pressure variation of the adsorbent bed, evaporator and condenser during the adsorption and desorption processes.

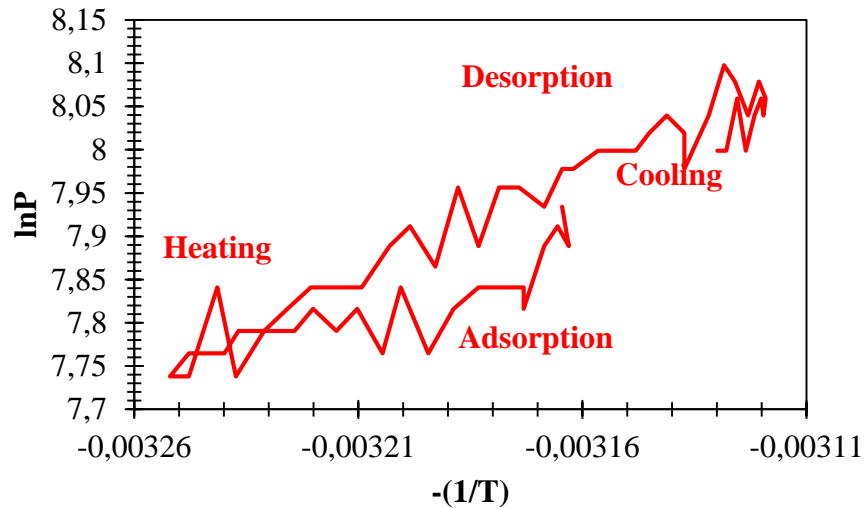


Figure 9.15. (c) Clapeyron Diagram of the adsorbent bed.

In table 9.2 the contribution of the suggested hybrid system on the performance of a household refrigerator is calculated when ambient temperature is 20°C. Table 9.2 presents the enhancement of performance of a household refrigerator with using an adsorption heat pump. Figure 3 illustrates the compressor outlet temperature of the refrigerant when the compressor is on or off. The compressor of a household refrigerator starts to work while the temperature of the cabinet of the refrigerator drops to a higher specified temperature. Similarly, when the temperatures of the inner cabinets of the refrigerator reach to the lower specified temperature, compressor stops. The period of on and off of the compressor changes by the inner set temperature of the cabinets, type of the refrigerator, type of compressor etc. Based on the performed

experimental data, the period of on and off of the compressor were taken 30 min and 35 min in this study, respectively. Based on this information, the heat of evaporation is calculated for a household refrigerator according to the different working periods. The heat of evaporation is calculated for adsorption cycle for the duration of adsorption is 20 minutes, 3 hours, 6 hours and 24 hours. The coefficient of performance of a household refrigerator improve by using an adsorption heat pump as seen from Table 9.2.

Table 9.2. The contribution of the proposed hybrid system on the performance of a household refrigerator is calculated when ambient temperature is 20°C.

	Q_{evap} (joule)	COP
<hr/>		
Household refrigerator		
(1 hour)	338400	1.68
Adsorption Cycle		
(20 min.)	215000	2.769
		% improvement of COP 64.867
<hr/>		
Household refrigerator		
(6 hours)	2030400	1.68
Adsorption Cycle		
(3 hours)	875000	2.540
		% improvement of COP 51.212
<hr/>		
Household refrigerator		
(12 hours)	4060800	1.68
Adsorption Cycle		
(6 hours)	1080000	2.144
		% improvement of COP 27.627
<hr/>		
Household refrigerator		
(48 hours)	8121600	1.68
Adsorption Cycle		
(24 hours)	4425000	2.616
		% improvement of COP 55.743
<hr/>		

CHAPTER 10

CONCLUSION

In this study, the importance of adsorption heat pump, advantages, and disadvantages with its working principle in detail. The hybrid cooling systems were reviewed according to the classification as single-loop and double-loop hybrid cooling cycle. Numerical studies were performed to investigate the effects on the performance of adsorption heat pumps. Also, an experimental setup was designed and constructed. As a result of this experimental study, the enhancement of performance of a household refrigerator by using an adsorption heat pump is calculated.

Firstly, a hybrid refrigerator system involves of a vapor compression and an adsorption heat pump cycle is studied theoretically. The study is presented in Section 8.1 of this thesis. The following remarks can be concluded in accordance with the performed numerical study based on designing a bed for utilization of heat released from hot gas and condenser;

- The adsorption heat pump cycle is combined by vapor compression cycle to utilize heat which is released by the condenser. Hence, the cooling effect and consequently the COP value of the vapor compression system are improved.
- The system includes two separate refrigeration cycles. For the vapor compression system, the refrigerant is R600a and the silica gel-water pair is used for the adsorption heat pump cycle. For the low ambient temperatures up to 35°C, the suggested hybrid cycle can increase the COP value of the vapor compression refrigerator from 33 to 21%.
- However, further studies with different type of adsorbent –adsorbate pairs should be performed in order to investigate the improvement of COP by combination of vapor compression and adsorption heat pump cycle.

The heat and mass transfer in a rectangular shape adsorbent bed with silica gel RD–water pair during an adsorption heat pump cycle for different volume fractions aluminum additive is numerically studied by using Comsol software. The study is

presented in Section 8.2 of this thesis. The following remarks can be concluded from the performed study;

- The adsorbent bed design is in rectangular box shape and the heat and mass transfer equations are written in two dimensional Cartesian coordinate system with metal additive.
- The aim of the present study is to analyze the heat transfer rate through a granular adsorbent bed by addition of metal pieces. The use of metal additives enhances the heat transfer rate inside of the adsorbent bed. But the increase of volume fraction of metal additives should be considered well due to reduction of silica gel by increasing of metal additive amount.
- The reduction of silica gel amount causes decrease on SCP based on total mass of the bed. The volume fraction of silica gel-Al mixture have to be optimized by the researchers and optimum weight of the aluminum additive should be considered for the best cooling performance.
- Further studies on the effect of shape and the size of metal additives have to be performed.

The optimum parameters have been investigated to get optimum design for the proposed adsorbent bed by using Taguchi method. Four parameters with three different levels are selected in order to search the optimum design of the adsorbent bed for optimal SCP. Runs and the Taguchi method calculations were performed with Comsol and the Minitab 17.0 software, respectively. The study is presented in Section 8.3 of this thesis. The results of the study can be concluded as follows:

- By using the Taguchi method, the $3^4=81$ runs reduced to 9 runs. In order to optimize parameters for the adsorbent bed, there is no need to run many variations with these parameters. Taguchi method was successfully applied to the present study with limited experiments and in a very short time.
- In order to optimize the SCP with the considered parameters, the optimum design parameters for the considered bed design is found $A_1B_1C_1D_2$ and the

optimum values of the parameters are $L=5$ mm (A_1), $H=5$ mm (B_1), $r_p=0.25$ mm (C_1), $\Delta T=40^\circ\text{C}$ (D_2).

- The contribution analysis showed that, the most effective parameter on the performance of the adsorbent bed is the radius of the adsorbent particle with 40.1%, the second effective parameter is the height of the bed with 25.1% contribution ratio. The temperature difference between adsorbent bed and the ambient temperature has minimum effect on the performance of the adsorbent bed with the contribution ratio of 12.8%.

An experimental work was also performed for silica gel-water. An experimental setup was designed and constructed based on the simulation results. The small leakage rate was achieved for the experimental setup.

- The experiments were performed for the duration of adsorption process is 20 minutes, 3 hours, 6 hours and 24 hours.
- According to the results of revised experimental setup, the coefficient of performance (COP) of a household refrigerator enhances %64 for the duration of adsorption is 20 minutes, %51 for duration of adsorption is 3 hours, %27 duration of adsorption is 6 hours and % 55 duration of adsorption is 24 hours.

REFERENCES

- Banker, N D, Dutta, P, Prasad, M, and Srinivasan K. (2008). Performance studies on mechanical-adsorption hybrid compression refrigeration cycles with HFC 134a. *International Journal of Refrigeration*, Vol. 31, 1398-1406.
- Ben Amar, N., Sun, L.M., Meunier, F., (1996). Numerical analysis of adsorptive temperature wave regenerative heat pump. *Applied Thermal Engineering*, Vol.16, 405-418.
- Bird, B.R., Stewart, E.W., Lightfoot, N.E., (2002). Transport Phenomena, Second edition, John Wiley and Sons Inc., New York, 189–191.
- BSH Bosch und Siemens Hausgeräte GmbH, 81739, München, Federal Republic of Germany, DE102010040085 (2010).
- Cengel Y., and M. A. Boles (2002). Thermodynamics: An engineering approach, McGraw Hill.
- Chua, H.T., Ng, K.C., Chakraborty, N., Oo, M., Othman, A., (2002). Adsorption Characteristics of silica gel-water systems. *Journal of Chemical & Engineering Data*, vol.47, p. 1177-1181.
- Demir, H., Mobedi, M., Ülkü, S., 2008, A review on adsorption heat pump: problems And solutions, *Renewable and Sustainable Energy Reviews*, vol. 12, p. 2381–2403.
- Demir, H., Mobedi, M., Ulku S., (2008). Adsorption heat pumps, difficulties and solution, *Renewable and Sustainable Energy Reviews*, vol. 12, 2381-2403.
- Demir H., Mobedi M., Ulku S., (2009). Effects of porosity on heat and mass transfer in a granular adsorbent bed, *International Communications in Heat and Mass Transfer*, vol. 36: 372–377.
- Demir, H., Mobedi, M., Ulku S., (2010). The use of metal piece additives to enhance heat transfer rate through an unconsolidated adsorbent bed, *International. J. Refrigeration*, vol. 33, 714-720.
- Gundogan C.S., (2014). Determination of characteristics of adsorbent for adsorption heat pumps. Chemical Engineering. İzmir, İzmir Institute of Technology. Master of Science.
- Hau O.B., (2010). Thermodynamic analysis of absorption refrigeration systems (ARS). Chemical Engineering. Malaysia. Bachelor of Science.
- Ilis G. G., Mobedi M., Ulku S., (2010). A parametric study on isobaric adsorption process in a closed adsorbent bed. *International Communications in Heat and Mass Transfer*, vol. 37, 540–547.

- Ilis, G.G., Mobedi, M., Ulku S., (2011). A dimensionless analysis of heat and mass transport in an adsorber with thin fins; uniform pressure approach, *International Communications in Heat and Mass Transfer*, vol. 38, 790–797, 2011.
- Ilis, G. G., Mobedi, M., Ulku S., (2011). A dimensionless analysis of heat and mass transport in an adsorber with thin fins; uniform pressure approach. *International Communications in Heat and Mass Transfer*, vol. 38, 790–797.
- Ilis, G.G., (2012). An experimental and numerical study on heat and mass transfer in adsorbent bed of adsorption heat pump performance. Mechanical Engineering. İzmir, İzmir Institute of Technology. Doctor of philosophy.
- Ilis, G. G., Arslan, G., Mobedi, M., Ulku S., (2013). Study on performance analysis of vapor compression-adsorption hybrid refrigeration cycle, *Climamed'13*, p. 531-539, Istanbul, Turkey.
- Ilis G. G., Mobedi M., Ulku S., (2013). Comparison of Uniform and Non-uniform Pressure Approaches Used to Analyze an Adsorption Process in a Closed Type Adsorbent Bed. *Transport Porous Media* vol. 98, 81–101.
- Ilis, G. G., Arslan, G., Mobedi, M., Ulku S., (2014). Simulation of Heat and Mass Transfer in Adsorbent Bed of Adsorption Heat Pump Operating with Released Heat of a Household Refrigerator, *ISHPC 2014*, Maryland, USA
- Ilis, G. G., Mobedi, M., Ulku S., (2014). Adsorption cycle system for household type refrigerators, Publication No: EP2775236
- Ilis, G. G., Mobedi, M., and Ulku S., 2013b, Hibrit Adsorpsiyon Çevrimi, TPE Patent Application, No. 2013/02766.
- Karger J. and Ruthven M.D. (1992). Diffusion in zeolites and other microporous solids. *A Wiley-Interscience Publications.*, New York.
- Kato Y., Yamashita N., Kobayashi K., Yoshizawa Y., (1996). Kinetic study of the hydration of magnesium oxide for a chemical heat pump, *Applied Thermal Engineering*, vol. 16, 853-862.
- Kawasaki H., Watanabe T., Kanzawa A., (1999). Proposal of a chemical heat pump with paraldehyde depolymerization for cooling system, *Applied Thermal Engineering*, vol. 19, p. 133-143.
- Leong, K.C., Liu, Y., 2004, Numerical study of a combined heat and mass recovery adsorption cooling cycle, *International Journal Heat Mass Transfer*, vol. 47, p. 4761–4770.
- Liu, Y. and K. C. Leong (2006). "Numerical study of a novel cascading adsorption cycle" *International Journal of Refrigeration-Revue Internationale Du Froid*, vol. 9, p. 250-259.

- Li Yong, Sumathy, K., (2004). Comparison between heat transfer and heat mass transfer models for transportation process in an adsorbent bed, *International Commutation Heat Mass Transfer*, vol. 47, p.1587–1598.
- Li Yong and Ruzhu Z. Wang, (2007). Adsorption Refrigeration: A Survey of Novel Technologies, *Recent Patents on Engineering*, vol. 1, p. 1-21.
- Maggio, G., Gordeeva, L.G., Freni, A., Aristov, Y.I., Santori, G., Polonara, F., Restuccia, G., (2009). Simulation of a solid sorption ice-maker based on the Novel composite sorbent “lithium chloride in silica gel pores”, *Applied Thermal Engineering*, vol. 29, p. 1714-1720.
- Marletta, L., Maggio, G., Freni, A., Ingrassiotta, M., Restuccia, G., (2002). A non uniform temperature non-uniform pressure dynamic model of heat and mass transfer in compact adsorbent beds, *International Journal Heat Mass Transfer*, vol. 45, p. 3321-3330.
- Maxwell, J.C., A Treatise on Electricity and Magnetism, Clarendon Press, Oxford, 1873, p. 365.
- Ng, K, Chua, H, Chung, C Y, Kashiwagi, T, Akisawa, A, and Saha B B. (2001). Experimental investigation of the silica gel-water adsorption isotherm characteristic, *Applied Thermal Engineering*, vol. 21, p. 1631-1642.
- NV Philips’ Gloeilampen-fabrieken, (Netherlands), Groenewoudseweg 1, 5621 BA Eindhoven, The Netherlands (1983).
- Pino L., Aristov Yu., Cacciola G., Restuccia G., (1996). Composite materials based on zeolite 4A for adsorption heat pump, vol. 3, p. 33-40.
- Rezk A., Al-Dadah R.K., Mahmoud S., Elsayed A., (2013). Effects of contact resistance and metal additives in finned-tube adsorbent beds on the performance of silica gel/water adsorption chiller, *Applied Thermal Engineering*, vol. 53, p. 278-284.
- Saha, B.B., Chakraborty, A., Koyama, S., Aristov, Y.I., (2009). A new generation Cooling Device employing CaCl₂ in silica gel water system, *International Journal Heat Mass Transfer*, vol. 52, p. 516-524.
- Saha, B. B., K. Habib, I. I. El-Sharkawy and S. Koyama (2009). "Adsorption characteristics and heat of adsorption measurements of R-134a on activated carbon" *International Journal of Refrigeration-Revue Internationale Du Froid* , vol. 32, p. 1563-1569.
- Sun, L.M., Ben Amar, N., Meunier, F., (1995). Numerical study on coupled heat and mass transfers in an adsorber with external fluid heating, *Heat Recovery System*, vol. 15, p.19-29.
- S. Inoue, S. Honda,: JP11211261 (1999).

- Sward, B K and LeVan M D. (1999). Examination of the performance of a compression Driven adsorption cooling cycle, *Applied Thermal Engineering*, vol. 19, p. 21-20.
- Taguchi G., (1987). Taguchi Techniques for Quality Engineering, Quality resources, New York.
- Ulku S., Adsorption Heat Pumps, (1986). *J. Heat Recovery Systems*, vol. 6, p. 277-284.
- Ulku S., Mobedi M., Inan C., (1987). Adsorpsiyonlu Isı Pompaları, vol. 6, p. 989-418, Ankara.
- Ulku, S., Mobedi, M., (1989). Adsorption in energy storage, Proceedings of the NATO Advanced Study Institute on Energy Storage Systems, *Series E., Applied Science*, vol.167, p. 487–507.
- Ulku S., Mobedi M, Adsorption in Energy Storage, (1989). *Energy Storage, Kluwer Academic Pub.*, vol. 167, p. 487-507.
- Ulku S., Mobedi M., Zeolites in Heat Recovery, (1989). *Studies in Surf-Science and Catalysis, Elsevier Science Pub.*, vol.49, Zeolites:Facts Figures Future, p. 511-518,
- Wolf GmbH, 84048, Mainburg, Federal Republic of Germany DE102008057110 (2008).
- Van der Pal, M., A. Wemmers, S. Smeding, V. Jakobert, N. Jan-Aiso Lyclama (2011). Experimental results and model calculations of a hybrid adsorption-compression heat pump based on a roots compressor and silica gel-water sorption, *10th IEA Heat Pump International Heat Pump website Conference*.
- Yıldırım E.Z., (2011). A Study on isotherm characteristics of adsorbent/adsorbate pair used in adsorption heat pump. Energy Engineering. İzmir, İzmir Institute of Technology. Master of Science.
- Zhang, X J and Wang, R Z. (2002). A new combined adsorption-ejector refrigeration and heating hybrid system powered by solar energy, *Applied Thermal Engineering*, vol. 22, p. 1245-1258.

APPENDIX A

TABLE OF PROPERTIES

Table A.1. Thermophysical properties of adsorbent granule and adsorbate considered in the studies as presented in the Chapter 8.

Parameter	Symbol	Value
Molecular weight of water, kg/mol	M	18
Density of adsorbent, kg/m ³	ρ_s	700
Specific heats of adsorbate at 303 K, kJ/kgK	C_{p_w}	4.178
Specific heats of adsorbate at 360 K, kJ/kgK	C_{p_w}	4.203
Specific heats of adsorptive at 303 K, kJ/kgK	C_{p_v}	1.895
Specific heats of adsorptive e at 330 K, kJ/kgK	C_{p_v}	1.911
Specific heats of adsorptive at 360 K, kJ/kgK	C_{p_v}	1.983
Thermal conductivity of adsorbent, kW/mK	λ_s	0.594×10^{-3}
Thermal conductivity of adsorbate, kW/mK	λ_w	1.96×10^{-5}
Heat of adsorption for water on silica gel, kJ/kg	ΔH	2693
Reference diffusivity, m ² /s	D_o	2.9×10^{-4}
Collision diameter for Lennard-Jones Potential, A	σ	2.641
Collision integral	Ω	2.236
Boltzmann's constant, J/K molecule	k	1.38×10^{-23}
Tortuosity	τ	3
Viscosity of water vapor, kN s /m ² at 303 K	μ	9.09×10^{-9}
Viscosity of water vapor, kN s /m ² at 360 K	μ	11.49×10^{-9}

APPENDIX B

DERIVATION OF THE HEAT AND MASS TRANSFER EQUATIONS

In this appendix, heat and mass transfer equations for a rectangular adsorbent bed are derived. The governing equations for the heat and mass transfer for a granular type adsorbent bed are the continuity, Darcy flow and energy equation for the adsorptive, mass transfer equation for the adsorbent particle and ideal gas equation when a non-uniform approach is used. Furthermore, the heat and mass transfer equations for an adsorbent bed single are also derived and presented in this appendix.

The heat and mass transfer equations (which are conservation of mass for adsorbent bed, mass transfer equation for the adsorbent particle, Darcy Law equation for the water vapor velocity in the bed and energy equation) are listed below in detail.

B.1. Derivation of Heat and Mass Transfer Equations for the Annular Adsorbent Bed

The conservation of mass states that the accumulation of mass in a fixed control volume is balanced by the difference between the amount of mass entering and leaving the control volume. It is an expression of a fundamental conservation principle, namely, that of mass conservation. It is a statement that fluid mass is conserved: all fluid particles that flow into any fluid region must flow out. To obtain this equation, we consider a rectangular control volume inside a fluid. Mass conservation requires that the net flow through the control volume is zero. In other words, all fluid that is accumulated inside the control volume and all fluid that is flowing into the control volume must be equal to the amount of fluid flowing out of the control volume.

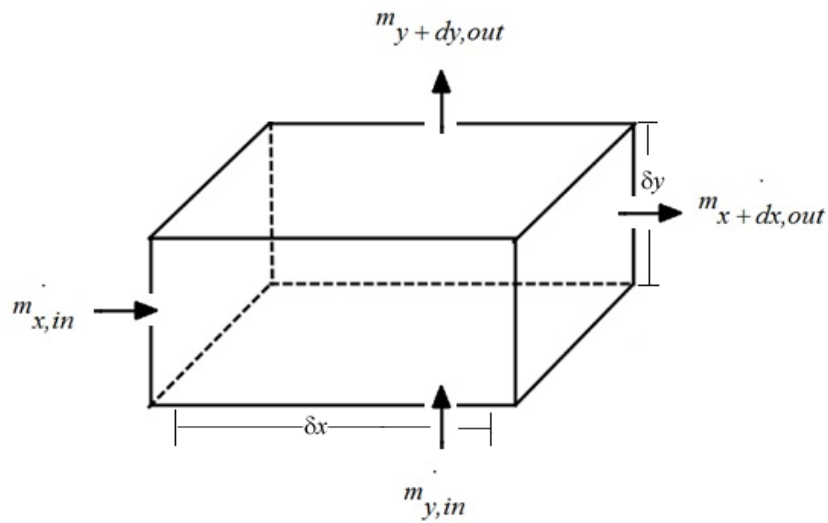


Figure B.1. Control volume for mass balance.

Mass balance of the control volume can be written as:

$$\dot{m}_{x,in} + \dot{m}_{y,in} + \dot{m}_{gen} = \dot{m}_{x,out} + \dot{m}_{y,out} + \dot{m}_{stored} \quad (\text{B.1})$$

The mass flow inlet from the inner x direction surface is:

$$\dot{m}_{x,in} = \rho_v V_x dy \quad (\text{B.2})$$

where V_x is Darcy velocity in x direction.

The mass flow outlet from the outer x direction surface ($x+dx$) is:

$$\dot{m}_{x,out} = \rho_v V_x dy + \left[\frac{\partial}{\partial x} (\rho_v V_x) dx \right] dy \quad (\text{B.3})$$

The mass flow inlet from the inner y direction surface is:

$$\dot{m}_{y,in} = \rho_v V_y dx \quad (\text{B.4})$$

The mass flow inlet from the inner y direction surface ($y+dy$) is:

$$\dot{m}_{y,out} = \rho_v V_y dx + \left[\frac{\partial}{\partial y} (\rho_v V_y) dy \right] dx \quad (\text{B.5})$$

where V_y is Darcy velocity in y direction.

The mass generation in the control volume can be written as:

$$\dot{m}_{gen} = (1 - \phi) \rho_s \frac{\partial \bar{W}}{\partial t} dy dx \quad (B.6)$$

The stored mass can be written as:

$$\dot{m}_{stored} = \phi \frac{\partial \rho_v}{\partial t} dy dx \quad (B.7)$$

If the equations from (A.2) to (A.7) are substituted into the mass balance equation (A.1), the following equation will be found as:

$$\frac{(1 - \phi)}{\phi} \rho_s \frac{\partial \bar{W}}{\partial t} = \frac{\partial}{\partial x} (\rho_v v_x) + \frac{\partial}{\partial y} (\rho_v v_y) + \frac{\partial \rho_v}{\partial t} \quad (B.8)$$

Also it can be written as in this form:

$$\frac{(1 - \phi)}{\phi} \rho_s \frac{\partial \bar{W}}{\partial t} - \frac{\partial \rho_v}{\partial t} = \nabla \cdot (\rho \mathbf{V}) \quad (B.9)$$

B.2. Darcy Law

In two dimensions, V_x is water vapor velocity and can be calculated by Darcy law. It can be written as:

$$\mathbf{V} = \mu K_{app} \nabla P \quad (B.10)$$

where the K_{app} is the apparent permeability and P is the pressure. where K_{app} and μ are apparent permeability of the silica gel bed and the water vapor viscosity. The ideal gas relation is used to calculate the pressure change of the water vapor in the silica gel bed. The apparent permeability of the silica gel bed, K_{app} , can be calculated by the following relation when porosity is equal 0.45.

$$K_{app} = \frac{r^2 \epsilon^3}{37.5(1 - \epsilon)^2} \quad (B.11)$$

The Equation (A.10) can be written for the annular bed in x and y directions as (Bejan 1984):

$$\frac{\partial P}{\partial x} = -\frac{\mu}{K_{app}} V_x \quad , \quad \frac{\partial P}{\partial y} = -\frac{\mu}{K_{app}} V_y \quad (B.12)$$

B.3. Energy Equation

In a rectangular bed in two directions, the conservation of energy for an unsteady process can be derived as follows:

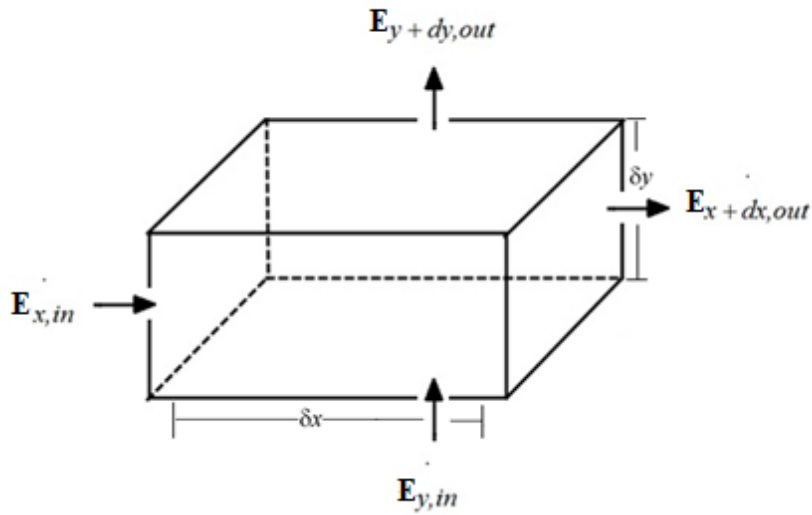


Figure A.2. Control volume for conservation of energy.

Energy balance of the control volume can be written as:

$$\dot{q}_{x,in} + \dot{q}_{y,in} + \dot{q}_{gen} = \dot{q}_{x,out} + \dot{q}_{y,out} + \dot{q}_{stored} \quad (\text{B.13})$$

The energy inlet from the inner x direction surface is:

$$\dot{q}_{in} = \dot{q}_{cond} + \dot{q}_{conv} \quad (\text{B.14})$$

$$\dot{q}_{x,in} = -k \frac{\partial T}{\partial x} dy + \rho_v C_p V_x T dy \quad (\text{B.15})$$

The energy outlet from the outer x direction surface is:

$$\dot{q}_{x,out} = \left[-k \frac{\partial T}{\partial x} + \rho_v C_p V_x + \frac{\partial}{\partial x} \left(-k \frac{\partial T}{\partial x} dx + \rho_v C_p V_x T dx \right) \right] dy \quad (\text{B.16})$$

The energy inlet from the inner y direction surface is:

$$\dot{q}_{y,in} = -k \frac{\partial T}{\partial y} dx + \rho_v C_p V_y T dx \quad (\text{B.17})$$

The energy outlet from the outer y direction surface is:

$$\dot{q}_{y,out} = \left[-k \frac{\partial T}{\partial y} + \rho_v C_p V_y + \frac{\partial}{\partial y} \left(-k \frac{\partial T}{\partial y} dy + \rho_v C_p V_y T dy \right) \right] dx \quad (\text{B.18})$$

The energy generation can be written as:

$$\dot{q}_{gen} = (1-\phi) \rho_s \frac{\partial \bar{W}}{\partial t} dy dx \quad (\text{B.19})$$

The stored energy in the control volume can be written as:

$$\dot{q}_{stored} = (\rho C_p)_{eff} \frac{\partial T}{\partial t} dy dx \quad (\text{B.20})$$

If these equations from (B.14) to (B.20) are substituted into the energy balance equations, energy balance equation (B.13) becomes as:

$$(1-\phi) \rho_s \Delta H_{ads} \frac{\partial \bar{W}}{\partial t} + \frac{\partial}{\partial x} (\lambda_{eff} \frac{\partial T}{\partial x}) + \frac{\partial}{\partial y} (\lambda_{eff} \frac{\partial T}{\partial y}) = \frac{\partial}{\partial x} (\rho_v c_v v_x T) + \frac{\partial}{\partial y} (\rho_v c_v v_y T) + (\rho c_p)_{eff} \frac{\partial T}{\partial t} \quad (\text{B.21})$$

where

$$\rho_{eff} C_{eff} = (1-\phi) \rho_s C_s + \phi \rho_v C_v + (1-\phi) \rho_s C_l W \quad (\text{B.22})$$

$$\lambda_{eff} = (1-\phi) \lambda_s + \phi \lambda_v \quad (\text{B.23})$$

Also conservation of energy law can be written as in this form:

$$(1-\phi) \rho_s \Delta H_{ads} \frac{\partial \bar{W}}{\partial t} + \nabla(k \nabla T) = \rho_v c_v v_y \nabla T + (\rho c_p)_{eff} \frac{\partial T}{\partial t} \quad (\text{B.24})$$

APPENDIX C

COMSOL MODEL REPORT

The following is a sample model report generated by Comsol Multiphysics. The table of contents are followed during the numerical solution of an adsorption cycle that comprised of four processes as: isobaric adsorption, isosteric heating, isobaric desorption and isosteric cooling.

C.1. Table of Contents

1. Global Definitions

1.1. Variables

2. Model 1 (mod1)

2.1. Definitions

2.2. Model Properties

2.3. Geometry 1

2.4. Darcy's Law (dl)

2.5. PDE (u)

2.6. Heat Transfer in Porous Media (ht)

2.7. Mesh 1

3. Solver Configurations

3.1. Time Dependent Solver

3.2. Postprocessing

C.1. Global Definitions

C.1.1. Variables

Name	Expression	Description
deff	$DD \cdot \exp(ert)$	Effective diffusivity
rp	0.0005	Radius of the silica gel particles
aa	$15 \cdot deff / rp^2$	Coefficient term of LDF Model
ros	$670 [\text{kg}/\text{m}^3]$	Density of the silica gel
gam	$aa \cdot (\text{ue} \cdot \text{mod1.u})$	LDF Model
mol	$18 \cdot 10^{-3} [\text{kg}/\text{mol}]$	
delh	$2693000 [\text{J}/\text{kg}]$	Heat of Adsorption
giz	$gam \cdot (1 - \text{poros}) \cdot (1 - fi) \cdot ros \cdot delh$	Part of heat transfer equation
kapp	$rp^2 \cdot \text{poros}^3 / (37.5 \cdot (1 - \text{poros})^2)$	Apparent permeability
poros	0.45	Porosity
RR	$8.315 [\text{J}/\text{mol}/\text{K}]$	Ideal gas constant
mu	$10.29 \cdot 10^{-6} [\text{Pa} \cdot \text{s}]$	Water vapor viscosity
gascon	RR / mol	Gas constant
qm	$(\text{poros} - 1) \cdot (1 - fi) \cdot ros \cdot gam$	Part of heat transfer equation
atsay	$7.3 \cdot 10^{-10}$	Coefficient term of Toth's isotherm equation
wmm	0.45	Coefficient term of Toth's isotherm equation
DD	$2.54 \cdot 10^{-4} [1/\text{s}]$	Reference diffusivity
E	$-(4.2 \cdot 10^4) [\text{K}]$	Diffusion activation energy
ert	$(E / (8.315 \cdot \text{mod1.T}))$	Coefficient of effective diffusivity
ue	$atsay \cdot \exp(\text{delh} / (RR / \text{mol}) \cdot \text{mod1.T}) \cdot (\text{mod1.p} / 1000) / ((1 + (atsay / wmm \cdot \exp(\text{delh} / (RR / \text{mol}) \cdot \text{mod1.T})) \cdot (\text{mod1.p} / 1000))^{12})^{1/12}$	Toth's isotherm equation
fi	0	Term for metal additive

C.2. Model 1 (mod1)

C.2.1. Definitions

Settings	
Name	Value
Coordinate names	{t1, n, to}
Create first tangent direction from	Global Cartesian

C.2.2. Model Properties

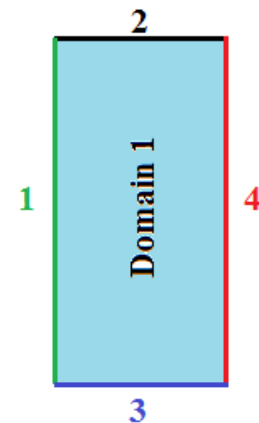
Property	Value
Default element type	Lagrange - Quadratic
Analysis type	Transient
Species diffusion	Inactive
Turbulence model	None
Predefined multiphysics application	Off
Frame	Frame (ref)
Weak constraints	Off
Constraint type	Ideal

C.2.3. Geometry

Units	
Length unit	mm
Angular unit	deg

Property	Value
Space dimension	2
Number of domains	1
Number of boundaries	4

C.2.3.
1. Recta



ngle 1

Settings	
Name	Value
Position	{0, 0}
Width	5
Height	10
Size	{5, 10}

C.2.4. Darcy's Law

Selection	
Geometric entity level	Domain
Selection	Domain 1

Settings	
Description	Value
Equation form	Time dependent

Equations

$$\frac{\partial}{\partial t}(\rho \varepsilon_p) + \nabla \cdot (\rho \mathbf{u}) = Q_m$$

$$\mathbf{u} = -\frac{\kappa \nabla p}{\mu}$$

C.2.4.1. Fluid and Matrix Properties

Selection	
Geometric entity level	Domain
Selection	Domain 1

Equations

$$\frac{\partial}{\partial t}(\rho \varepsilon_p) + \nabla \cdot (\rho \mathbf{u}) = Q_m$$

$$\mathbf{u} = -\frac{\kappa \nabla p}{\mu}$$

Settings	
Description	Value
Density	Ideal gas
Dynamic viscosity	User defined
Dynamic viscosity	mu
Permeability	User defined
Permeability	{{kapp, 0, 0}, {0, kapp, 0}, {0, 0, kapp}}
Porosity	User defined
Porosity	porous
Specific gas constant	User defined
Specific gas constant	gascon
Temperature	Temperature (ht/fluid1)
Absolute pressure	Pressure (dl/dlm1)
Reference pressure	0

C.2.4.2. No Flow 1

Selection	
Geometric entity level	Boundary
Selection	Boundaries 1-4

C.2.4.3. Initial Values 1

Selection	
Geometric entity level	Domain
Selection	Domain 1

Settings	
Description	Value
Pressure	775

C.2.4.4. Mass Source 1

Selection	
Geometric entity level	Domain
Selection	Domain 1

Settings	
Description	Value
Mass source	qm

Equations

$$\frac{\partial}{\partial t}(\rho \epsilon_p) + \nabla \cdot (\rho \mathbf{u}) = \underline{q}_m$$

$$\mathbf{u} = -\frac{\kappa}{\mu} \nabla p$$

C.2.5. PDE (u)

Selection	
Geometric entity level	Domain
Selection	Domain 1

C.2.5.1. Coefficient Form PDE 1

Selection	
Geometric entity level	Domain
Selection	Domain 1

Settings	
Description	Value
Diffusion coefficient	{{0, 0}, {0, 0}}
Absorption coefficient	aa
Source term	ue*aa

Equations

$$e_a \frac{\partial^2 u}{\partial x^2} + d_a \frac{\partial u}{\partial t} + \nabla \cdot (-c \nabla u - \alpha u + \gamma) + \beta \cdot \nabla u + a u = f$$

$$\nabla = \left[\frac{\partial}{\partial x}, \frac{\partial}{\partial y} \right]$$

C.2.5.2. Zero Flux 1

Selection	
Geometric entity level	Boundary
Selection	Boundaries 1-4

Equations

$$-\mathbf{n} \cdot (-c\nabla u - au + \gamma) = 0$$

$$\nabla = \left[\frac{\partial}{\partial x}, \frac{\partial}{\partial y} \right]$$

C.2.5.3. Initial Values 1

Selection	
Geometric entity level	Domain
Selection	Domain 1
Settings	
Description	Value
Initial value for u	0.073

C.2.6. Heat Transfer in Porous Media

Selection	
Geometric entity level	Domain
Selection	Domain 1

Equations

$$(\rho C_p)_{eq} \frac{\partial T}{\partial t} + \rho C_p \mathbf{u} \cdot \nabla T = \nabla \cdot (k_{eq} \nabla T) + Q$$

C.2.6.1. Porous Matrix 1

Description	Value
Equation form	Time dependent
Heat transfer in porous media	On
Default model	Porous matrix

Selection	
Geometric entity level	Domain
Selection	Domain 1

Equations

$$(\rho C_p)_{eq} \frac{\partial T}{\partial t} + \rho C_p \mathbf{u} \cdot \nabla T = \nabla \cdot (k_{eq} \nabla T) + Q$$

$$k_{eq} = \theta_p k_p + (1 - \theta_p) k$$

$$(\rho C_p)_{eq} = \theta_p \rho_p C_{p,p} + (1 - \theta_p) \rho C_p$$

Settings	
Description	Value
Thermal conductivity	User defined
Thermal conductivity	{{0.198, 0, 0}, {0, 0.198, 0}, {0, 0, 0.198}}
Density	User defined
Density	ros
Specific heat capacity	User defined
Specific heat capacity	880
Volume fraction	1-poros

C.2.6.2. Heat Transfer in Fluids 1

Geometric entity level	Domain
Selection	Domain 1

Equations

$$(\rho C_p)_{eq} \frac{\partial T}{\partial t} + \rho C_p \mathbf{u} \cdot \nabla T = \nabla \cdot (k_{eq} \nabla T) + Q$$

$$\rho = \frac{p_A}{R_s T}$$

Settings	
Description	Value
Thermal conductivity	User defined
Thermal conductivity	{{0.09838, 0, 0}, {0, 0.09838, 0}, {0, 0, 0.09838}}
Specific gas constant	User defined
Specific gas constant	gascon
Heat capacity at constant pressure	User defined
Heat capacity at constant pressure	1907
Fluid type	Ideal gas
Absolute pressure	Pressure (dl/dlm1)
Velocity field	Darcy's velocity field (dl/dlm1)
Reference pressure	0

C.2.6.3. Thermal Insulation 1

Selection	
Geometric entity level	Boundary
Selection	Boundaries 1-3

Equations

$$-\mathbf{n} \cdot (-k \nabla T) = 0$$

C.2.6.4. Initial Values 1

Selection	
Geometric entity level	Domain
Selection	Domain 1

Settings	
Description	Value
Temperature	312[K]

C.2.6.5. Heat Source 1

Selection	
Geometric entity level	Domain
Selection	Domain 1

Settings	
Description	Value
Heat source	giz

Equations

$$(\rho C_p)_{eq} \frac{\partial T}{\partial t} + \rho C_p \mathbf{u} \cdot \nabla T = \nabla \cdot (k_{eq} \nabla T) + \dot{Q}$$

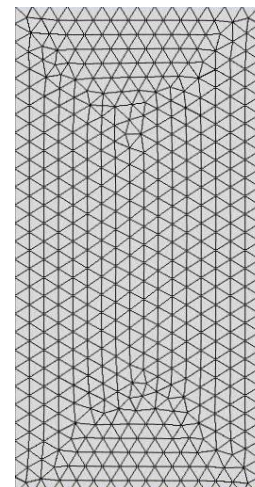
C.2.6.6. Cooling

Selection	
Geometric entity level	Boundary
Selection	Boundary 4

Equations

C.2.7. Mesh 1

Mesh	
Property	Value
Minimum element quality	0.7618
Average element quality	0.9862
Triangular elements	950
Edge elements	82
Vertex elements	4



C.2.7.1. Size

Settings	
Name	Value
Maximum element size	0.37
Minimum element size	0.00125
Resolution of curvature	0.25
Maximum element growth rate	1.25
Predefined size	Finer
Heat Transfer in Porous Media (ht)	Physics

C.3. Solver Configurations

C.3.1. Time-Dependent Solver

Solve using a script: off

Analysis type	Transient
Auto select solver	On
Solver	Time dependent
Solution form	Automatic
Symmetric	auto
Adaptive mesh refinement	Off
Optimization/Sensitivity	Off
Plot while solving	Off

C.3.1.2. Direct (UMFPACK)

Solver type: Linear system solver

Parameter Value Pivot threshold	0.1
Memory allocation factor	0.7

C.3.1.3. Time Stepping

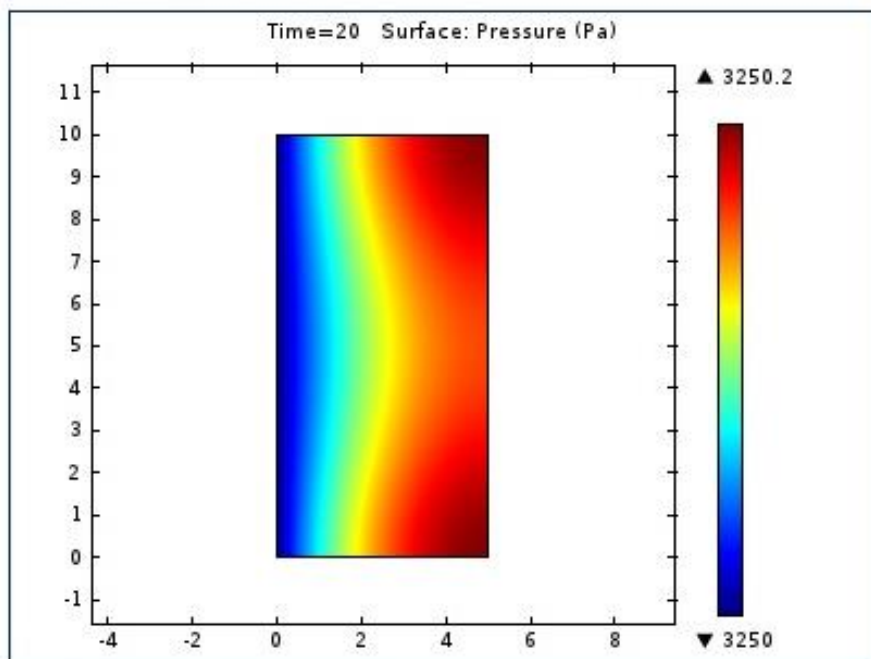
Parameter	Value
Relative tolerance	0.01
Absolute tolerance	0.001
Times to store in output	Specified times
Time steps taken by solver	Free
Maximum BDF order	2
Singular mass matrix	Maybe

Consistent initialization of DAE systems	Backward Euler
Error estimation strategy	Include algebraic
Allow complex numbers	Off

C.3.1.4. Advanced

Parameter	Value
Constraint handling method	Elimination
Null-space function	Automatic
Automatic assembly block size	On
Assembly block size	1000
Use Hermitian transpose of constraint matrix and in symmetry detection	Off
Use complex functions with real input	On
Stop if error due to undefined operation	Off
Store solution on file	Automatic
Type of scaling	
Manual scaling	On
Row equilibration	Off
Manual control of reassembly	On
Load constant	On
Constraint constant	On
Mass constant	On
Damping (mass) constant	On
Jacobian constant	On
Constraint Jacobian constant	On

C.3.2. Postprocessing



APPENDIX D

FURTHER EXPERIMENTAL RESULTS

- Experiment No and Date: 1 / 06.01.2015

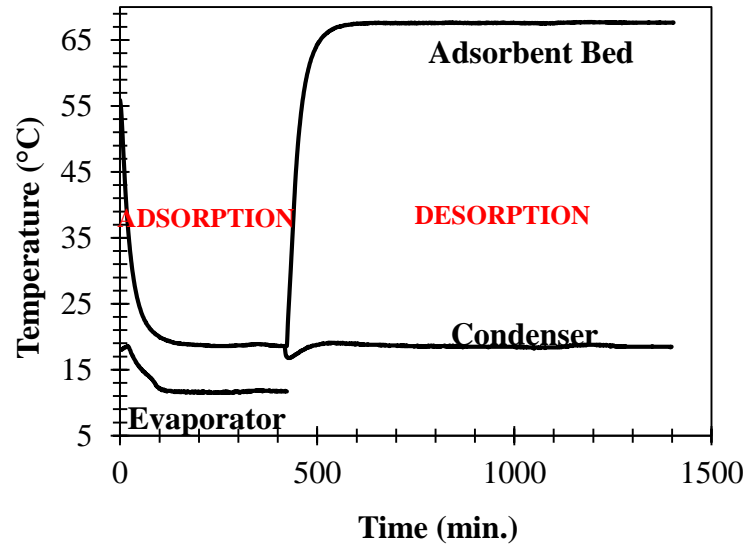


Figure D.1 (a). Temperature diagram of adsorbent bed, condenser and evaporator for experiment no: 1 conditions.

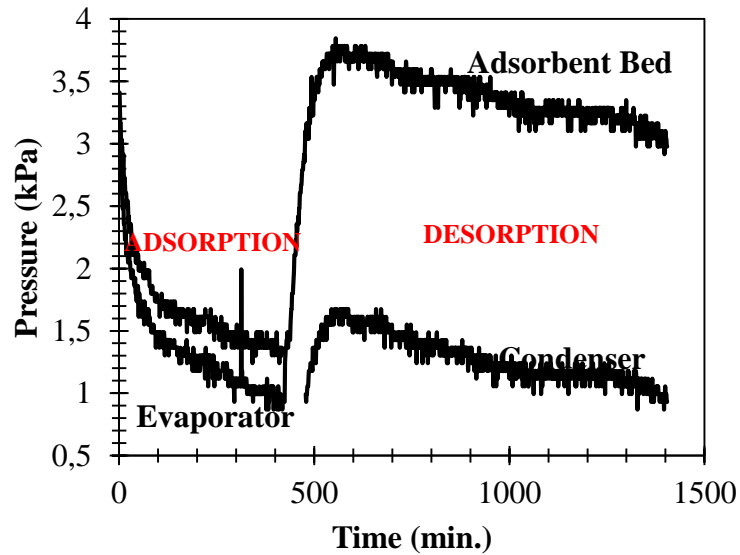


Figure D.1 (b). Pressure diagram of adsorbent bed, condenser and evaporator for experiment no: 1 conditions.

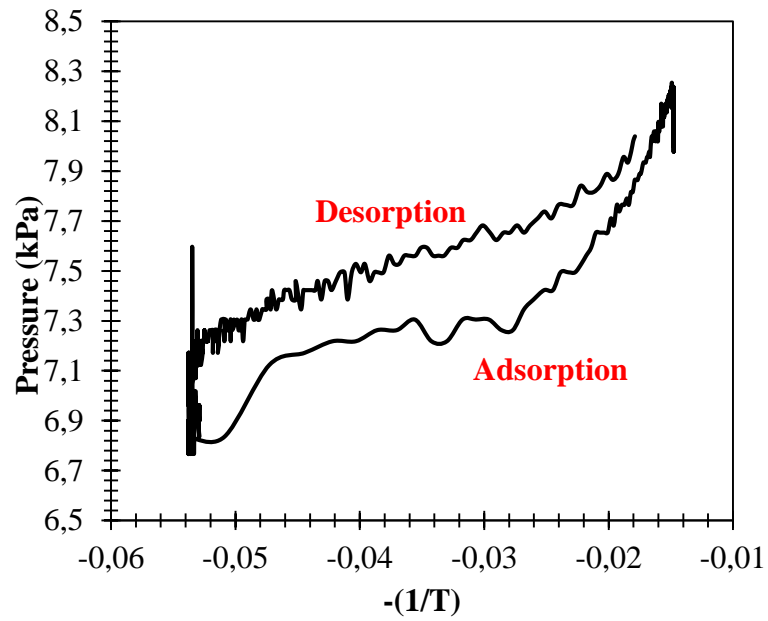


Figure D.1 (c). Clapeyron diagram of adsorbent bed for experiment no: 1 conditions.

- Experiment No and Date: 2 / 08.01.2015

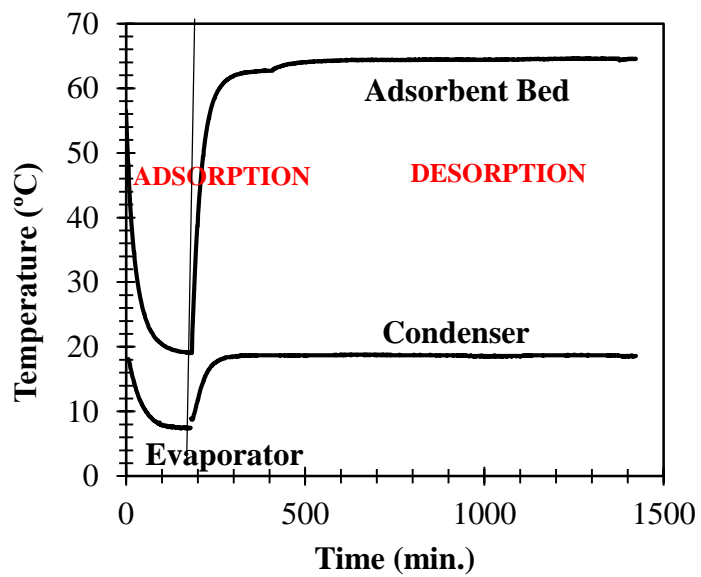


Figure D.2 (a). Temperature diagram of adsorbent bed, condenser and evaporator for experiment no: 2 conditions.

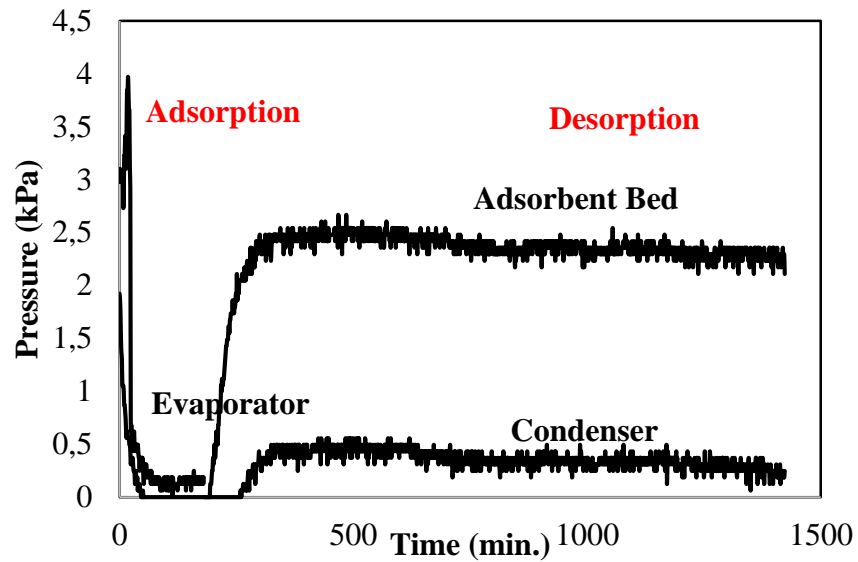


Figure D.2 (b). Pressure diagram of adsorbent bed, condenser and evaporator for experiment no: 2 conditions.

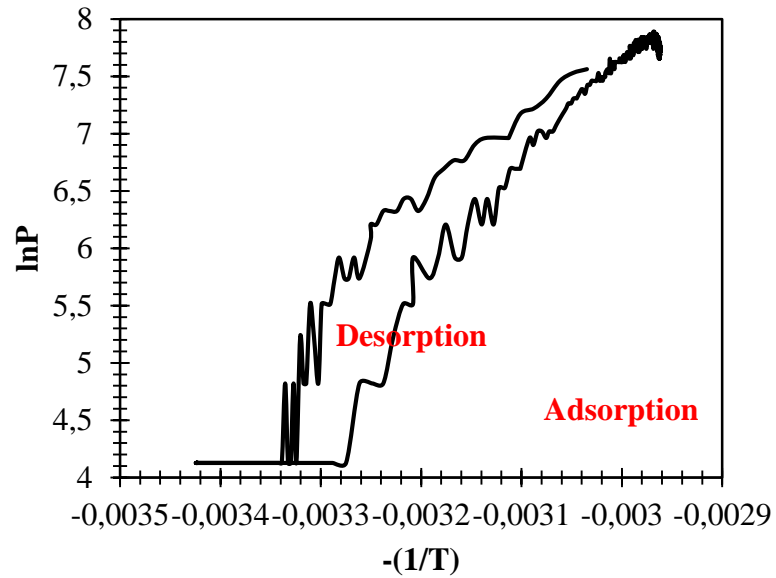


Figure D.2 (c). Clapeyron diagram of adsorbent bed for experiment no: 2 conditions.

- Experiment No and Date: 3 / 12.01.2015

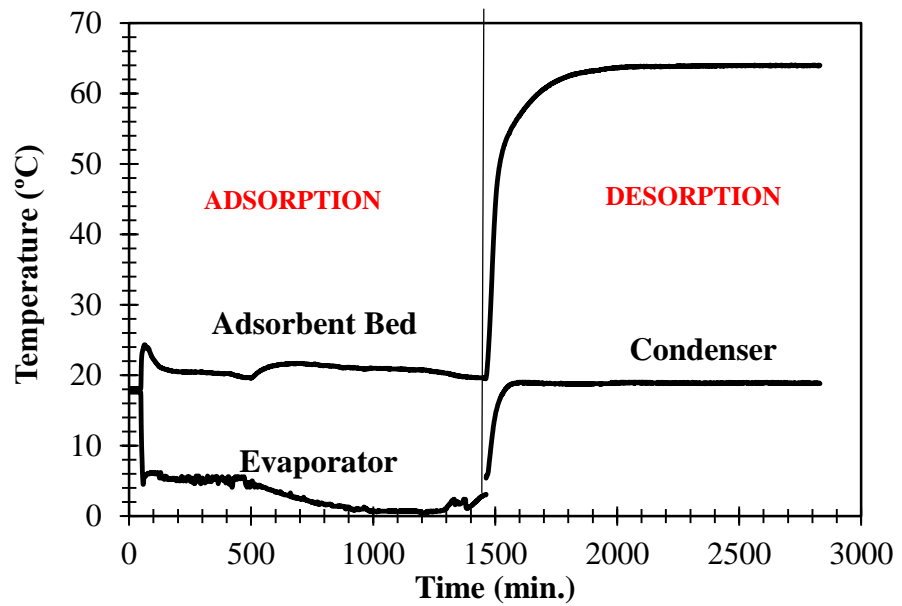


Figure D.3 (a). Temperature diagram of adsorbent bed, condenser and evaporator for experiment no: 3 conditions.

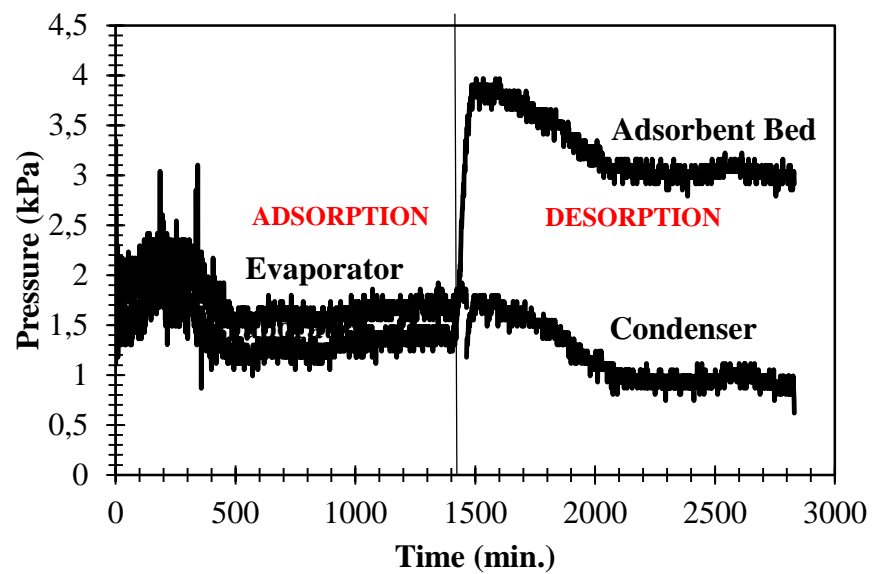


Figure D.3 (b). Pressure diagram of adsorbent bed, condenser and evaporator for experiment no: 3 conditions.

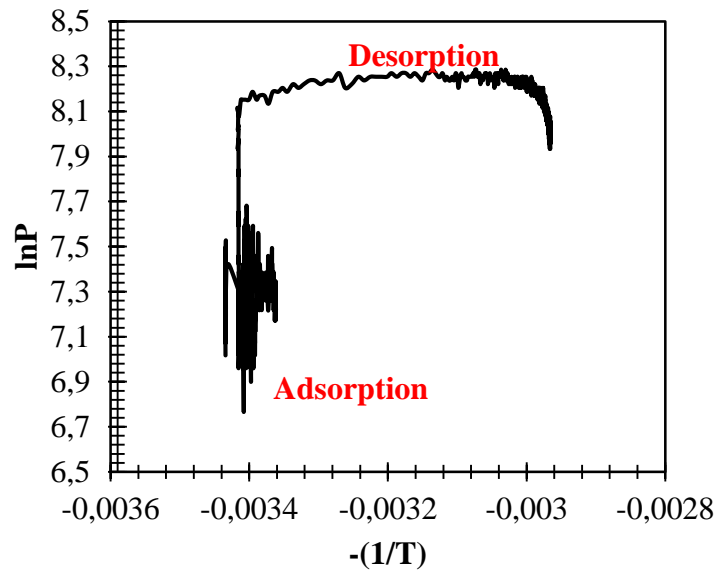


Figure D.3 (c). Clapeyron diagram of adsorbent bed for experiment no: 3 conditions.

- Experiment No and Date: 4 / 15.01.2015

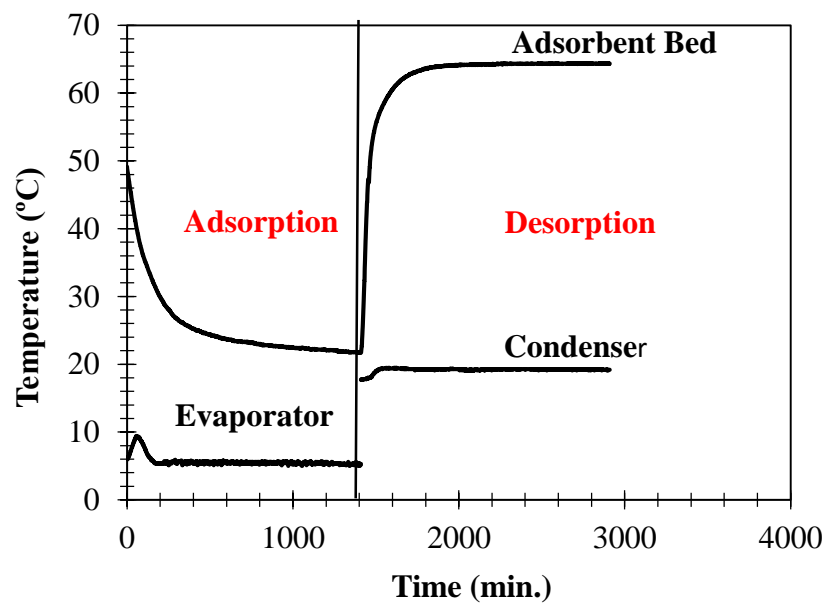


Figure D.4 (a). Temperature diagram of adsorbent bed, condenser and evaporator for experiment no: 4 conditions.

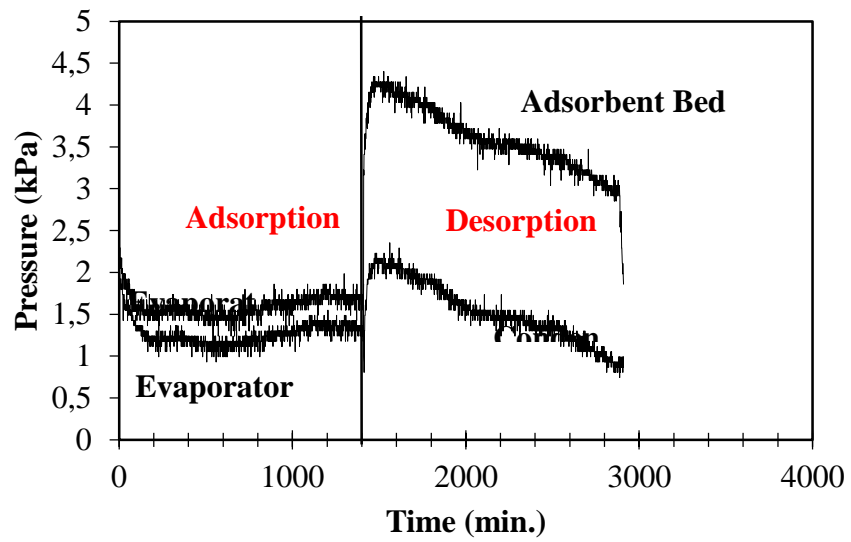


Figure D.4 (b). Pressure diagram of adsorbent bed, condenser and evaporator for experiment no: 4 conditions.

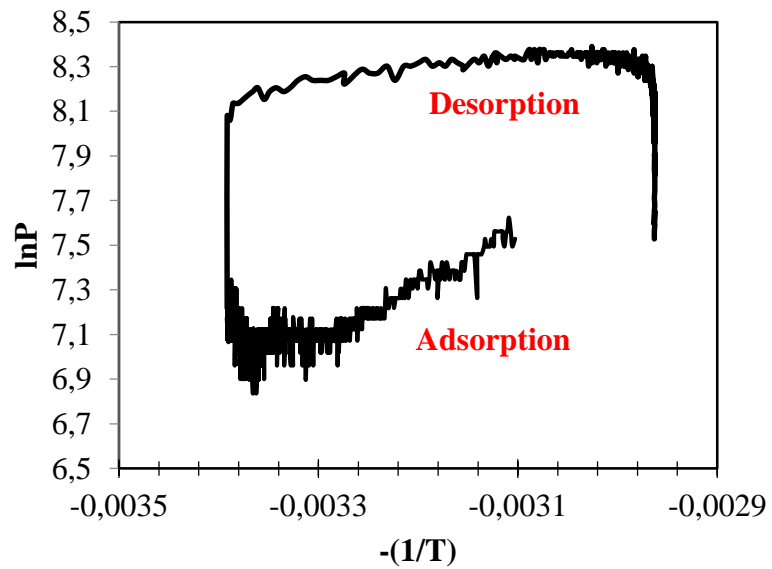


Figure D.4 (c). Clapeyron diagram of adsorbent bed for experiment no: 4 conditions.

- Experiment No and Date: 5 / 20.01.2015

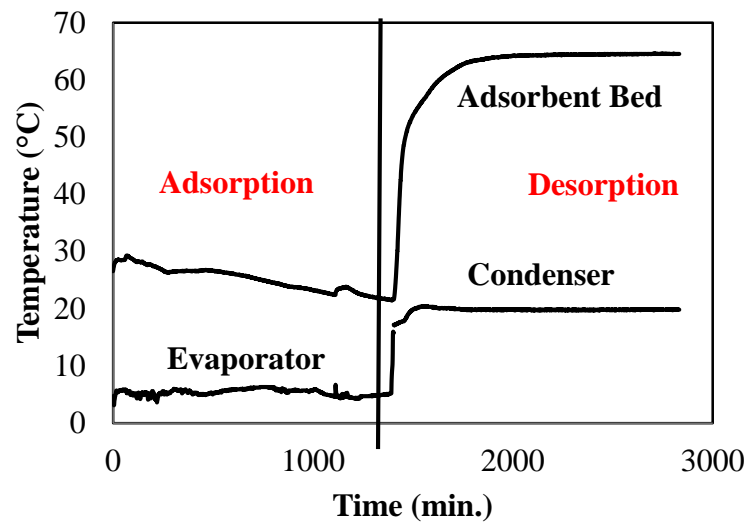


Figure D.5 (a). Temperature diagram of adsorbent bed, condenser and evaporator for experiment no: 5 conditions.

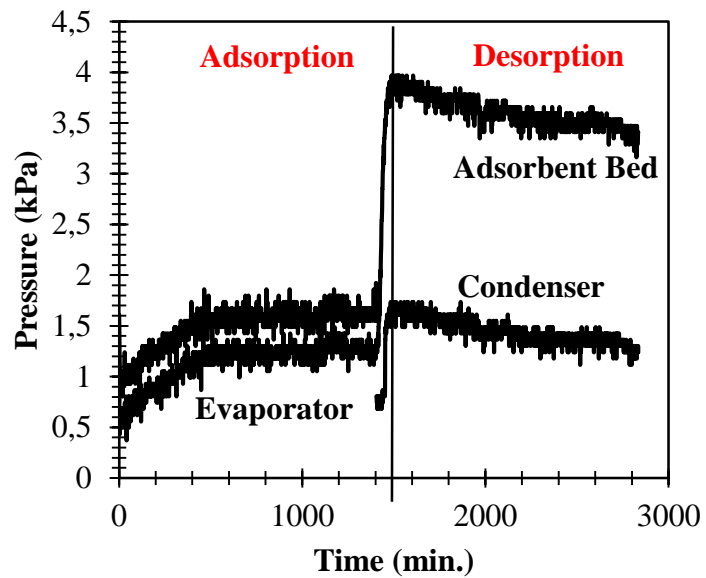


Figure D.5 (b). Pressure diagram of adsorbent bed, condenser and evaporator for experiment no: 5 conditions.

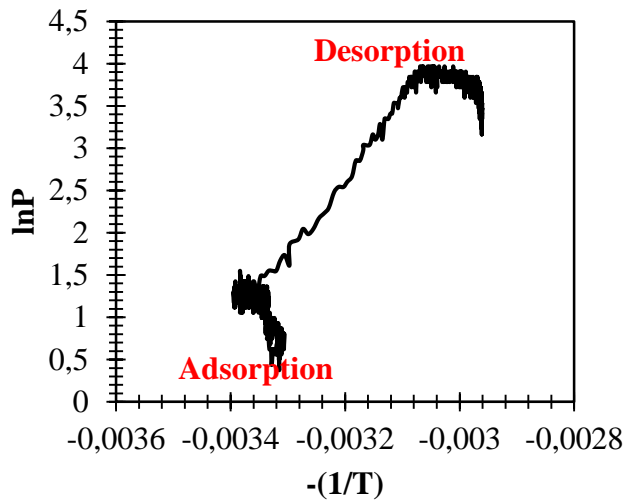


Figure D.5 (c). Clapeyron diagram of adsorbent bed for experiment no: 5 conditions.

- Experiment No and Date: 6 / 21.01.2015

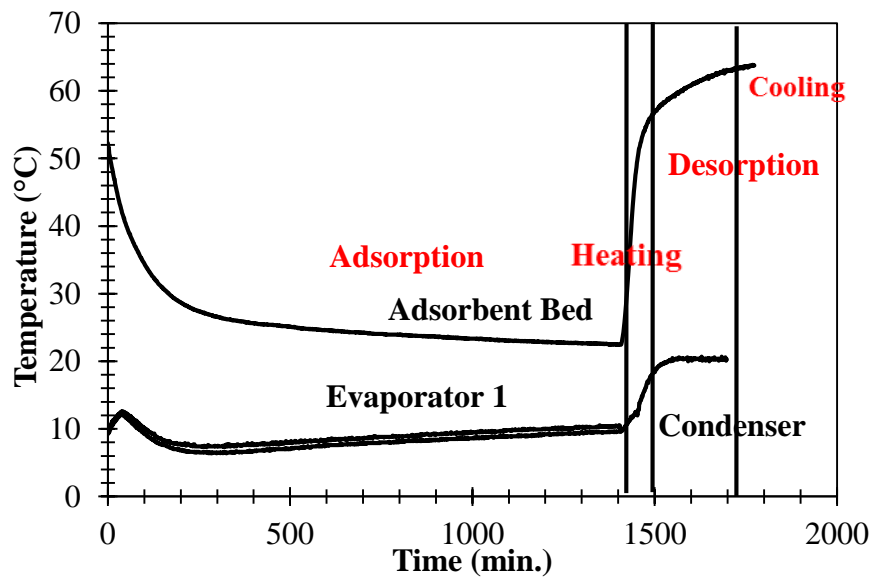


Figure D.6 (a). Temperature diagram of adsorbent bed, condenser and evaporator for experiment no: 6 conditions.

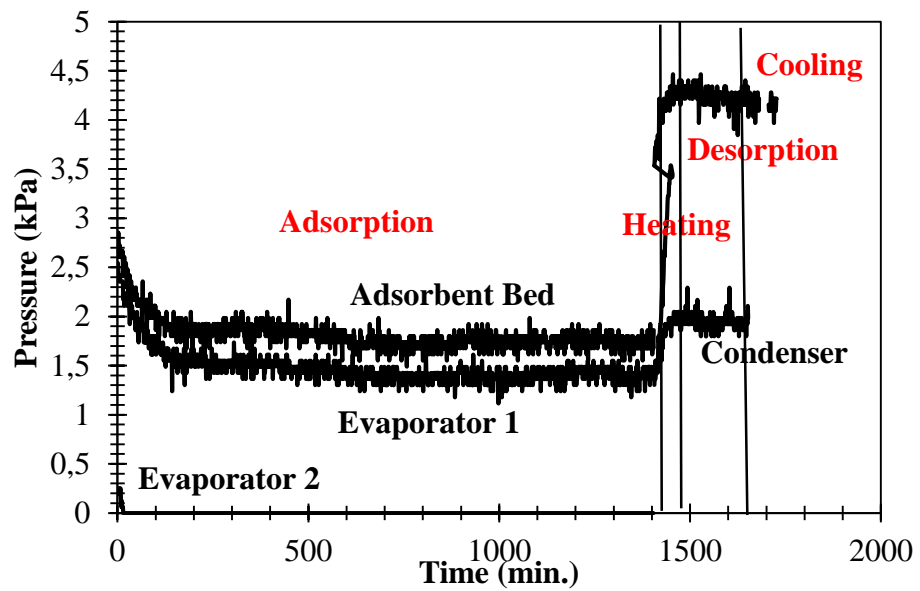


Figure D.6 (b). Pressure diagram of adsorbent bed, condenser and evaporator for experiment no: 6 conditions.

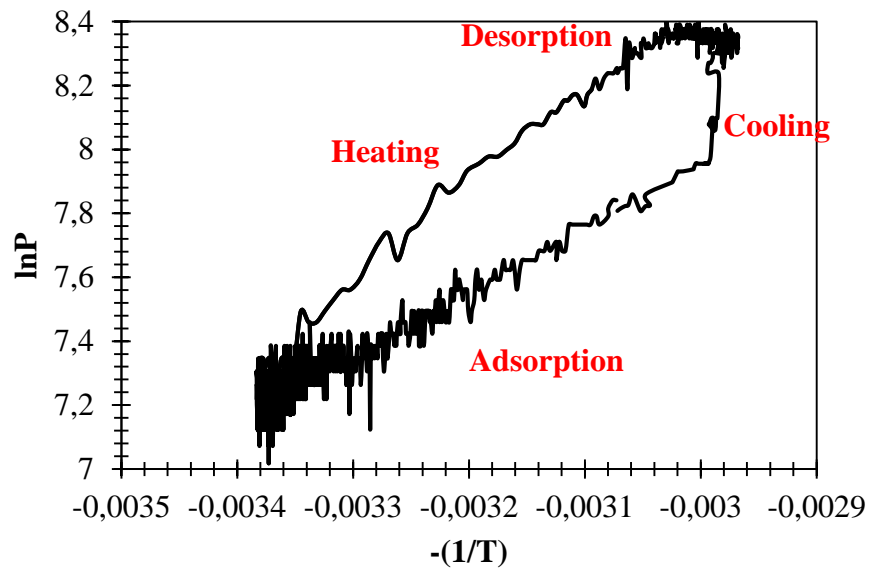


Figure D.6 (c). Clapeyron diagram of adsorbent bed for experiment no: 6 conditions.

- Experiment No and Date: 7 / 26.01.2015

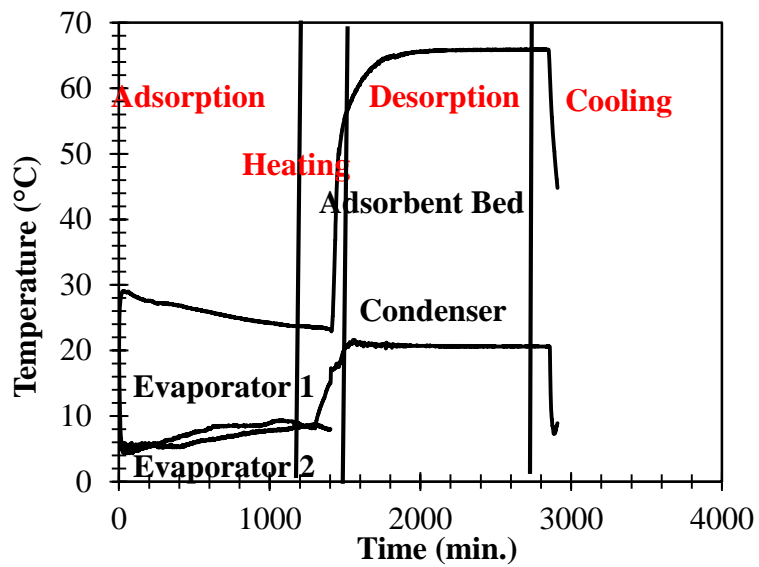


Figure D.7 (a). Temperature diagram of adsorbent bed, condenser and evaporator for experiment no: 7 conditions.

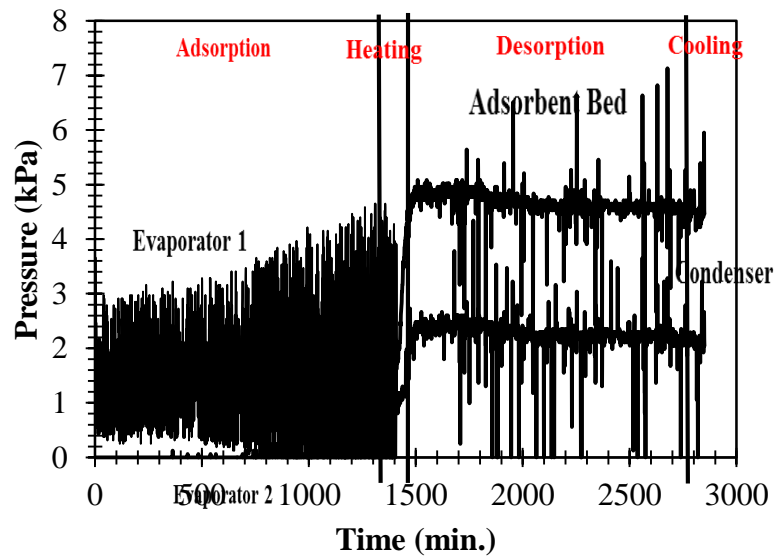


Figure D.7 (b). Pressure diagram of adsorbent bed, condenser and evaporator for experiment no: 7 conditions.

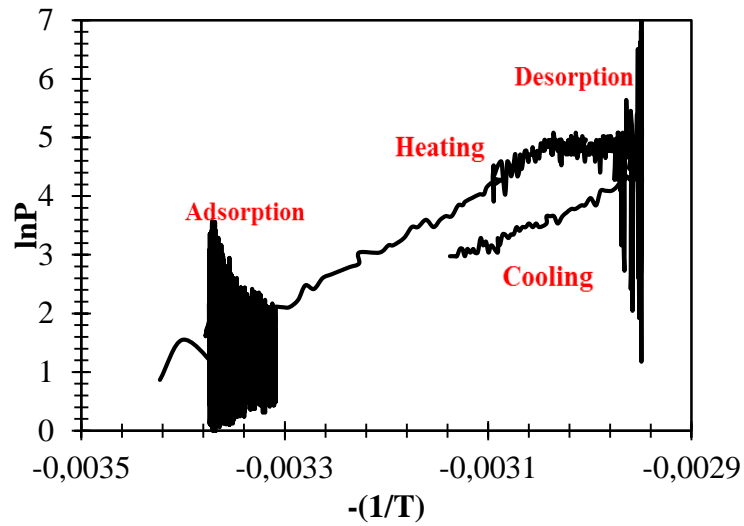


Figure D.7 (c). Clapeyron diagram of adsorbent bed for experiment no: 7 conditions.

- Experiment No and Date: 8 / 28.01.2015

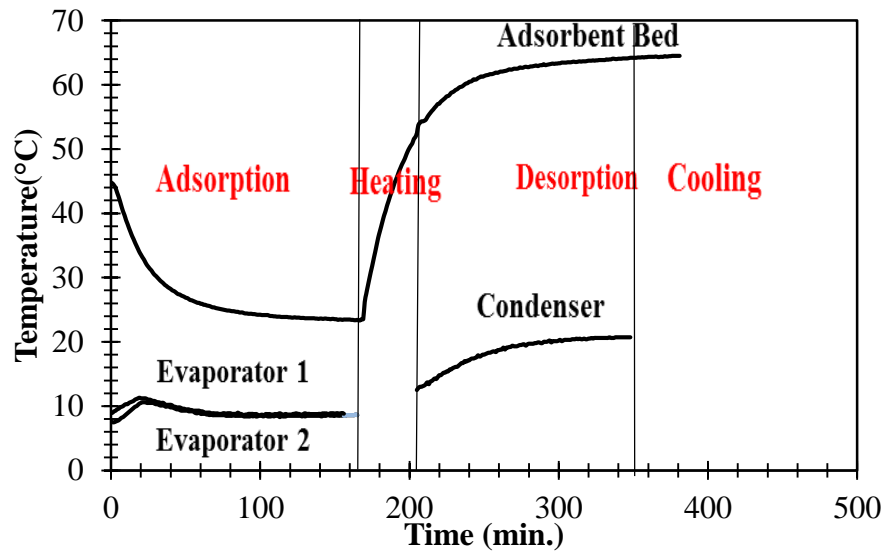


Figure D.8 (a). Temperature diagram of adsorbent bed, condenser and evaporator for experiment no: 8 conditions.

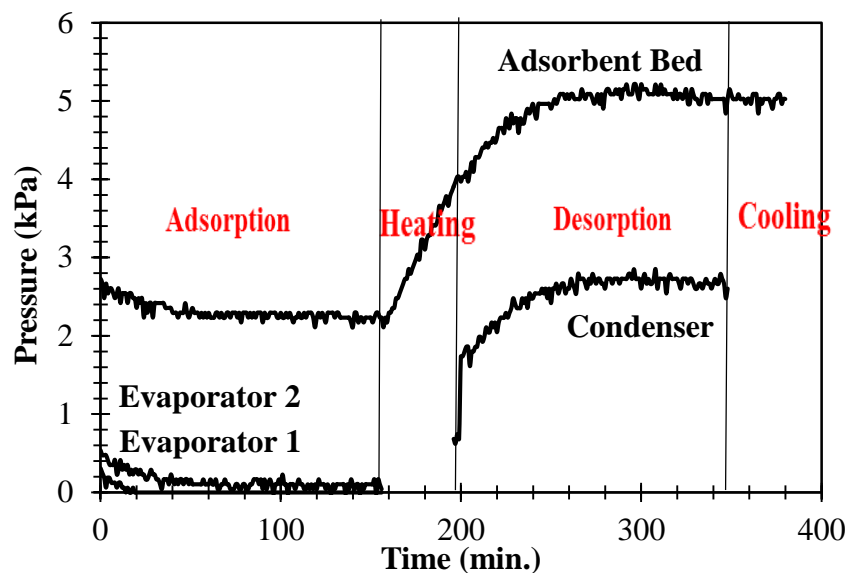


Figure D.8 (b). Pressure diagram of adsorbent bed, condenser and evaporator for experiment no: 8 conditions.

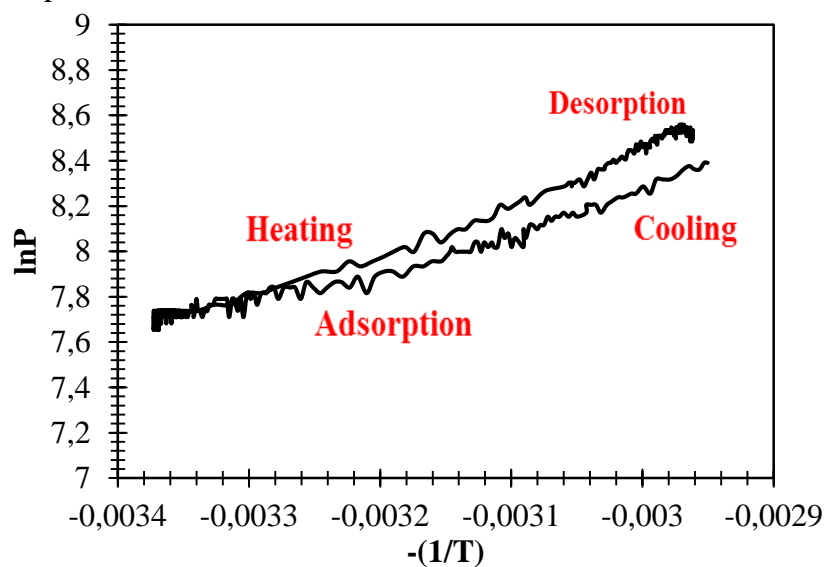


Figure D.8 (c). Clapeyron diagram of adsorbent bed for experiment no: 8 conditions.

- Experiment No and Date: 9 / 29.01.2015

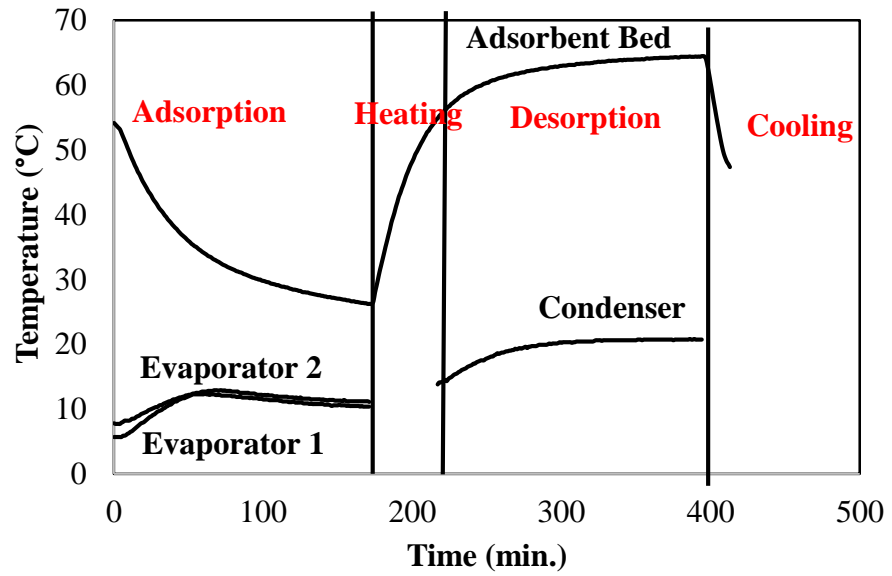


Figure D.9 (a). Temperature diagram of adsorbent bed, condenser and evaporator for experiment no: 9 conditions.

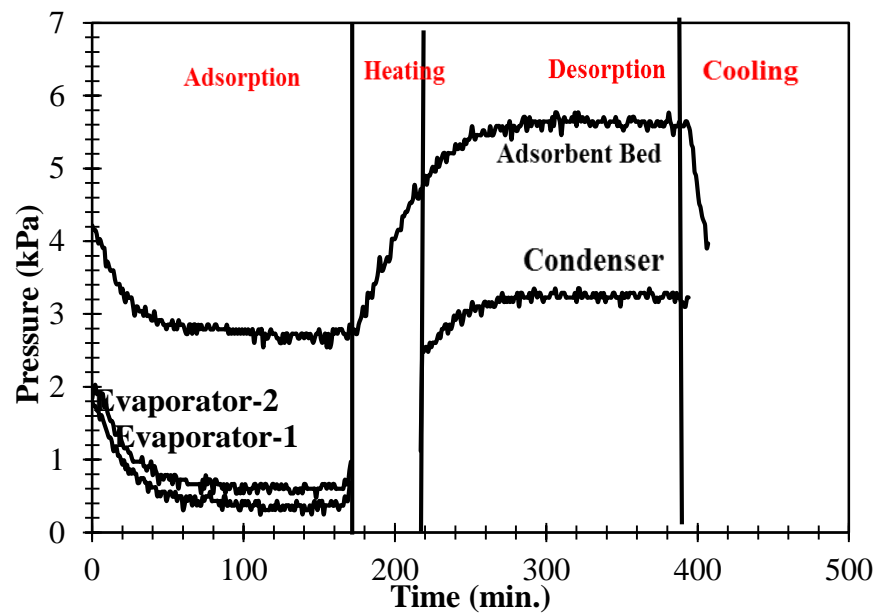


Figure D.9 (b). Pressure diagram of adsorbent bed, condenser and evaporator for experiment no: 9 conditions.

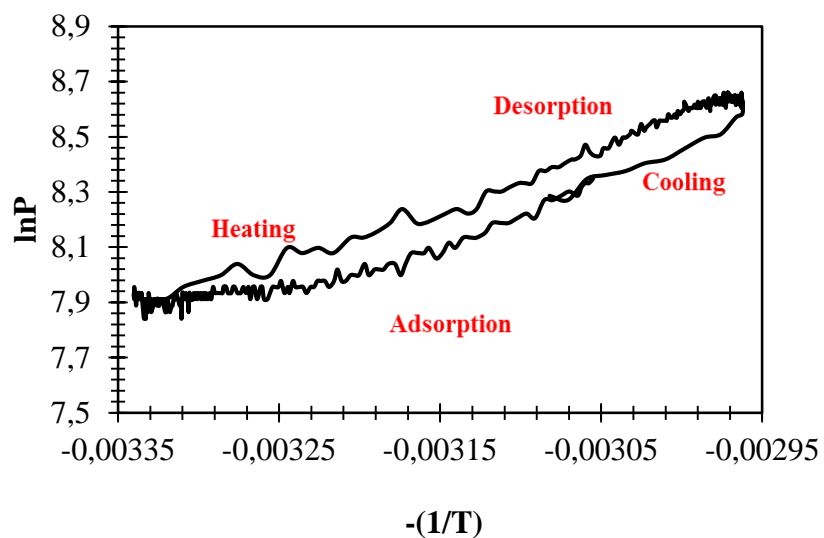


Figure D.9 (c). Clapeyron diagram of adsorbent bed for experiment no: 9 conditions.

- Experiment No and Date: 10 / 30.01.2015

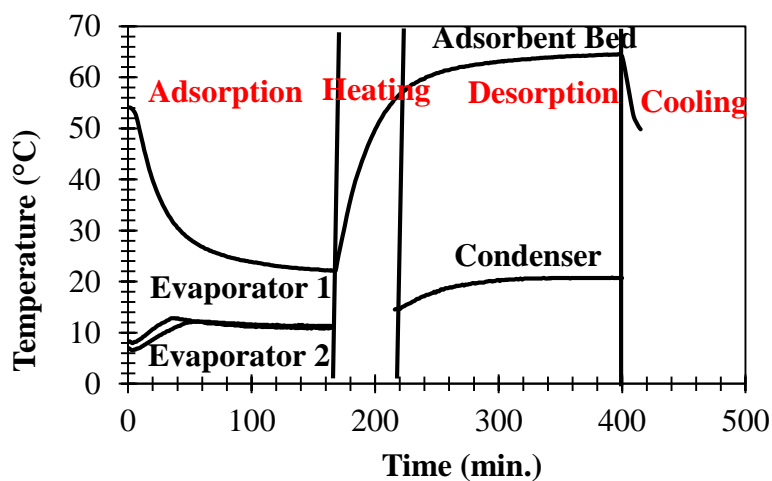


Figure D.10 (a). Temperature diagram of adsorbent bed, condenser and evaporator for experiment no: 10 conditions.

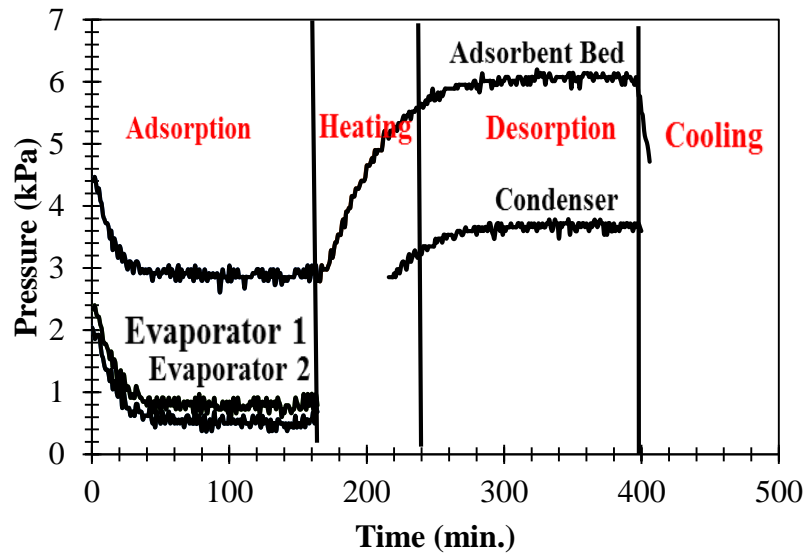


Figure D.10 (b). Pressure diagram of adsorbent bed, condenser and evaporator for experiment no: 10 conditions.

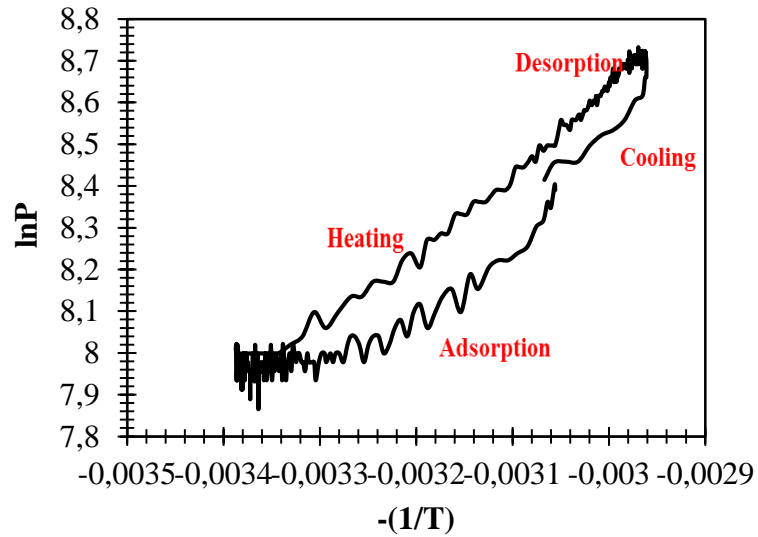


Figure D.10 (c). Clapeyron diagram of adsorbent bed for experiment no: 10 conditions.

• Experiment No and Date: 11 / 03.02.2015

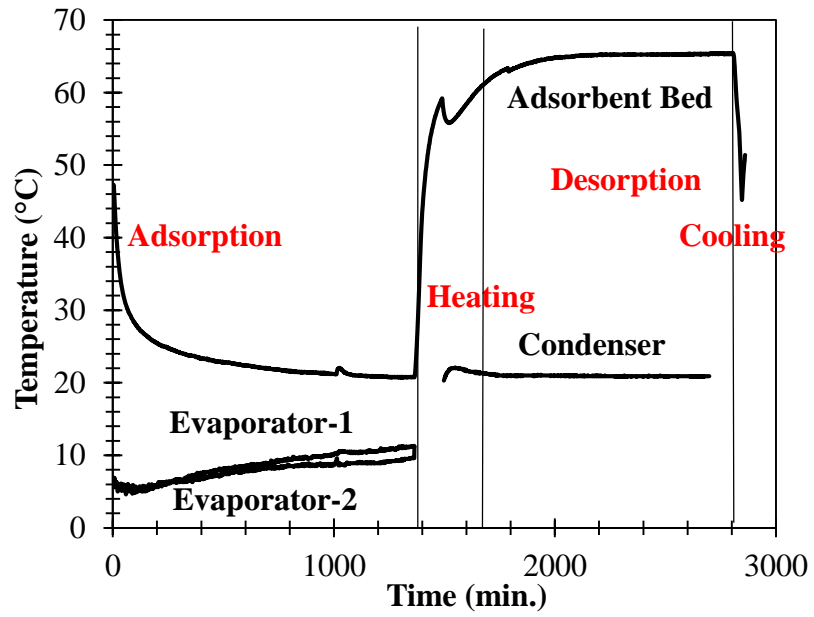


Figure D.11 (a). Temperature diagram of adsorbent bed, condenser and evaporator for experiment no: 11 conditions.

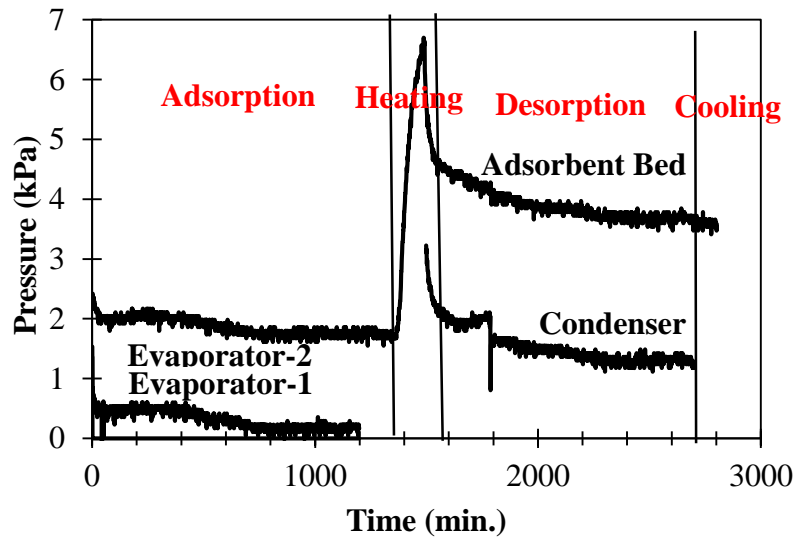


Figure D.11 (b). Pressure diagram of adsorbent bed, condenser and evaporator for experiment no: 11 conditions.

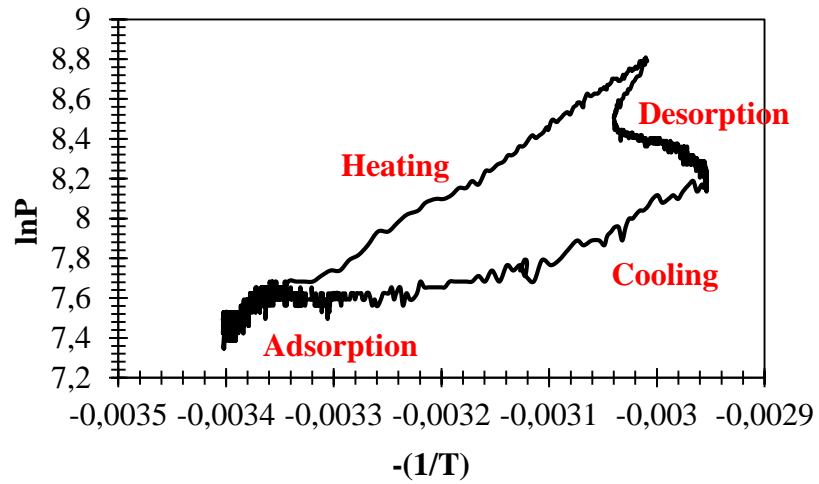


Figure D.11 (c). Clapeyron diagram of adsorbent bed for experiment no: 11 conditions.

- Experiment No and Date: 12 / 05.02.2015

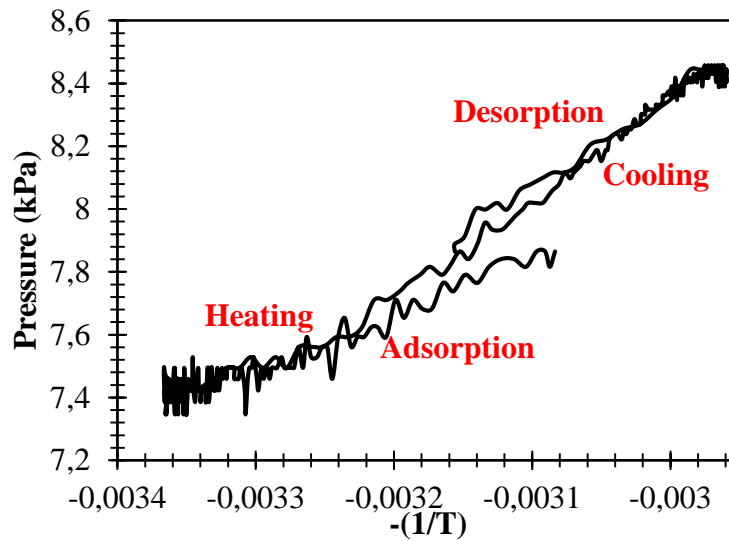


Figure D.12 (a). Temperature diagram of adsorbent bed, condenser and evaporator for experiment no: 12 conditions.

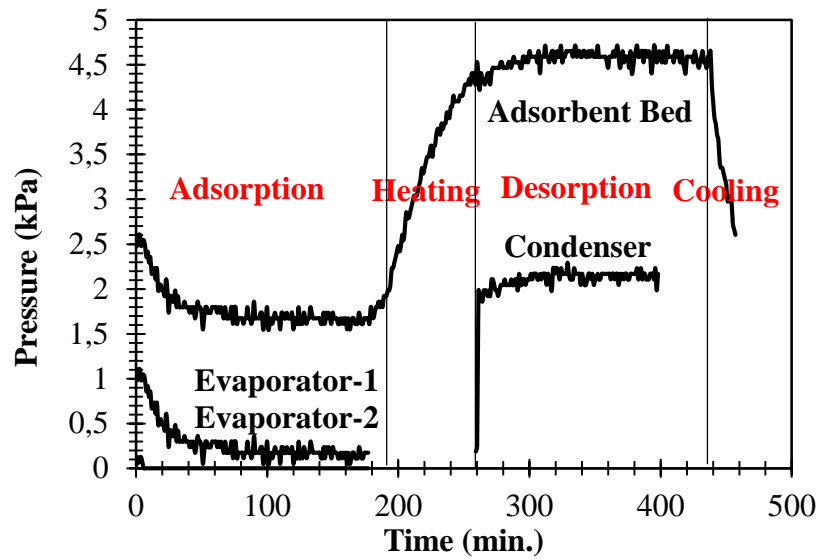


Figure D.12 (b). Pressure diagram of adsorbent bed, condenser and evaporator for experiment no: 12 conditions.

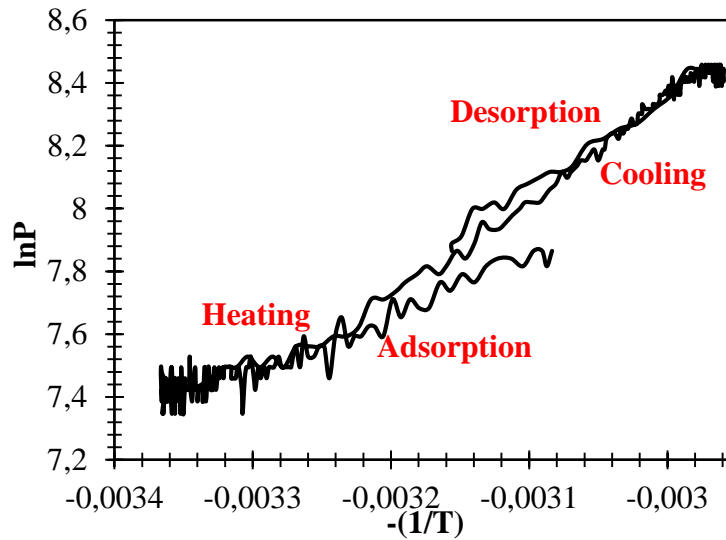


Figure D.12 (c). Clapeyron diagram of adsorbent bed for experiment no: 12 conditions.

- Experiment No and Date: 13 / 06.02.2015

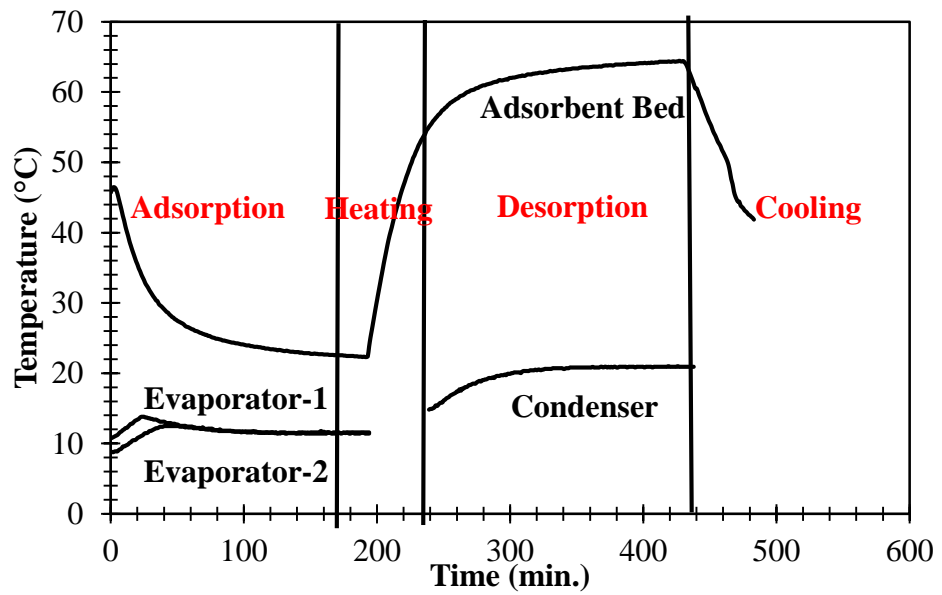


Figure D.13 (a). Temperature diagram of adsorbent bed, condenser and evaporator for experiment no: 13 conditions.

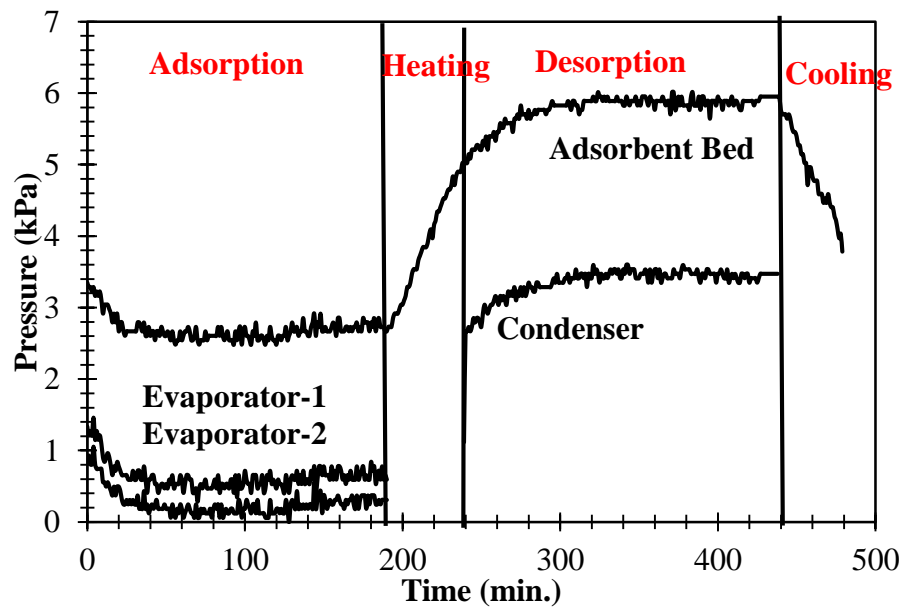


Figure D.13 (b). Pressure diagram of adsorbent bed, condenser and evaporator for experiment no: 13 conditions.

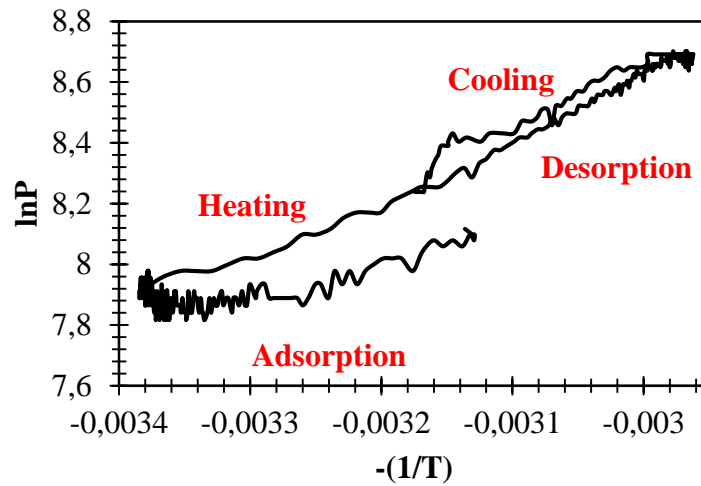


Figure D.13 (c). Clapeyron diagram of adsorbent bed for experiment no: 13 conditions.

- Experiment No and Date: 14 / 09.02.2015

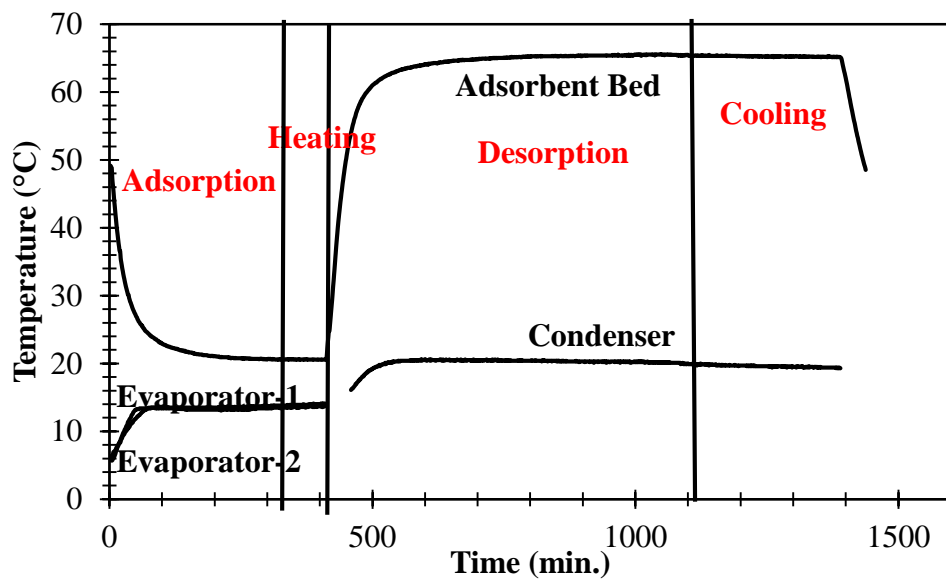


Figure D.14 (a). Temperature diagram of adsorbent bed, condenser and evaporator for experiment no: 14 conditions.

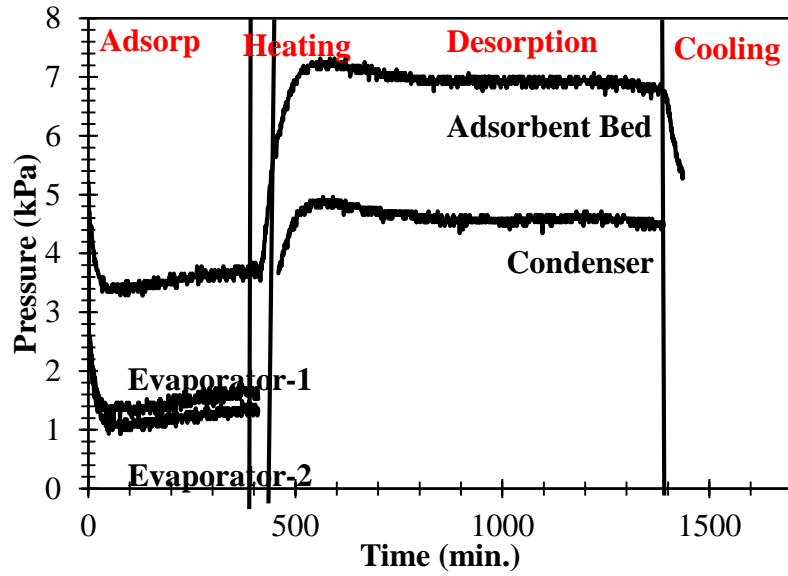


Figure D.14 (b). Pressure diagram of adsorbent bed, condenser and evaporator for experiment no: 14 conditions.

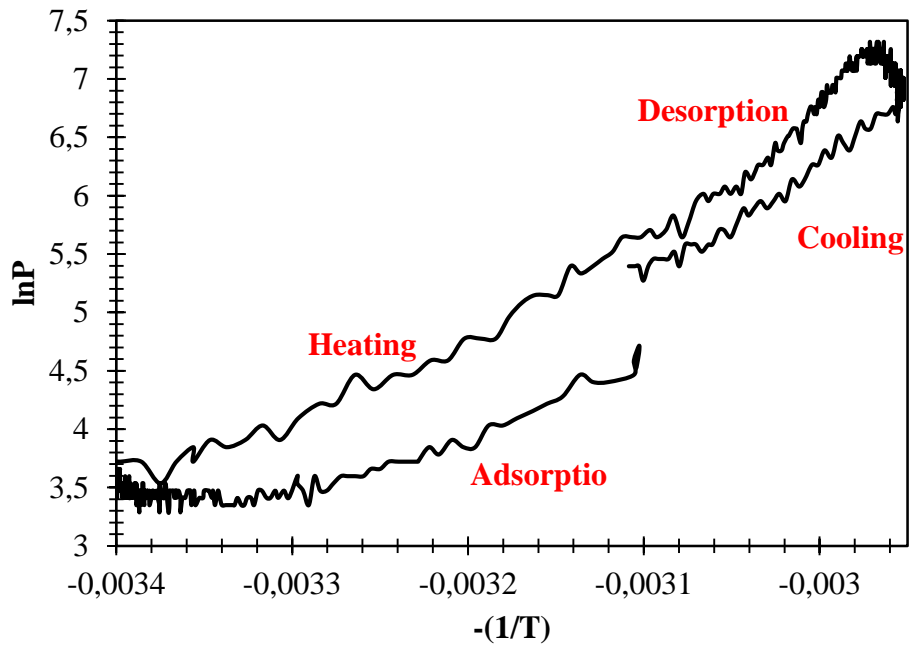


Figure D.14 (c). Clapeyron diagram of adsorbent bed for experiment no: 14 conditions.

- Experiment No and Date: 15 / 10.02.2015

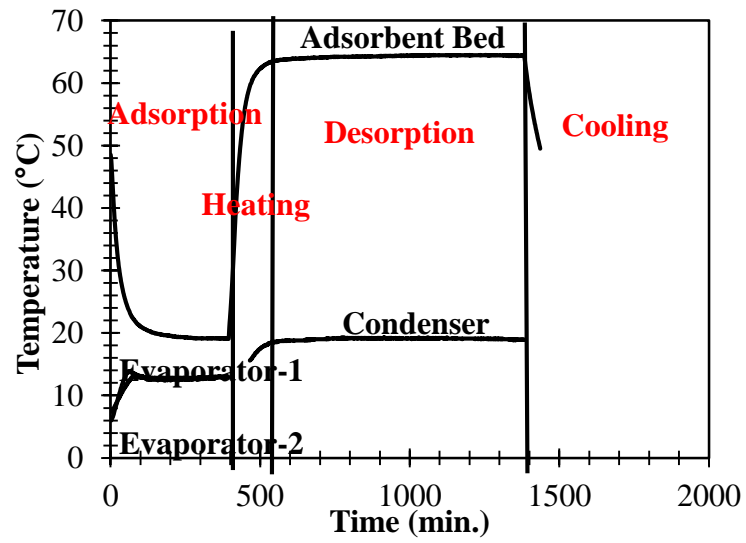


Figure D.15 (a). Temperature diagram of adsorbent bed, condenser and evaporator for experiment no: 15 conditions.

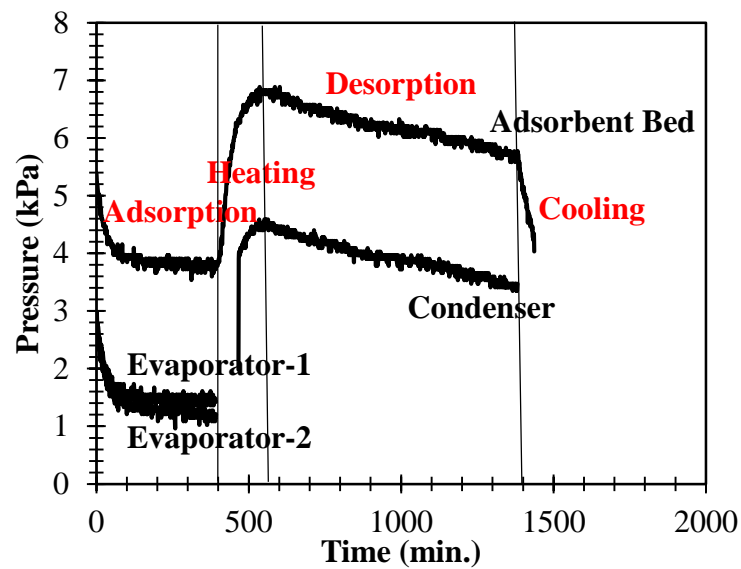


Figure D.15 (b). Pressure diagram of adsorbent bed, condenser and evaporator for experiment no: 15 conditions.

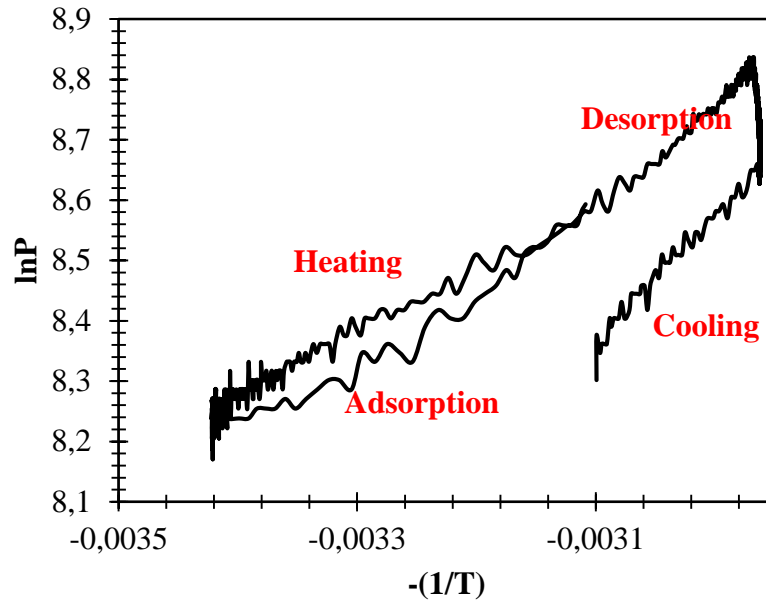


Figure D.15 (c). Clapeyron diagram of adsorbent bed for experiment no: 15 conditions.

- Experiment No and Date: 16 / 11.02.2015

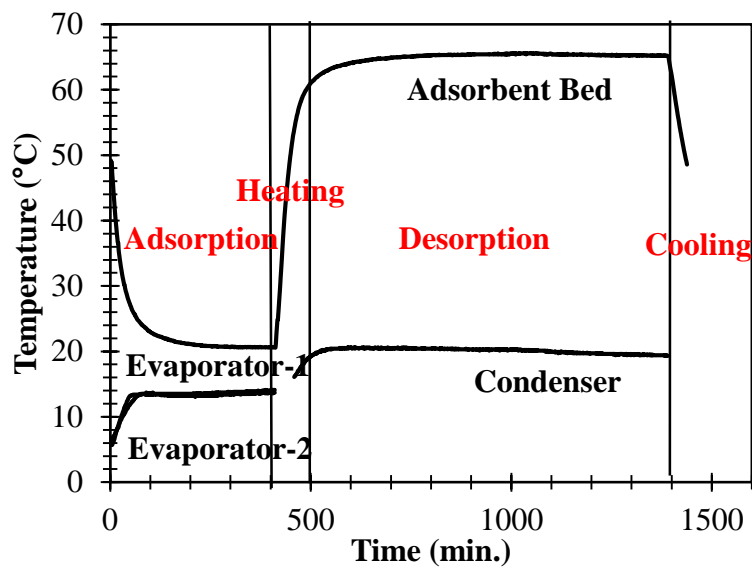


Figure D.16 (a). Temperature diagram of adsorbent bed, condenser and evaporator for experiment no: 16 conditions.

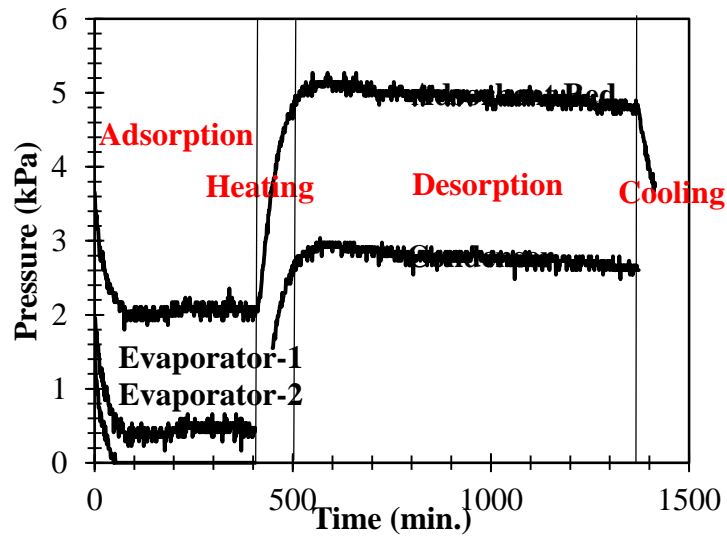


Figure D.16 (b). Pressure diagram of adsorbent bed, condenser and evaporator for experiment no: 16 conditions.

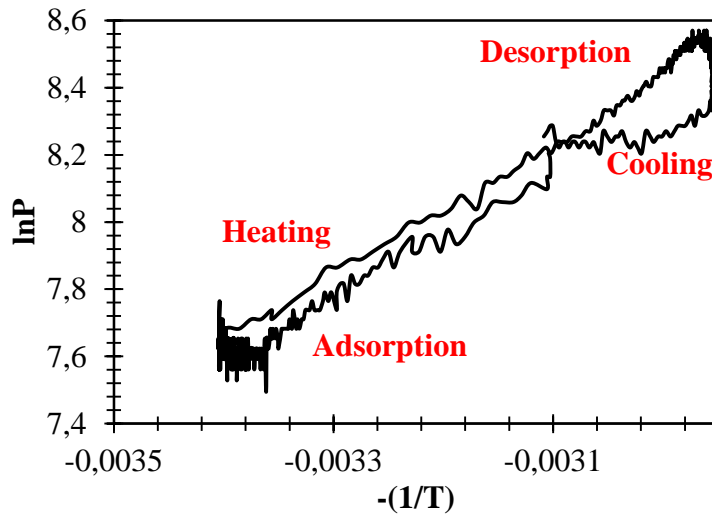


Figure D.16 (c). Clapeyron diagram of adsorbent bed for experiment no: 16 conditions.

- Experiment No and Date: 17 / 12.02.2015

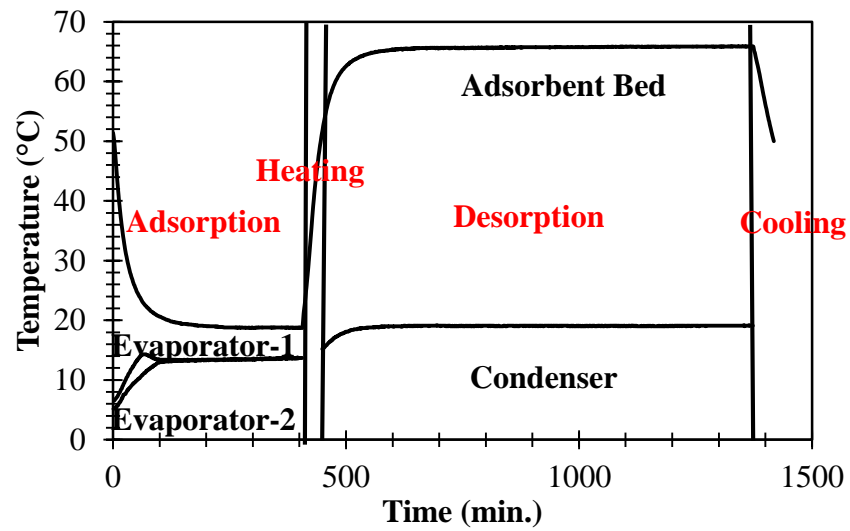


Figure D.17 (a). Temperature diagram of adsorbent bed, condenser and evaporator for experiment no: 17 conditions.

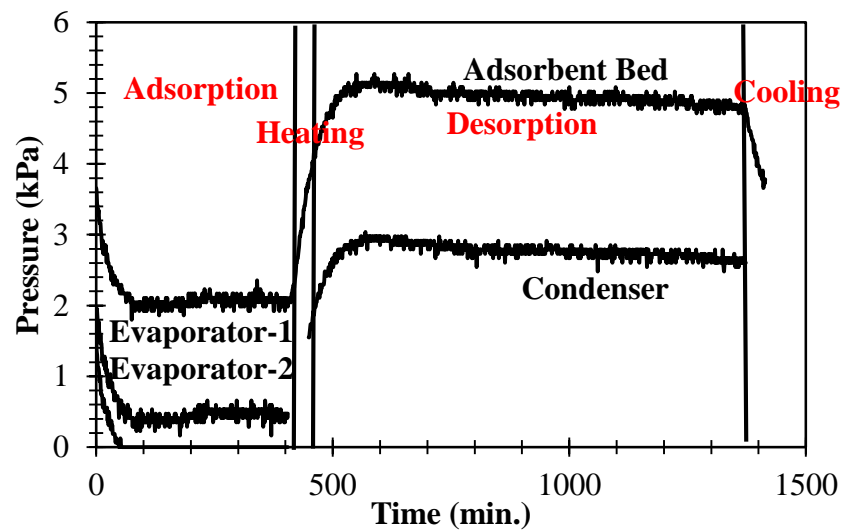


Figure D.17 (b). Pressure diagram of adsorbent bed, condenser and evaporator for experiment no: 17 conditions.

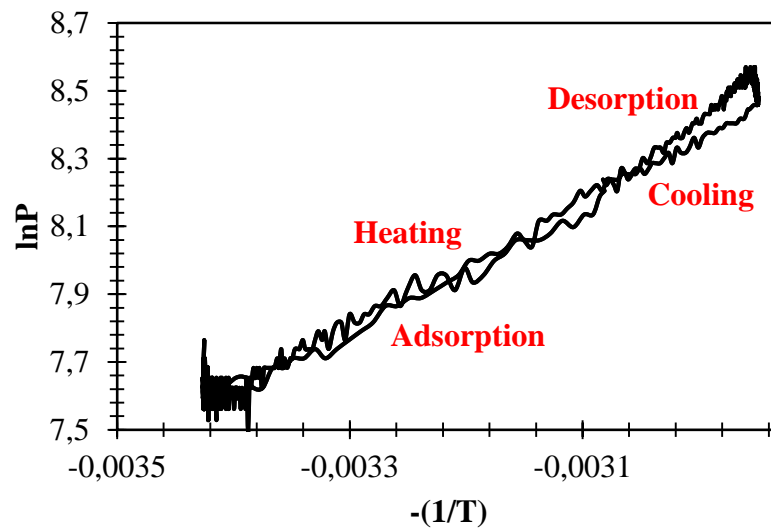


Figure D.17 (c). Clapeyron diagram of adsorbent bed for experiment no:20 conditions.

- Experiment No and Date: 18 / 19.02.2015

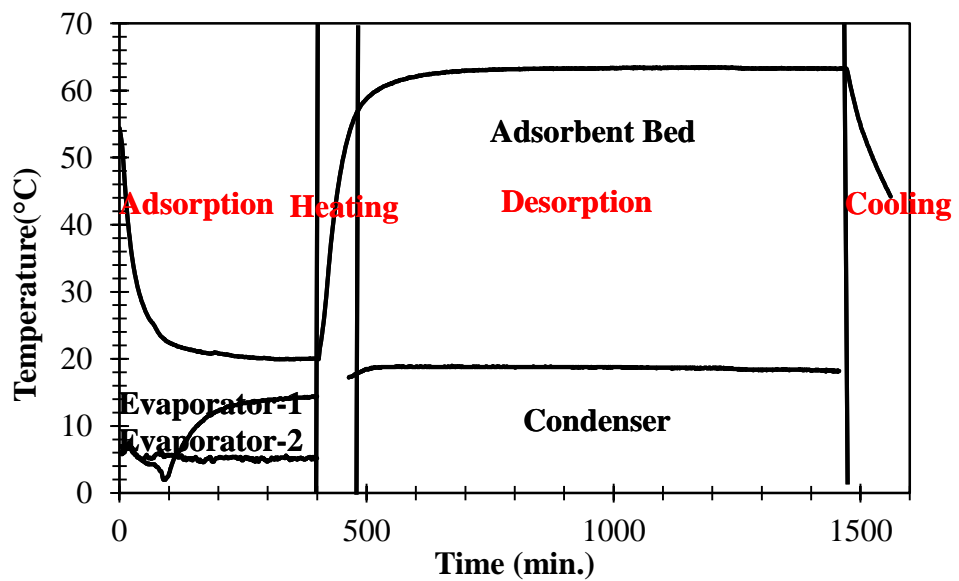


Figure D.18 (a). Temperature diagram of adsorbent bed, condenser and evaporator for experiment no: 18 conditions.

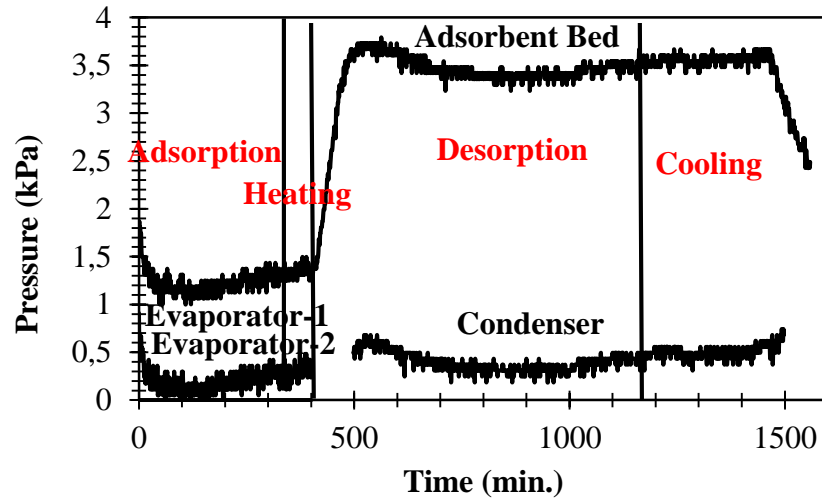


Figure D.18 (b). Pressure diagram of adsorbent bed, condenser and evaporator for experiment no: 18 conditions.

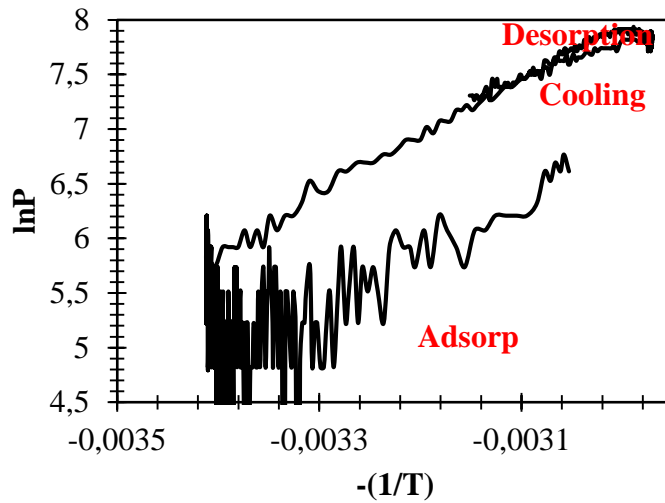


Figure D.18 (c). Clapeyron diagram of adsorbent bed for experiment no: 18 conditions.

Table D.1. The results of the whole experiments during this thesis.

DATE	Adsorption Time (hour)	h_{evaporation} (cm)	Desorption Time (hour)	h_{condensation} (cm)
06.01.2015	7	1	16	1
08.01.2015	3	2.2	20	2
10.01.2015	24	14	24	12.5
14.01.2015	24	8	24	8
19.01.2015	24	16	24	13
21.01.2015	24	12	5	10
26.01.2015	24	18	24	13
28.01.2015	3	3	3	1.5
29.01.2015	3	1	3	0.5
30.01.2015	3	1.5	3	1.5
03.02.2015	24	23	24	23
05.02.2015	3	4.3	3	2
06.02.2015	3	3	3	1,5
09.02.2015	7	2.2	16	4
10.02.2015	7	1.7	16	2.5
11.02.2015	6	3.5	16	2
12.02.2015	6	1.2	16	1.5
19.02.2015	7	1.5	16	0.9

(Cont. on next page)

Table D.1. (cont.)

Cycle Time (sec)	Water Mass (kg)	Qevap (W)	COP	SCP
16200	0,069	10,684	0,531	2,671
27000	0,086	8,013	0,582	2,003
88200	0,086	2,453	0,582	0,613
88200	0,190	5,396	0,733	1,349
178200	1,211	16,998	0,898	4,249
178200	0,692	9,713	0,870	2,428
178200	1,384	19,426	0,902	4,856
109800	1,038	23,646	0,891	5,911
178200	1,557	21,855	0,906	5,463
27000	0,259	24,040	0,778	6,010
27000	0,086	8,013	0,582	2,003
27000	0,129	12,020	0,666	3,005
178200	1,990	27,925	0,913	6,981
27000	0,372	34,458	0,820	8,614
27000	0,259	24,040	0,778	6,010
88200	0,190	5,396	0,733	1,349
88200	0,147	4,170	0,689	1,042
84600	0,302	8,951	0,798	2,237
84600	0,103	3,069	0,621	0,767
88200	1,298	3,796	0,900	1,199

APPENDIX E

UNCERTAINTY ANALYSIS

Measurement uncertainties can come from the measuring instrument, from the item being measured, from the environment, from the operator, and from other sources. W is a function of x_1, x_2, \dots, x_n . The effect of W of an error measuring an individual x_i may be estimated by analogy to the derivative of a function. A variation, δx_i in x_i would cause W to vary according to;

$$(B.1) \quad \frac{\partial W}{\partial x_i} \delta x_i = \delta W_i$$

If the equation is divided to W and multiplied with x_i ;

$$(B.2) \quad \frac{\delta W_i}{W} = \frac{x_i}{W} \frac{\partial W}{\partial x_i} \frac{\delta x_i}{x_i}$$

$\frac{\delta x_i}{x_i}$ is the definition of uncertainty because of variation in x_i , where δx_i is the accuracy of measurement. Uncertainty of the results is calculated by using Eqn. (B.3).

$$(B.3) \quad u_W = \sqrt{\left(\frac{x_1}{W} \frac{\partial W}{\partial x_1} u_1\right)^2 + \left(\frac{x_2}{W} \frac{\partial W}{\partial x_2} u_2\right)^2 + \dots + \left(\frac{x_n}{W} \frac{\partial W}{\partial x_n} u_n\right)^2}^{1/2}$$

In this thesis, Toth's isotherm equation is evaluated using pressure and temperature values of the adsorptive. Toth's isotherm equation is given in Chapter 6. Toth's isotherm equation depends on pressure and temperature parameters. Thus, the uncertainty analysis should be performed based on the accuracy of devices used to measure the quantities of these parameters. The measurement devices and accuracies of them are given in Table (E.1)

Table (E.1). Accuracies and uncertainties of measured parameters.

Measurement	Device	Accuracy	Uncertainty
Pressure	EW-07356-60	0.4%	±0.004
Height	-	1.5%	±0.015
Temperature	RT03-IP05-5 1/2 NPT	0.3%	±0.003
Mass	Kern-cb6k-1	1%	±0.01

The uncertainty is calculated from this equation:

$$u_W = \bar{\mp} \left[\left(\frac{P}{W} \frac{\partial W}{\partial P} u_P \right)^2 + \left(\frac{T}{W} \frac{\partial W}{\partial T} u_T \right)^2 \right]^{1/2} \quad (\text{B.4})$$

$$u_W = \bar{\mp} \left[\left(\frac{PT^{1/n} P^{1/n}}{P^{1/n} T^{1/n}} \right)^2 + \left(\frac{TT^{1/n}}{P^{1/n}} (-T) \left(-\frac{1}{n} - 1 \right) P^{1/n} u_T \right)^2 \right]^{1/2}$$

$$u_W = \bar{\mp} \left[((1) \bar{\mp} u_P)^2 + ((-1) \bar{\mp} u_T)^2 \right]^{1/2}$$

$$u_W = \bar{\mp} \left[((1) \bar{\mp} 0.004)^2 + ((-1) \bar{\mp} 0.003)^2 \right]^{1/2}$$

$$u_W = \bar{\mp} 0.005$$

The uncertainty of the experimental study on isotherm is found 0.005.

The concentration change in the bed is correlated with the data given in this equation.

$$W = \frac{\Delta m_v}{m_s} = \frac{\rho_v \pi (R_0^2 - R_i^2) H}{m_s} \quad (\text{B.5})$$

where H is the height water height in the evaporator. The uncertainty can be calculated from this equation:

$$u_W = \bar{\mp} \left[\left(\frac{H}{W} \frac{\partial W}{\partial H} u_H \right) + \left(\frac{m_s}{W} \frac{\partial W}{\partial m_s} u_m \right) \right]^2 \Bigg]^{1/2} \quad (\text{B.6})$$

$$u_W = \bar{\mp} \left[\left(\frac{H m_s}{H} \frac{1}{m_s} u_H \right) + \left(\frac{m_s^2 - H}{H} \frac{-H}{m_s^2} u_m \right) \right]^2 \Bigg]^{1/2}$$

$$u_W = \bar{\mp} \left[((1) \bar{\mp} u_H)^2 + ((-1) \bar{\mp} u_m)^2 \right]^{1/2}$$

If the uncertainty is calculated:

$$u_W = \bar{\mp} \left[((1) \bar{\mp} 0.015)^2 + ((-1) \bar{\mp} 0.01)^2 \right]^{1/2} = \bar{\mp} 0.018$$

The achieved calculations and results should be evaluated considering this uncertainty quantity.

